UNIVERSITÀ DEGLI STUDI DI SALERNO

UNIVERSITÀ DEGLI STUDI DI SALERNO
Dipartimento di Farmacia

PhD Program
in **Drug Discovery and Development**
XXXI Cycle   —   Academic Year 2018/2019

PhD Thesis in

Computational Chemistry techniques for the design and the synthesis of molecules with anti-inflammatory and anti-tumor activity

Candidate

Marianna Potenza

Supervisor

Prof. *Giuseppe Bifulco*

PhD Program Coordinator: Prof. Dr. *Gianluca Sbardella*

Dedicated to my father and my mother

Preface

My three-year PhD course in Drug Discovery and Development at the Department of Pharmacy of Salerno University was started in November 2015 under the supervision of Prof. Giuseppe Bifulco.

My research project mainly focused on the application of computational chemistry techniques for the design and/or the identification of new anti-tumor and anti-inflammatory molecules, and their synthesis for the subsequent biological evaluation.

In detail, basing on a project founded by AIRC (Associazione Italiana per la Ricerca sul Cancro, Italian Association for Cancer Research) I was interested in the identification of new inhibitors of a membrane enzyme, microsomal Prostaglandin E_2 Synthase-1 (mPGES-1). A second part of the research activity concerned the discovery of new inhibitors of a molecular chaperone, Heat Shock Protein 90 (Hsp90). Both the targets have been shown to be involved in inflammation and cancer processes.

Biological tests on small molecules that I designed and/or synthesized were performed in collaboration with Prof. Oliver Werz of Friedrich Schiller University (Germany).

Furthermore, in order to improve my knowledge on synthetic chemistry, I moved to the Department of Chemistry and Applied Biosciences of ETH (Zurich) in 2018 (March until the end of October 2018) under the supervision of Prof. Jeffrey W. Bode.

During the period of my internship in their laboratory of Organic Chemistry, I applied new synthetic strategies developed in the last few years. I mainly worked on SnAP chemistry, using it as chemical route for the synthesis of pharmacologically promising compounds.

List of publications related to the scientific activity performed during the three years PhD course in Drug Discovery and Development

Papers:

1. Terracciano, S.; Russo, A.; Chini, M. G.; Vaccaro, M. C.; **Potenza, M**.; Vassallo, A.; Riccio, R.; Bifulco, G.; Bruno, I., Discovery of new molecular entities able to strongly interfere with Hsp90 C-terminal domain. *Sci Rep* **2018,** *8* (1), 1709.

2. Lauro, G.; Cantone, V.; **Potenza, M**.; Fischer, K.; Koeberle, A.; Werz, O.; Riccio, R.; Bifulco, G., Discovery of 3-hydroxy-3-pyrrolin-2-one-based mPGES-1 inhibitors using a multi-step virtual screening protocol. *MedChemComm* **2018,** *9* (12), 2028-2036.

3. Chini, M.G.; † Giordano, A.;† **Potenza, M**.; Vaccaro, M.C.; Terracciano, S.; Bruno, I.; Riccio, R.; Werz, O.; Koeberle, A.; Bifulco, G., "Targeting mPGES-1 by combinatorial approach: identification of aminobenzothiazole scaffold as new PGE$_2$/LTs modulator in human cancer cells". Manuscript in preparation.

Conference proceedings:

1. **M. Potenza**, M.G. Chini, A. Russo, S. Terracciano, G. Bifulco "Computational chemistry methods for the identification of new Hsp90 inhibitors", European-Winter School on Physical Organic Chemistry (E-WISPOC 2016), Bressanone (Italy), January, 31- February, 5, 2016.

2. **M. Potenza**, M.G. Chini, A. Giordano, G. Bifulco "Computational chemistry methods for the identification of new mPGES-1 inhibitors", XLI International Summer School on Organic Synthesis "A. Corbella" (ISOS 2016), Gargnano (Italy), June, 12-17, 2016.

3. **M. Potenza**, M.G. Chini, A. Giordano, G. Bifulco "Computational chemistry methods for the identification of new mPGES-1 inhibitors", European-Winter School on Physical Organic Chemistry (E-WISPOC 2017), Bressanone (Italy), January, 29-February, 3, 2017.

4. **M. Potenza**, M.G. Chini, G. Bifulco. "SnAP reagents for the development of new potential mPGES-1 inhibitors" XLII International Summer School on Organic Synthesis "A. Corbella" (ISOS 2017), Gargnano (Italy), June, 18-22, 2017.

5. **M. Potenza**, S. Terracciano, A. Russo, M.G. Chini, M.C. Vaccaro, A. Vassallo, R. Riccio, G. Bifulco and I. Bruno "Discovery of new molecular entities able to strongly interfere with Hsp90 C-terminal

domain" XXVI International meeting of Italian Chemical Society, Paestum (Italy), September, 10-14, 2017.

6. **M. Potenza**, M.G. Chini, G. Lauro, J.W. Bode, G. Bifulco. "From SnAP reagents to substituted saturated heterocycles as new potential mPGES-1 inhibitors" XXXVIII National Meeting of Italian Chemical Society, Organic Chemistry Division, Milano (Italy), September, 9-13, 2018.

Abstract

In the last few years, computational chemistry has played an important role in disclosing novel compounds with relevant biological activity. Inflammation and cancer processes have been recently linked, and the identification of new molecular entities able to interfere with biological targets involved in these pathologies is strongly needed. The analysis of ligand-macromolecule interactions and the evaluation of possible "binding modes" are the starting points in the design and the identification of new and more powerful drugs. Also, *in silico* Virtual Screening campaigns of large libraries of compounds on a specific target allow the selection of the most promising, leading the identification of new hits. Moreover, the coupling between versatile synthetic approaches and computational protocols is a powerful tool to obtain optimal results with time optimization. Thus, in this thesis both topics are applied at the same time, as they are connected to each other.

The research work was mainly focused on mPGES-1 (microsomal Prostaglandin E_2 Synthase) as a promising target for the treatment of the pathologies above. This enzyme is a homotrimeric membrane protein involved in the arachidonic acid cascade and it acts as downstream synthase in the cyclooxygenase pathway, catalyzing the conversion of the unstable peroxidic intermediate prostaglandin H_2 (PGH_2) in prostaglandin E_2 (PGE_2). Among the three different isoforms of the enzyme, selective inhibition of the inducible mPGES-1 may be considered a valid therapeutic approach to interfere with inflammation-induced PGE_2 formation, avoiding to block the biosynthesis of constitutive prostanoids. Also, it is over-expressed in tumor pathologies. In light of this, in order to identify novel molecular platforms able to inhibit the activity of the enzyme strongly, a structure-based multi-step computational

protocol was applied starting from selected privileged scaffolds coupled to a synthetic chemical route. Specifically, new libraries of 2-aminobenzothiazole, 2-aminothiadiazole and 2-carboxamidepyrrole-based molecules were generated, and they were docked onto the 3D structure of mPGES-1 (PDB code: 4BPM) crystallized in 2014. Using the interactions with the receptor counterpart as a qualitative filter, a collection of compounds for each library was selected, synthesized and submitted to biological investigation. Finally, cell-free and cell line assays confirmed some of them (benzothiazole derivatives **1**, **3**, **6**, **9** and **13**, thiadiazole derivatives **18-20** and **22**, pyrrole derivatives **45** and **47**) as novel promising mPGES-1 inhibitors.

Furthermore, the same computational approach focused on mPGES-1 was applied on substituted saturated N-heterocycles, whose synthesis was performed at the Department of Chemistry and Applied Biosciences at ETH (Zurich). In detail, the libraries were docked onto the crystal structure co-crystallized with the inhibitor 6PW (PDB code: 5K0I), leading to the selection of 21 compounds (**62-82**). The synthesis was performed using the SnAP (Stannyl Amine Protocol) chemistry, which consists of a reaction between an aminotributylstannane and an aldehyde to form an imine as the first step, followed by an intramolecular cyclization. Biological investigations are in progress on the synthesized compounds.

In order to deeply combine computational tools and this versatile and suitable synthetic approach, a large database of about 1,300,000 synthetically accessible compounds was created *in silico* starting from iSnAP (Iterative SnAP) reagents, a new generation of SnAP reagents bearing a further functional group. The prepared database was then submitted to virtual screening studies on pharmacologically promising targets (mPGES-1 up to

now), in order to select the best candidates for the synthesis and the biological evaluation.

Finally, the application of multi-step computational protocols including both ligand and structure based approaches took place in the identification of two novel 3-hydroxy-3-pyrrolin-2-one-based hits (compounds **87** and **88**) as promising mPGES-1 inhibitors, starting from a large library of commercially available compounds.

A second research work regarded Hsp90, a molecular chaperone involved in the development, survival and proliferation of cancer cells, regulating the homeostasis of oncoproteins. Most of the developed Hsp90 inhibitors interact with the N-terminal domain, but this type of modulation induces toxicity issues connected to the induction of the deleterious heat shock response (HSR). Contrariwise, since C-terminus inhibitors do not produce this effect and only a few of them have been developed so far, an aim of this research work consisted of the individuation of novel C-terminus binders. Thus, a biological screening on a small library of 48 commercially available compounds was performed and two novel inhibitors were identified (compounds **100** and **103**) able to interact selectively with the C-terminal domain. Starting from these results, a computational rationalization was performed, applying Induced Fit Docking studies and Molecular Dynamic Simulations.

In conclusion, in order to perform an optimization campaign, three large libraries of derivatives of compound **103** were generated using the multi-step computational protocol above, and a total number of 21 molecules have been selected for the synthesis and the biological evaluation.

-INTRODUCTION-

-CHAPTER 1-

Inflammation and Cancer

1.1 Inflammation and cancer

The connection between inflammation and cancer is a concept disclosed as early as 1863, when Virchow confirmed the sites of chronic inflammation as a potential source for cancer development.[1] A sequence of factors is involved in neoplastic risk, since the proliferation of cells alone does not induce cancer, and an environment rich in inflammatory cells and related agents potentiates and supports its growth. The purpose of the inflammatory response is to repair and regenerate tissues exposed to injury associated with wounding. When the damage is repaired, proliferation is blocked and inflammation goes out. In tumors, the proliferation of damaged cells persists in microenvironments of inflammation.[2] In the next sections, the fundamental pathways of connection between the two pathologies will be described. Moreover, although the relationship between cancer and inflammation is broadly known, many of the molecular and cellular mechanisms useful for well understanding the development of the cancer-related inflammation are not disclosed.[3]

1.2 Inflammation: an overview

The word "inflammation" derives from the Latin "*inflammation*", whose meaning is "fire". This single word is a resume of the five signs of the pathology: *calor* (heat and fever), *tumor* (swelling), *rumor* (redness), *dolor* (pain), *functio laesa* (inability of the area affected by inflammation to maintain its functionalities).

The inflammatory response is triggered by pathogens or tissue traumas caused by several factors, such as physical or chemical insults.[4] Several physiological changes follow the exposure to these factors to contrast the

damages[5]. After the invasion of pathogens, for example, the release of peptides, carbohydrates and nucleic acids stimulates the tissues to produce substances such as uric acid, extracellular ATP and other dendrites. The immune response is induced by the binding of these molecules to PRR (Pattern Recognition Receptors) proteins (an example are the Toll-Like Receptors, TLRs) expressed by dendritic cells, macrophages, monocytes, neutrophils in the innate immune response.[6] Thus, the granulocytes product substances involved in the ongoing inflammatory response (histamine, tumor necrosis factor α, nitric oxide), and the subsequent dilatation of blood vessels and the increasing of the levels of cellular junctions induce the release of plasma proteins in the tissue. In some cases, platelets and plasma proteins penetrate the tissue and recruit components of the matrix, taking part in the formation of clots.[6] Vascularization damage releases platelets and blood cells into the tissue. Although in the absence of physical trauma, cytokines and granulocytes may increase permeability through endothelial junctions, allowing plasma fluid and proteins to filter through the wall and to wet the surrounding tissue. This way, fibronectin and fibrinogen components induce the three-dimensional extracellular matrix to repair the tissue with immediate cell infiltration. Then, growth factors carried from blood regulate the recruitment of immune cells. [7, 8]

Furthermore, the flow of plasma through the interstitium and the structural remodeling of matrices act as a signal for the recruitment of plasma proteins and growth factors into damaged tissue, and the mechano-biological activation is useful for the migration of leukocytes and fibroblasts.[9] Also, the filtration of plasma through the vessel is responsible of the increasing of blood

concentration near the vessel wall. The combination of this with vessel dilatation increases erythrocyte aggregation.[9]

Endothelial adhesion molecules (ICAM-1, VCAM-1, PECAM-1, E-selectin and P-selectin) are regulated by growth factors such as histamine, interleukins, ROS and TNF,[10] deriving from granulocytes. The leukocytes flow along the wall of the blood vessel and stop in the tissue. Some of the cytokines produced during the inflammatory process act as chemokines, generating chemical gradients.[10] At this point, cells of the inflammatory response are recruited. Neutrophils are involved in phagocytosis of assaulting agents, and in the generation of neutrophilic traps, known as NET (neutrophil extracellular traps), that may trap and kill extracellular bacteria without phagocytosis processes.[11] Hypoxia conditions may occur considering the high grade of activities in the repair of the damage. In response to these events new blood vessels can be generated in order to increase the oxygen availability, a phase which presents as main components angiogenic growth factors, such as VEGF (vascular endothelial growth factor).[12]

In a successful inflammatory response, these processes are able to restore homeostasis. Several control mechanisms, such as a short half-life of mediators of inflammation and the ability to reorganize the tissue microanatomy after removing the insult, are fundamental for the resolution. Unfortunately, this safety mechanism is limited in pathological and chronic inflammation.[7, 8]

1.2.1 Inflammation mediators

One of the main mediators of inflammatory processes is prostaglandin E_2 (PGE_2), as it is involved in different roles such as induction of redness, edema,

fever, hypersensitivity of peripheral neurons, and it acts as a chemotactic and mitogenic factor. [13] Once released, it is able to interact with four different G-protein coupled receptor subtypes (EP1, EP2, EP3, EP4), taking part in the inflammatory effects.[14] Moreover, PGE_2 plays a series of different roles in the organism to maintain homeostasis: vascular regulation,[15] female reproduction,[16] protective gastric mucosa[17] and renal function.[18] Also, it participates in tumor development, since it promotes tumor growth, immune suppression, angiogenesis and apoptosis inhibition.[13] Recently, some studies reported that the concentration of PGE_2 increases in a wide variety of human tumors,[19] such as colorectal[20] and breast cancers.[21]

Fundamental mediators of the inflammatory response are other eicosanoids (prostacyclins, thromboxanes and leukotrienes).[22, 23] In particular, prostacyclin interferes with the formation of blood clots and induces vasodilatation; thromboxane has also vasodilating effects, but favours platelet aggregation and bronchospasm; leukotrienes are responsible for the delayed phase of the asthmatic reaction, acting as powerful bronchoconstrictors.[24]

Other examples of molecules able to act as mediators in the inflammatory performances are histamine, NO (nitric oxide), TNF-α (tumor necrosis factor α) and NF-κB (nuclear factor kappa-light-chain-enhancer of activated B cells), whose activities will be described in the next sections. [25-27]

1.2.2 Eicosanoids biosynthesis

A brief description of the biosynthesis of eicosanoids in the inflammatory cascade is reported, since a purpose of this research work is to interfere with the activity of an enzyme involved in the synthesis of prostaglandins.

Eicosanoids derive from the oxidation of arachidonic acid (AA), characterized by a 20 carbons chain and released from cell membranes due to the activity of Phospholipase A2 (PLA2).[22, 23] The activation of the mentioned lipase is by mechanical, physic or chemical stimuli (for example an increase of intracellular Ca^{2+} levels)[28] or the interaction of inflammation mediators with G-protein coupled receptors. Then, AA may be undergone to two different enzymatic pathways: cyclooxygenase (COX)[29] or lipoxygenase (LOX) activities.[30] In particular, cyclooxygenase leads to the formation of prostaglandins, thromboxane and prostacyclin,[29] whereas lipoxygenase is involved in the synthesis of leukotrienes and lipoxins (Figure 1). [30]

In details, in the COX pathway it is possible to distinguish two cyclooxygenases: COX-1, constitutively expressed, and COX-2, inducible isoform. Both of them firstly lead to the formation of the AA-derived endoperoxide PGG_2 in the cyclooxygenase site of the COXs,[31] then reduced at the peroxidase site of COXs into the unstable peroxide intermediate prostaglandin H_2 (PGH_2).[32] The latter is converted to the stable isomer prostaglandin E_2 (PGE_2) by prostaglandin E_2 synthase, or other prostaglandins (PGD_2, $PGF_{2\alpha}$), prostacyclin (PGI_2) and thromboxane (TXA_2) by the proper synthase (Figure 1). [23, 33] PGE_2 and the other prostaglandins interact with G-protein coupled membrane receptors (GPCR) and perform their functions.[34]
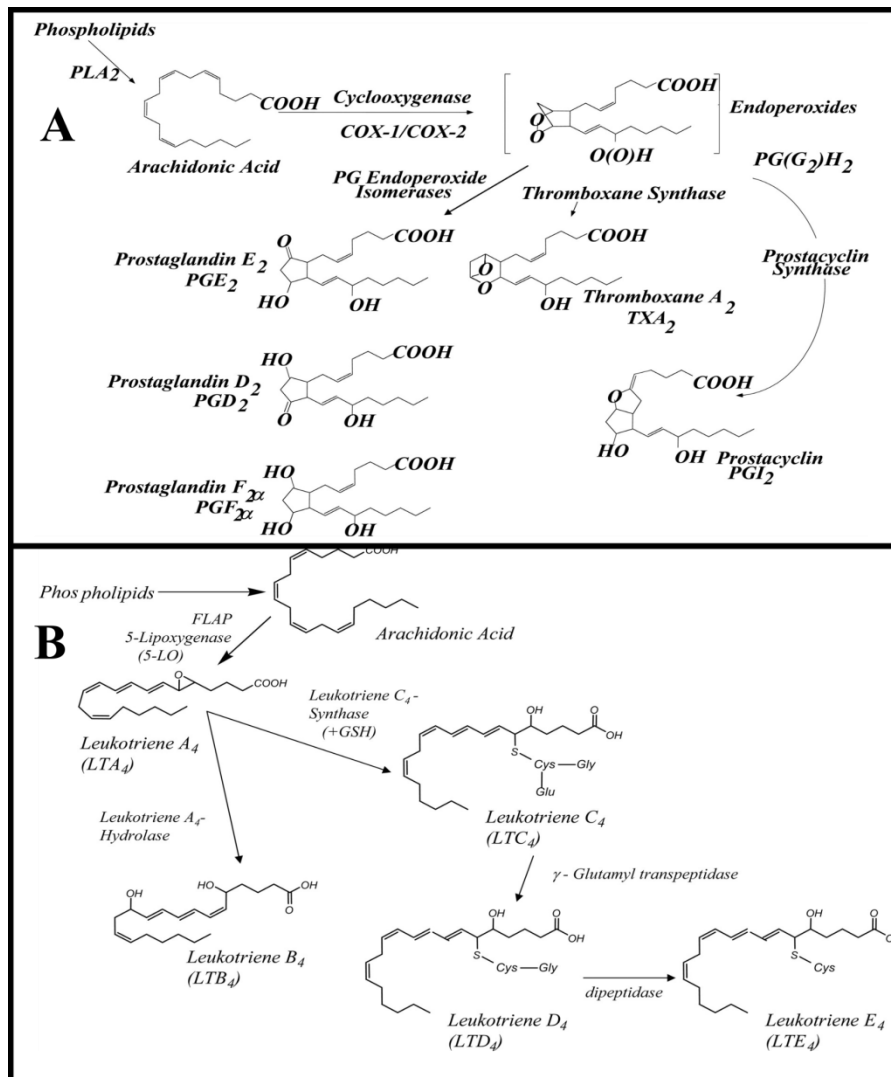
Figure 1 Biosynthesis of prostaglandins (**A**) and leukotrienes (**B**).[23]

1.2.3 From acute to chronic inflammation

In inflammation, all recruited cells play a crucial role in defense of the damaged tissue against infection. Control of the duration of the response is fundamental to avoid exposure to an inflammatory environment from lasting

too long and the generation of the conditions for cancer development.[35] In the shift from tissue damage to tissue repair both pro-inflammatory and anti-inflammatory mechanisms are implicated, since a balance between promoting and suppressing is crucial for the retaining of the homeostasis. Different molecules take part in this equilibrium, performing the two activities by the case. A dual job is carried out from prostaglandin E_2,[36] transforming growing factor-β,[37] reactive oxygen and nitrogen intermediates.[38] A programmed removal of inflammatory cells from the tissue with a following resolution of the response is provided by dendritic cells, macrophages, and phagocytes, inducing apoptosis and phagocytosis.[11, 39]

Moreover, if the breaking down of the inflammatory response is dysregulated, a shift to a chronic response is induced. In this situation, the persistence of macrophages and other inflammation cells in the microenvironment develops growth factors, cytokines and reactive oxygen and nitrogen species, and may cause DNA damages. The described conditions may lead to the progression of a tumoral state. [1, 8]

1.3 Cancer: an overview

A neoplasm is an abnormal and extensive growth (*neoplasia*) of a tissue, which usually forms a mass called tumor.[40] In a benign neoplasm, cells are not differentiated from those of the original tissue and lack the ability of invasion.[41] Moreover, the main problem is the need for space as it may become dangerous if it exerts pressure on nearby vital structures. The malignant evolution of a neoplasm is called cancer. Cancer cells, likely to generate in almost every organ and tissue, are endowed with metastatic growth that can be caused by a combination of factors, such as genetic and

environmental agents.[4] Cancer development is a multi-step process, in which uncontrolled cell growth follows the activation of oncogenes and/or the deactivation of tumor suppression genes. Six several characteristics (hallmarks)[42] lead to the progression of cancer: evading apoptosis and extension of the number of cells; self-sufficiency in growth signals and insensitivity to anti-growth signals, where in contrast a normal cell cannot proliferate in absence of external stimulatory signals; tissue invasion and metastasis that requires a down-regulation of cell adhesion receptors as well as an up-regulation of receptors involved in cell motility; limitless replicative potential, deriving from growth signals autonomy; substained angiogenesis, which ensures the supply of nutrients and oxygen for the survival of cells. [42] Epigenetic alterations are also implicated in cancer and may be considered another hallmark. In fact, modifications affecting histones and DNA residues are crucial in the generation of cancer progenitor cells. [43]

The evolution of cancer is complicated and a combination of different signaling processes. Moreover, it is essential to stress the correlation between chronic inflammation and carcinogenic conditions.

1.4 Connecting inflammation and cancer

As reported above (section 1.1), the connection between inflammation and cancer was first presented in the nineteenth century. It is estimated that 20% of cancers derive from persistent inflammation.[1] Two different pathways can be distinguished: an extrinsic, in which inflammatory conditions increase the risk of cancer development, and an intrinsic, in which genetic alterations are reason of inflammation and tumor. In the intrinsic path the expression of oncogenes and inactivation of tumor suppressor genes are performed. (Figure 2).

Moreover, both the pathways converge to the activation of transcription factors.

Macrophages populate the environment as the main cellular component in chronic inflammation. Those and other leukocytes are responsible of the production of reactive oxygen and nitrogen species, whose persistence in the tissue is dangerous, since they may generate mutagenic agents able to react with DNA.[44] Furthermore, the release of tumor necrosis factor-α (TNF-α) and macrophage migration inhibitory factor contribute to the damage, determining an accumulation of oncogenic mutations.[45]
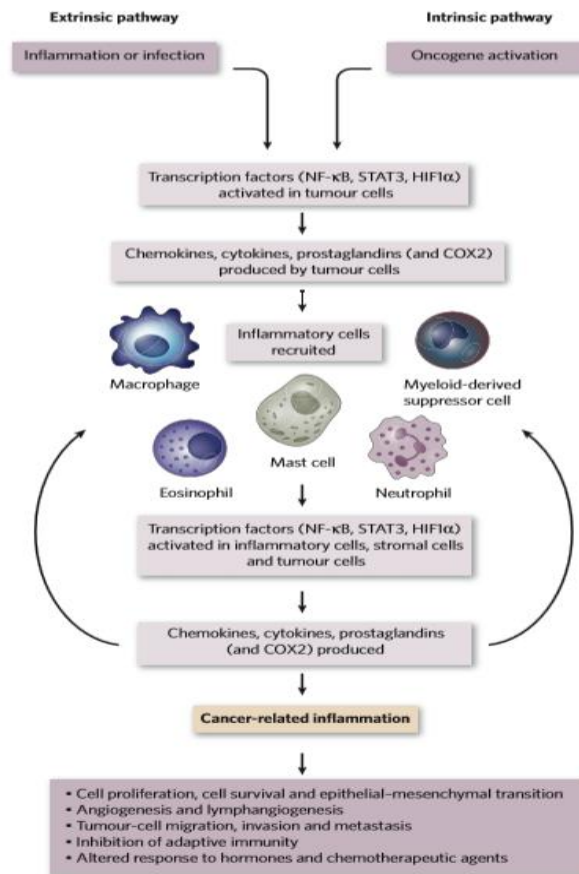
Figure 2 Cancer-related inflammation: intrinsic and extrinsic pathways.

A description of the key regulatory molecules involved in the conversion from chronic inflammation to cancer is useful for understanding some mechanisms. Key endogenous (intrinsic) factors can be defined, such as transcription factors (NF-κB, STAT3) and cytokines (IL-1β, IL-6, IL-23 and TNF-α named above). TNF-α was discovered first as a mediator locally expressed by cells of the immune system, with a therapeutic role.[25] Moreover, it was demonstrated that TNF-α is also involved in most of the processes for the development of cancer, since it stimulates other inflammatory mediators

and it is produced by tumoral cells, performing the role of an endogenous tumor promoter. It modulates cellular transformation, proliferation, angiogenesis, invasion, metastasis.[26]

Also, NF-κB is an endogenous mediator involved in the promotion of cancer and the progression. It is a coordinator of innate immunity and inflammation, and it operates downstream, in the Toll-like receptor (TLR)-MyD88 signaling pathway. In both tumor and inflammatory cells, NF-κB is responsible for the expression of genes which encode cytokines, angiogenic factors, enzymes involved in the synthesis of prostanoids (COX-2) or inducible nitric oxide synthase (iNOS). In light of this, NF-κB is an important mediator which plays a fundamental role in both inflammatory and cancer pathologies.[27]

A list of mediators that take part in the key molecular mechanisms of connection between the two pathological states is reported below. In conclusion, molecular and cellular components of the inflammatory response are crucial in cancer development.

Potential linkers	Functions in linking inflammation to cancer
IL-6	Promotion of tumor growth
TNF-α	Induction of DNA damage and inhibition of DNA repair Promotion of tumor growth Induction of angiogenic factors
Chemokines	Promotion of tumor growth Invasion and metastasis by directing tumor cell migration and promoting basement membrane degradation
NF-κB	Inflammation progress, promoting chronic inflammation Promotion of production of mutagenic reactive oxygen species

	Protection of transformed cells from apoptosis Promotion of tumor invasion and metastasis Feedback loop between proinflammatory cytokines
iNOS	Induction of DNA damage and disruption of DNA damage response Regulation of angiogenesis and metastasis
COX-2	Production of inflammation mediator prostaglandins Promotion of cell proliferation, antiapoptotic activity, angiogenesis, and metastasis
HIF-1α	Promotion of chronic inflammation Involved in angiogenesis, tumor invasion, and metastasis by transactivating VEGF
STAT3	Promotion of proliferation, apoptosis resistance, and immune tolerance
Nrf2	Anti-inflammatory activity Protection against DNA damage
NFAT	Regulation of proinflammatory cytokine expression Involved in cell transformation

Table 1 Molecular connection between inflammation and cancer.

1.5 Aim and outline of this thesis

According to the importance and relevance of the described related pathologies, the aim of this research project was the identification of new potential anti-inflammatory and anti-tumor molecules. The side effects of the well-known non-steroidal anti-inflammatory drugs (NSAIDs), for example on the gastrointestinal tract and the cardiovascular system, require the discovery and exploration of new classes of anti-inflammatory drugs, more specific and

safer,[46] especially for long term therapies.[47] Prostagrandin E_2 Synthase (PGES) is an enzyme involved in the inflammatory response, since it catalyzes the conversion of the unstable peroxide intermediate prostaglandin H_2 (PGH_2) in its isomer prostaglandin E_2 (PGE_2) (Figure 1). In particular, the enzyme is placed downstream in the inflammatory cascade, performing its function in a specific step which follows the upstream COX activity (Figure 1).[23] The increase of the level of PGE_2 in several types of cancer[19] and its support in cancer cell proliferation and tumor growth[13] are fundamental factors to consider the inhibition of the activity of PGES as a promising method for the development of novel anti-cancer drugs.[48] Herein, it is important to stress the existence of three different isoforms of PGES: the cytosolic cPGES and the microsomal mPGES-1 and mPGES-2. This project is mainly focused on the discovery and the design of novel mPGES-1 inhibitors, since it has been demonstrated in recent studies an up-regulation of this specific isoform in concert with COX-2 after exposure to various inflammatory stimuli and mediators,[49] whereas a constitutively expression of mPGES-2 and cPGES, and ubiquitous mPGES-1 at low concentration have been confirmed.

Basing on the objectives above, the research group in which the entire project was developed follows a specific multitasks protocol (Figure 3) as a guideline for the identification of new mPGES-1 inhibitors. A detailed description of its application to this research work will be reported in chapter 3.

Computational chemistry techniques have been a handy and powerful tool in the development and the progress of the project. The study of ligand-protein interactions played a fundamental role in the design of promising compounds, and the computational approaches permitted the analysis of a broad range of

chemical stereotypes for the individuation of new hits. Furthermore, the experimental part was essential to confirm *in silico* developed studies. Versatile and fast synthetic methods were performed for the generation of the compounds and the subsequent biological evaluation.
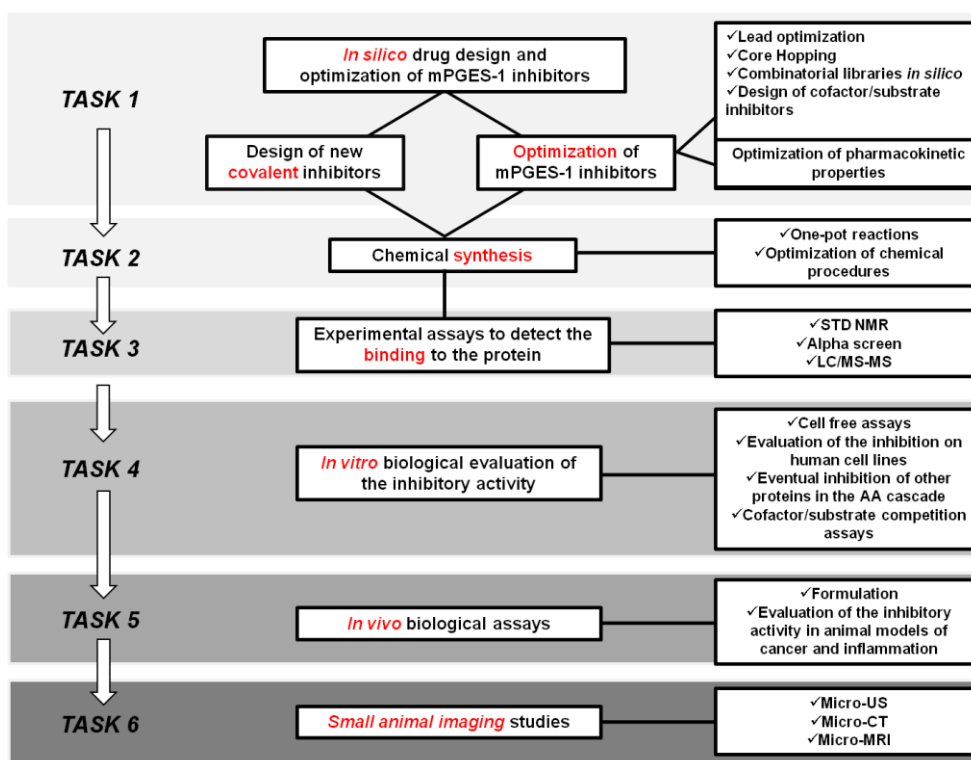
Figure 3 General Workflow.

The whole project has been founded by AIRC (Associazione Italiana per la Ricerca sul Cancro, Italian Association for Cancer Research).*

Furthermore, a second part of the project was the identification of novel inhibitors of Hsp90, protein target implicated in cancer development and

progression, belonging to the family of heat shock proteins (HSPs). Molecular chaperone activities of these proteins is noteworthy, since they are involved in the mechanisms of proteostasis in both physiological and stressful conditions.[50] The regulation of three-dimensional folding, assembly and disassembly, translocation and degradation of macromolecular protein structures during normal cellular growth and development are examples among many activities for which they are responsible.[50] Also, the members of this family take part in the refolding and reactivation of unfolded and misfolded proteins, damaged by stress conditions.[51] Hsp90 clients include different classes of protein macromolecules involved in signal transduction, such as kinases and many steroid hormone receptors.[51] In the last years, research on Hsp90 has been relevant, considering that most of Hsp90 clients are agents active in cancer progression.[51, 52] Also, Hsp90 is an interesting target for our purposes, since it is over-expressed in many tumors (breast and lung cancers).[53, 54] In the last years, the campaign of the discovery of Hsp90 inhibitors led to the identification of many inhibitors able to interact with the N-terminal domain of the protein,[55] whereas a few C-terminal inhibitors exist.[56-59] A detailed description of the protein and its conformational cycle associated with its chaperone activity,[50] and the importance of the individuation of C-terminal binders in comparison to N-terminal inhibitors[60] will be stressed below in this thesis[1].

-CHAPTER 2-

Computational Chemistry Techniques

2.1 Computational Chemistry in Drug Discovery

In the last three decades, computational chemistry techniques have played a major role in the development of therapeutically important small molecules.[61] A brief description of the adopted methods is reported in the next sections.

Computer-aided drug discovery (CADD) is employed for the exploration of the molecular basis of bioactive compounds pharmacological activity as well as for the development of derivatives with improved activity. Three main aims of CADD in drug discovery campaign are noteworthy:

1. the filtration of large libraries of compounds in order to select a small promising set for the biological evaluation;
2. the optimization of hit compounds, increasing the affinity for the protein target or optimizing the pharmacokinetic parameters (absorption, distribution, metabolism, excretion, and the potential for toxicity) at least from a calculate perspective;
3. the design of novel compounds, using "growing" strategies of molecules or combining fragments into new chemotypes. [61]
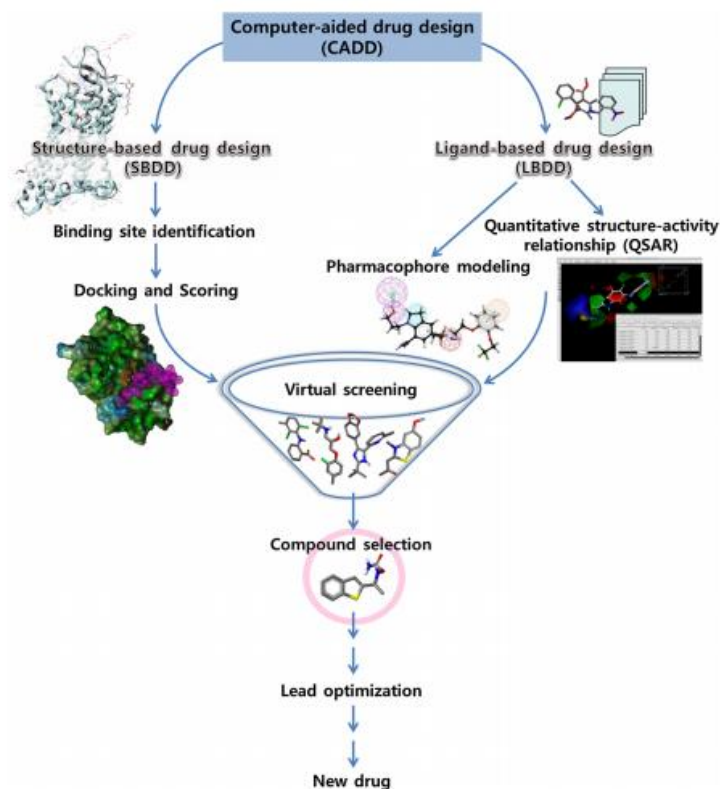
Figure 4 CADD in drug discovery/design pipeline.

2.2 Drug design

Drug design, also named rational drug design or rational design,[62] is a convenient method for the research of compounds targeting biological macromolecules. This approach appreciates a detailed knowledge of the targets involved in the pathology of interest, in order to decide the most promising for the design of new molecules. The choice of the target is based on:

1. its importance and its involvement in the pathology.

2. the druggability,[63] its ability to bind a small molecule able to change its physiological activity. Hopkins and Groom introduced the term druggable[64]. They wanted to identify a set of about 3,000 genes in the human genome which encode proteins related to the disease for which it is possible to develop drug-like compounds.[65] Therefore, the previous definition of druggability included those macromolecules capable of binding the molecules that comply with the Lipinski rule.[66] Today, a druggable structure is a protein which is implicated in the pathways involved in the pathology, whose activity can be modulated by drug-like molecules. [63]

It is also essential the knowledge of the existent modulators of the selected macromolecule, in order to define the chemical-physical properties and to compare them with the designed molecules, since the main aim of drug design is to generate compounds with an improved biological activity on the target.

In the last few years, computational modeling techniques were used for the drug design.[67] They consist of the application of molecular mechanic methods[68] to perform computational simulations of the binding between a ligand and a macromolecule. As a crucial component in pharmaceutical research, CADD reduced costs and time of screening significantly without compromising the quality of the lead compound discovery.

2.2.1 Structure-based Drug Design (SBDD)

Structure-based drug design (SBDD) approach[69] is based on the requirement that the 3D structure of the macromolecule is available. Protein Data Bank (PDB) is the most important database wherein crystal structures of

proteins, determined by NMR, X-ray crystallography or homology modeling[70, 71] methods, have been deposited since 1976.

As the design of the molecules is performed starting from the 3D structure of the protein, the active site is identified. Two cases are possible:

1. a co-crystallized ligand, known inhibitor, is placed in the active site. The entire process of calculation is carried out in the ligand binding site (LBS).

2. It is necessary to determine the possible binding sites using specific software, such as SiteMap[72] (Schrödinger LCC), Qsite Finder,[73] CASTp.[74] SiteMap[72] analyzes several chemical-physical parameters of the protein (volume, solvent exposure, hydrophobic and hydrophilic spaces, individuation of acceptor and donor hydrogen bonds) in order to calculate *Site Score* (SScore) and *Druggability Score* (DScore).

The compounds or the fragments of compounds are located in the active site and a score is assigned, according to the analysis of the interactions with the receptor counterpart. Based on the methodology applied to perform the structure-based drug design, two approaches can be used:

1. *de novo* approach, in which new ligands are tested into the binding site. A preliminary analysis of volume and shape of the site and the study of the key interactions for the determination of the biological activity are critical in this methodology. Fragments of molecules with specific functional groups are placed in the active site in order to establish the key interactions, and are connected to obtain the final promising compound.

2. virtual screening approach, in which several sized libraries of compounds are docked onto the LBS (Ligand Binding Site) in order to select the most promising. The libraries can be commercially available or built starting from the synthons of a synthetic accessible route.

2.2.2 Ligand-based Drug Design (LBDD)

If the three-dimensional structure of the protein is not available, the ligand-based drug design approach[75] is used in drug design. Basically, it consists of starting from the information obtained from known binders of the biological target of interest, in order to indentify novel modulators. The identification of a pharmacophore as a model is fundamental in this approach. Pharmacophore screening aims to identify compounds containing different scaffolds, but with a similar three-dimensional arrangement of key functional groups.[76] In light of this, 3D-QSAR (3D structure-activity relationship) and shape similarity are both important tools in the ligand-based drug design.

2.3 Methodologies employed

In the next sections, the computational methodologies applied in this research work are briefly described.

2.3.1 Molecular docking

One key methodology is the molecular docking that estimates conformation and orientation of molecules within a targeted binding site. Many different programs have been developed, of which DOCK,[77] FlexX,[78] GOLD 120[79] Autodock,[80, 81] Autodock Vina,[82] and Glide [83-87] are among the most popular. The mentioned tools are based on a range of different concepts, and each

comes with its own set of strengths and weaknesses. However, the placing of a flexible ligand into a rigid binding site is a feature common to most of docking software. The use of a rigid macromolecule in the docking calculations reduces the number of freedom degrees, as only conformational changes of docked compounds are considered.

Most molecular docking software has two key parts:

    1) a search algorithm

    2) a scoring function.[88, 89]

The highest efficiency of the calculation is reached if both these parts are accurate and fast, but speed and accuracy are often in opposition to each other.[90, 91]

2.3.1.1 Conformational search

The search algorithm is involved in the sampling of conformations and orientations of ligands in the binding site of the macromolecule. In light of this, it is possible to stress that the number of degrees of freedom of the docked small molecule influences the difficulty of this step. Three different categories of search methods can be identified: systematic methods, random or stochastic methods (Monte Carlo and genetic algorithms), and simulation methods (molecular dynamics, energy minimization).

In the systematic search algorithms, all the degrees of freedom in a molecule are explored, generating a considerable number of conformations.[92]

The random methods or stochastic methods perform random changes of a single ligand or a population of ligands. At each step, the variations of energy related to the modification of the dihedral angles are analyzed, and the

molecular space of the available conformations is explored. A pre-defined probability function is used for the examination of the obtained ligand.

Molecular dynamics (MD)[93, 94] is currently the most popular simulation method for the rationalization of the biological activity of macromolecules, calculating the time-dependent behavior of a molecular system. Detailed information about conformational changes of proteins and nucleic acids, and the nature and stability of binder-protein complexes can be provided by means of this computational tool, which plays now an important role in drug discovery.[95]

The determination of protein motions requires the description of quantum-mechanical motions and chemical reactions, that are too complex for even the best supercomputers. Molecular dynamics simulations were developed in the late 1970s[96] and they were able to overcome this limitation, as simple approximations based on Newtonian physics are used for the calculations. Position and moment of each particle belonging to a molecular system are important for the determination of the state of the system. In detail, 6 coordinates (3 for the position and 3 for the moment) for each particle occupy the so-called *phase space*. The initial instant is the minimized state of the molecule. Then, a moment with random direction is applied, whose intensity depends on the temperature of the system. The collection of a subsequent series of points in specific intervals of time provides a trajectory which is an estimation of the natural situation.

Since only local energy minima can be reached using energy minimization methods, the latter are rarely used in comparison with molecular dynamics methods.

2.3.1.2 Scoring function

After the conformational search by means of search algorithms, the scoring function evaluates the results predicting the affinity for the biological target. Several factors influence this function, such as enthalpic and entropic components, limited resolution of X-ray crystals, induced fit or other adopted conformational changes, the presence of water-bridge molecules in macromolecule–ligand interactions. It is possible to group the scoring functions in three categories: force field (FF),[97] empirical and knowledge-based.

In the force fields there is the contribution of two energetic components, the protein–ligand interaction energy and the internal ligand energy, as a single conformation of the protein is considered and the calculation of the internal protein energy can be omitted.

The sum of electrostatic and van der Waals terms, and the hydrogen bonds established between ligand and biological target contribute to the determination of the enthalpic value. The van der Waals potential energy for the general treatment of non-bonded interactions is often modeled by a Lennard–Jones 12–6 function (Equation 1):

$$E_{vdW}(r) = \sum_{j=1}^{N} \sum_{i=1}^{N} 4\varepsilon \left[\left(\frac{\sigma_{ij}}{r_{ij}} \right)^{12} - \left(\frac{\sigma_{ij}}{r_{ij}} \right)^{6} \right]$$

Equation 1

where ε is the well depth of the potential and σ is the collision diameter of the respective atoms i and j. The exp(12) is responsible for small-distance

repulsion, whereas the exp(6) is related to an attractive term which approaches zero as the distance between two atoms increases (Equation 2).

The Lennard–Jones 12–6 function is also used to describe the hydrogen bond in macromolecule-ligand complex, but is less smooth and angle dependent if compared to the Van der Waals function (Figure 6)

A) van der Waals   **B) H-bond**   **C) Electrostatic**

Energy — Distance (r_{ij})
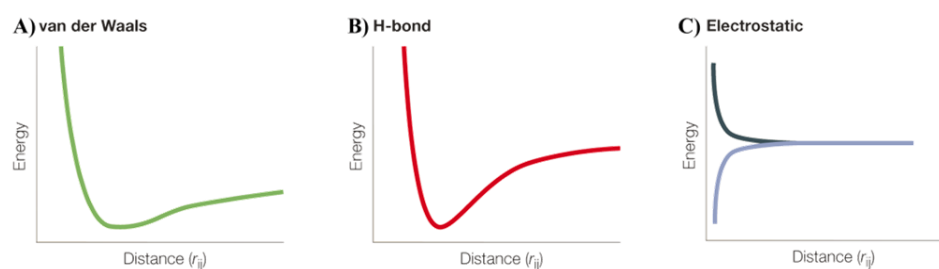
Figure 5 Schematic representation of functions used to model pair-wise interactions that contribute to binding. Interactions are calculated as a function of the distance (*rij*) between two atoms *i* and *j*. **A**) van der Waals interaction given by a 12–6 Lennard–Jones potential. **B**) hydrogen bond potential given by a 'harder' 12–10 Lennard–Jones potential. **C**) electrostatic potential for two like (blue) or opposite (black) charges of same magnitude calculated using a distance dependent dielectric constant.

The electrostatic potential energy is represented as the sum of Coulombic interactions, as described in equation 2:

$$E_{coul}(r) = \sum_{i=1}^{N_A} \sum_{j=1}^{N_B} \frac{q_i q_j}{4\pi\varepsilon_0 r_{ij}}$$

Equation 2

where N is the number of atoms in molecules A and B, respectively, and q the charge on each atom. The internal ligand energy is in general very similar

to the protein–ligand interaction energy. Its value, in fact, is given by van der Waals contributions and/or electrostatic terms.

The empirical scoring function considers the sum of a set of weighted empirical energy terms, (Van der Waals, hydrogen bonding and electrostatic energies, etc.):

$$\Delta G = \sum_i W_i \cdot \Delta G_i$$

Equation 3

where ΔG is the summation of the individual empirical energy terms multiplied by the corresponding coefficients, which are determined by reproducing the binding affinity data of a training set of protein-ligand complexes with known three-dimensional structures, using least squares fitting (some examples of empirical scoring functions are GlideScore, [83-87] LUDI,[98] LigScore[99]).

2.3.1.3 Glide: an overview

The named Glide[83-87] software was used in this research work for docking analysis. It searches for possible locations of the test compound in the active-site of the crystal structure of the protein, using a hierarchical set of filters (Figure 6). A grid determines shape and properties of the receptor, defined by a series of fields. A broad conformational search and a heuristic screen are both main actors in the removal of unsuitable conformations. Each ligand is divided into a core and rotamer groups, which are attached directly to the core and do not have further rotable bonds. Carbon and nitrogen with hydrogens

(CH$_3$, NH$_2$, NH$_3^+$), located at the end of a rotamer group are not considered rotatable. In the generation of conformers, core conformations are generated, generally fewer than 500. The number is related to the quantity of rotatable bonds, the presence of conformationally labile rings and asymmetric pyramidal trigonal nitrogen centers. The core and all possible conformations of rotamer groups are docked as a unique object.
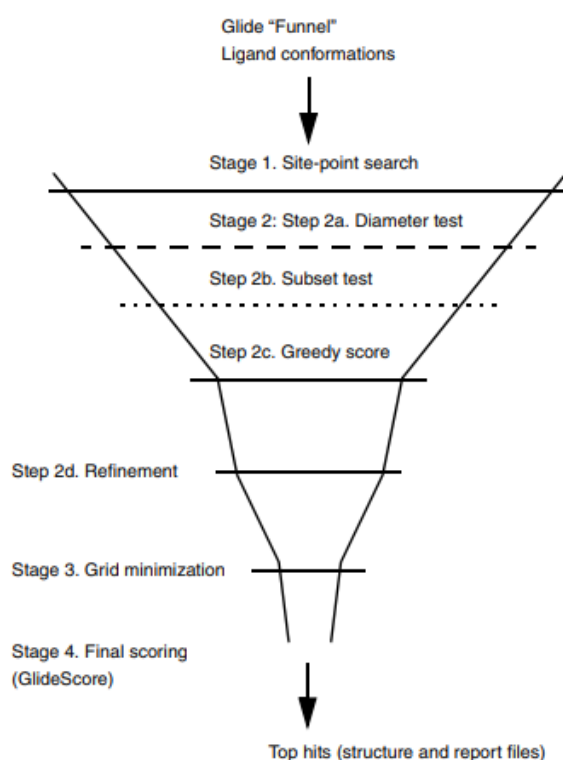
Figure 6 Glide docking hierarchy.

The research of the possible locations and orientations of each conformer is carried out following a set of stages. The first consists of the calculation of a site point of width 2 Å which covers the active site region. A calculation of the

distances from the site point to the receptor surface is performed, which are sorted into distance ranges of width 1 Å. The same way, the distances between the ligand center and the ligand surface are calculated and sorted as described. A comparison between the distance ranges from the site point to the receptor surface and those from the ligand center to the ligand surface is carried out. The selection is based on the evaluation of the match between the ligand center and the site point.

A second stage is divided in several steps. The diameter test (2a) focuses on the calculation of the distances between the most separated atoms inside the conformer (ligand diameter). The specific orientation is skipped if there are many steric clashes with the receptor. In the next step (2b), ligand diameter is considered rotatable and a first evaluation of the scoring deriving from the interactions of a subset of atoms able to establish hydrogen bonds or ligand-metal interactions with the receptor is carried out, and if the calculated value is good, all the interactions with the receptor counterpart are inclused in the score (2c). Schrödinger's ChemScore[100] empirical scoring function is involved in these three tests. It is an algorithm which recognizes favorable hydrophobic interactions, hydrogen bonds and metal-ligations, whereas penalizes steric clashes. In this case, score evaluation for each atom depends on its position onto the receptor, but also on the best possible score which it may present by changing its position ±1 Å in x, y or z (greedy scoring). The final step provides a re-scoring of the top poses deriving from the previous step using a refinement procedure, in which the test compound may move rigidly ±1 Å in *x*, *y* or *z*.

Only a few poses (100–400) enter the third stage, in which an energetic minimization is performed. A set of van der Waals and electrostatic grids were

smoothed in order to reduce the wide energy deriving from too-close interatomic contacts. Then, a sampling of the top-ranked poses is performed, in which local-minima core and the torsion angles of rotamer groups are evaluated, with the aim of improving the score.

A re-scoring of the minimized selected poses is the last stage. GlideScore[83-87] is the main actor of this phase. It is based on ChemScore, [100] but includes a series of other terms decribed in the equation 4.

$$GScore = 0.05 * vdW + 0.15 * Coul + Lipo + hbond + Metal + Rewards + ROTB + Site$$

Equation 4

where vdW and Coul are the van der Waals and coulomb energy respectively, Lipo, Hbond and Metal are the lipophilic, hydrogen-bonding and metal-binding terms. It also evaluates rewards and penalties, such as buried polar terms, hydrophobic enclosure terms, amide twist penalties. Emodel[83-87] is engaged in the final choice of the best poses for each ligand, and considers the energy grid score and the binding affinity provided by GlideScore. Herein, the docking score is calculated which includes GlideScore and Epik[101, 102] state penalties.

2.3.2 A flexible docking: Induced Fit Docking

A more detailed computational protocol for docking experiments is the Induced Fit Docking (IFD), [103-105] as the flexibility of the amino acids placed in the binding site of the protein is considered in the calculations. The classical molecular docking described above, in fact, consists of placing flexible ligands onto the rigid structure of the target. The binding of a molecule in the active

site of a protein induces conformational changes and resolving the X-ray structure of the complex protein-ligand is frequently infeasible. The IFD protocol is one of the most useful instrument to overcome this limitations. The workflow is composed by a job sequence in which ligands are docked with Glide (first step)[103-105], then Prime Refinement is used to allow the receptor to relax (second step),[105, 106] and the ligands are redocked onto the relaxed receptor with Glide (third step).

2.3.3 Ligand-based approach: Shape similarity

The evaluation of the shape similarity between designed molecules and known inhibitors of the biological target is another fundamental component for the generation of promising libraries.[107] The shape filter allows to take into account for the next steps only the structures showing a specific binding mode. Among different shape-based research software, Phase[108, 109] is one of the most famous for ligand-based design. The determination of the three-dimensional disposition of the functional groups of active compounds by analyzing the chemical properties that confer activity against the target is the tool that the approach is based on. Then, Phase searches for novel structures with a similar shape from an internal database that can be updated or modified. Overlapping two structures A and B, the volume occupied by both structures (VA∩B) is normalized by the total volume (VAUB) to obtain SimAB, whose value is from a minimum of 0.00 to a maximum of 1.00, according to the similarity grade (Equation 5).

$$SimAB = V \cap B/VA \cup B$$

Equation 5

As an alternative to atom-based methods, Phase represents a structure as a set

32

of pharmacophore sites that encode the positions of acceptor and donors hydrogen bonds, hydrophobic regions, positive and negative ionizable functions and aromatic rings. Another tool of Phase software is the Isosteric matching of the Core hopping software, useful for the research of bioisosters of a specific chemical item.[108, 109]

2.3.4 Calculation of pharmacokinetic parameters and filters application

Pharmacokinetic parameters have fundamental importance to evaluate if a molecule is a right candidate to become a drug, or if its properties are not appropriated to consider it in the development of new hit compounds. With a prediction of these properties, it is possible to select exclusively drug-like compounds by discarding the remaining compounds from the calculation.

In this field, the hydrophobic/hydrophilic balance in a compound influences its intestinal adsorption, or the distribution in the several compartments of the organism, the metabolism (higher hydrophobic properties make more difficult the metabolic processes) and the elimination.

QikProp[110, 111] is a module of Schrödinger LLC for the prediction of ADME (adsorption, distribution, metabolism, elimination) properties of molecules (e.g. belonging to a combinatorial library obtained with CombiGlide[112, 113], described above) applying filters that eliminate the compounds unable to comply with some important rules and parameters. With the *in silico* prediction, it is possible to exclude not-drug-like molecules before the synthesis, reducing the time and the costs needed.

QikProp[110, 111] uses similarity in property space to increase the accuracy of the predictions of the ADME parameters, comparing each molecule to a

database of known drugs. The similarity can be from a value of 0.0 (no similarity) to a value of 1.0 (maximum similarity).

The software considers three cases:

1. A similarity less than 0.9: the QikProp prediction is used.
2. A similarity greater than or equal to 0.9: the predicted property (P_{pred}) is:

$$Ppred = SPexp + (1 - S)PQP$$

Equation 6

where S is similarity, P_{exp} the experimental prediction, P_{QP} the QikProp prediction.

3. A similarity of 1.0: the software reports the experimental value.

In addition, it takes into account 30 different reactive functional groups, which could be responsible for false positives in *high throughput screening* (HTS) assays, instability and toxicity of the molecules.

In the calculation of the pharmacokinetic parameters, the rule of Lipinski (also called the rule of 5)[114] is one of the most important in order to estimate the adsorption of valid candidates. The researcher Christopher Lipinski in 1997[66] defined this rule according to which a molecule must:

- not have a molecular weight higher than 500 (MW <500);
- have no more than 5 hydrogen bond donors;
- have no more than 10 hydrogen bond acceptors;
- have a logP less than 5 (logP< 5);

There are extensions of the Rule of 5^{115} such as the "Rule of 3", used for the construction of fragment libraries for lead generation.[116] These are generalized rules for assessing drug-likeliness and bioavailability of compounds.

QikProp[110, 111] can perform the calculation in two different modes: normal and fast (*fast mode*). The fast mode calculates fewer properties, in particular omits the *PM3 calculation*, which determines the dipolar moment, the ionization potential and the electron affinity, and is particularly suitable when a large number of molecules is available.

Some of the properties calculated by the software are:

➢ QPlogBB, an index of the permeability of the blood-brain barrier (BEE);

➢ QPlogPo/w, the octanol / water partition coefficient;

➢ QPlogS, predicted aqueous solubility;

➢ QPPC which indicates the permeability through the Caco-2 cells, as a model of human intestinal barrier;

➢ QPPMDCK indicates permeability through MDCK cells; QikProp predictions consider non-active transport;

➢ QPlogHERG, predicts IC_{50} value for blockage of HERG K^+ channels;

➢ RtvFG, the number of reactive functional groups;

➢ SASA, the surface accessible to the solvent, expressed in Angstrom (Å);

➢ FISA, a hydrophilic component of the solvent-accessible surface area (SASA) on N, O, H bound to hetero-atoms and carbonyl C;

> ➤ HumanOralAbsorption, predicts human oral absorption, with values 1 (low), 2 (medium) and 3 (high), which can also be expressed as a percentage.

At the end of the calculation, only drug-like molecules are selected from the previous libraries resulting from Combiglide.[112, 113]

Then**,** LigFilter[117, 118] is applied. This is a function of Maestro[117, 118] through which you can set precise values for pharmacokinetic parameters and filter the libraries basing on these (for example molecular weight, logS, logP, FISA).

2.4 Application of combinatorial chemistry to computational chemistry

Combinatorial chemistry techniques have made possible the synthesis of large libraries of compounds and revolutionized the process involved in the discovery of new bioactive compounds.[119]

The assumption that maximizing structural diversity would increase the chances of finding new hits has led to the design of libraries characterized by different compounds. However, in the design of a library other factors have to be considered, such as chemical-physical properties of molecules, costs, availability of reagents and synthetic accessibility. The techniques developed for the design of combinatorial libraries can be divided into *reagent-based*[120] and *product-based.*[121]

Reagent-based. This approach does not provide the use of a scaffold, but it starts from the available reagents, which are synthons of a synthetic strategy, and applies *selection algorithms* based on the calculation of their chemical-

physical diversity in order to obtain the most representative molecules of all the possible synthesizable compounds.[120]

Product-based. Generally, it is used for the development of scaffolds. It consists of the use of a genetic algorithm (GA) which starts from a set of several scaffolds and alters atoms and molecular fragments in order to generate molecules that adapt to the indicated constraints. This algorithm can generate and optimize a large number of hits, taking into account weight and molecular volume, number of stereogenic centers, number and type of bonds, and other parameters.[121] Combinatorial chemistry Lab (CCLab)[122] is one of the software which uses this algorithm.

2.4.1 Reagent Preparation

Reagent Preparation is a function which provides the preparation of several fragments for the decoration of the *core*. It works by the generation of SMARTS (representation of chemical structures through text string), and defines precisely the fragment and the functional group that will be removed with Combiglide (Schrödinger, LLC) [112, 113] in the next step, to perform the connection to the core. Using the SMARTs it is possible to determine the breaking point of the collection of reagents, indicating the atom of the molecule that has to be preserved (rpc1) and the one that has to be removed (rpc2) (Figure 7).
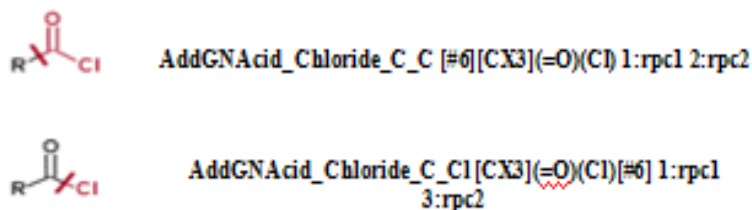
Figure 7 Commercially available compound and correspondents SMARTs for the two possible fragments.

2.4.2 Combiglide and generation of libraries

CombiGlide[112, 113] allows the choice of the specific points on the scaffold for the addition of the prepared fragments, applying the interactive enumeration function. It works following a combinatorial chemistry approach to obtain all the possible combinations of the different reagents with the core, starting from the synthons of a selected synthetic strategy. The links scaffold-fragments are not necessarily the bonds that are cleaved in the real chemical reactions, taking into account that Combiglide considers the final product synthetizable using the selected synthetic strategy, and generates all the possible final compounds. Then, this is an important tool for the design of very large libraries of molecules, all the possible compounds starting from all the commercially available reagents, synthons of the synthetic route. Anyway it is not possible to synthesize all the designed compounds, but with the use of appropriate filters the most synthetically accessible molecules can be selected.

Finally, LigPrep (Schrödinger, LLC) [123, 124] software performs:

1. energetic minimization of the whole library using *Optimized Potentials for Liquid Simulations* (OPLS) *2005 force field,*[125] considering all the energetic components.

2. preparation of each compound, by the calculation of the stereoisomers, the tautomeric and ionization states, and the determination of three-dimensional ring conformations at physiological pH.

3. Application of rules to eliminate possible mistakes in the structures of the molecules.

The described computational methodologies and approaches were widely applied in multi-step protocols adopted in this thesis, for the identification of new potent hits on the protein targets. A detailed description is reported in the next chapters.

-RESULTS AND DISCUSSION-

-CHAPTER 3-

Discovery of new inhibitors of

microsomal Prostaglandin E_2

Synthase

3.1 Microsomal Prostaglandin E$_2$ Synthase (mPGES-1)

Prostagrandin E$_2$ Synthases (mPGES-1, mPGES-2, cPGES) are enzymes involved in the inflammatory response, since catalyze downstream the conversion of prostaglandin H$_2$ (PGH$_2$) in its isomer prostaglandin E$_2$ (PGE$_2$) (Figure 8), as described in the introduction of this thesis. Microsomal PGES-1 is ubiquitous, but its concentration is up-regulated after exposure to various inflammatory stimuli and mediators, for example, cytokines (LPS, IL-1β and TNF-α).[126] Different studies reported by Jackobsson *et al.*[127] demonstrated its belonging to the superfamily of membrane-associated proteins involved in eicosanoid and glutathione metabolism (MAPEG),[128] together with 5-lipoxygenase-activating protein (FLAP), leukotriene C4 synthase (LTC4S) and microsomal glutathione transferases (MGST1, MGST2, MGST3).[129]
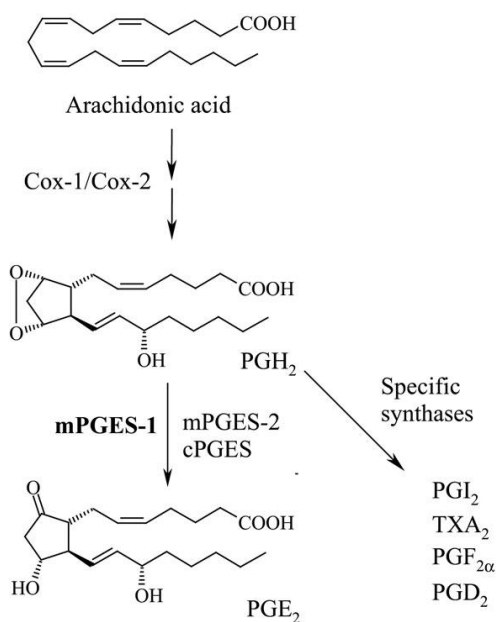
Figure 8 mPGES-1 in the inflammatory cascade.

42

3.1.1 Structure, Catalytic Mechanism and Binding Site

The first structure was reported in 2008 by 3D-electron crystallography at low resolution,[130] and Sjögren *et al* reported in 2013 the high resolution (1.16 Å) X-ray crystal of mPGES-1 in the active conformation, in complex with its cofactor glutathione.[131] Structurally, it is a membrane protein of 16 kDa with a total number of 153 amino acids in mouse and rat, and 152 amino acids in human because of the absence of the 11th amino acid. The tridimensional disposition of the enzyme consists of a homotrimer in the endoplasmic reticulum membrane, and each monomer is organized in four helices, named TM1, TM2, TM3 and TM4. Three equivalent active sites are placed in the three monomers, within the membrane-spanning region at each monomer interface. Each active site is oriented towards the cytoplasmic part of the protein, between the N-terminal parts of TM2 and TM4 of one monomer and the C-terminal part of TM1 and the cytoplasmic domain of the next monomer (Figure 9). [131]
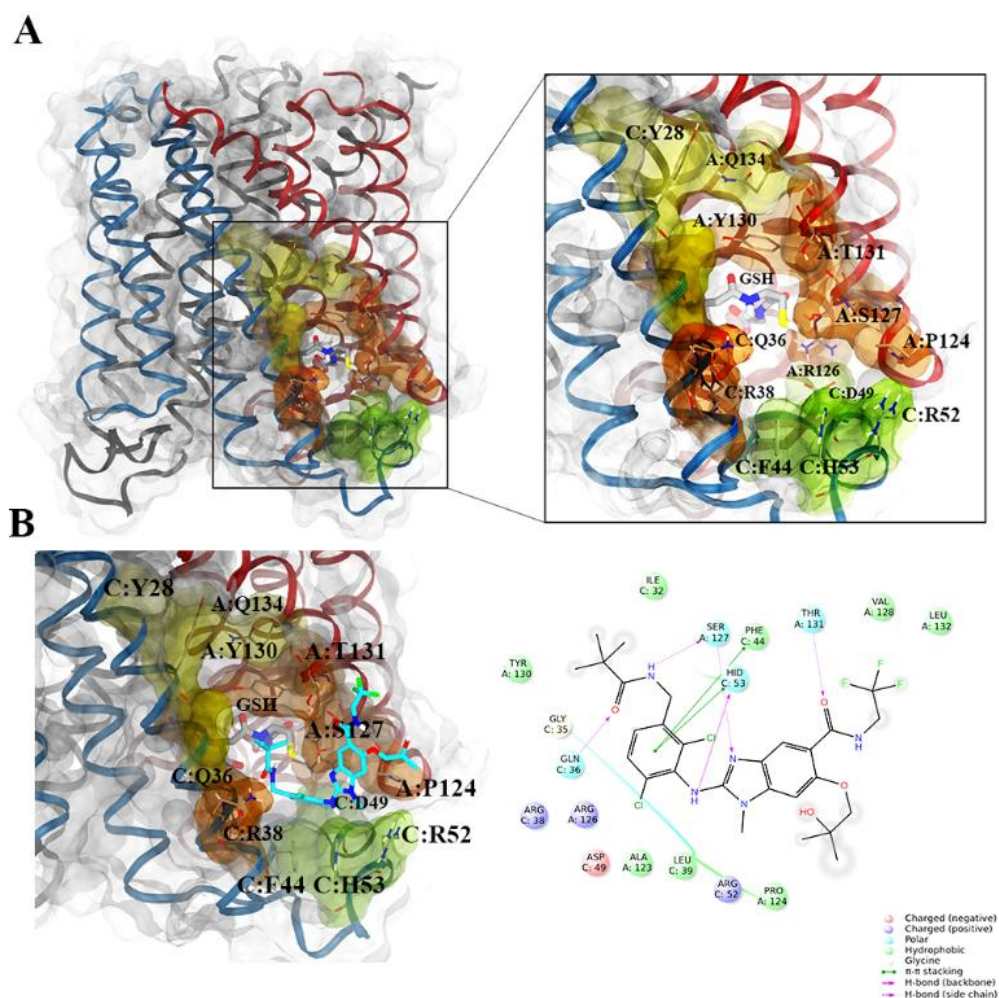
Figure 9 A) on the left, transparent molecular surface representation of mPGES-1, with chains A, B and C depicted in red, black, and blue ribbons, respectively; on the right, representation of the mPGES-1 binding site with the co-factor (GSH). **B)** on the left, mPGES-1 co-complexed with LVJ inhibitor (PDB code: 4BPM, LVJ represented in sticks, C cyan, O red, N blue, polar H white, Cl green, F light green); on the right, 2D representation of LVJ and interactions with the residues in mPGES-1 binding site.

According to Jegerschöld et al.,[130] mPGES-1 has to perform a change from the closed to the open conformation in order to allow access of PGH_2 to the

active site. In the last few years, the tridimensional X-ray structures of the enzyme have been crystallized in the open conformation. The investigation of the involvement of GSH cofactor in the catalytic mechanism by the replacing of cysteine residue by a serine residue in GSH molecule, confirmed the fundamental role of the thiol moiety in the conversion of PGH_2 in PGE_2.[132] The access of inhibitors is blocked by the so-called "gate keepers" (Thr131, Leu135 and Ala138, probably Arg52 and His53 too). Regarding Ser127 residue, it was considered able to activate the thiol moiety of the cofactor for starting the catalytic cycle, but recent studies including a combination of site-directed mutagenesis (Ser 127 has been replaced by an Alanine) and activity assays with a structural dynamics analysis, demonstrated Ser127 is not essential for catalysis.[132] Conversely, similar investigations corroborated the crucial role of Arg126 and Asp49 in the catalysis. In details, the interaction between the positively charged Arginine and the negatively charged Aspartate is the key of the whole mechanism (Figure 10). Also, analysis of the active site showed that a water molecule forms a hydrogen-bonding network between the α-carboxylate and the thiol moiety of GSH, inducing the deprotonation of the latter and the formation of the thiolate which is stabilized by interaction with the guanidine moiety of Arg126. Two different mechanisms have been proposed (Figure 10):

A. The thiolate attacks upon endoperoxide ring at the C-9 position, the O-O bond is cleaved, and S-O bond is formed. Simultaneously, Asp49 reduces the pKa of the C-9 proton, and this leads spontaneously to the yield of the PGE_2 isomer.

B. The thiolate as a base removes the C-9 proton, inducing the cleavage of the unstable O-O bond and the formation of the product.
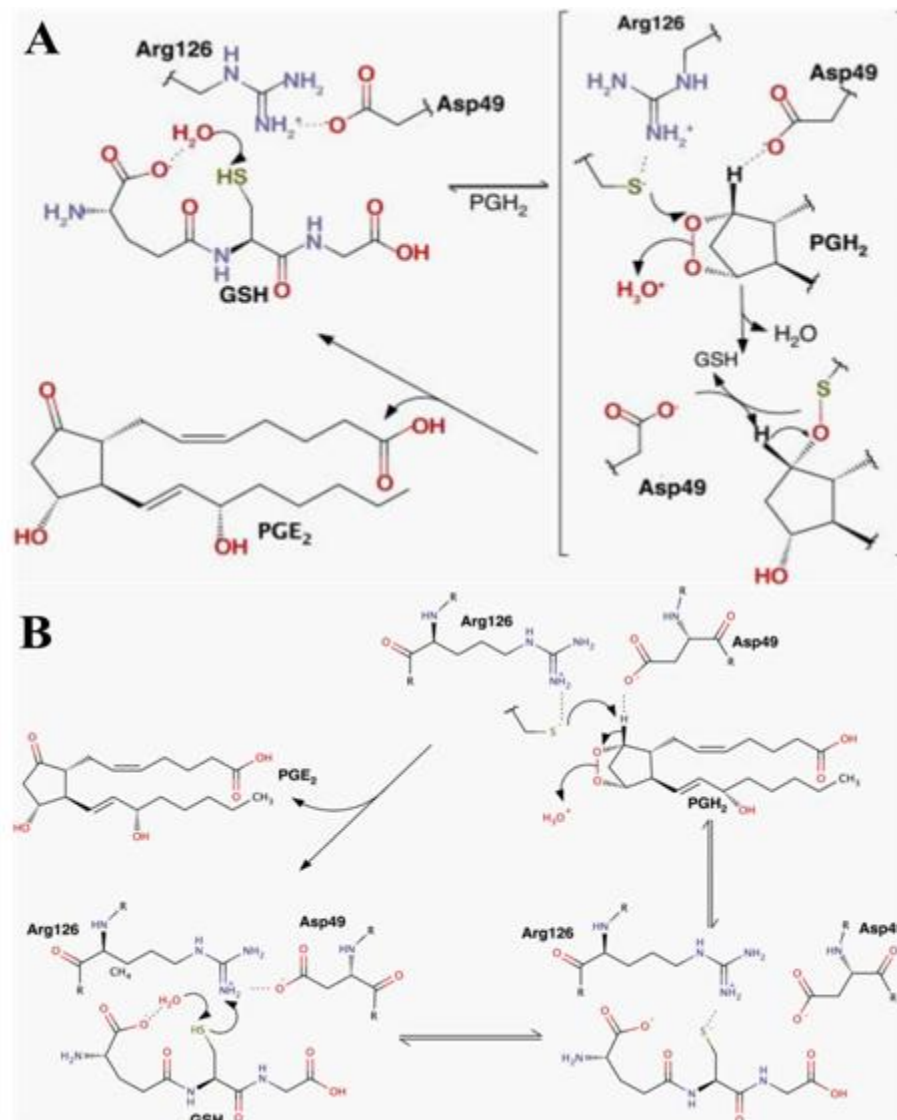
Figure 10 A) Proposed mechanism of mPGES-1; **B)** Alternative mechanism of mPGES-1.[132]

From a meticulous analysis of the binding site of the enzyme moving from the cytoplasmic to the opposite part of the membrane, three sub-regions including hydrophobic/polar residues have been identified:

46

1. a groove between the GSH binding site and a region close to the cytoplasmic part (colored in green, Figure 9). Herein, mPGES-1 known binders (co-crystallized LVJ, 4DV, 4DZ, 4U8, 4U9)[133] establish π-π contacts with aromatic residues, such as $Phe44_{chain C}$, $His53_{chain C}$. Polar interactions with $Arg52_{chain C}$ and $Asp49_{chain C}$ residues (the latter essential for mPGES-1 catalysis) located in this region, take part in the set of the key interactions with the enzyme.

2. the cofactor binding region (colored in orange, Figure 9). In detail, the U-shape conformation of GSH stemmed from the interactions between its two terminal carboxylic functions and the positively charged residues Arg38 and Arg73 of chain C. Also, in this part of the protein is placed the Ser127 of chain A mentioned above.

3. a binding groove between TM1 of chain C and TM4 of chain A (colored in yellow, Figure 9), with polar ($Gln134_{ChainA}$), aliphatic ($Val24_{ChainC}$) and aromatic residues ($Tyr28_{ChainC}$ and $Tyr130_{ChainA}$).

3.1.2 mPGES-1 inhibitors

Considering the importance of the above described enzyme in the individuation of novel selective anti-inflammatory and anti-cancer drugs, several mPGES-1 inhibitors have been discovered and developed in the last years as result of long and difficult research works. Among these, only two inhibitors entered the clinical trials and none is in the market.

Endogenous fatty acids (arachidonic acids, docosahexaenoic acid) and eicosanoids (leukotriene C4, PGJ_2 and 15-deoxy-Δ12, 14-PGJ_2) demonstrated in some studies the ability of weakly inhibit the activity of the enzyme,[134] but the first synthetic inhibitor was the indole derivative **MK-886** (Figure 11)

47

which has been discovered earlier as a FLAP inhibitor with an IC_{50} value of 2.5 nM.[135] Instead, the IC_{50} value presented in the cell-free assay on mPGES-1 was higher (1.6 μM).[136] Also, **MK-866** inhibitor showed low activity in the whole blood assay and is able to interfere with the activity of COX-2 at higher concentration (8 μM). The **MK-866** synthesized derivatives are more potent and selective than the starting compound. For example, the analogue reported in figure 10 showed an IC_{50} of 3 nM in the cell-free assay on mPGES-1, and a 100-fold selectivity over mPGES-2, thromboxane synthase and FLAP.[136]
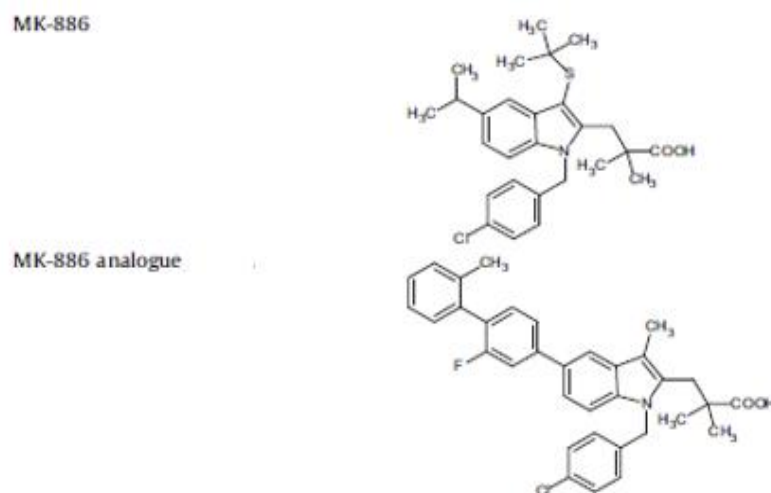
Figure 11 MK-866 inhibitor and its analogue.[136]

A chemical class of developed mPGES-1 inhibitors includes Phenanthrene imidazoles, characterized by a 2,6-dicyano-substituted phenyl ring at position 2 of the imidazole. In detail, three inhibitors have been developed, presenting low values of IC_{50}. Compound **MF-63** (Figure 12) showed an IC_{50} of 0.42 μM in the A549 whole cell assay in the presence of 50% fetal bovine serum, and

an IC_{50} of 1.3 μM in human whole blood assay. Also, **MF-63** inhibited the human mPGES-1 (IC_{50}=1.3 nM) and presented a 1000-fold selectivity over mPGES-2, PGI_2, PGD_2 and TX synthases, and a similar selectivity was tested against COX-1, COX-2, 5-lipoxygenase (5-LO). It is also able to strongly inhibit guinea pig mPGES-1 (IC_{50}=0.9 nM).[137] Other inhibitors are 2,4 biarylimidazoles (Figure 12, compound **I**) and trisubstituted ureas (Figure 12, compound **II**) that presented low IC_{50} value in both cell-free and whole blood assay. Compound **AF3485** (Figure 12) is a benzoyl derivative of 3-aminocarbazole. It showed promising value of IC_{50} in the *in vitro* assays versus human mPGES-1 expressed in bacterial membrane and microsomal PGES-1 in A549 cells, results confirmed by the cell-based assay. In the *in vivo* experimentation, its ability to contrast inflammatory pain in a dose-dependent manner in mice was demonstrated, and it presented high value of absorption by the intestinal barrier and high bioavailability. It is also able to reduce the level of PGE_2 in A431 epithelial tumor cells, but the antitumor activity of this compound could be related to the inhibition of EGFR signaling.[138] Furthermore, the investigation of the activity of three imidazopyridine carboxamides led to the selection of compound **III** (Figure 12) as a very promising inhibitor, presenting an IC_{50} of 1 nM in the cell-free assay. Another important class of inhibitors consists of 2-arylamino benzimidazoles. This broad class of inhibitors includes a high diversity of the arylamino moiety. Unsuccessful, it was demonstrated that the compounds selected in the first step presented different results in the enzyme and cell-based assays, showing different potencies in the two tests. Thus, biological evaluation of another class of benzimidazole derivatives was carried out in 2012, and the most efficient inhibitors for mPGES-1 were discovered. The investigation of

49

derivatives bearing the 2,4-dichlorobenzyl pivalamide group (Figure 12, compounds **IV** and **V**) seems to have provided compounds presenting an IC_{50} of 1 nM in the enzyme assay and IC_{50} less than 1 nM in the A549 cell-based assay. A further modification was the removal of the carboxamide residues of the benzimidazole ring, which afforded compound **VI** as an efficient mPGES-1 inhibitor, showing an IC_{50} value of 1.3 nM.

Considering another class of inhibitors, the introduction of the imidazole moiety on benzamides derivatives provided molecules with higher efficiency in the inhibition of the enzyme, as confirmed from different performed biological assays. Among these, compound **VII** (IC_{50}=12 nM in *ex vivo* human whole blood assay) was submitted to the monoiodoacetate (MIA) *in vivo* model for knee pain in comparison with diclofenac, and both significantly reduced pain in a dose-dependent manner. It also presented absorption, distribution, metabolism and excretion properties and **VII**·H_3PO_4 was defined as proper for clinical development. Compound **PF-4693627**, a benzoxazole piperidine carboxamide, exhibited an IC_{50} value of 3nM in the cell-free assay and of 109 nM in the whole blood assay. This compound has been advanced in clinical studies for the treatment of rheumatoid arthritis and osteoarthritis.[139] Another interesting compound is the methyl-piperidine **VIII** in Figure 12, (IC_{50}=1.93 nM in the cell-free assay, IC_{50}=2 nM in human whole blood assay, IC_{50}=4.71 nM in the cell-based assay). [140]

Bis-sulfonylamino derivatives were also developed for the target. In particular, compound **IX** showed promising results in the enzyme assay (IC_{50}=3.2 nM)[141]
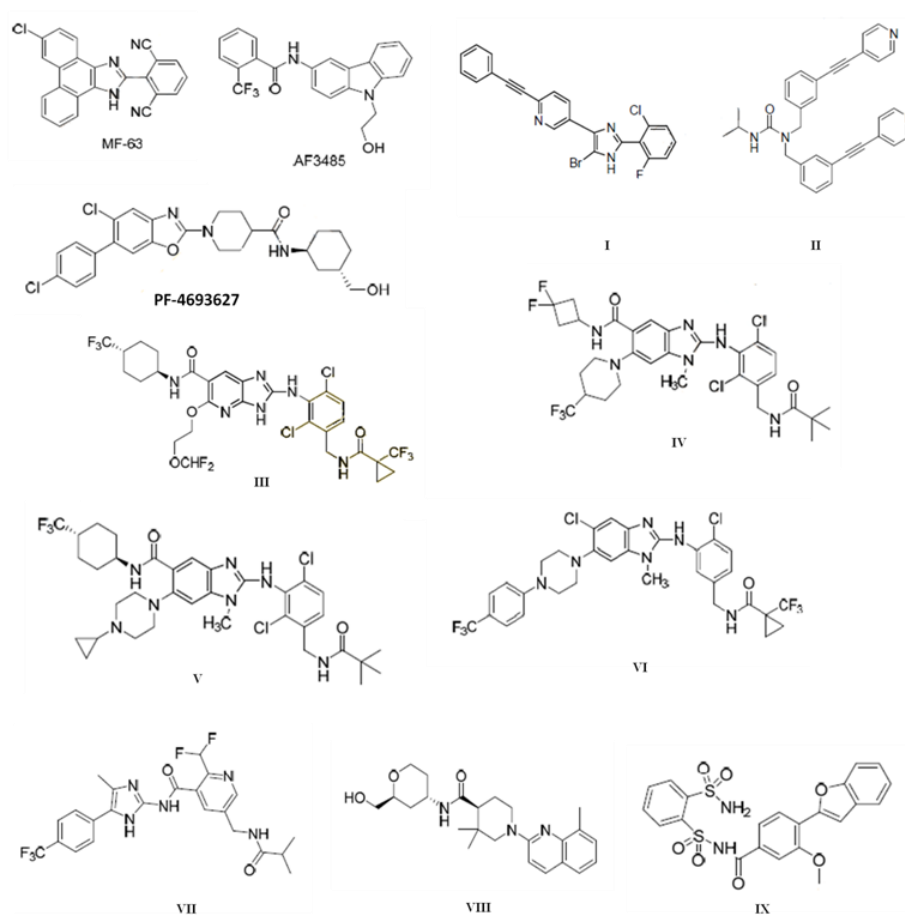
Figure 12 Known mPGES-1 inhibitors.

Also, it is necessary to mention compound **CAY10526** (Figure13), since it was used as a control in some biological assays performed on compounds developed in this thesis. It inhibits PGE_2 production through the selective modulation of mPGES1 expression, but it does not affect COX-2.[142]
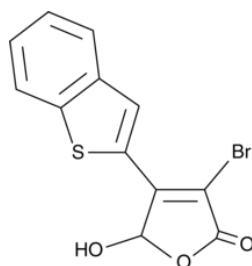
Figure 13 CAY10526 inhibitor.

To date, two different compounds entered the clinical trials:

1. **GRC27864** (Figure 14) was developed by Glenmark and belongs to the substituted pyrimidine chemical class. It showed an IC_{50} value of 5 nM in the cell-free assay and 376 nM in human whole blood assay, and was able to interfere with the production of PGE_2 in synovial fibroblasts and chondrocytes deriving from tissues affected by rheumatoid arthritis and osteoarthritis. Other biological assay demonstrated that it is also a potent inhibitor of recombinant guinea pig mPGES-1 enzyme (IC_{50}=12 nM) and 1000-fold selective over COX-1, COX-2, mPGES-2, cPGES, PGI2, PGD_2 and TXA_2 synthases and did not inhibit cytosolic phospholipase A2 (cPLA2).[143] It showed safety and no side effects in Phase 1 of the clinical trials, and is currently in phase 2.

2. **LY3023703**, developed by Lilly, whose structure has not yet been disclosed. A group of 48 patients took part in the experimentation of the efficacy of the compound. In detail, mPGES-1 inhibitor, celecoxib (400 mg) or a placebo once a day for 28 days were administered. From the results, **LY3023703** is more potent than

celecoxib in the inhibition activity of the enzyme. The identified side effects were diarrhoea, abdominal pain, and one of the patients reported an increase of the level of aminotransferase, which is index of liver toxicity.[144]
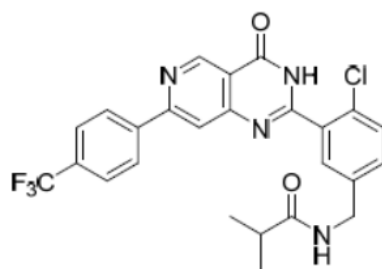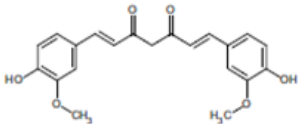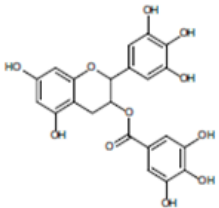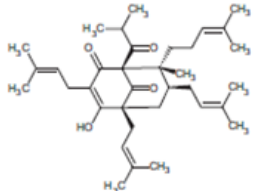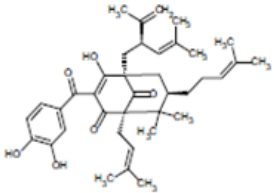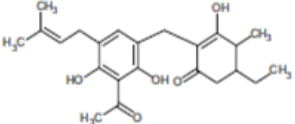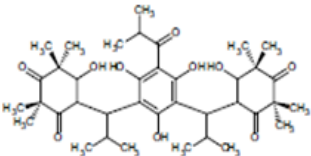
Figure 14 GRC27864 mPGES-1 inhibitor.

In this section only the most significant mPGES-1 synthetic inhibitors are reported.

Regarding natural products (NPs), several compounds obtained from different plant species are able to inhibit the activity of mPGES-1. The suppression of PGE_2 synthesis was observed in both cell-free and whole cell assay, with IC_{50} values close to low micromolar concentrations. Most of the reported natural mPGES-1 inhibitors also interfere with the activity of 5-LO at similar concentrations, confirming no selectivity for the enzyme. [145-148]

Substance	Chemical structure	IC$_{50}$ (mPGES-1) cell-free	IC$_{50}$ (PGE$_2$) cell-based	PGE$_2$ reduction in vivo
Curcumin (*Curcuma longa*; turmeric)		0.3 μM	15 μM	n.d.
Epigallocatechin-3-gallate (*Camellia sinensis*; green tea)		1.8 μM	≥30 μM	n.d.
Hyperforin (*Hypericum perforatum*; John's wort)		1 μM	3 μM	Yes (rat pleurisy)
Garcinol (*Garcinia indica*)		0.3 μM	10 μM approx. 30 μM	n.d.
Arzanol (*Helichrysum italicum*)		0.4 μM	9 μM 30 μM	Yes (rat pleurisy)
Myrtucommulone A (*Myrtus communis*)		1 μM	30 μM	n.d.
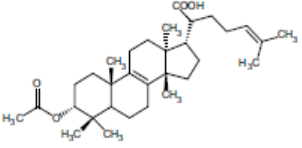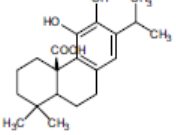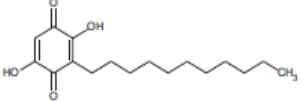
54

Substance	Chemical structure	IC$_{50}$ (mPGES-1) cell-free	IC$_{50}$ (PGE$_2$) cell-based	PGE$_2$ reduction in vivo
3α-Acetoxy-8,24-diene-tirucallic acid (*Boswellia* spec.)		0.4 μM	n.d.	n.d.
Carnosic acid (*Salvia officinalis*)		5 μM	9.3 μM	n.d.
Embelin (*Embelia ribes*)		0.2 μM	n.d.	n.d.

Table 2 Natural inhibitors of mPGES-1.[145-148]

3.2 The importance of the research of new mPGES-1 inhibitors

The discovery of inhibitors of mPGES-1 is even more aimed, since its inhibition could be a new promising strategy for the treatment of inflammation in order to avoid the side effects connected to NSAIDs. Furthermore, the relevance of mPGES-1 in pathological conditions such as pain,[149, 150] rheumatoid arthritis,[151] cardiovascular diseases,[152] fever[153] and cancer,[154] is noteworthy. Considering its over-expression in a large number of tumors, it is involved in the progression of brain cancers,[155] gastrointestinal cancers,[156] breast cancer,[157] thyroid cancer,[158] and several cancers derived from epithelium (lungs,[159] cervix,[160] ovary,[161] etc.). For example, an important

evidence of the involvement of mPGES-1 in cancer progression is its up-regulation correlated with prognosis in late stages in colorectal cancer.[162]

Moreover, a crucial point is the disclosing of selective inhibitors. Some binders, in fact, are endowed with a dual activity on both mPGES-1 and 5-lipoxygenase (5-LO), the latter involved in the synthesis of leukotrienes. Also, quite few inhibitors present activity on other prostanoid synthases, such as mPGES-2, PGI_2, PGD_2 and TX synthases, or are able to interact and modulate the activity of COX-1 and COX-2. However, the dual activity on mPGES-1 and 5-LO has been considered an innovative and effective strategy for the treatment of inflammation in the last few years.[163, 164]

In the research group where this research work has been mostly carried out, several derivatives able to strongly inhibit the activity of the enzyme have been developed using computational chemistry techniques, whose grade of promiscuity demonstrates the key role of exploring different chemical items in order to increase the possibility of discovering new important hits (Figure 15).
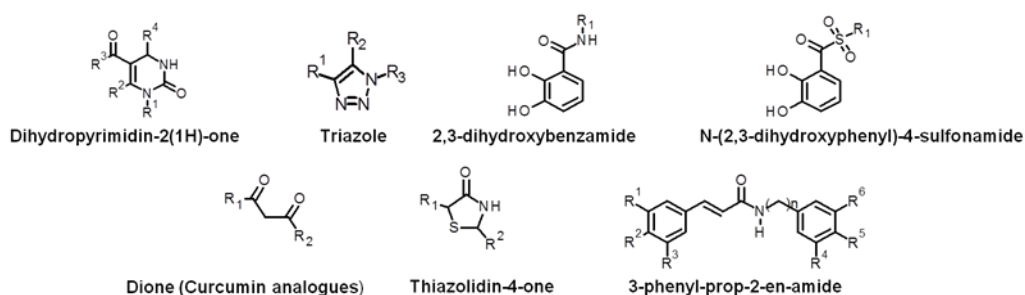
Figure 15 Examples of scaffolds of derivatives developed in the research group using computational chemistry techniques and virtual screening.[164-166]

56

3.3 General workflow of the project and additional procedures

The main part of the project is focused on a general workflow (Figure 16) which includes:

1. The choice of a synthetic strategy, whose building blocks are used as a starting point for the *in silico* design of new large libraries of molecules, following a combinatorial chemistry approach. Afterwards, a multi-step computational protocol is applied to the generated libraries for the selection of the most promising according to the virtual docking studies on the protein target (phase 1).

2. Synthesis of the molecules applying the selected synthetic route and purification of the crude by flash chromatography, HPLC (high performance liquid chromatography) and crystallization techniques; characterization of the synthesized molecules by nuclear magnetic resonance techniques, such as ^{1}H NMR, ^{13}C NMR, COSY experiments and by ESI-HRMS (high resolution electrospray ionization mass) and LC-MS (Liquid Chromatography Mass Spectrometry) (phase 2).

3. Biological assays on the targets and cell line tests for the experimental evaluation and quantification of the activity of the synthesized molecules. If the compounds are able to interfere with the functions of the protein target, they are the starting point for an optimization step, with the goal of improving their pharmacokinetic properties or their performance in the modulation of the activity of the protein. This may include a second application of the multi-step

57

computational protocol using a combinatorial or a 3D-QSAR (three-dimensional quantitative structure-activity relationships) approach[167] for the generation of analogues of the new disclosed hits. Instead, if the results show an inability to inhibit the activity or a very low inhibition, the protocol foresees a ''recycling'' (namely a repurposing) of the synthesized compounds. A computational technique named *Inverse Virtual Screening*, [168] developed in the last years in the research group in which the whole research project was carried out, is very useful for the individuation of a specific target in a panel of targets. Briefly, *Inverse Virtual Screening*[168] is an inverse screening in which a molecule or a small set of molecules are docked versus a panel of proteins involved in the development of cancer and inflammation. Thus, this approach is the opposite of the *direct virtual screening* in which a large library of compounds is docked onto the crystal structure of a unique macromolecule.
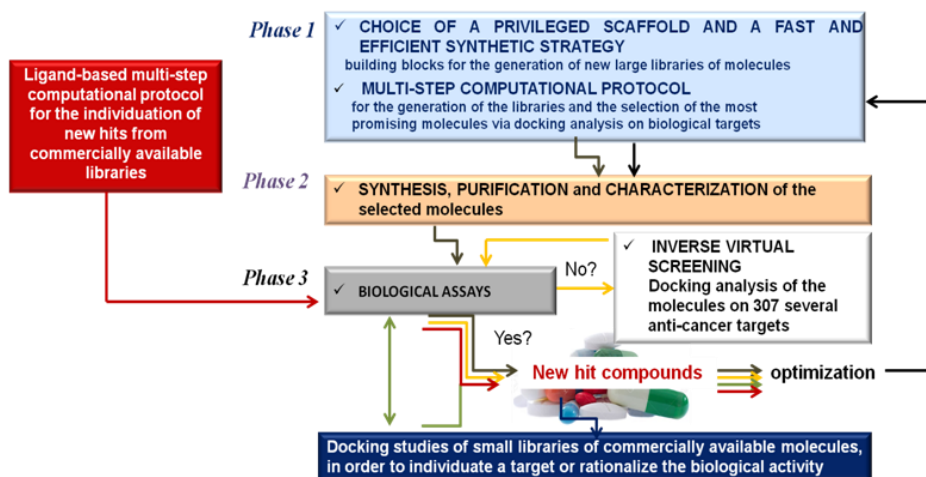
Figure 16 General Workflow.

58

Also, the workflow consists of the application of other specific multi-step computational protocols on large libraries of commercially available compounds in order to individuate interesting novel scaffolds involved in the inhibition of the enzyme (Figure 16, red box). A detailed example is reported in chapter 4 of this thesis.

Finally, an important place in the computational developed studies was occupied by docking analysis of small libraries of commercially available compounds on the biological target (Figure 16, blue box) in order to rationalize the activity presented in biological assays (chapter 5). Also in this case, the research work continued with an optimization campaign on the disclosed novel biologically active compounds, as described previously.

The reason for defining "additional procedures" the last two points (red and blue boxes) is not related to the importance of the discovery. This preference in the classification derives from a distinction between the main scheme which most of the research project was based on, and these second activities that gave very interesting results.

3.3.1 Selection of the scaffold

The design of new compounds potentially able to inhibit the activity of microsomal prostaglandin E_2 synthase as a new promising anti-inflammatory and anti-tumor drugs started with the selection of "privileged scaffolds". This definition was described by Evans in 1998 and indicates specific building blocks consisting of different ring systems (either heterocyclic or not, saturated or aromatic) as a source for an appropriate functionalization and

production of molecules targeting a broad variety of receptors, and that perform different biological activities.[164]

A previous knowledge of existent modulators reported in literature and a detailed study of their pharmacodynamic and key interactions with the receptor counterpart are essential in the choice of new scaffolds as a starting point for the individuation of new hits.

Since the large number of compounds targeting mPGES-1 developed so far is characterized by structural and pharmacokinetic properties with an extensive variability, this research project aimed to approach different categories of scaffolds to evaluate their ability to inhibit the activity of the protein. Also, this approach was employed to expand the probability to discover hits with a considerably increased activity in comparison to known inhibitors. According to the importance of heterocyclic compounds in medicinal chemistry in the last few decades, several heterocyclic cores have been considered.[169]

3.3.2 Selection of the chemical route

A study of the possible chemical routes for each scaffold was useful to select a very efficient and fast method for the synthesis of the final selected compounds and to individuate the commercially available synthons for the design phase. At this point, it is important to emphasize that the choice of the methods for the synthesis and the generation of libraries of molecules are strongly connected since the synthons of the synthetic strategy are the building blocks of each designed compound.

3.3.3 Multi-step computational protocol

Before starting the discussion concerning the obtained results, it is appropriate to introduce the adopted computational protocol which the main

part of the developed research project was based on. The aforementioned combinatorial computational approach allows the design of a large number of potentially biologically active compounds with a substantially lower time needed in comparison to the classical QSAR methods. However, a QSAR approach is also suitable in the optimization phase, in order to improve the biological activity of the new discovered hit compounds (see section 3.3).

The applied computational method is represented in figure 17, and is based on a sequence of techniques described above (see chapter 2). In detail, two phases can be distinguished:

1) Selection of the scaffold and generation of new libraries of molecules containing drug-like compounds. Combiglide[112, 113] was used for the generation of all the possible compounds deriving from the combination of the commercially available reagents with the core, according to the selected synthetic route. LigPrep[123, 124] includes all protonated states at physiological pH, tautomers and stereoisomers. Regarding QikProp,[110, 111] it was applied for the prediction of pharmacokinetic parameters, such as evaluation of Lipinski rule, logP, permeability through Caco-2 cell lines, toxicity against HERG K^+ channel, permeability through the blood-brain barrier (BEE), in order to modify the number of all the possible synthesizable compounds to a lower number of synthesizable drug-like compounds. LigFilter[117, 118] was applied to define certain restrictions:

➢ $150 <= MW <= 500$;

➢ $-3 <= logPo/w <= 6.5$;

➢ $logS >= -7$;

61

➤ reactive groups = 0

2) Docking analysis on the built new libraries for the selection of the best candidates by means of virtual screening workflow (VSW, Glide software). [83-87, 117, 118] The latter is a computational method for the screening of large libraries of ligands versus one or more biological targets. Generally, the ligand files for the docking analysis is previously prepared using several software described above. If a file with 2D structures is used, it is possible to run the LigPrep to obtain the MAE format, since the workflow contains a Ligand Preparation and a Filtering part as well. Since in this case the preparation of the libraries and the application of filters was performed separately, the virtual screening workflow was restricted to the docking analysis. The docking path works at three different levels, which operate with a gradually increasing precision:

➤ HTVS (high throughput virtual screening)

➤ SP (standard precision)

➤ XP (extra precision)

For each level, it is possible to keep a percentage of top-ranked poses using docking score as a selection parameter. The selected are then submitted to the next docking step, which outperforms the previous for both sampling and scoring. The analysis of the final screened compounds is based on the interactions with the receptor counterpart, binding energy, superimposition with a known binder that is co-crystallized in the three-dimensional crystal structure of the protein available in the protein data bank (PDB) database.

1. Generation of libraries

Combiglide (combinatorial chemistry approach)
• Decoration of the selected scaffold with libraries of commercially available reagents and generation of new libraries

LigPrep
• Generation of all possible tautomers and stereoisomers of each molecule at pH value 7.4 ±1

QikProp
• Determination of pharmacokinetics parameters

LigFilter
• Application of some specific filters

2. Docking studies on the final libraries
Virtual Screening Workflow (Glide software) for **docking** studies-three phases:

HTVS *(high throughput virtual screening)*

SP *(standard precision)*

XP *(extra precision)*

Figure 17 Multi-step computational protocol.

3.3.4 Synthesis of the molecules selected via structure-based drug design

The selected chemical routes were applied for the synthesis of the compounds generated and filtered via structure-based drug design. In some specific cases, the synthetic procedure has been slowed down by several issues, concerning the solubility or the reactivity of the involved reagents.

63

Based on the analysis of the specific chemical conditions, the reaction optimization was very useful to overcome the limitations and for the obtainment of the desired products.

In total, 42 molecules have been synthesized as promising inhibitors of mPGES-1.

3.3.5 Biological evaluation of mPGES-1 inhibition

A cell-free assay was performed on the synthesized compounds in collaboration with Prof. Oliver Werz of the University of Jena (Germany).[170] For the performance of the enzyme assay, A549 human lung epithelial cancer cells are treated for 48 h with interleukin-1β (1 ng/ml) and the expression of mPGES-1 is induced. Centrifugation and resuspension in a buffer solution of the microsomal fraction are carried out, the total protein concentration are determined, and microsomes are diluted in potassium phosphate buffer (0.1 M, pH 7.4) containing 2.5 mM glutathione. Then, the test compounds are added and incubated at 4 °C for 15 min. A 20 μM PGH_2 solution is used for starting the reaction, which is stopped after 1 min adding the stop solution (40 mM $FeCl_2$, 80 mM citric acid, and 10 μM 11β-PGE_2). Solid-phase extraction and RP-HPLC (reverse-phase high performance liquid chromatography) are used for the determination of the amount of PGE_2 which defines the percentage of inhibition activity of the enzyme in the presence of the test compounds.[170]

In order to deeply investigate and confirm the inhibition activity presented in the cell-free assay, the effect of the test compounds on PGE_2 production in cells was evaluated. In details, interleukin-1β-treated A549 cells were incubated for 24 h with the test compounds and the amount of PGE_2, secreted into the culture medium, was measured using ELISA assay. Furthermore, in

order to ensure that the PGE$_2$ reduction of the active compounds derives from the inhibition of the activity of mPGES-1 and not from compound-induced cytotoxicity, the cell viability was examined using MTT assay.

Also, the anti-proliferative or cytotoxic effects of the active compounds were evaluated on A375 human melanoma cells. It was demonstrated that in this cell line mPGES-1 is over-expressed, and its inhibition blocks the melanoma cell survival.[171] The cells were incubated for 72 h with increasing concentrations (from 5 µM to 150 µM) of compounds and cell viability was investigated by means of MTT assay. The known inhibitor CAY10526, which is a selective modulator of mPGES-1 and does not interfere with COX-2 activity,[142] was used as a control in the experiments. Finally, the analyses of the cell cycle progression of A375 cancer cells was performed on the compounds able to inhibit cell proliferation or to induce cell death. The cell line was treated with concentrations close or higher to the IC$_{50}$ values of the compounds, and the flow cytometry analysis was used for the determination of the cell cycle progression and the apoptosis induction.

Detailed results of the mentioned performed biological assays on the synthesized molecules will be reported in the following sections, with explicit reference to the individual chemical class.

3.4 Application of the protocol with 2-amino-1,3-benzothiazole and 2-amino-1,3,4-thiadiazole items

One of the scaffolds selected for the generation of new large libraries of molecules using a combinatorial approach is the 2-aminobenzothiazole building block (Figure 18), due to its incidence in antitumor, anti-inflammatory and antibacterial agents and other biologically active

molecules.[172-174] Furthermore, the synthetic versatility and accessibility of this scaffold is noteworthy, and a wide range of chemical routes for the generation of derivatives has been explored and optimized, taking into account the possibility to use it as both reactant and reaction intermediate; the presence of NH_2 group and endocyclic *N* functions, in fact, may assist reactions with common bis electrophilic reagents to form a diverse fused heterocyclic scaffold.[169] Also, other recent studies demonstrated that molecules with a 2-aminothiazole moiety are able to inhibit the activity of the enzyme *in vitro*.[175] In light of this, the 2-aminobenzothiazole has been chosen to explore the ability of its derivatives to inhibit the activity of the enzyme, with the fundamental purpose to obtain compounds more promising than the 2-aminothiazole derivatives.

Figure 18 From 2-aminothiazole to 2-aminobenzothiazole.

A compared rationalization was adopted in the choice of the 2-amino-1,3,4-thiadiazole (Figure 19) according to the biological activity of 2-aminothiazole compounds.

Starting from the analysis of the binding mode of ligands 4UJ[175] and 4UK[176] (Figure 20) co-crystallized in 2016, it seemed appropriate to modify the disposition of the molecular moieties, in order to further optimize the

distances between the compound and the key amino acids of the active binding site.

The translation of the aromatic moiety from position 4 to position 5 of the 2-aminothiazole, and the insertion of the nitrogen on the aromatic ring at position 4 afforded the new scaffold for the design of new potential hits (Figure 19). In this way, the nitrogen could be potentially able to establish additional hydrogen bonds with the receptor counterpart and induce a three-dimensional conformation such that the substituted aromatic ring gets able to interact with Tyr130 and Gln134 by π-π and other specific interactions, according to the importance of these amino acids in the binding mode of known inhibitors.

Figure 19 From 2-amino-1,3-thiazole to 2-amino-1,3,4-thiadiazole.
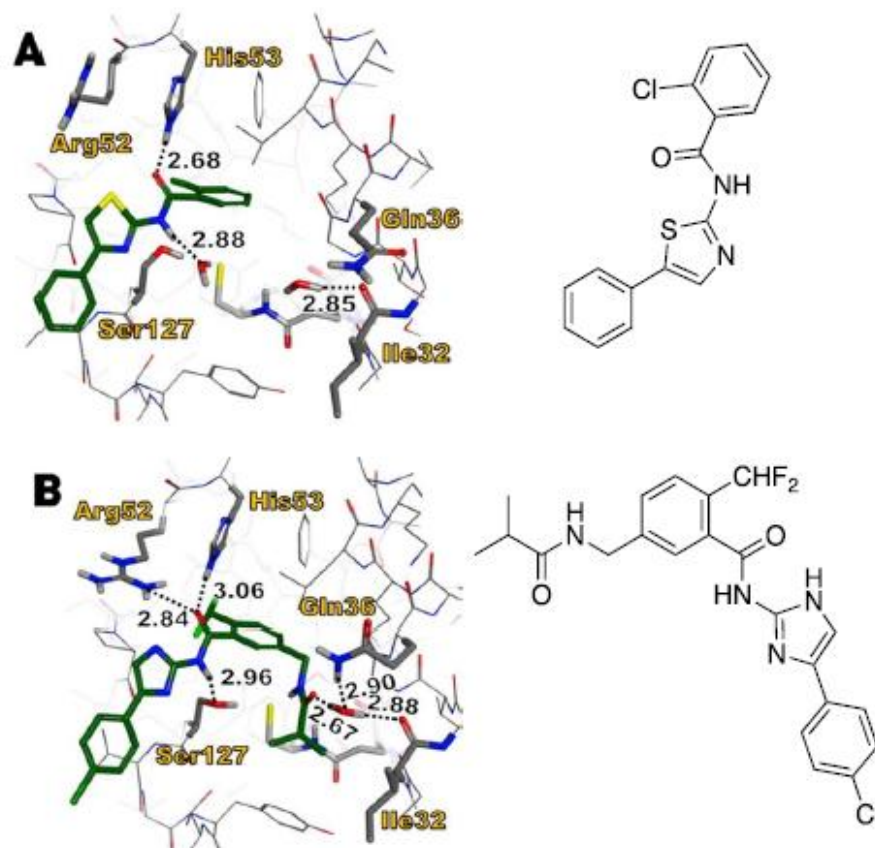
Figure 20 Binding mode of ligands 4UJ (A) and 4UK (B) in the binding site of mPGES-1.

Furthermore, the broad diffusion of several isomers (Figure 21) of 1,3,4-thiadiazole in the pharmaceutical field and the vast spectrum of pharmacological activities led to the selection of this scaffold for the application of the computational protocol used for the individuation of new hits.
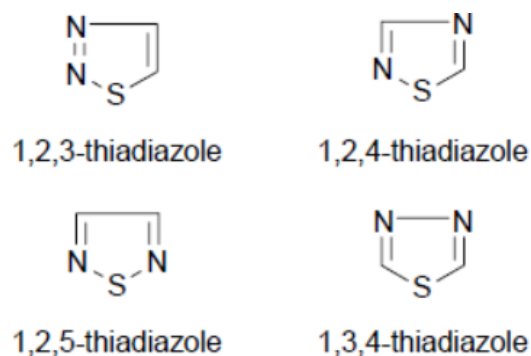
Figure 21 1,3,4-thiadiazole scaffold and its isomers.

Thiadiazole scaffold is involved in analgesic, antidepressant and anxiolytic, antihypertensive, anticonvulsant, anti-inflammatory and anaesthetic activities.[177] The pharmacological profile was attributed to the presence of the portion -N=C-S,[178] but the isosterism is also noteworthy. The 1-3-4-thiadiazole, in fact, is the bioisoster of pyridazine, which is implicated in different pharmacological activities. (Figure 22).[177] In particular, the main reason for the choice of the thiadiazole instead of the pyridazine scaffold is focused on the lipophilicity-hydrophilicity balance, as the substitution of − CH=CH moiety with −S increases the lipophilic properties. These characteristics could lead to an increase in oral absorption and bioavailability.[177]

Figure 22 Bioisosters.

An important factor is the possibility of 1,3,4-thiadiazole derivatives to produce mesoionic salts (Figure 23), which consist of a pentatomic heterocyclic ring endowed with a positive charge counterbalanced by a formal negative charge. The formation of these salts improves the ability of interaction with biological macromolecules (for example, DNA and proteins) of this chemical class of compounds.[177]
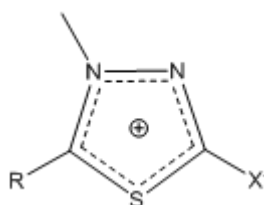
Figure 23 Mesoionic salt.

The 2-amino-1,3,4-thiadiazole derivatives are the most promising and studied, considering the experimented cytostatic activities of this core and the reactivity of the amine group.[177] According to the considerations above, the 2-amino-1,3,4-thiadiazole building block is an excellent candidate for the design of potential hit compounds.

3.4.1 Synthetic strategy for 2-amino-1,3-benzothiazole and 2-amino-1,3,4-thiadiazole derivatives

For the synthesis of 2-aminobenzothiazole and 2-amino-thiadiazole derivatives, the same chemical route was selected. In both, a two steps strategy was chosen: a Suzuki-Miyaura reaction and a nucleophilic substitution, inverted on the case according to the synthetic accessibility. In particular, starting from 2-amino-5-bromobenzothiazole, 2-amino-6-bromobenzothiazole

and 2-amino-5-(4-bromophenyl)thiadiazole starting materials (Figure 24, A, B and C respectively) the strategy provided the coupling on the aromatic ring bearing the bromine using boronic acids and a nucleophilic substitution reaction on acyl chlorides with the amino group.
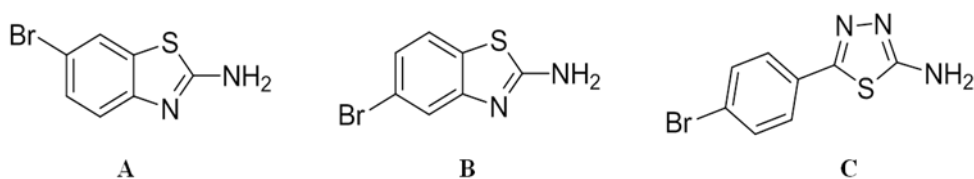
Figure 24 A) 2-amino-6-bromobenzothiazole, **B)** 2-amino-5-bromobenzothiazole; **C)** 2-amino-5-(4-bromophenyl)thiadiazole starting materials.

The Suzuki-Miyaura reaction was first published in 1979 by Akira Suzuki,[179-181] and improved in the following years modifying base, temperature and solvent conditions. It is a coupling reaction between an organohalide (alkenyl, vinyl, aryl halides) and a boronic acid (organometallic compound), catalyzed by a palladium (0) complex in basic conditions, which lays to the formation of C-C bonds (Figure 25). Considering the efficiency and versatility of this reaction, and the stability and low toxicity of the organometallic partner in comparison to others, it is often applied for the synthesis of highly functionalized biaryls.
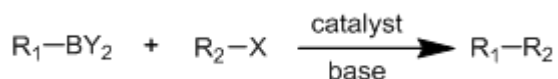
Figure 25 Suzuki reaction between boronic acid (R_1-BY_2) and halide (R_2-X).

71

The use of palladium is related to its characteristics, as it has an electronegativity similar to the carbon. The bond C-Pd, in fact, is quite strong due to its poor polarity. In the Suzuki reaction, palladium (Pd) takes part in the catalytic cycle, which is divided into three steps: oxidative addition, transmetalation, reductive elimination.[179-181]
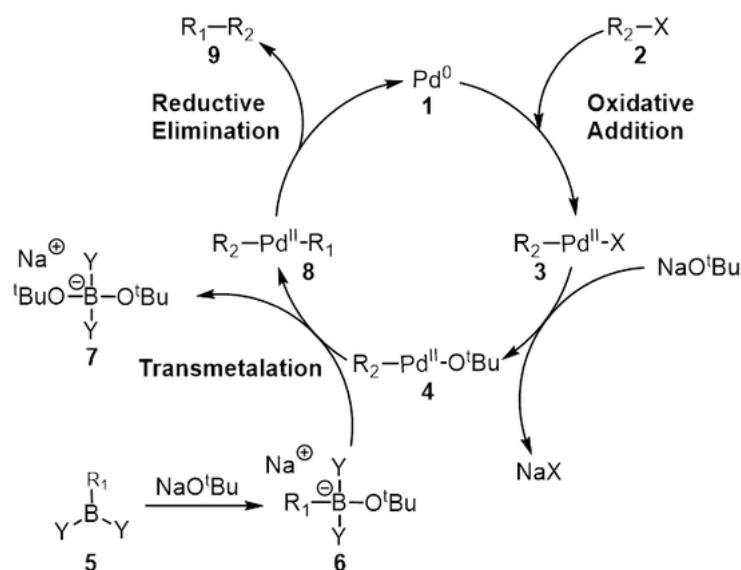
Figure 26 Catalytic cycle of Suzuki reaction.

The oxidative addition is the rate determining step of the reaction. During this step, palladium is oxidized from palladium (0) to palladium (II) and is coupled with the alkyl halide forming an organopalladium complex, in which it is placed between the halogen and the R_2 group (Figure 27). The reaction time is determined by the halogen, according to the scale of halogen reactivity: I >OTF> Br >> Cl.
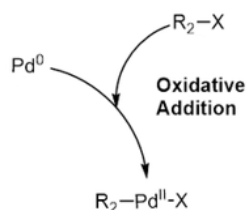
Figure 27 Oxidative Addition and formation of complex R_2-Pd^{II}-X.

The second step is the transmetalation, which consists of an exchange of ligands between two chemical species (Figure 28). In particular, in this case the organic moiety of the boronic acid switches to the organopalladium complex, giving the final R_2-Pd^{II}-R_1. A detailed mechanism of the transmetalation phase is not known to date. Moreover, the presence of the base is essential, since it plays an important role in the activation of the organoboron compound as well as is involved in the formation of R_2-Pd^{II}-OtBu complex, from which the resulting complex is formed.
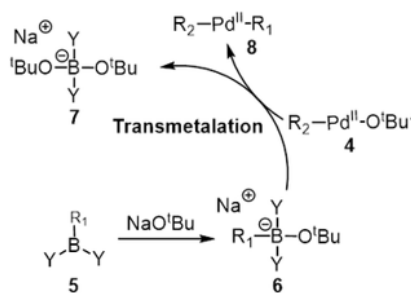
Figure 28 Transmetalation step and formation of R_2-Pd^{II}-R_1 complex.

The third step is the reductive elimination in which the palladium (II) eliminates the product (R_1-R_2) and palladium (0) is regenerated (Figure 29).[179-181]
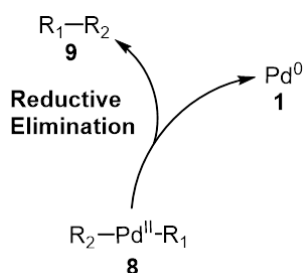
Figure 29 Reductive Elimination and formation of the product (R_1-R_2).

3.4.2 Generation of libraries of 2-aminobenzothiazole and 2-aminothiadiazole derivatives

Based on the application of the multi-step computational protocol, a set of different libraries was built starting from the selected cores.

Benzothiazoles. Starting from the synthons of the selected synthetic strategy, Combiglide[112] was used for the decoration of 2-amino-6-bromobenzothiazole and 2-amino-5-bromobenzothiazole with 318 acyl chlorides at position 2 and 570 boronic acids at position 5 and 6 respectively. After the combination of the scaffold with the prepared reagents (Figure 30) two large libraries were obtained:

1) 2-arylacylamino-6-arylbenzothiazoles (**A**)
2) 2-arylacylamino-5-arylbenzothiazoles (**B**)

each containing 181,260 molecules. Then, the libraries were processed with LigPrep,[123] in order to generate all the possible stereoisomers, tautomers and protonation states at a pH of 7.4 ± 1.0. The application of QikProp[110] for the determination of pharmacokinetic parameters and

LigFilter[117] (150<MW<500, $-3<=logP_{O/W}<=6.5$, logS >= -7, reactive groups=0) afforded the final libraries **A** and **B**.
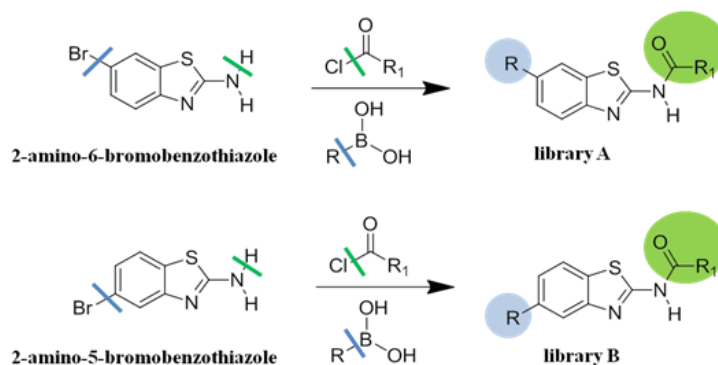
Figure 30 Generation of two libraries: **A**)2-arylacylamino-6-arylbenzothiazoles from 2-amino-6-bromobenzothiazole; **B**)2-arylacylamino-5-arylbenzothiazoles from 2-amino-5-bromobenzothiazole.

Thiadiazoles. The same reagents prepared for the generation of the previous libraries were used for the decoration of 2-amino-1,3,4-thiadiazole core. A library of 181,260 *N*-(5-(4-arylphenyl)-1,3,4-thiadiazol-2-yl)arylcarboxamides (**C**) was generated by means of Combiglide[112] (Figure 31). LigPrep[123] calculations and the same filters enumerated above were applied, obtaining the resulting library **C**.

2-amino-5-(4-bromophenyl)thiadiazole
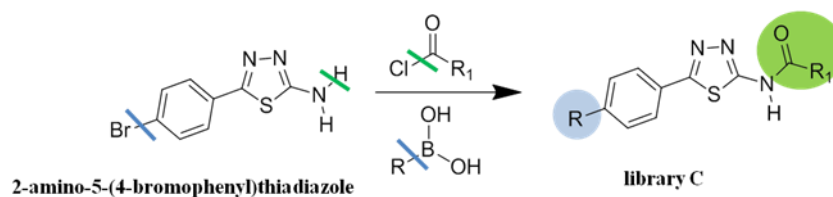
library C

Figure 31 Generation of a library of N-(5-(4-arylphenyl)-1,3,4-thiadiazol-2-yl)arylcarboxamides starting from 2-amino-1,3,4-thiadiazole (**C**).

3.4.3 2-aminobenzothiazole and 2-aminothiadiazole derivatives targeting mPGES-1

The second phase was the structure-based virtual screening of the libraries on mPGES-1. Semi-flexible docking experiments were carried out on the three libraries of compounds. The screened molecules were analyzed considering docking score, binding mode and interactions established with the receptor counterpart, basing on the reported key interactions.[165, 182, 183] In total, 13 benzothiazole (Figure 32) and 9 thiadiazole (Figure 33) derivatives were chosen for the synthesis and the biological evaluation of their anti-inflammatory/anti-tumor activity, inhibiting mPGES-1.
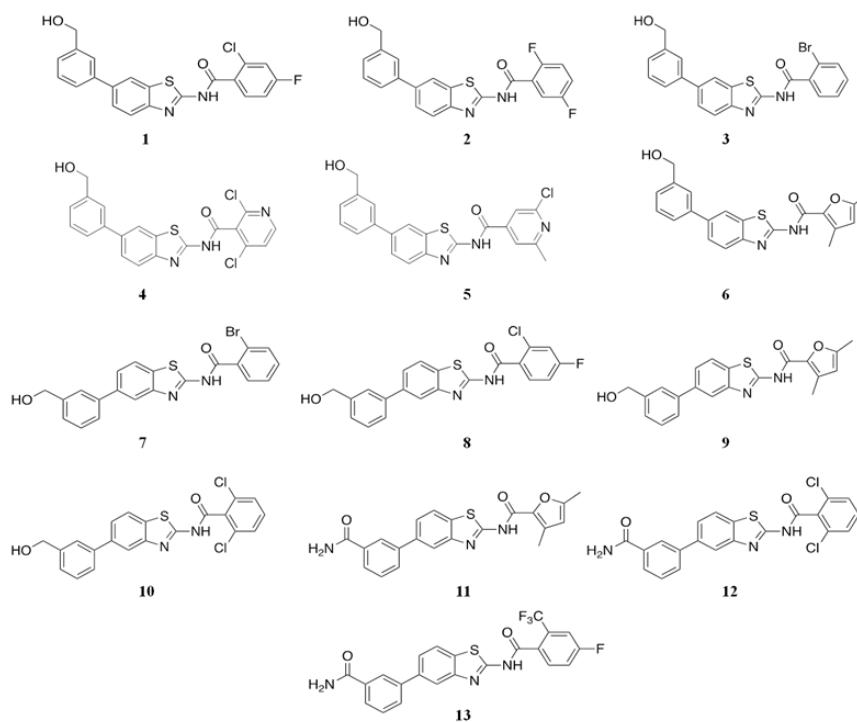
Figure 32 2-amino-1,3-benzothiazole derivatives selected for mPGES-1 via structure-based drug design.
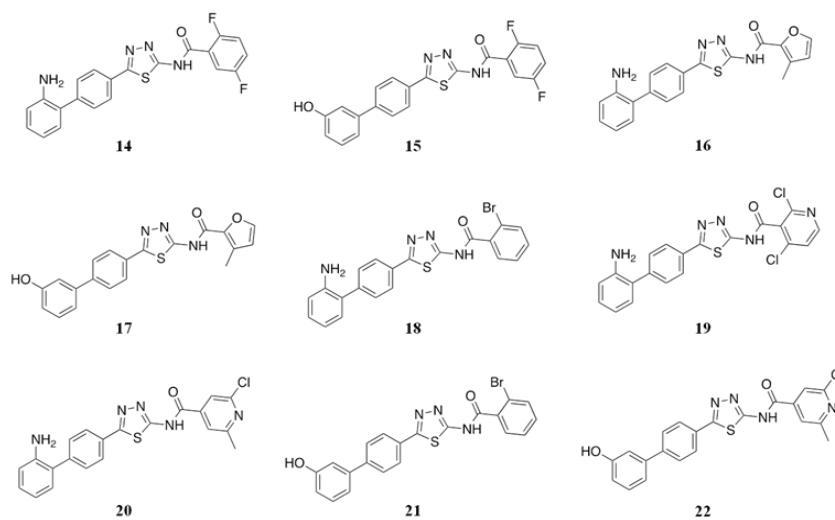
Figure 33 2-amino-1,3,4-thiadiazole derivatives selected for mPGES-1 via structure-based drug design.

77

Among them, a representative description of the binding mode in the active site of the novel ligands series is reported, taking into account the most promising compounds: compound **3** for the 2-aminobenzothiazole item and compound **18** for the 2-aminothiadiazole item.

Considering compound **3**, the 2-amino-6-bromobenzothiazole scaffold centers the ligand binding site along the three different regions (see section 3.1.1), establishing contacts and interactions with aromatic and polar residues. For this specific molecule, the substituents decorating the scaffold perform peculiar contacts: a) bromine atom establishes halogen bonds with Thr34$_{ChainC}$ and Asn46$_{ChainC}$ (Figure 35); b) -OH group is able to interact with Gln134$_{ChainA,}$ Tyr130$_{ChainA}$ and Ile32$_{ChainC}$ by hydrogen bonds, while -NH group of the amide establishes hydrogen bond with Ser127$_{ChainA}$; c) benzothiazole interacts with Tyr130$_{ChainA}$ and the other aromatic rings with Tyr130$_{ChainA}$ and His53$_{ChainC}$ respectively, all of them by π-π stacking interactions (Figure 34).

Figure 34 2D panel representation of compound **3** in the ligand binding site of mPGES-1. Positive charged residues are colored in violet, negative charged residues are colored in red, polar residues are colored in light blue, hydrophobic residues are colored in green. The π-π stacking interactions are indicated as green lines, and H-bond are reported as dotted pink arrows.

Figure 35 Three-dimensional representation of compound **3** in the active binding site of mPGES-1. Purple lines represent specific halogen bonds with the receptor counterpart. A selective representation of halogen bond interactions is reported.

Regarding the thiadiazole moiety of compound **18**, it is placed in the middle of the ligand binding site and interacts with the closest key amino acids (Gly35$_{ChainC}$, Ser127$_{ChainA}$) by hydrogen bonds. The centered position is retained in all the selected compounds, with a peculiarity in the interactions of the substituents with the receptor counterpart. The aromatic rings are able to establish π-π stacking interactions with His53$_{ChainC}$ on the cytoplasmic region and with Tyr130$_{ChainA}$ on the other side. In this case, the bromine on the amidic moiety of the molecule establishes halogen bonds with Asn46$_{chainC}$ (Figure 37), while the amino group interacts with Tyr130$_{ChainA}$ and Gln134$_{ChainA}$ by hydrogen bonds (Figure 36).
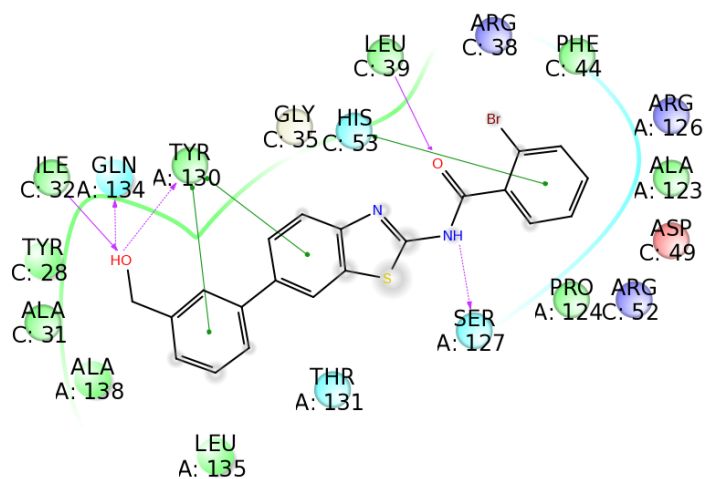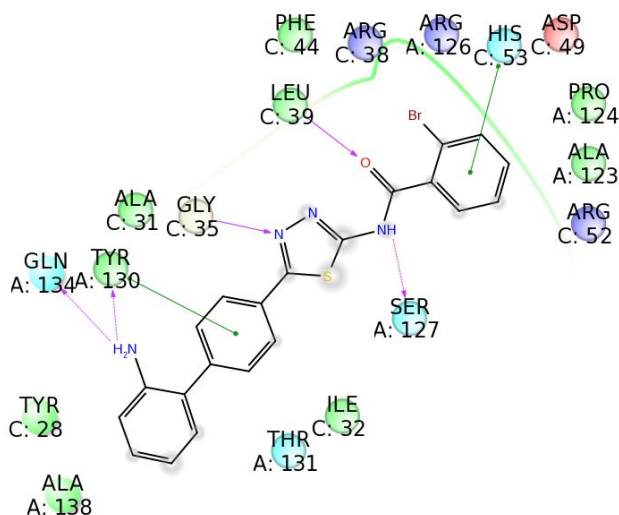

Figure 36 2D panel representation of compound **18** in the ligand binding site of mPGES-1. Positive charged residues are colored in violet, negative charged residues are colored in red, polar residues are colored in light blue, hydrophobic residues are colored in green. The π-π stacking interactions are indicated as green lines, and H-bond are reported as dotted pink arrows.
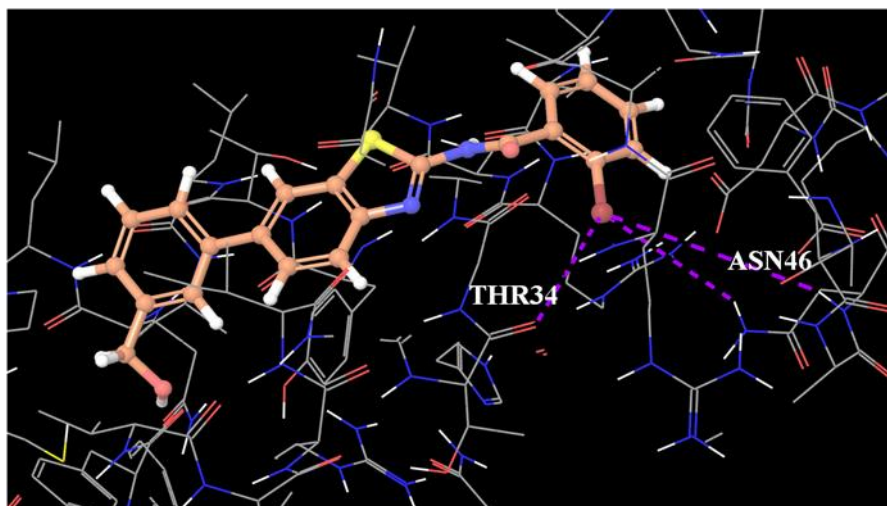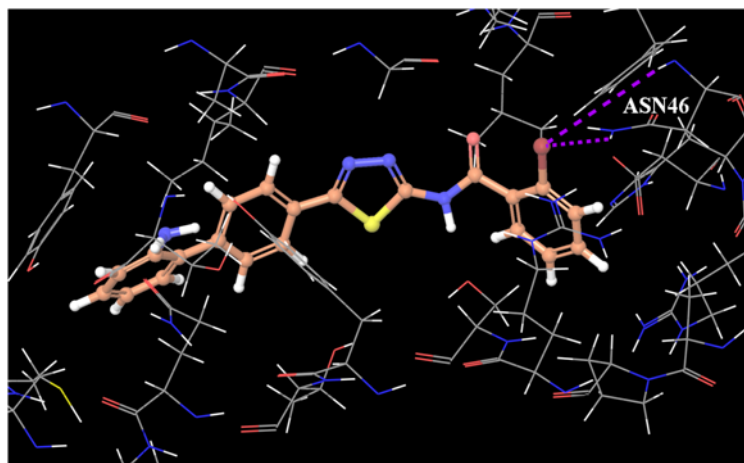
Figure 37 Three-dimensional representation of compound **18** in the active binding site of mPGES-1. Purple lines represent specific halogen bonds with the receptor counterpart. A selective representation of halogen bond interactions is reported.

3.4.3.1 Pan-Assay Interference compounds (PAINS) screening

A current problem in drug discovery is the existence of chemical species able to not specifically bind numerous biological macromolecules, thus giving false positives in high-throughput screens. A preliminary computational tool focused on the prediction of ADME parameters was used in order to avoid this specific issue. SwissADME[184] web tool evaluates the presence of chemical moieties belonging to "Pan-Assay Interference Compounds" (PAINS) chemical class, implemented from the paper by Baell et al. [185]

Since the promiscuity of 2-aminothiazoles is well-known, selected 2-aminobenzothiazole (**1-13**) and 2-aminothiadiazole (**14-22**) based compounds were analyzed with SwissADME in order to apply a further filter focused on PAINS identification. All the molecules belonging to the small library selected for the synthesis (**1-22**) passed the filter, as they do not contain PAINS.

3.4.4 Synthesis of 2-amino-1,3-benzothiadiazole derivatives

It is possible to distinguish three different groups in the 13 benzothiazoles candidates for the synthesis, according to the chemical structure of the coupling partner. The first two groups are different for the position of the 3-(hydroxymethyl)phenyl moiety on the benzothiazole since one shows the substituent at position 6, the other one at position 5 (Figure 38). The third class, instead, contains a 3-aminocarbonylphenyl substituent at position 5 (Figure 38).

In the synthesis of the 13 molecules, two different commercially available starting materials were used: 2-amino-6-bromo-1,3-benzothiazole for the first group, and 2-amino-5-bromo-1,3-benzothiazole for the second and third groups. Suzuki coupling reaction was performed at position 6 of the benzothiazole using 3-(hydroxymethyl)phenylboronic acid for the synthesis of compounds **1-6**, and at position 5 for the synthesis of compounds **7-10** (Figure 39). The cross-coupling was performed under standard conditions using Pd(PPh$_3$)$_4$ as catalyst (0.2 eq.) and aqueous carbonate as base (3.0 eq.) in a mixture of dioxane (80%) and water (20%) at 80 °C. Reactions afforded the product with good yields (75% and 88%).
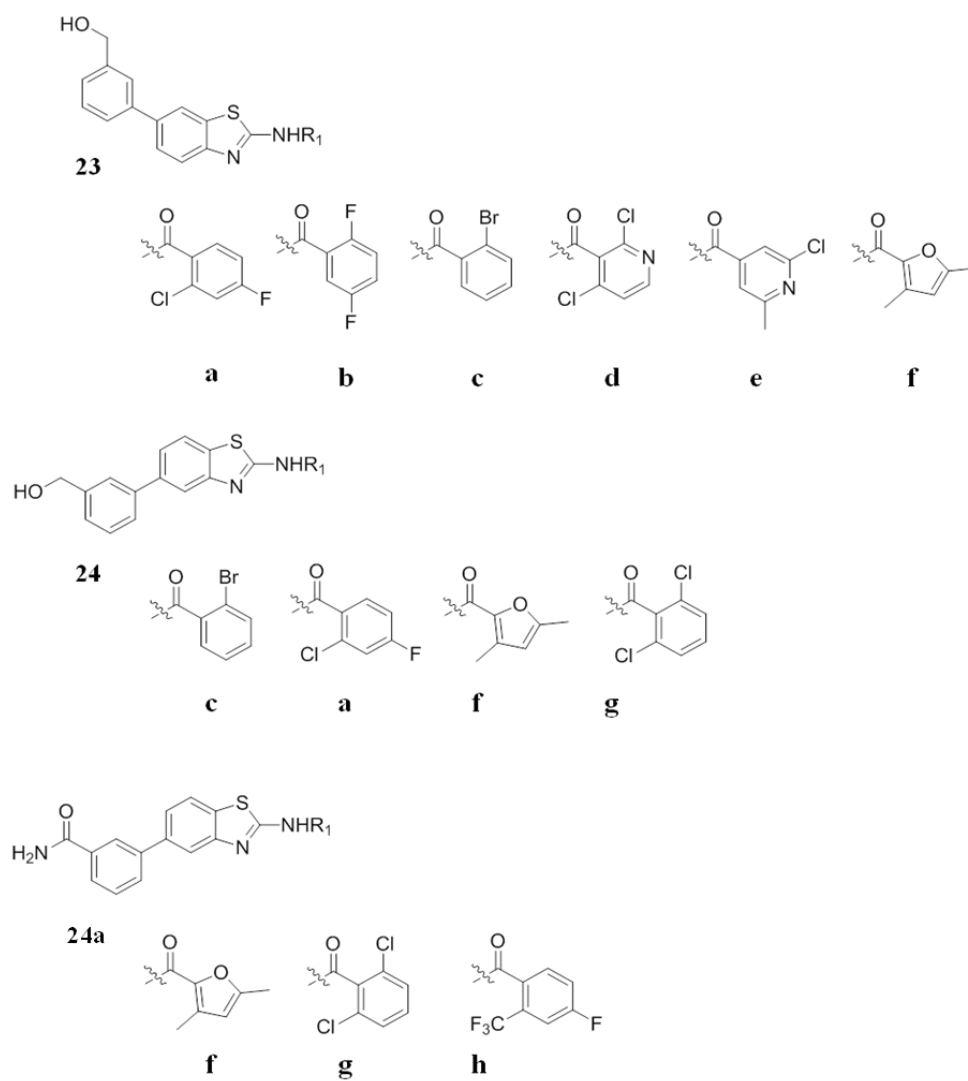
Figure 38 Three groups of selected compounds.
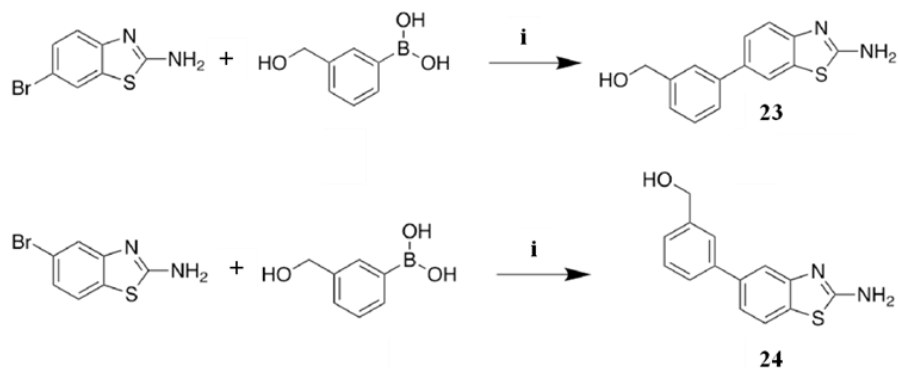
Figure 39 Coupling reaction for the synthesis of **23** and **24**; **i**: Pd(PPh₃)₄, K₂CO₃, H₂O-Diox, 80°C.

Then, the proper acylation reaction was performed on the resulting intermediates **23** and **24** to obtain compounds **1-6** and **7-10** respectively. Moreover, the hydroxyl group of the two Suzuki intermediates could perform a substitution reaction on the acyl chloride. A transient protection by trimethylsilyl ether was performed *in situ* in dry acetonitrile with pyridine at room temperature, before adding the proper acyl chloride in the reaction mixture. The protective group was then removed with acidic work-up (Figure 40).
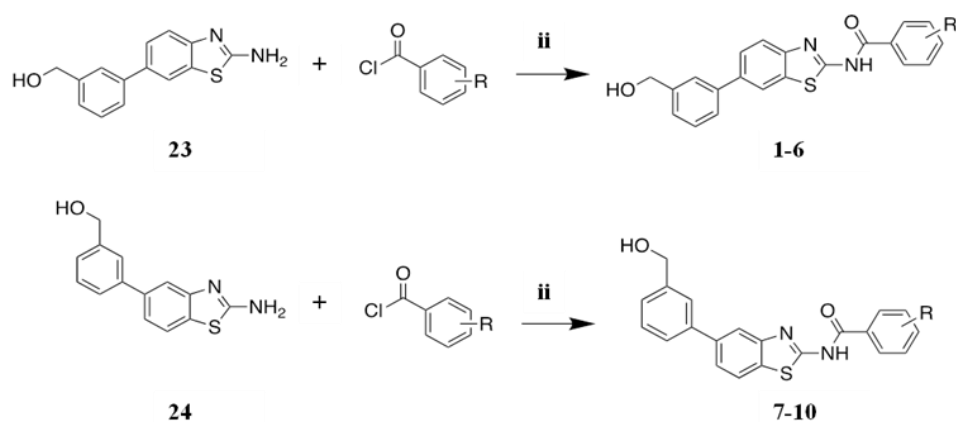
Figure 40 Acylation reaction for the synthesis of the final products **1-6** and **7-10**; **ii:** pyridine, CH₃CN dry, TMSCl, r.t.

Compounds **11-13** belonging to the third group were synthesized inverting the sequence of the reactions, considering the less polarity of **25**, **26** and **27** intermediates and a consequent easier purification. The acylation reaction with the proper acyl chloride was the first step, conducted in dry acetonitrile with pyridine at room temperature. Then, a coupling with 3-aminocarbonylphenyl boronic acid was carried out on the acylated intermediates (Figure 41) to afford **11-13**.

All compounds were purified by reversed phase HPLC (high performance liquid chromatography) or by flash column chromatography, and were obtained with >98% purity.
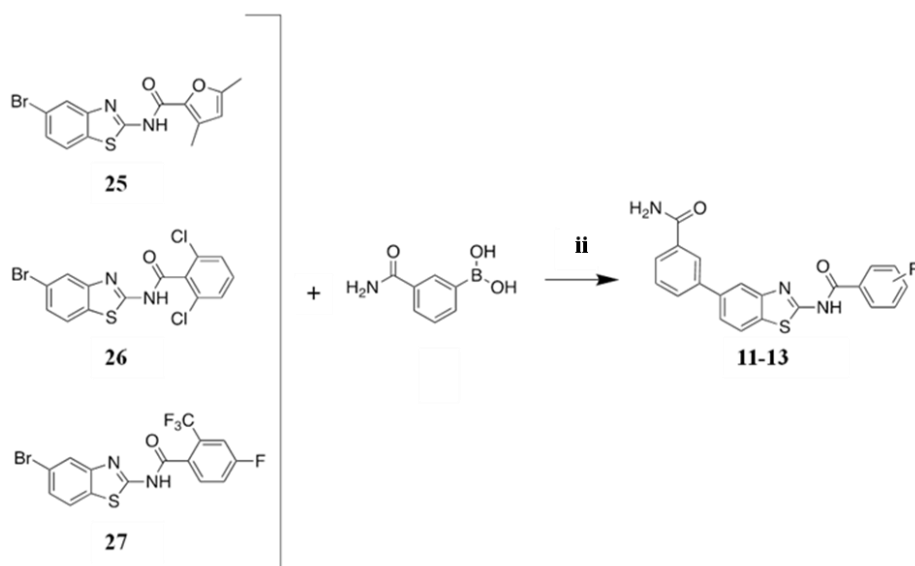
Figure 41 Suzuki reaction on the acylated intermediates **25**, **26** and **27** for the synthesis of the final products **11-13**; **ii**: Pd(PPh$_3$)$_4$, K$_2$CO$_3$, H$_2$O-Diox, 80°C.

3.4.5 Biological evaluation of benzothiazole derivatives

The cell-free assay on mPGES-1 expressed in IL-β-treated A549 cells was performed on compounds **1-13**.[170] The benzothiazole derivatives bearing the (hydroxymethyl)phenyl moiety at position 5 (**7-10**) showed a residual activity higher than 30% at 10 μM. The replacement of the (hydroxymethyl)phenyl with 3-aminocarbonylphenyl group at position 5 of compounds **9** and **10** did not provide an improvement of the results, since compounds **11** and **12** presented a comparable inhibitory activity. Conversely, the introduction of a 4-fluoro-2-(trifluoromethyl)phenyl acyl group in compound **13** of this series showed better results, with an IC$_{50}$ value of 1.7±0.2 μM. The introduction of the (hydroxymethyl)phenyl at position 6 afforded an improved inhibitory activity, as it was demonstrated in the cell-free assay on compounds **1** and **3**.

Moreover, the presence of a pyridine acyl group provided a reduction of the activity in compounds **4** and **5**, whereas the 2,5-dimethylfuran in compounds **6** determined an IC_{50} value of 2.6±0.1 µM. Thus, compounds **1**, **3**, **6** and **13** presented a promising inhibitory activity in the enzyme assay on mPGES-1.

Selectivity studies are in progress for the most promising compounds, in order to investigate the possibility of modulating the activity of COXs and 5-LO.

According to the cell-based assay performed on IL-β-treated A549 cell lines, a reduction of PGE_2 production into the culture medium was demonstrated with compounds **1**, **3**, **6** and **13**, and interestingly with compound **9** in a concentration-dependent manner. The MTT assay confirmed the reduction of PGE_2 is not dependent from compounds cytotoxicity, since there was not a significant difference in cell viability with respect to control group. Compound **9** showed inhibition of 20% of cell viability at 10 µM and the PGE_2 production value was normalized taking into account the percentage of cell viability.

In light of this, in order to deeply understand the activity of the test compounds **1**, **3**, **6**, **9** and **13**, their effect on cancer cell viability and on cell cycle progression were evaluated in A375 human melanoma cells (see section 3.3.5, biological assay for details). All the compounds inhibited the cancer cell vitality according to the MTT proliferation assay. In detail, the compounds **1**, **3**, **9** showed the best IC_{50} values of 18.3 ± 1.5, 12.1 ± 0.8 and 20.3 ± 1.1 µM, respectively, while IC_{50} value for CAY10526 under the same conditions was 4.7 ± 0.5 µM.[148] In the flow cytometry analysis for the investigation of their effects on the cycle progression, **1** and **9** displayed a cytostatic activity in time and dose-dependent manner with a G0/G1 or S phase arrest, respectively

(Figure 43, A and C). Compound **1** induced a modest apoptotic effect after 48h or after 72h at high concentration, whereas compound **9** did not induce cell death (Figure 43, A and C). Conversely, compound **3** caused both cytostatic and pro-apoptotic effect in dose-dependent manner (Figure 43, B).

Compound	$IC_{50} \pm SD$ (µM)
1	1.4±0.2
3	0.7±0.1
6	2.6±0.1
9	>10 (55.3±10.3)
13	1.7±0.2

Table 3 IC_{50} values deriving from the cell-free assay.
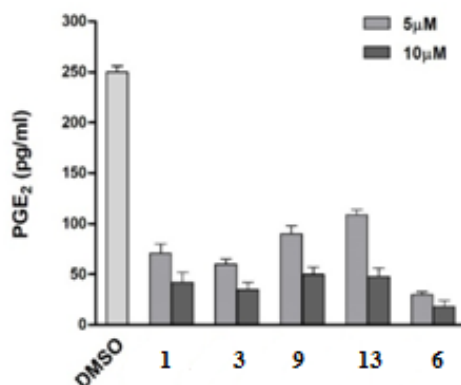
Figure 42 Cell-based assay on IL-β-treated A549 cell line.

Compound	IC$_{50}$ ± SD (µM)
1	18.3 ± 1.5
2	98.2 ± 1.3
3	12.1 ± 0.8
6	90.5 ± 1.4
7	46.0 ± 1.4
8	42.5 ± 1.7
9	20.3 ± 1.1
10	97.5 ± 1.9
12	31.3 ± 1.7
13	41.7 ± 1.3
CAY10526	4.7 ± 0.5

Table 4 Anti-proliferative effect of mPGES-1 inhibitors in A375 human melanoma cancer cell line.
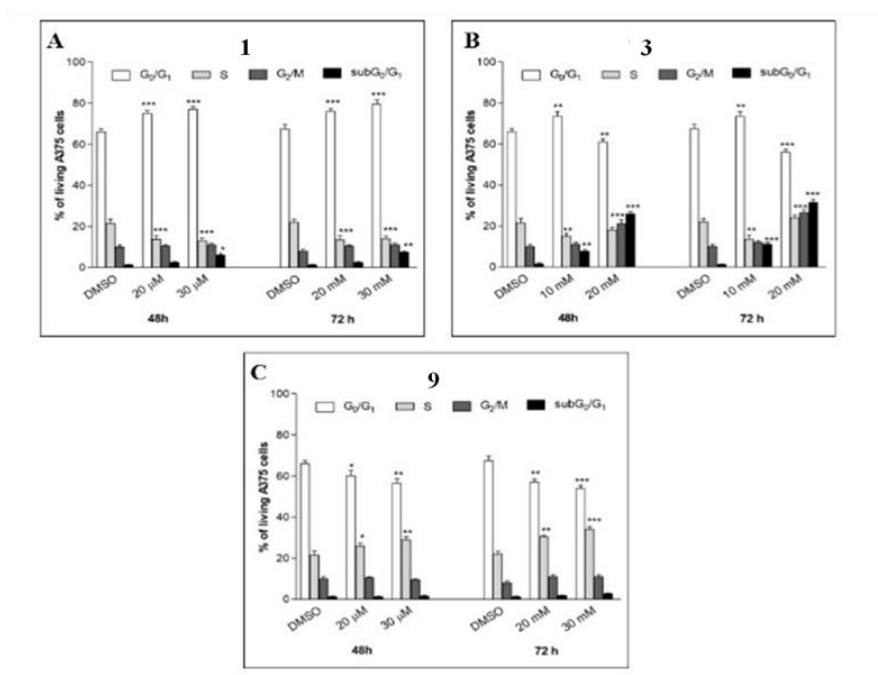
Figure 43 Cell cycle progression analysis by flow cytometry.

3.4.6 Synthesis of 2-amino-1,3,4-thiadiazole derivatives

The 2-amino-1,3,4-thiadiazole derivatives selected in the virtual screening workflow can be classified into two different groups: the first one bearing a 2-aminophenyl and the second one a 3-hydroxyphenyl as coupling partner moiety (Figure 44). In the second group, four acyl chlorides (R_1) of the first group are involved in the substitution reaction.
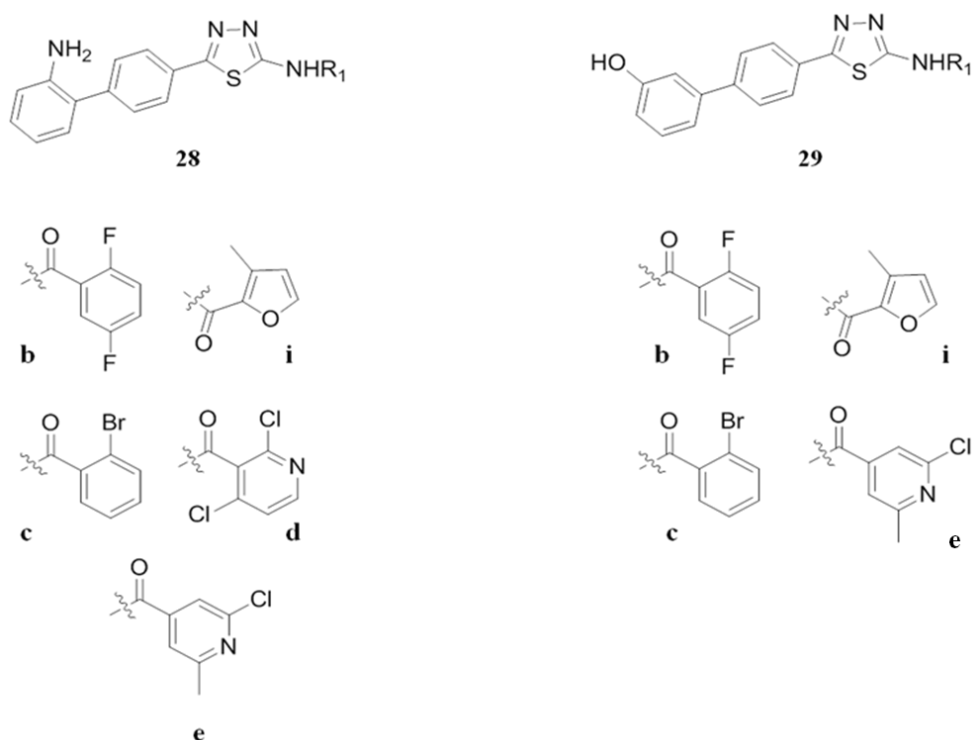
Figure 44 On the left, the group of selected compounds bearing the 2-aminophenyl moiety; on the right, the group bearing the 3-hydroxyphenyl moiety. R_1=Acyl chlorides moiety.

As in the synthetic procedure of 2-aminobenzothiazole derivatives, the synthesis adopted for the 9 thiadiazolic compounds consists of the same two main steps. Starting from 2-amino-5-(4-bromophenyl)thiadiazole, the general route provides the acylation reaction on the amino group, followed by the Suzuki-Miyaura coupling on the 4-bromophenyl ring (Figure 45).
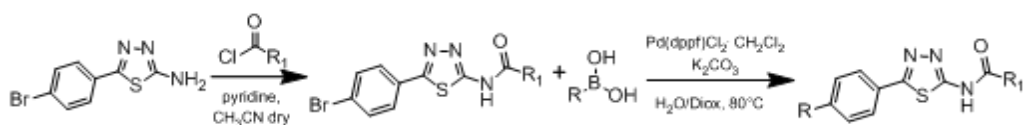
Figure 45 General synthetic route (compounds **14-17**).

91

Among the 9 selected compounds, **14-17** were synthesized retaining the same sequence of reactions. In the synthesis of the rest of the molecules, an inversion of the steps was adopted, performing the coupling in the first step and the acylation reaction in the second step. The halogens on the aromatic rings of the acylated intermediates, in fact, would have been able to interfere with the coupling on the phenyl ring of the 2-amino-5-(4-bromophenyl)thiadiazole, considering mainly the high reactivity of bromine. Also, the nucleophilic groups (-OH, -NH$_2$) of the two Suzuki intermediates may be involved in the substitution reaction of the acyl chloride. The use of protective groups, with a further step for the final deprotection, was essential to avoid this problem. For the analogues bearing an amino group, the tert-butoxycarbonylamino (Boc) protected boronic acid, commercially available, was used in the first step (Figure 46). After the acylation step with the proper acyl chloride, the protecting group was removed with a mixture of DCM (50%) and TFA (50%) stirring over three hours at room temperature, and the final compounds were obtained.

In the synthesis of the analogues with the hydroxyl group, the intermediates deriving from the coupling reaction were protected with TMSCl (trimethylsilyl chloride), and the acyl chlorides were added *in situ*. The following acidic work-up removed the trimethylsilyl protecting group, affording the desired products (Figure 46).

92
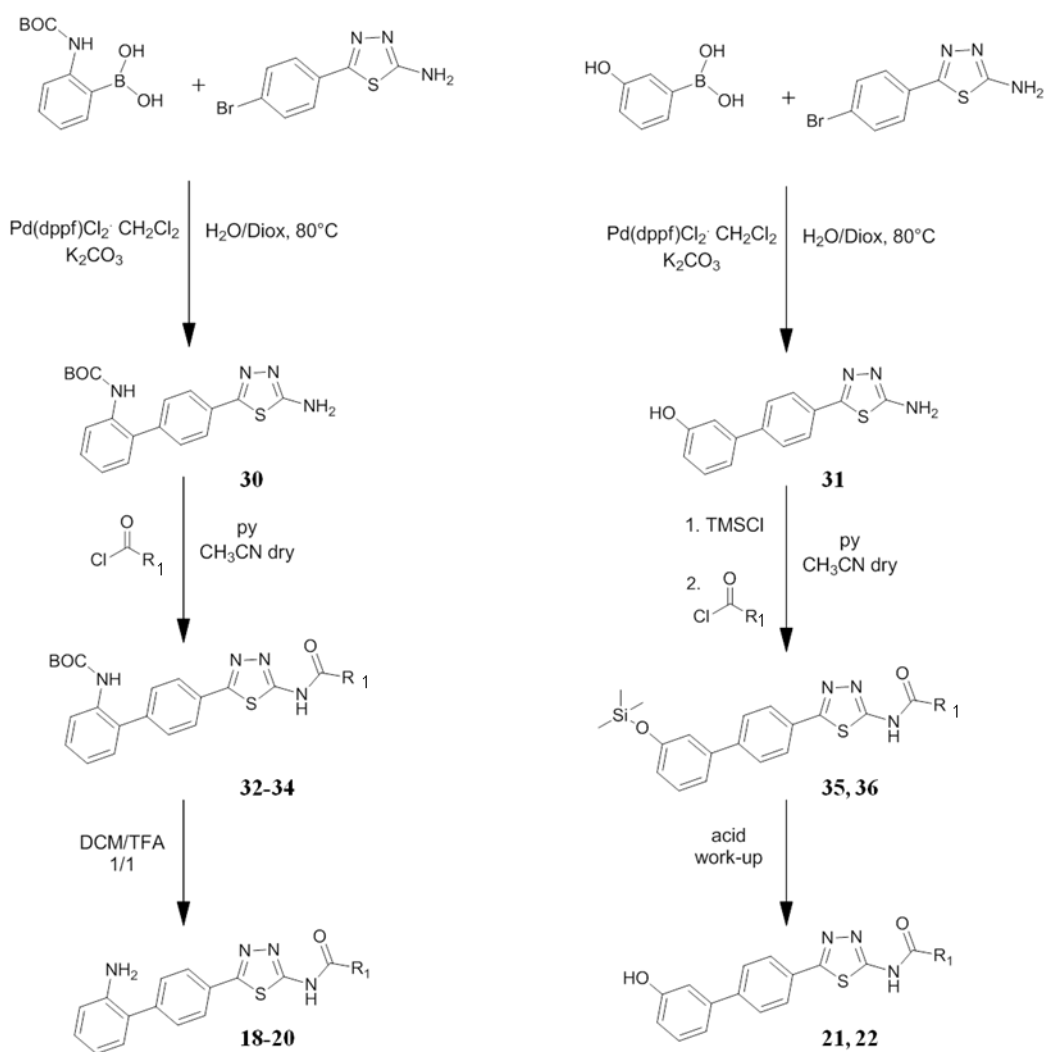
Figure 46 Synthetic strategy for compounds **18-22**.

Another important problem observed in the synthesis of 2-aminothiadiazole derivatives is related to the tautomeric equilibrium (Figure 47). Amino-heterocycles, in fact, may exist in two tautomeric forms: amino (A) and imino (B). In the last few years, different experiments demonstrated that the

tautomerism affects the orientation of the substitution and increases the number of possible products.[186, 187]
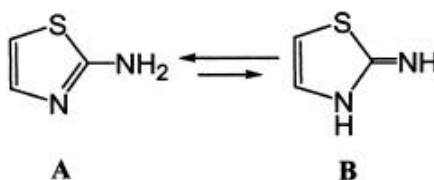
Figure 47 Tautomeric equilibrium of 2-aminothiazole.

In light of the peculiarity of this class of compounds, the acylation step in the synthesis of 2-amino-1,3,4-thiadiazole derivatives represented a limitation in the synthetic route. In this case, in fact, the reaction may afford two different products, as demonstrated by NMR and LC-MS analysis:

1. The product bearing the amidic group at position 2 of the thiadiazole, deriving from the substitution of the amino group.
2. A product deriving from a double acylation, in which a further substitution reaction on the nitrogen at position 3 of the thiadiazolic ring provides a di-amide.
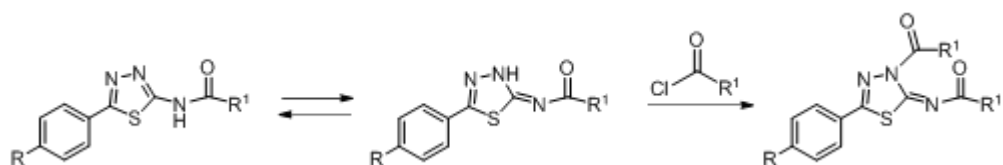
Figure 48 Tautomeric equilibrium leading to double acylation.

For this reason, the reaction gave the product with low yields (10-20%). In order to optimize the yields, a reduction of reaction time was adopted, and a considerable increase of the desired product was observed.

94

3.4.7 Biological evaluation of thiadiazole derivatives

Among the synthesized compounds reported above, the cell-free assay[170] was performed on **14** and **16-20**, and is in progress for the remaining compounds. All test compounds presented a residual activity higher than 30% at 10 µM. Compounds **18-20** showed a promising IC_{50} value. Furthermore, the cell-based assay on A549 cell line was performed on **15** and **18-22**. Compounds **18-20** confirmed the results of the cell-free assay, while compound **22** presented an interesting high inhibitory activity (Figure 49, A). A further performed analysis was the cell viability assay (MTT). Human fibroblast cells were incubated with DMSO or compounds **18-20** and **22** at 10 µM or 50 µM for 24 hours. No cell viability inhibition was observed for all test compounds (Figure 49, B).

Compound	$IC_{50} \pm SD$ (µM)
18	0.2±0.0
19	1.7±0.3
20	3.3±0.8

Table 5 IC_{50} values deriving from the cell-free assay.

95
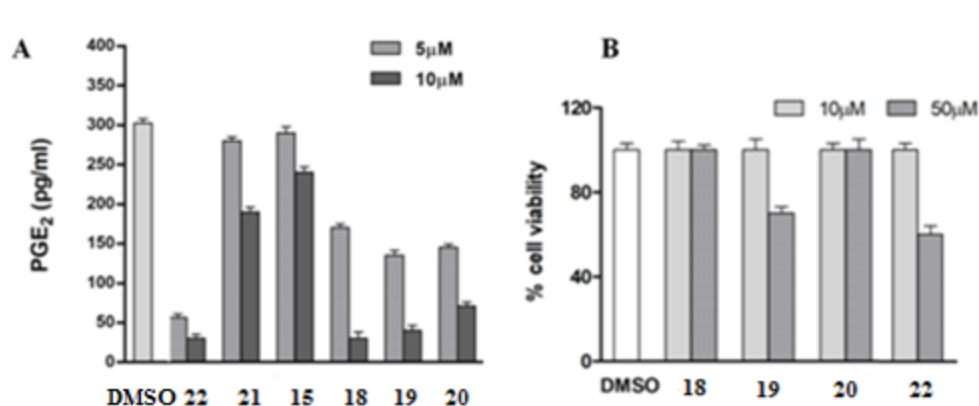
Figure 49 A) Cell-based assay on IL-β-treated A549 cell line; **B)** Cell viability assay on human fibroblast cells (10 μM or 50 μM).

3.5 Application of the protocol with 2-carboxamide pyrrole

A pyrrolic scaffold was also chosen as a new promising mPGES-1 targeting moiety, considering the broad spectrum of biological activities (anti-bacterial,[188, 189] anti-inflammatory,[190] antifungal,[188] anticancer[191]).

In a research work developed in 2012,[192] a set of different pyrroles was synthesized and tested on mPGES-1. Starting from the 4-acylpyrrol-2-ylpropionic acid (Figure 50), a known inhibitor of mPGES-1 with an IC_{50} value of 0.80 μM, the synthesis of analogues was carried out in order to obtain compounds with an improved activity on the enzyme. In details, the modifications provided the variation of the dodecanoyl residue, the substitution of the methyl groups with hydrogen, phenyl and benzyl, length modifications of the acid chain, and bioisosteric replacement of the carboxylic acid group. In spite of the large number of synthesized analogues, quite a few

96

of pyrrole derivatives were able to inhibit the activity of the target.[192] Also, it was demonstrated that such flat structures are nuisance inhibitors of mPGES-1, since they lost activity at 10 μM in the presence of Triton X-100.

In this research project, other modifications of the pyrrolic scaffold were explored in order to overcome the issues above, and a rationalization of the binding mode of the pyrrole alkanoic acid derivatives reported in Table 6 was carried out, in order to compare them with the new pyrroles selected via structure-based virtual screening.
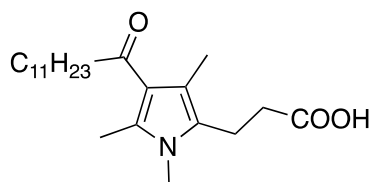
Figure 50 3-(4-dodecanoyl-1,3,5-trimethyl-1H-pyrrol-2-yl)propanoic acid, mPGES-1 inhibitor (IC$_{50}$ = 0.80 μM).

In particular, the 2-carboxamide pyrrole building block was considered for the design of derivatives, due to its incidence in a broad range of pharmacological activities, such as antimicrobial and antifungal.[188, 193, 194]

3.5.1 Synthetic strategy for 1*H*-pyrrole-2-carboxamide derivatives

The pyrrole analogues chemical route consists of a synthetic method developed by Prof. Anna Ramunno at the Department of Pharmacy of Salerno University.[191] In detail, the reaction between (±)-serine methyl ester hydrochloride and p-toluenesulfonyl chloride affords the tosyl protected compound, which reacts in turn with tert-butyl pyrocarbonate, (Boc)$_2$O, and a

catalytic amount of 4-dimethylaminopyridine (DMAP) to give the dehydroalanine. Then, β-diketones are used for the synthesis of pyrrole using Cs_2CO_3 as base and 10% THF in dichloromethane. The next hydrolysis of the methyl-ester and the amide formation provides the desired products (Figure 51, A).[191] β-diketones may be commercially available or synthesized starting from ethyl esters and a methyl-ketone (Figure 51, B).[195]
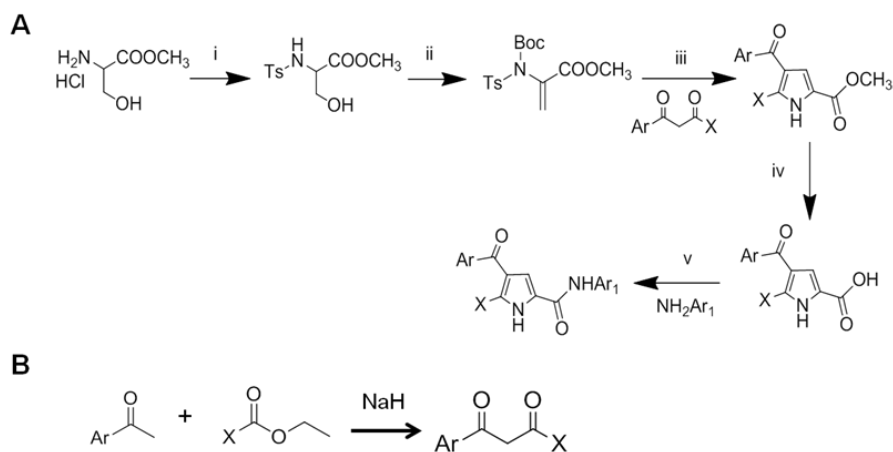
Figure 51 A) Synthetic strategy for pyrrole derivatives; **i**=tosyl chloride, TEA, DMC, 0°C to rt, overnight,; **ii**= (Boc)$_2$O, DMAP, CH$_3$CN,rt; **iii**= Cs$_2$CO$_3$, dry CH$_3$CN; **iv**=NaOH , MeOH; **v**=EDC, DMAP, DCM, rt.[191] **B)** Synthesis of β-diketones starting from methyl-ketones; X=methyl, phenyl.[195]

3.5.2 Generation of libraries of 1*H*-pyrrole-2-carboxamides

Two large libraries of molecules were prepared starting from two pyrrolic cores differentially substituted at position 5. Considering some structures of

the previously developed pyrrole derivatives include an alkylic moiety,[192] a modification was its substitution with a bulky substituent as an aromatic ring. Also, the acidic group was functionalized to an amidic group. Two different cores were designed:

1) 5-methyl-1*H*-pyrrole-2-carboxamide
2) 5-phenyl-1*H*-pyrrole-2-carboxamide

Since the synthons of the synthetic method are methyl ketones and aromatic amines, commercially available reagents were used for the decoration of the scaffolds (Figure 52) using Combiglide.[112] Starting from the two cores and the prepared reagents, two final libraries were generated:

1) 4-aryl-5-methyl-*N*-aryl-1*H*-pyrrole-2-carboxamides
2) 4-aryl-*N*,5 diaryl-1*H*-pyrrole-2-carboxamides

each containing 11,312 compounds. To simplify, the two libraries are named respectively **D** and **E**. Again, LigPrep[123] calculation was performed for the addition of all the tautomers, stereoisomers and protonation states at physiological pH, and QikProp[110] for the estimation of pharmacokinetic parameters. Specific filters[117] were applied (see section 3.4.2) and the final libraries **D** and **E** were determined.
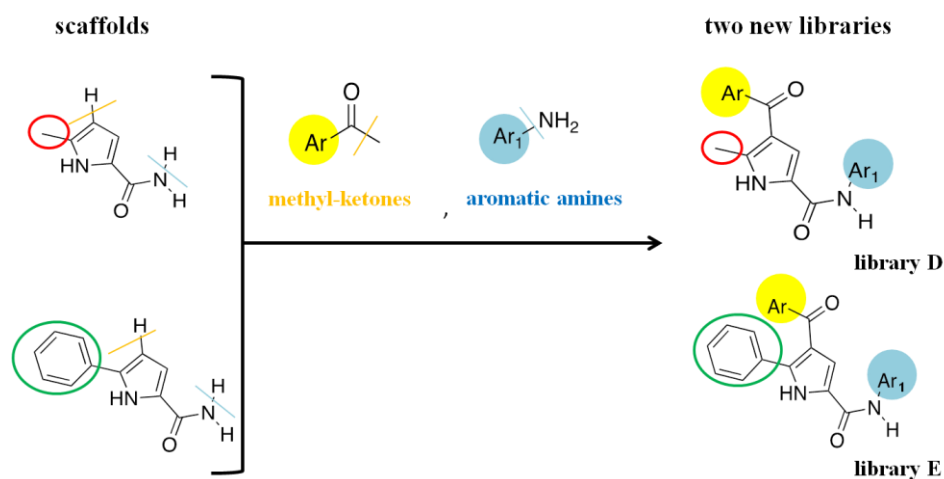
Figure 52 Generation of two libraries: **D**) 4-aryl-5-methyl-*N*-aryl-1*H*-pyrrole-2-carboxamides; **E**) 4-aryl-*N*,5 diaryl-1*H*-pyrrole-2-carboxamides.

3.5.3 Selection of the most promising 1*H*-pyrrole-2-carboxamide derivatives

An accurate analysis of the XP poses resulted from the screening, respectively 388 and 116 for the libraries of 5-methylpyrroles and 5-phenylpyrroles derivatives, led to the selection of a total number of 24 molecules from the first named library (**D**).

As expected, the phenyl at position 5 of library **E** induces a shift of the molecules into the binding site, and some fundamental interactions are missing, such as the hydrogen bonds with Gln 36_{chainC} and π-π interactions with His 53_{chainC} and Phe 44_{chainC} (Figure 53). Considering these aspects, the compounds belonging to this structural class have been excluded in the selection.
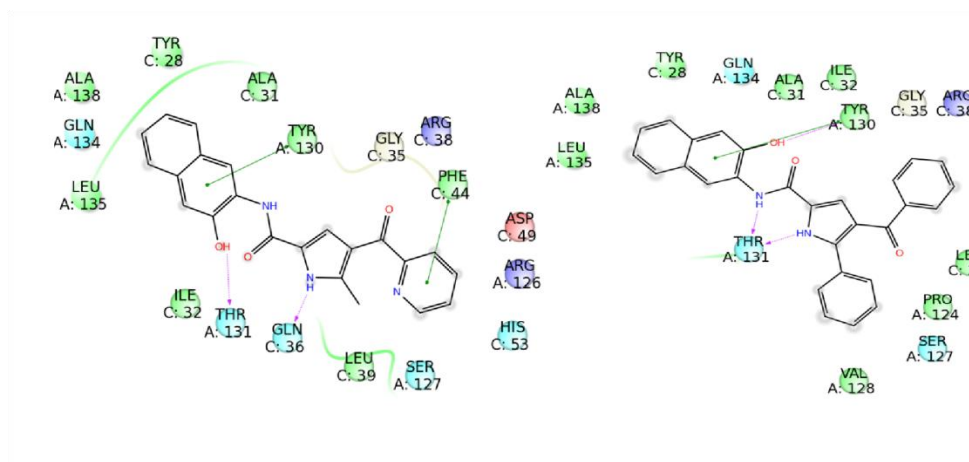
Figure 53 2D binding mode comparison of two similar compounds of libraries **D** and **E**.

Based on the chemical structure of the methyl ketone moiety, it is possible to classify the selected compounds in 4 different categories: benzofuran-methylketone, naphthalene methyl ketone, benzene or pyridine methyl ketone and pyrrole or furan methyl ketone derivatives.

All the molecules presented a value of binding energy in the range of (−8.5)–(−7.0) kcal/mol and demonstrated to be able to establish the key interactions with the receptor counterpart: in most of the compounds, the aromatic moiety deriving from the methyl ketone building block is involved in π-π interactions edge to face or face to face with His 53 $_{chainC}$ and Phe 44 $_{chainC}$, while the amidic moiety interacts by specific hydrogen bonds and other π-π interactions with Gln134$_{chainA}$, Tyr130$_{chainA}$, Thr131$_{chainA}$, Tyr28$_{chainC}$. For the pyrrole-methyl ketone derivatives, a hydrogen bond interaction of the nitrogen of the pyrrole moiety with Gln134 $_{chainA}$ induces an overturning in the binding site, and the π-π interaction is established with the aromatic ring of the amidic moiety. A representative 2D binding mode of a compound for each class is reported below.

101
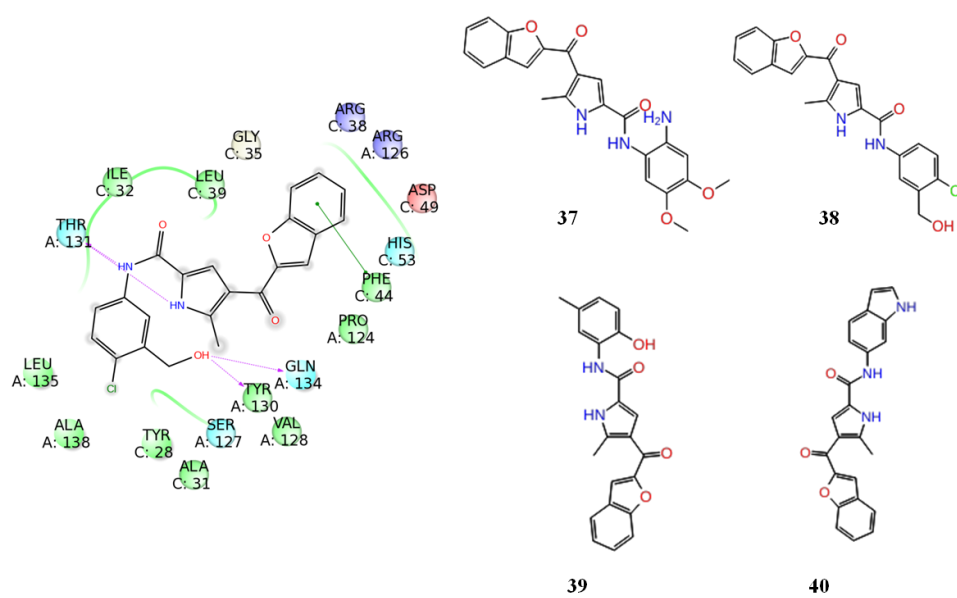
Figure 54 Benzofuran derivatives.
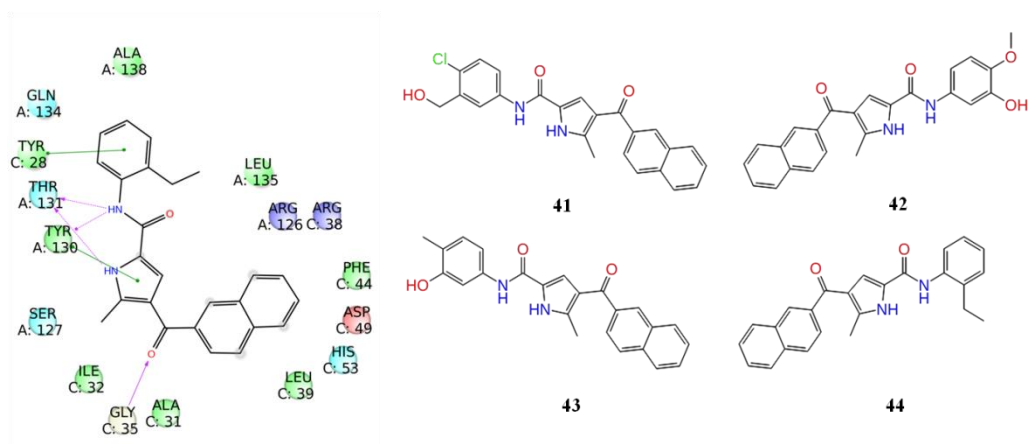
Figure 55 Naphthalene derivatives.

45

46

47

48

49

50

51

103
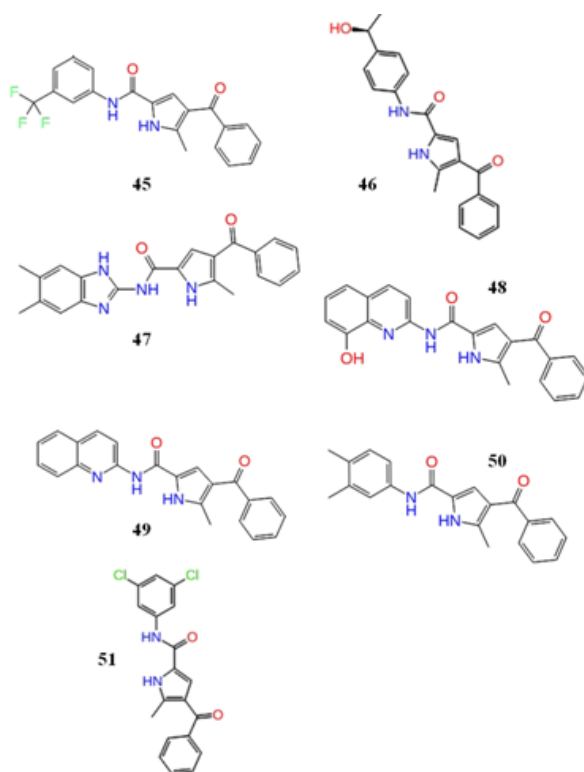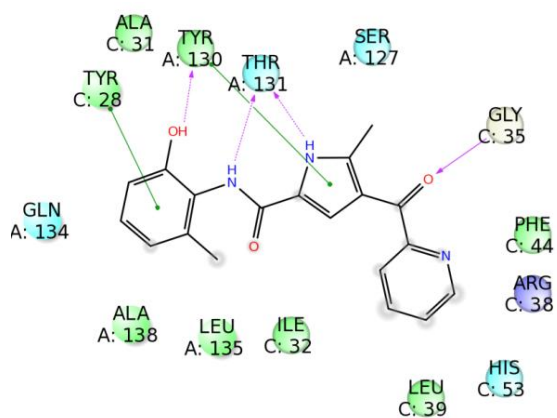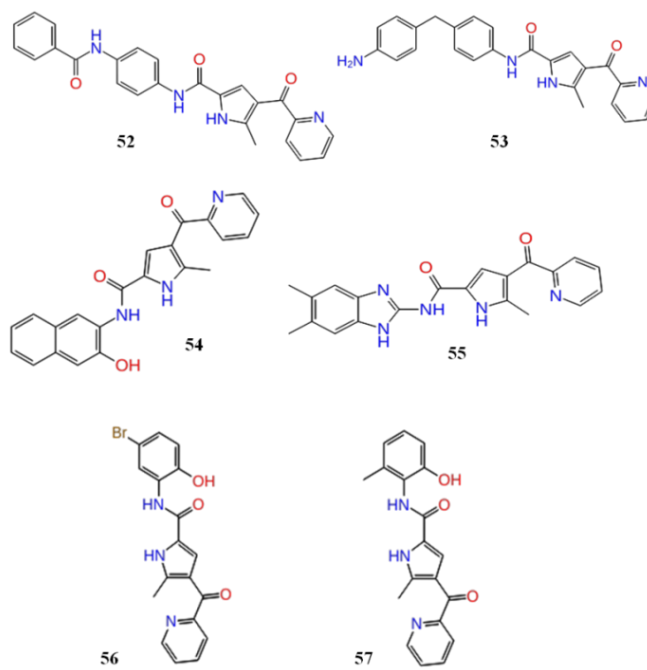
Figure 56 Phenyl-pyridil derivatives.
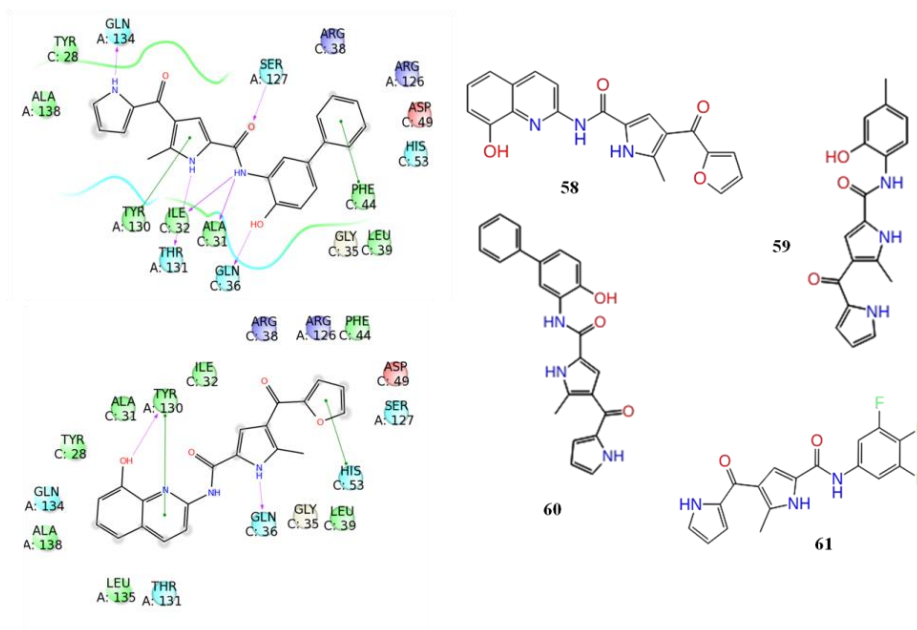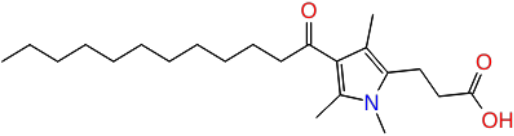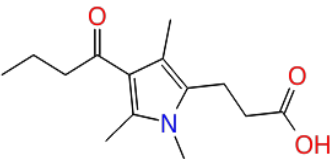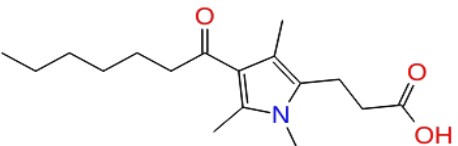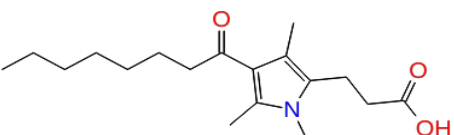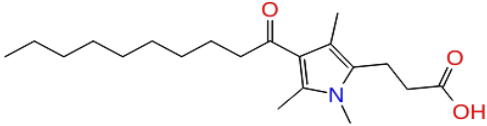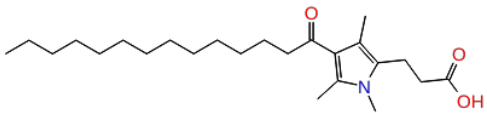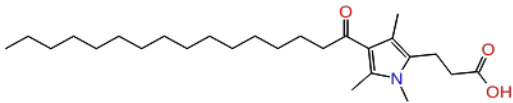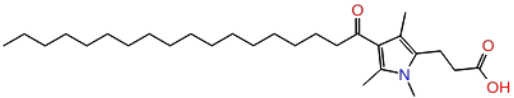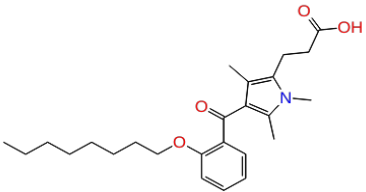
Figure 57 Heterocycles-based derivatives.

Finally, a binding mode comparison between the developed pyrroles alkanoic acid derivatives[192] and the compounds selected through virtual screening workflow was performed. The docked molecules are reported in Table 6. The analysis of the XP poses of the reported compounds showed a different binding mode compared to the designed compounds. Most of the interactions are focused in a lower region of the binding site, since the carboxylic group establishes hydrogen bonds with Arg38$_{chainC}$, Ala45$_{chainC}$, Asn46$_{chainC}$, Arg126$_{chainA}$. No overlapping with our selected molecules was observed.
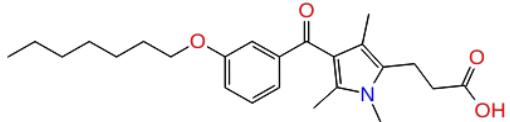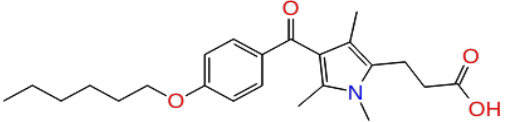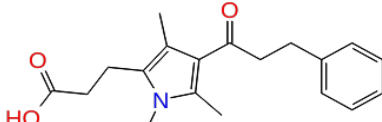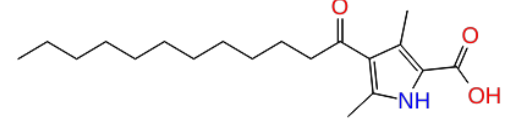
Reported compounds[192]	Inhibition of mPGES-1 from A549 cells at 3.3 µM [%]	Inhibition of human recombinant mPGES-1 at 1 µM [%]
X	74±8 (*n=5*)	54±8 (*n=7*)
XI	n.a.	n.a.
XII	n.a.	n.a.
XIII	55	n.a.

\n**XIV**	62	n.a.
\n**XV**	63	91
\n**XVI**	35	97
\n**XVII**	n.a.	97
\n**XVIII**	23	n.a.

107

 XIX	67	n.a.
 XX	64	32
 XXI	n.a	n.a.
 XXII	–	62

108
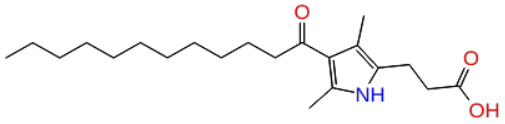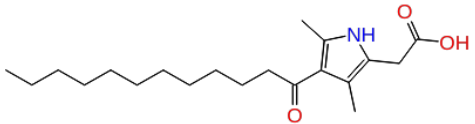
XXIII	–	38
XXIV	–	17

Table 6 Some reported pyrrole alkanoic acid derivatives and inhibitory activity on mPGES-1.[192]
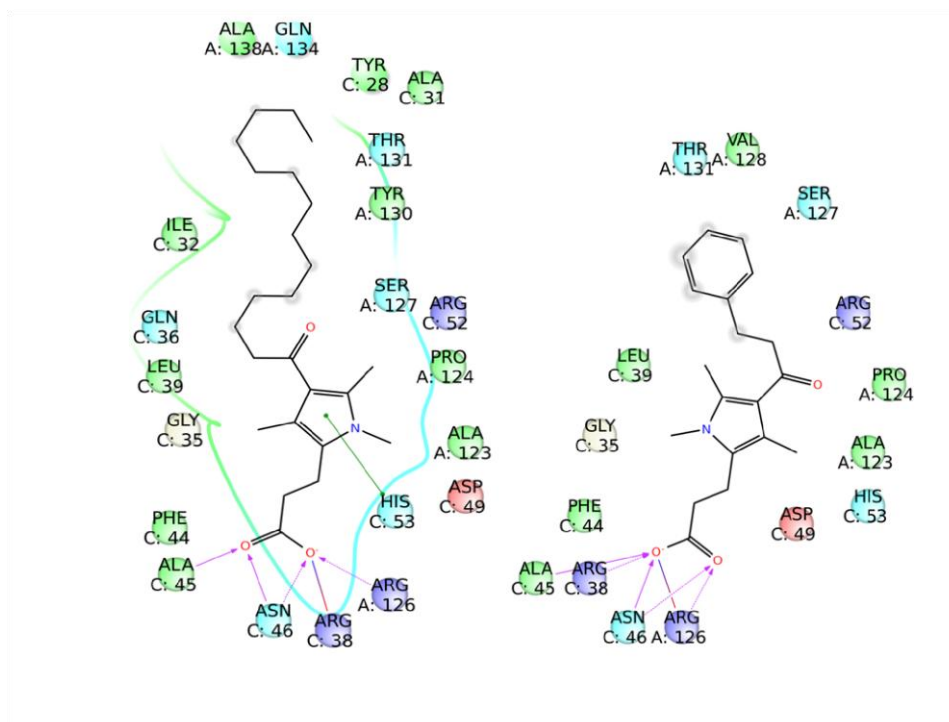
Figure 58 Representative examples of the binding mode of the reported pyrrole alkanoic derivatives.

3.5.3.1 PAINS screening

SwissADME[184] web tool was used for the individuation of chemical species belonging to "Pan-Assay Interference compounds" chemical class. Among compounds **37-61**, the pyridine derivative **53** did not pass the filter, since it was classified as belonging to PAINS. In light of this, 23 molecules were selected for the next step.

3.5.4 Synthesis of 2-carboxamide pyrrole derivatives

To date two among the 23 selected compounds have been synthesized in collaboration with Prof. Anna Ramunno (Figure 51). The applied synthetic strategy is previously reported. [191]

3.5.5 Biological evaluation of 2-carboxamide pyrrole derivatives

Compounds **45** and **47** were submitted to the cell-free assay.[170] Both of them showed inhibitory activity on mPGES-1, with a better result for the molecule bearing a dimethyl substituted benzene ring as amidic moiety ($IC_{50}=5.5\pm0.7$ μM).
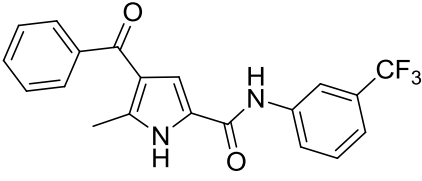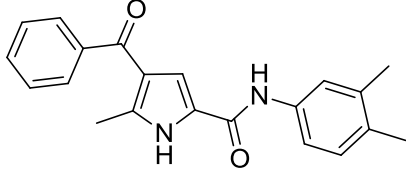
Compound	Structure	$IC_{50} \pm SD$ (μM)
45		>10 (75.0±5.3)
47		5.5±0.7

Table 7 IC_{50} values of compounds **45** and **47** in the cell-free assay.[170]

3.6 Application of the protocol with N-heterocycles

In conclusion, a set of saturated N-heterocycles cores was chosen since they are very common in the preparation of bioactive small molecules and are useful to overcome the limitations in solubility, pharmacokinetic parameters, and bioavailability of high-aromatic-ring-count.[196, 197]

111

Furthermore, since a biological evaluation of mPGES-1 inhibitory activity of saturated heterocycles presented positive response,[140] (Figure 59) it seems promising to consider this chemical class of molecules as building blocks of potential inhibitors of the enzyme. The co-crystallized ligand 6PW (Figure 59), in fact, co-complexed with a crystal structure of the human protein released in 2016 (PDB code: 5K0I)[140] is a 3,3-dimethyl substituted *N*-aryl piperidine, belonging to the saturated heterocyclic family. It presented an IC_{50} of 7 nM in an *ex vivo* human whole blood (HWB) assay. In addition, it showed no activity in human COX-1 or COX-2 assays at 30 µM and in the inhibition of mPGES-2 activity at 62.5 µM in a microsomal prep assay.[140]
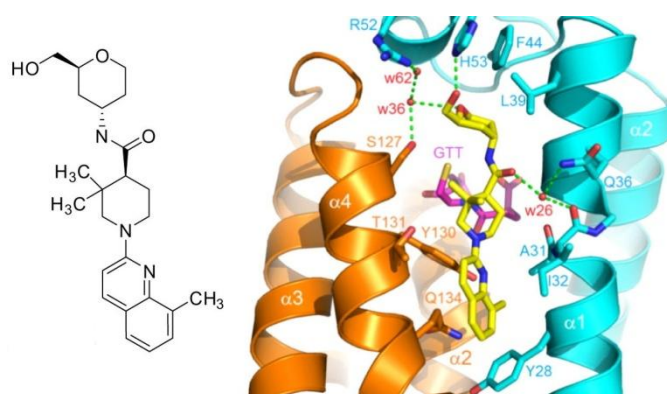
Figure 59 Ligand 6PW in the binding site of the X-ray structure of the human mPGES-1 (PDB code: 5K0I).[140]

According to these data, 4 different scaffolds were selected for our purposes: thiomorpholine, morpholine, piperazine, and ethyl thiomorpholine-3-carboxylate.

3.6.1 Synthetic strategy for thiomorpholine, morpholine, piperazine and ethyl thiomorpholine-3-carboxylate derivatives

Concerning the set of saturated heterocyclic scaffolds, the SnAP (Stannyl Amine Protocol) chemistry was selected as promising synthetic strategy. This approach was developed for the first time in 2013 from Jeffrey W. Bode et al.,[197] and it is considered a very useful synthetic tool.

Metal-catalyzed cross-coupling reactions have had a considerable role in organic chemistry in the last few decades. The application of cross-coupling synthetic strategies in the development of bioactive molecules induced the increase of aromatic-ring-count in the compounds, responsible for limitations such as solubility, pharmacokinetics and bioavailability. According to the considerations above, the use of saturated building blocks is getting privileged in the development of drug-like compounds (Figure 60), containing one or more heteroatoms.[197]
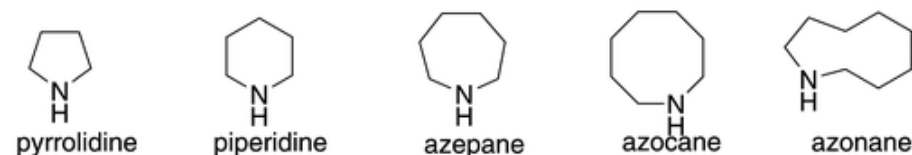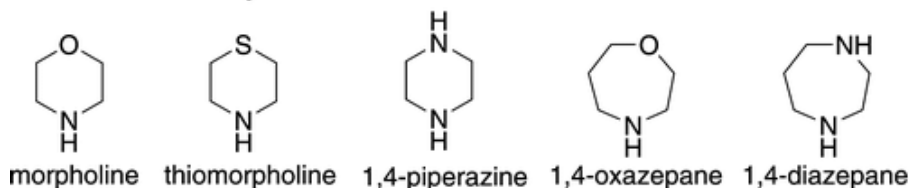
Figure 60 Saturated heterocycles building blocks used in medicinal chemistry.[198]

Most of the heterocycles are functionalized on the C-H bonds adjacent to nitrogen, due to their higher reactivity.[198] Different α-arylation of N-heterocycles have been proposed,[199-202] but a common difficulty of these reactions was the removal of N-aryl substituents. Herein, the proposed SnAP chemistry is a synthetic approach able to play a crucial role in the overcoming of the lacks of the previously studied mechanisms. In particular, the method leads to the direct formation of N-unprotected heterocycles, and the introduced substituents derive from stable and broadly commercially available functional groups in comparison to others. In detail, in the reaction are involved an aldehyde and an amino-tributylstannane (SnAP reagent) and consists of the formation of an imine bearing a pendant nucleophilic carbon, followed by an intramolecular radical cyclization.[197]
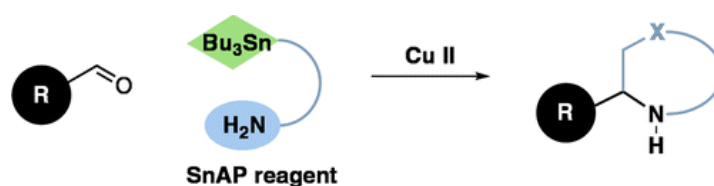
Figure 61 SnAP reaction; **X**=heteroatom.

Considering that in the intermolecular addition of organostannanes to *N*-phenyl imines reported by Kagoshima[203] a stoichiometric amount of $Cu(OTf)_2$ is used, the same was kept in the seeking of the most optimized conditions for the cyclization of the pre-formed imine. Different situations were explored, modifying the nature of the solvent, temperature and additive in the cyclization step of a fixed imine. In the end, the most promising conditions were:

➢ A mixture 4:1 CH_2Cl_2:HFIP (hexafluoroisopropanol) as solvent.

➢ Room temperature

➢ 2,6-lutidine as additive.
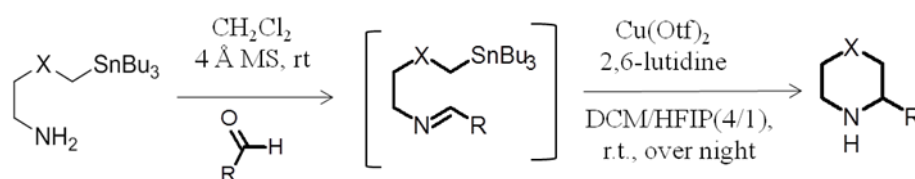
Figure 62 SnAP chemistry optimized conditions.

A general mechanism was also proposed and presented with experimental data. Kagoshima et al. proposed a role for the Cu^{II} as a Lewis acid in the nucleophilic addition of α-thioalkyl stannanes to *N*-phenyl or *N-para*-methoxyphenyl imines. Experimentally, other metal salts (such as $Zn(OTf)_2$ and $BF_3 \cdot OEt_2$) failed the cyclization, while the use of 2-pydirylaldehydes showed a poor reactivity although they could chelate Cu^{II}. Furthermore, with the addition of TEMPO (1.5 equiv.) in the reaction, no cyclization product was obtained, demonstrating the existence of a radicalic intermediate. In light of these considerations, it was hypothesized that Cu^{II} acts as an oxidant. Considering that organostannanes are able to form carbon-centered radicals under oxidative conditions, the mechanism below (Figure 63) was reported. [197]
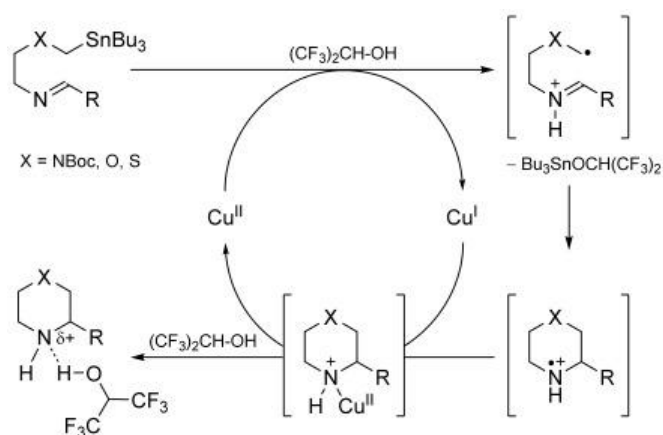
Figure 63 Proposed mechanism of SnAP chemistry.[196]

Iminotributylstannane is protonated in acidic conditions (HFIP). The one-electron oxidation with $Cu(OTf)_2$ gives Cu^I and the radical cation, which cyclizes with the intramolecular imine forming the radical cation, which is reduced by Cu^I.

The first reactions were performed using the Thiomorfoline SnAP reagent (SnAP-TM),[197] but the same approach was applied to others aminotributylstannanes belonging to the family of SnAP reagents, such as Morpholine (SnAP-M)[196, 204] and Piperazine (SnAP-PIP).[196, 204] Furthermore, more-substituted SnAP reagents were considered,[197] and bicyclic and spirocyclic.[205]
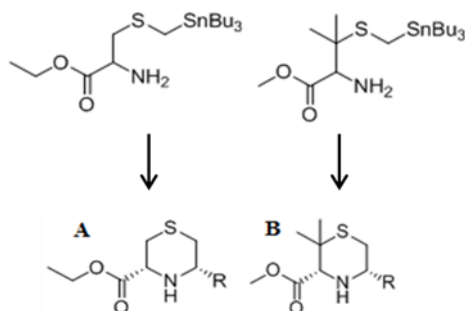
Figure 64 On the left, SnAP-Cys. On the right, SnAP-Pen, and the favored *cis*-products (**A**=SnAP-Cys, **B**=SnAP-Pen).

In particular, for the disubstituted SnAP-Cys and SnAP-Pen (Figure 64) was confirmed by X-ray crystallization a high diastereoselectivity (20:1) of the reaction for the *cis*-product, thermodynamically favored. [197]

Based on the considerations above, this is a widely efficient synthetic strategy for the generation of N-unprotected saturated heterocycles under mild conditions. For our purpose were considered Thiomorpholine (SnAP-TM), Morpholine (SnAP-M), Piperazine (SnAP-PIP) and ethyl thiomorpholine-3-carboxylate (SnAP-Cys).

3.6.2 Generation of libraries of thiomorpholine, morpholine, piperazine and ethyl thiomorpholine-3-carboxylate derivatives

Starting from the SnAP synthetic approach, morpholine, thiomorpholine, piperazine and ethyl thiomorpholine-3-carboxylate were decorated with commercially available aldehydes to obtain 4 final libraries of saturated N-heterocyclic derivatives. After the application of the filters mentioned above, the molecules which were undergone to docking analysis were 13,625 for the

morpholine, 13,625 for thiomorpholine and 26,578 for piperazine, 14,182 for ethyl thiomorpholine-3-carboxylate scaffolds.
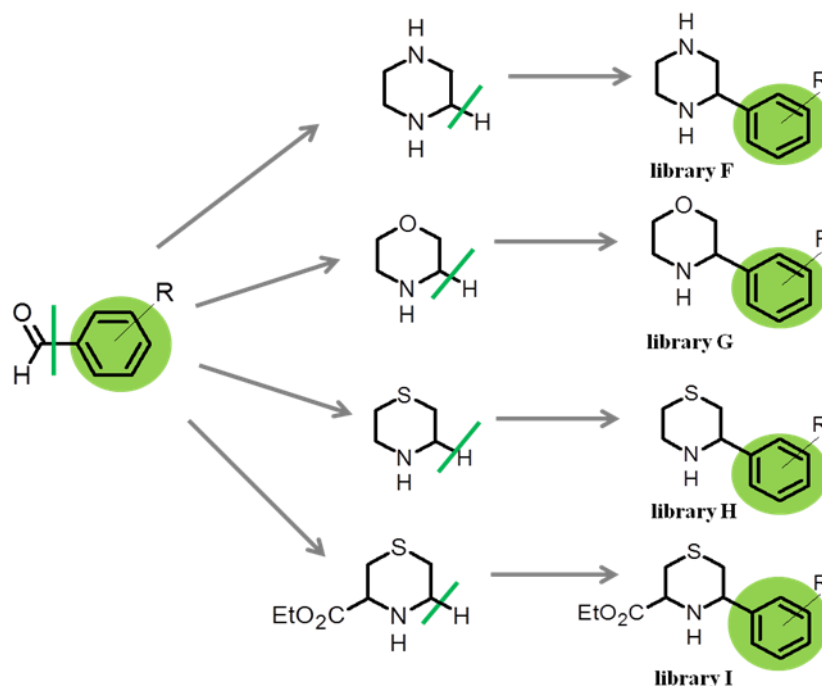
Figure 65 Generation of 4 libraries: **F)** Piperazine derivatives; **G)** Morpholine derivatives; **H)** Thiomorpholine derivatives; **I)** ethyl thiomorpholine-3-carboxylate derivatives.

3.6.3 Selection of the most promising thiomorpholine, morpholine, piperazine and ethyl thiomorpholine-3-carboxylate derivatives

In total, 17 SnAP-molecules have been selected from the 4 libraries for the synthesis (Figure 66), basing on a detailed *in silico* analysis of the binding mode and the interactions in the active site of the crystal structure of the enzyme. In particular, according to the small size of the scaffold compared to the other cores explored in this thesis, compounds bearing high molecular

weight aldehydic substituents presented the most promising results. All the selected compounds, in fact, center the binding site interacting with most of the key amino acids. In details, their saturated heterocyclic moiety establishes specific hydrogen bonds with $Gln134_{chainC}$, $Tyr28_{chainA}$, $Tyr130_{chainC}$. Moreover, a further binding mode is observed among the poses, in which the heterocyclic scaffold is oriented along the cytoplasmic region (section 3.1.1) and interacts by hydrogen bonds with $Ser127_{chainC}$ and $Arg52_{chainA}$ (see Figure 68). Interestingly, SnAP-Cys derivatives bearing the ethyl-ester group at position 3 interact by specific hydrogen bonds with the receptor counterpart, established between the ethyl-carboxylate moiety and $Arg52_{chainA,}$ $Ser127_{chainC}$ and $Arg126_{chainC}$ residues. Also, this class of selected compounds present a good superimposition with the co-crystallized 6PW inhibitor[140] (Figure 69). An advantage of the use of this specific scaffold is the possibility of a functionalization, for instance with commercially available aromatic amines.

Considering the susceptibility of the ester group to hydrolysis, a further docking analysis was performed on the acid analogues of the selected molecules. Specifically, 4 hydrolyzed compounds (Figure 67) are able to reproduce a similar binding mode onto the crystal structure of the enzyme, retaining the specific interactions reported above. Thus, in order to investigate the inhibitory activity on mPGES-1 of the acid analogues and to compare them with the biological results deriving from the assays performed on the esters, the 4 promising compounds were selected for the synthesis. In conclusion, 21 SnAP-molecules entered the next synthetic step.
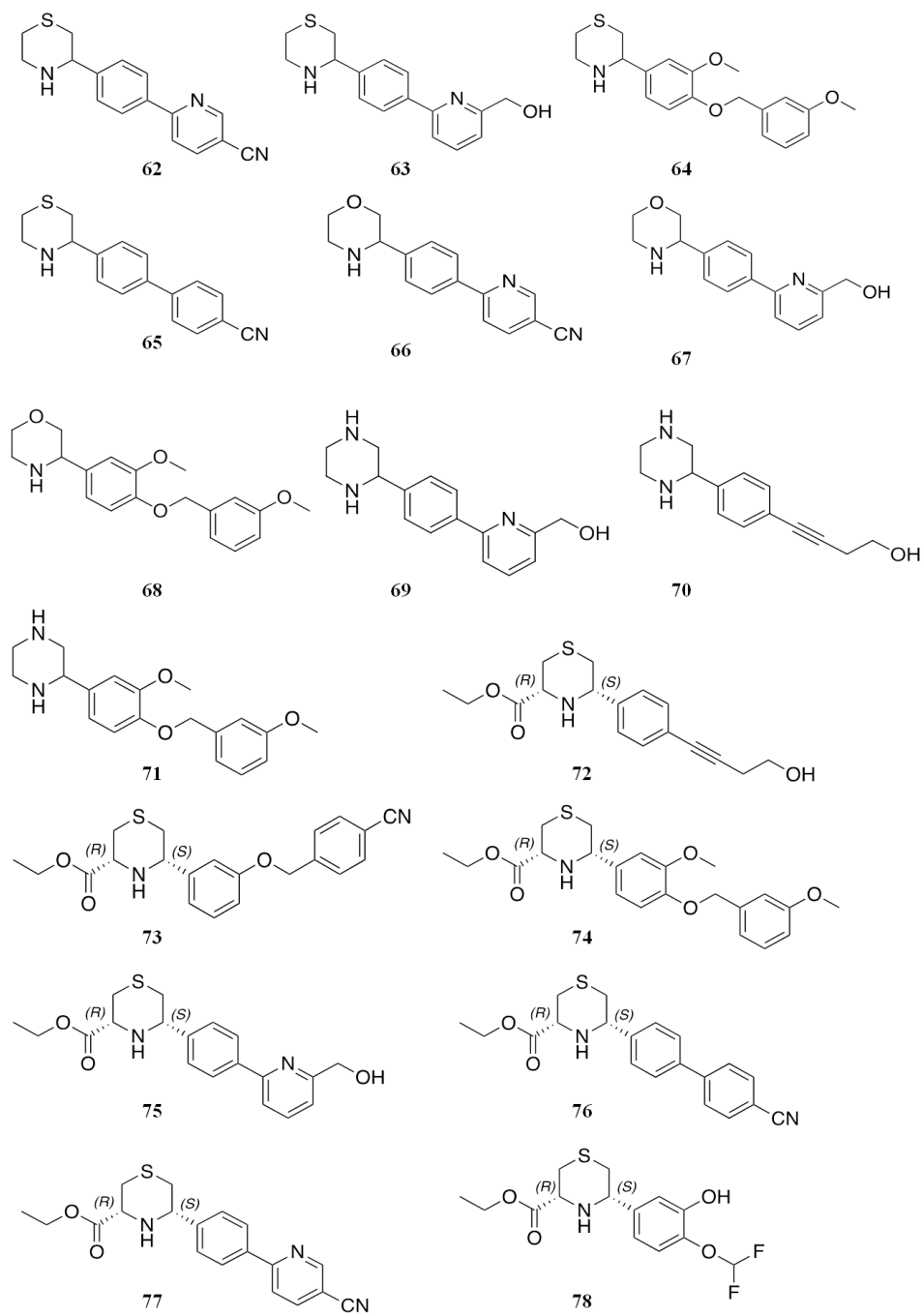
Figure 66 Selected SnAP-molecules.

120
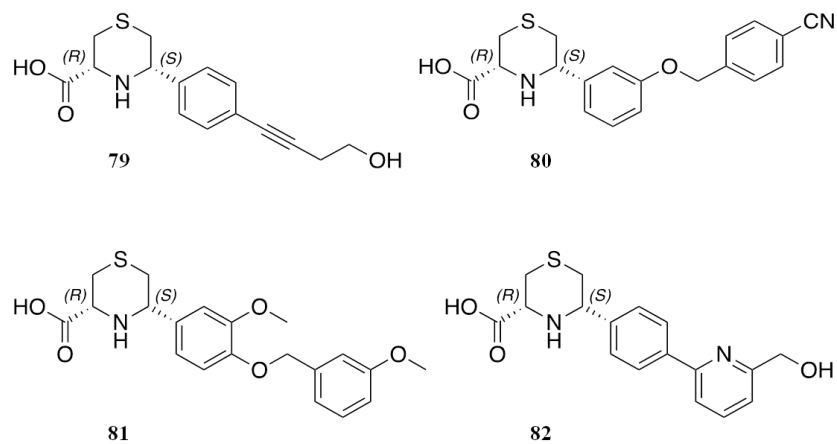
Figure 67 Selected acidic analogues.
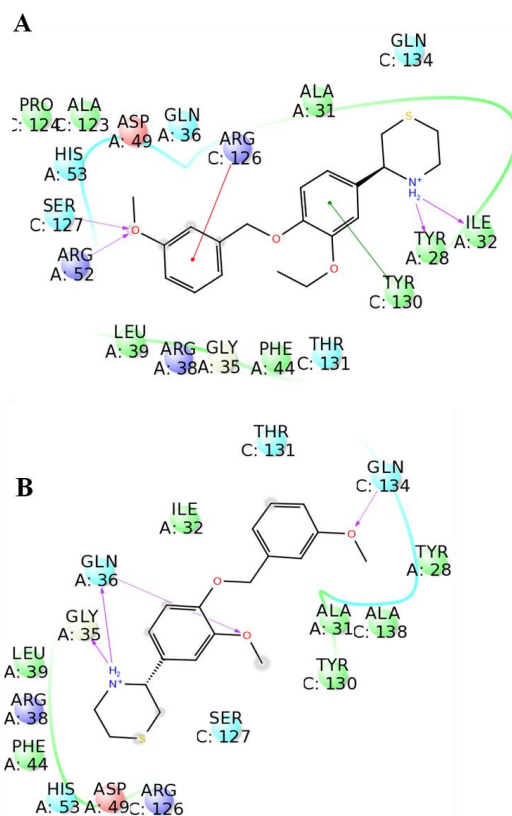
Figure 68 Two different binding modes (**A** and **B**) of compound **64.**
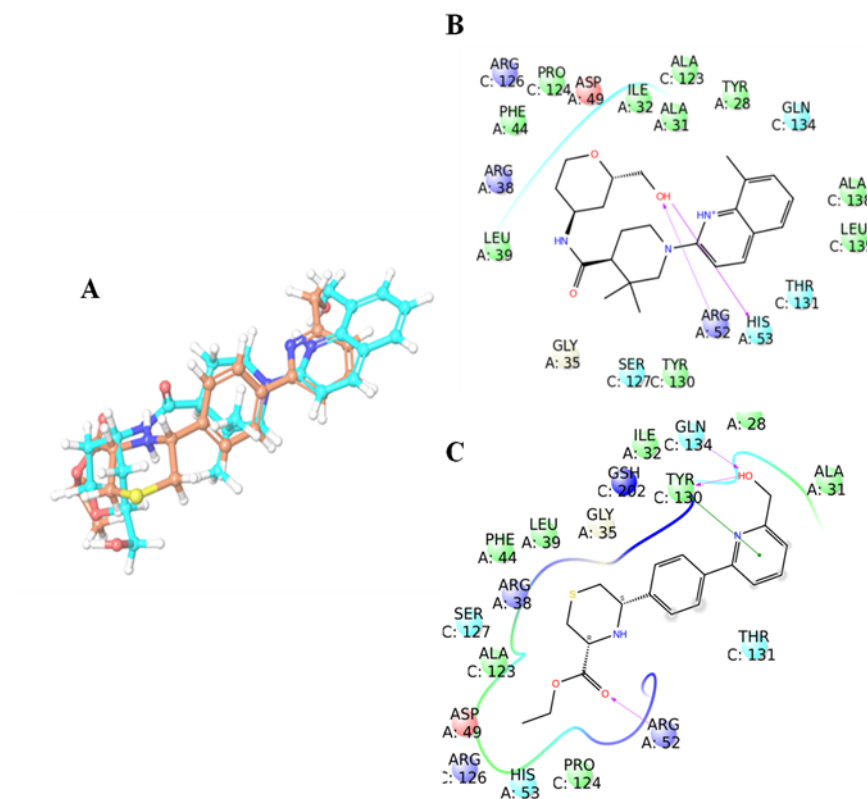
Figure 69 A) 3D superimposition of the co-crystallized ligand 6PW[140] (colored in light blue) and the selected compound (colored in pink); **B)** 2D representation of 6PW inhibitor in the binding site of mPGES-1; **C)** 2D representation of the 3D reported selected molecule in the binding site of mPGES-1.

3.6.3.1 PAINS screening

Each selected compound was submitted to SwissADME[184] analysis, with the purpose of identifying possible PAINS moieties in the structures. Compounds **62-82** passed the filter in this preliminary phase.

3.6.4 Synthesis of saturated N-heterocycles

The synthesis of the selected N-heterocycles was performed using the above described SnAP chemistry.[197-202] The whole synthetic project was carried out in the research group of the author of this approach, Prof. Jeffrey W. Bode, at the Department of Chemistry and Applied Biosciences of ETH. In the last few years, the group has had a lot of experience with SnAP chemistry, reaching important results that confirmed the versatility and utility of the chemistry in a broad range of applications. For the synthesis, the thiomorpholine (TM), morpholine (M), piperazine (PIP) and ethyl thiomorpholine-3-carboxylate (Cys) SnAP reagents were used as starting materials. The first three were synthesized previously in the group, while SnAP-Cys was synthesized by a one-step reaction[197] starting from tributyl(iodomethyl)stannane.[206] In the synthesis of SnAP-Cys reagent was performed a substitution reaction on tributyl(iodomethyl)stannane with L-ethyl-cysteine. In detail, an ethanol-water solution of tributyl(iodomethyl)stannane (**83**) and L-ethyl-cysteine hydrochloride (**84**) was stirred and refluxed at 70 °C for 4 hours in the presence of K_2CO_3. Purification via flash chromatography gave compound **85** (Figure 70).
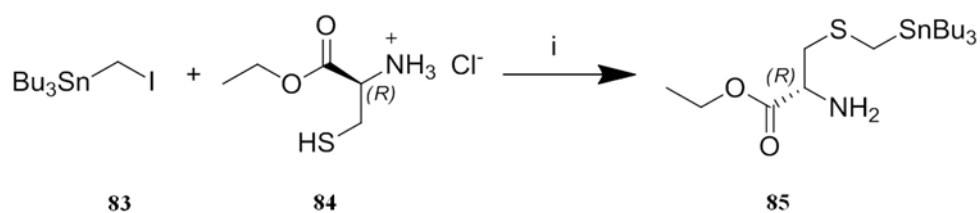
Figure 70 Synthesis of ethyl 2-amino-3-(((tributylstannyl)methyl)thio)propanoate; **i**: K_2CO_3, 4:1 EtOH:H_2O, 70°C, 4 hours.

For the synthesis of compounds **62-78** the optimized SnAP chemistry conditions were applied in the performance of the two steps reaction.

The imine formation was carried out between the amino group of the tributylaminostannane (SnAP reagent) and the proper aldehyde in dry CH_2Cl_2 in presence of 4Å MS, stirring overnight at room temperature. A filtration of the mixture through a short layer of Celite afforded the pure imine products. For the cyclization step, a suspension of anhydrous $Cu(OTf)_2$ in HFIP was prepared, and 2,6-lutidine was added in one portion. Then, a solution of the imine intermediate in CH_2Cl_2 was added to obtain a final solution 4:1 DCM:HFIP, and the resulting mixture was stirred overnight at room temperature. Schlenk techniques were applied to all reactions.

2,6-lutidine, copper triflate and HFIP suspension   **Cyclization reaction**   **Addition of 10% NH_4OH aqueous solution**
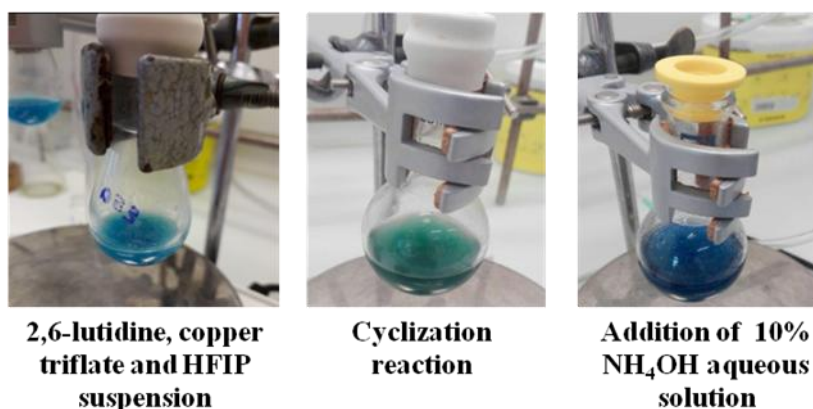
Figure 71 Application of SnAP chemistry.

Boc protective group of SnAP-PIP is useful to avoid the imine formation on the amine group close to tributyl stannyl moiety. Thus, the synthesis of SnAP products **69-71** required a third deprotection step, which was carried out using

a mixture 1:1 TFA:DCM (Figure 72). After work-up and purification, the final products were obtained with >98% purity.
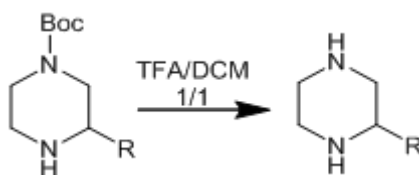
Figure 72 Deprotection of SnAP-PIP derivatives.

Also, for the synthesis of the acid analogues **79-82**, the hydrolysis of compounds **72-75** was performed, using a mixture 10% NaOH solution (50%) and CH_3OH (50%).
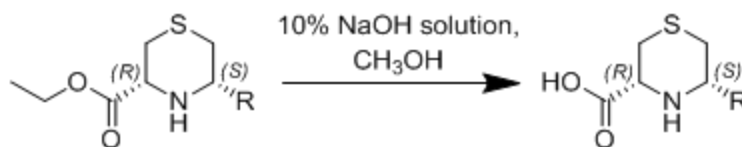
Figure 73 Synthesis of compounds **79-82.**

Some reactions were tried with electron-rich aldehydes, but because of their limited reactivity the imine formation was not complete, showing 50% of aldehyde by ^1H NMR analysis. An increase of the temperature gave an improvement of the yields, avoiding the use of carbonyl group activants such as titanium isopropoxide. This is the example of the imine precursor of compounds **64**, **71** and **74**, whose aldehyde is the 3-methoxy-4-((3-methoxybenzyl)oxy)benzaldehyde.
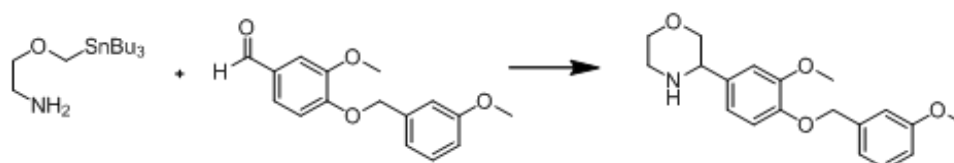
Figure 74 Failed synthesis of compound **68.**

Regarding the synthesis of compound **68**, (Figure 74) which involves the mentioned aldehyde and the SnAP-M (morpholine), it was possible to identify the signals of the product by ^{1}H NMR analysis carried out on the crude of the reaction. Purification by flash column chromatography did not afford the product. Again, the reaction was performed applying the same general conditions and a variation in the purification step. Silica column, in fact, was replaced with a small column of propyl sulfonic acid supported on silica (SCX$_2$), but the product was not isolated.
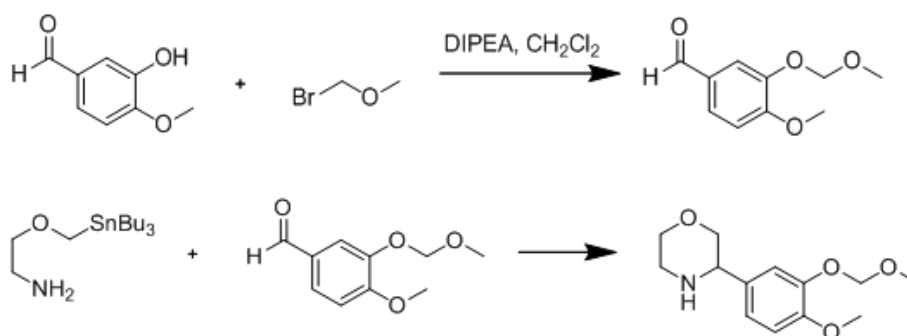
Figure 75 Test reaction.

In addition, in order to further investigate SnAP chemistry limitations, test reactions were carried out with SnAP-M (morpholine). Experimentally, the SnAP reactions with adehydes bearing cathecol did not work. Thus, the

126

reaction with –MOM (methoxymethyl) protected vanillin (Figure 75) was carried out, in order to analyze the reaction with less bulky substituent in comparison to compound **68**. Also in this case, the reaction did not work. Therefore, among the SnAP reagents used for the synthesis of promising mPGES-1 inhibitors, the use of SnAP-M presented more problems from a synthetic point of view, especially when combined with electron-rich aldehydes.

Other limitations included the purification of the crudes. Generally, flash chromatography was performed, using different mixtures of hexane-ethyl acetate as eluent and a solution 0.1% Et_3N in the solvent mixture was prepared for the most polar compounds. In many cases, traces of Tin were identified. For the removal of Tin, the product was dissolved in acetonitrile and washed with hexane. Traces of aldehyde (2-5%) in the product after flash chromatography were removed using SCX_2 for not basic aldehydes.

In conclusion, the SnAP chemistry was useful to synthesize most of the desired compounds, but with different yields based on the nature of the aldehyde moiety.

3.7 Generation of a database of compounds starting from the SnAP chemistry

The versatility and applicability of SnAP chemistry gave inspiration for the preparation of a database of synthetically accessible compounds.

Developments of the SnAP chemistry[197, 198] led to the generation of iSnAP (Iterative Stannyl Amine Protocol) reagents (Figure 76), organostannanes bearing ketones or amine groups potentially useful for further functionalization. Practically, a reductive amination on the ketone could be

carried out, or a substitution reaction of alkyl or acyl halides could be performed by the amino group. In this specific case, the synthetic route selected for the generation of the database is as follows:

1) The application of the classic SnAP chemistry between the involved amino-organostannane and the aldehyde;

2) Substitution reaction of acyl or alkyl halides on the amino group;

Therefore, the multi-step computational protocol was applied for the generation of the database. Starting from a library of 33 iSnAP-scaffolds, all possible diastereoisomers were generated for each item and a total of 98 scaffolds were prepared. At the same time, two large libraries of commercially available aldehydes and alkyl/acyl halides were divided into clusters according to 2D ligand properties, and for each class a representative reagent was selected.[207, 208] After this filtration, 129 aldehydes and 97 halides were selected for the next steps. Herein, using a combinatorial chemistry approach, the main tool of this research work, 98 iSnAP-molecules libraries were generated combining each scaffold with the aldehydes and the halides. A small sub-library of about 20,000 compounds was built for each isomer, considering all possible tautomers and protonation states at physiological pH. After the application of various filters, a database of 1,277,744 drug-like molecules synthesizable using SnAP chemistry was obtained, which can be subjected to virtual screening on biological targets. As proof of concept, virtual screening workflow was performed onto the crystal structure of mPGES-1 (PDB code: 4YL0),[133] and 38 molecules were selected. In details, 15 of the 98 iSnAP-scaffolds involved in the calculation showed promising results on the enzyme in the *in silico* docking analysis. Similar studies may be applied for the

individuation of iSnAP-derivatives in the database potentially able to interfere with the activity of pharmacologically interesting targets.

The structures of iSnAP-cores and the selected compounds are not reported in this thesis, as they have not yet been published.
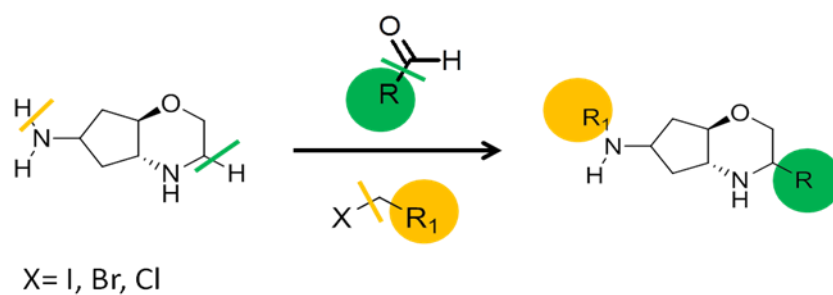
Figure 76 iSnAP reagents and generation of the database.

-CHAPTER 4-

A new multi-step computational protocol: discovery of novel 3-hydroxy 3-pyrrolin-2-one derivatives as mPGES-1 inhibitors

4.1 Multi-step computational protocol

Another computational protocol (Figure 77) adopted for the discovery of novel mPGES-1 inhibitors involved both ligand and structure based methods. A library of molecules containing 310,657 compounds, commercially available in Otava Ltd. (www.otavachemicals.com) and endowed with high chemical variability, was selected for the computational processes. The library above consists of both small fragments and high in weight compounds (16 Da ≤ molecular weight (MW) ≤ 1307 Da), presenting a broad range of hydrogen bond donors (HBD) and acceptors (HBA) (0 ≤ HBD ≤ 8; 0 ≤ HBA ≤ 16). Herein, the high degree of promiscuity is certainly useful for the individuation of new hits.

In the next sections, a detailed description of each step of the applied workflow is reported (Figure 77).
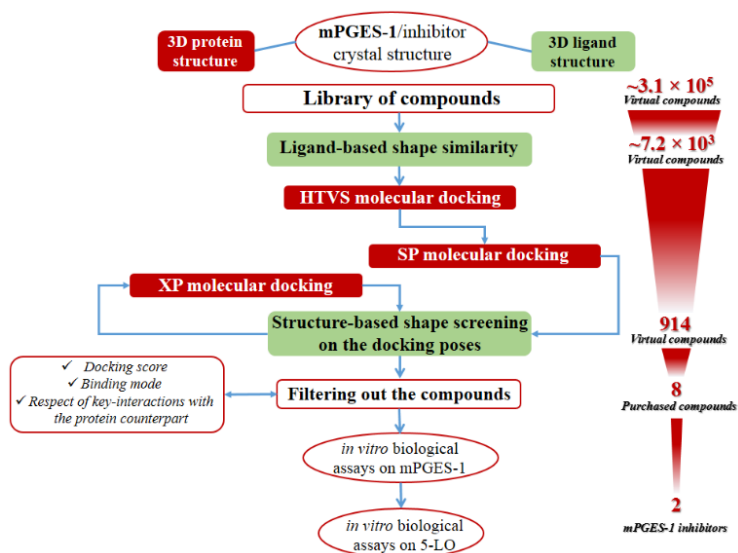
Figure 77 Protocol applied for the identification of the novel mPGES-1 inhibitors.

4.1.1 Ligand-based shape similarity screening

The starting library of compounds was obtained from the Otava Chemicals database. In order to reduce the number of the molecules, a preliminary analysis was carried out for the selection of the best candidates for the molecular docking experiments. The known potent inhibitor LVJ, co-crystallized in the crystal structure with the PDB code 4BPM[209], was chosen for a shape alignment study. Briefly, using a free conformational sampling for the alignment, the chemical shape of every molecule was compared to that of LVJ (Phase software, Schrodinger, LLC)[210]. This analysis stemmed from the demonstration, in several virtual screening studies,[211, 212] that similar molecules could bind the receptor counterpart in a similar way, thus showing a similar binding mode. In details, two steps can be distinct: conformational search and alignment of the resulting conformers with LVJ reference compound, calculating the similarity with the arithmetical parameter "shape similarity". The sampling was performed allowing the conformers around the amide bond to vary freely, and finally, 1000 maximum number of conformers were considered for the shape analysis. The shape similarity value can shift from 0 (no overlap between screened and reference compound) to 1 (all the atom overlap perfectly). Based on it, a ranking from the best to worst values was obtained, and a threshold of 0.627 was chosen reducing of 0.100 the best value (0.727).

After the application of this filter, the number of molecules was reduced to 7,220 items. Here, the new library featured only the most promising compounds, showing intrinsic conformational and pharmacophoric features, with high compatibility with LVJ reference compound.

4.1.2 Molecular docking and structure-based shape similarity screening

The 7,220 compounds were prepared using LigPrep software (Schrodinger Suite).[213] All the possible stereoisomers, tautomers, and protonation states at pH=7.4±1.0 were generated for each compound, and an energetic minimization was performed using OPLS 2005 force field.

Structure-based molecular docking experiments were carried out on the 3D crystal structure of mPGES-1 (PDB code: 4BPM), using Glide software[214].

In particular, the High-Throughput Virtual Screening (HTVS) was used for the first analysis. A maximum of 10 poses for each compound was generated, and a ranking based on docking score value was established. The first 10,000 ranked poses were selected, corresponding to 4546 different compounds. The second set of docking experiments provided the Standard Precision (SP) Glide precision mode. A maximum number of 10 poses for each of the 4,546 compounds was identified, and each of them was submitted to an "in place" shape screening against LVJ. This study is a shape comparison between the structure-based docking poses and the LVJ pose co-crystallized with the protein. Thus, in this case the shape similarity is performed on predefined poses of the molecules, and not on different conformers. The choice of a threshold of 0.400 led to the selection of 4,120 compounds. The third and last docking round was the Extra-Precision (XP) Glide mode which is more accurate in comparison to the SP mode for both sampling and scoring. A number of 100 maximum poses for each compound was saved and the "in place" shape similarity with the LVJ co-crystallized structure was performed. Considering a threshold of 0.500, 914 final molecules were selected for the next steps.

4.1.3 Evaluation of the key interactions

Starting from the selected promising molecules, presenting an elevated shape similarity to LVJ co-crystallized pose after docking experiments, an evaluation of the binding mode was useful to deeply screen the best items for the biological assays. A visual analysis of the key interactions in the presence of the cofactor was performed, in order to confirm the respect of those established between the reference compound and the receptor counterpart.

In details, the set of optimal interactions includes:

➢ edge-to-face π-π interaction with Phe44 and/or His53 of chain C;
➢ contacts with Pro124, Thr131 of chain A and with Asp49 of chain C;
➢ interactions with Tyr130 of chain A (hydrogen bonds or edge to face π-π contacts), which interacts with glutathione co-factor;
➢ contacts with glutathione.

As a result of this study, 296 poses were selected, corresponding to a total of 50 compounds.

4.1.4 Pan-Assay Interference compounds (PAINS) screening

A further evaluation of the 50 selected compounds was provided. SwissADME[184] web tool (section 3.4.3.1) was used in order to evaluate the presence of chemical moieties belonging to "Pan-Assay Interference Compounds" (PAINS) chemical class. The application of this added filter along with the preservation of the chemical variability and the optimal XP GlideScore value (Table 8) led to the selection of 8 final promising

compounds, that were subjected to biological assays with the goal of confirming the *in silico* predictions.

4.1.5 Biological assessment of mPGES-1 and 5-LO inhibition

The cell-free assay described above, which provides the use of the microsomal fractions of IL-1β-treated A549 cells (as source for mPGES-1), [170] was applied to demonstrate the ability of compounds **86-93** (Table 8) to interfere with the activity of mPGES-1.

In a first screening campaign, a solution 10 μM of each compound in DMSO was prepared for the biological test. From the preliminary results, the most promising compounds were those bearing a 3-hydroxy-3-pyrrolin-2-one (**87** and **88**), as presented from ~70 up to ~80% of mPGES-1 inhibition activity. Since this chemical core is endowed with a broad spectrum of biological activities (for instance anticancer and antiviral) and several chemical strategies have been reported for the synthesis of derivatives using multi-component reactions, the identification of these novel hits provided the foundations for the generation of new promising analogues in an optimization campaign. [215-217]

Also, compounds **90** and **93** showed a moderated activity, with a percentage from ~30 up to ~40% of inhibition activity. In light of this, additional investigations are helpful for the identification of the minimal pharmacophoric moieties in order to provide more potent derivatives.

A further investigation of the activity of compounds **87** and **88** afforded the determination of the IC_{50} values. Both the compounds are able to inhibit the activity of mPGES-1 in the low micromolar range (IC_{50} = 3.7± 2.7 μM for **87**; 1.9± 1.5 μM for **88**). In order to evaluate their selectivity, the two compounds

were tested at 10 μM concentration against 5-LO, another key enzyme involved in the AA cascade,[218] since a dual inhibition activity of both mPGES-1 and 5-LO was demonstrated for several kinds of compounds. From the results, compound **87** presented no inhibitory activity, while a modest inhibition was performed by compound **88** (See Table 8).

4.2 Analysis of the binding mode of compounds 87 and 88

The 3D representation of molecular docking poses of compounds **87** and **88** define their good accommodation onto the mPGES-1 binding site. Both of them establish specific hydrogen bonds and polar interactions with $Gln36_{chainC}$ by means of the 2-keto-3-hydroxy moiety, and the fundamental π-π interactions between $Tyr130_{chainA}$ and the aromatic ring of the keto-portion at position 4 of the pyrroline-based scaffold are noteworthy. Furthermore, it is important to highlight a variable set of interactions with the key amino acids: polar interactions with $Asp49_{chainA}$, $Ser127_{chainA}$, $Thr131_{chainA}$, $Arg38_{chainC}$, $His53_{chainC}$, H-bonds with $Ser127_{chainA}$, $Thr131_{chainA}$, $Arg52_{chainC}$, and π-π and π-cation contacts with $Phe44_{chainC}$, $His53_{chainC}$, $Arg52_{chainC}$ (docking poses featuring the highest shape similarity with LVJ reported in Figure 79 and 80).
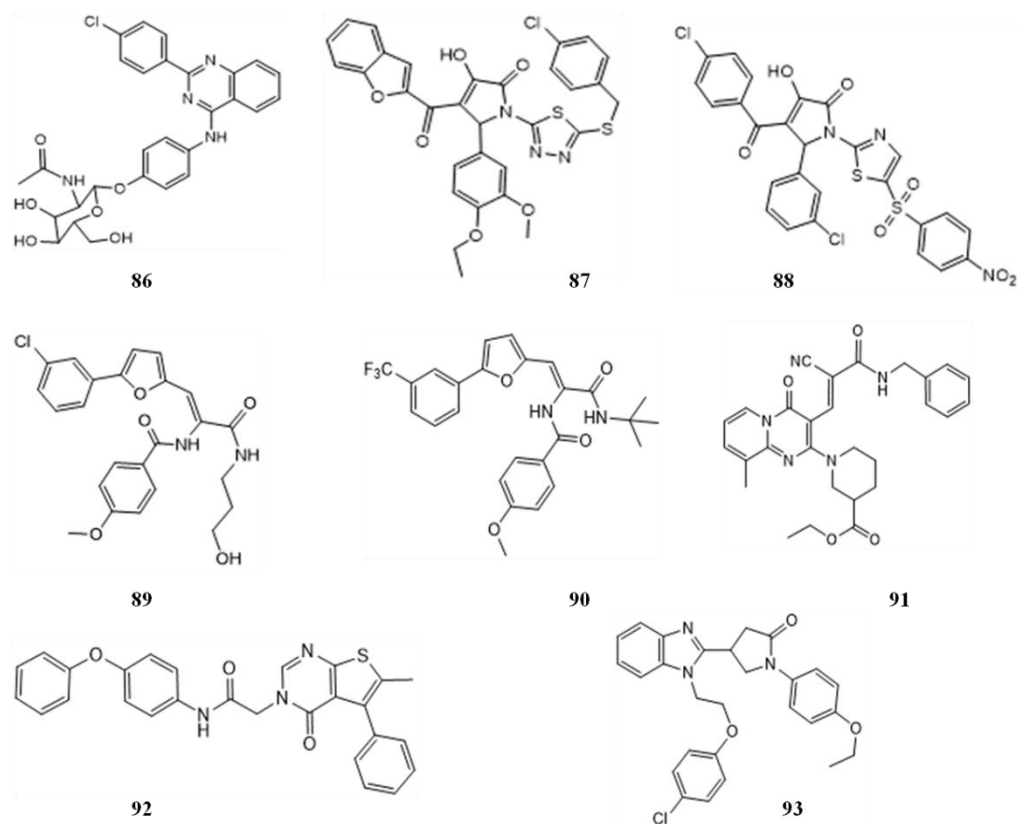
Figure 78 Chemical structures of compounds **86-93.**

ID	Glide XP Score	LVJ shape similarity	mPGES-1 (residual activity at 10 μM)	mPGES-1 IC$_{50}$ (μM)	5-LO (residual activity at 10 μM)
86	-7.462	0.506	80.1 ± 3.9	-	-
87	-6.494	0.585	30. 5 ± 3.4	3.7± 2.7	92.5 ± 10.0
88	-6.406	0.538	25.0 ± 6.5	1.9± 1.5	56.6 ± 8.5
89	-6.323	0.657	86.8 ± 4.2	-	-
90	-6.284	0.660	72.1 ± 4.1	-	-
91	-6.241	0.517	88.6 ± 3.7	-	-

92	-6.193	0.515	82.6 ± 2.4	-	-
93	-6.155	0.507	65.3 ± 11.1	-	-

Table 8 Glide XP Score, best shape similarity value (related to LVJ reference crystallized conformation), mPGES-1 and 5-LO residual activities tested at 10 μM ligand concentration, and mPGES-1 IC_{50} values of compounds **86-93.**
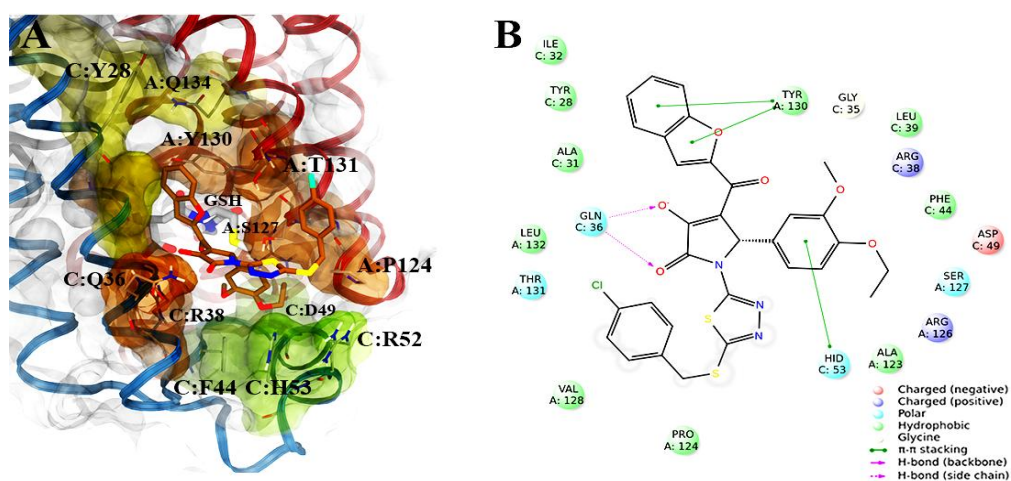
Figure 79 A) Selected 3D pose of **87** (colored by atom types: C, ochre; N, blue; O, red; S, yellow; polar H, light grey; Cl, light green) featuring the highest shape similarity to **LVJ**, in docking with mPGES-1 (chains A, B and C depicted in red, black, and blue ribbons, transparent molecular surface on the binding site colored in yellow, orange, and green, see text for details, glutathione (GSH) cofactor and key residues in the mPGES-1 binding site are represented in sticks, C grey, O red, N, blue, polar H white); **B)** related two-dimensional panels representing interactions.
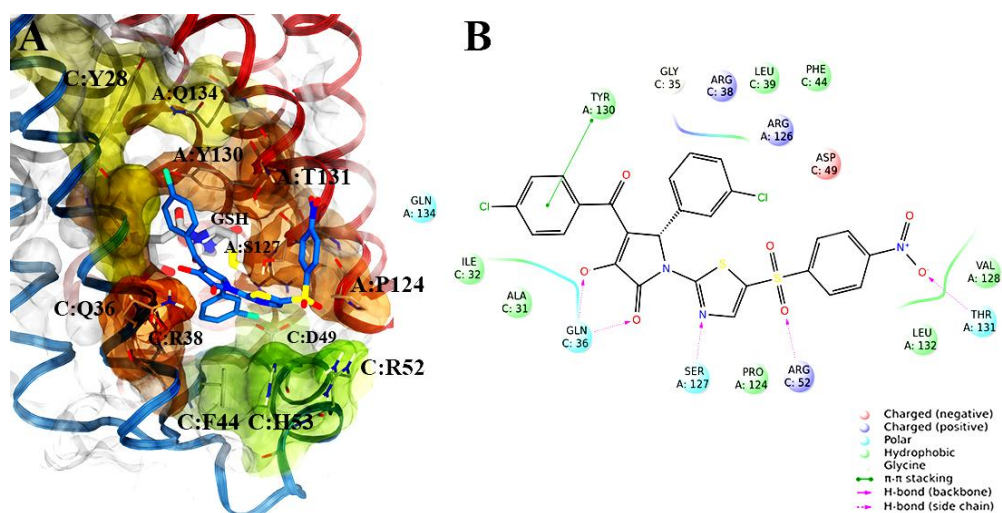
Figure 80 A) Selected 3D pose of **88** (colored by atom types: C, indigo blue; N, blue; O, red; S, yellow; polar H, light grey; Cl, light green) featuring the highest shape similarity to **LVJ**, in docking with mPGES-1 (chains A, B and C depicted in red, black, and blue ribbons, transparent molecular surface on the binding site colored in yellow, orange, and green, see text for details, glutathione (GSH) cofactor and key residues in the mPGES-1 binding site are represented in sticks, C grey, O red, N, blue, polar H white); **B)** related two-dimensional panels representing interactions.

-CHAPTER 5-

Heat Shock Protein 90

5.1 Heat shock proteins

Heat shock proteins (Hsps) is a family of ubiquitous proteins named according to the specific molecular weight (kilodaltons), which cells product in response to exposure to high temperatures[219] or to a variety of physiological and environmental insults (cold, UV light, bacterial or viral infections, oxidative stress or during wound healing and tissue remodeling).[220-222] According to their several and dynamic roles in protein homeostasis, many of the Hsps are mainly located in the cytoplasm, but also in other organelles such as the endoplasmic reticulum, mitochondria, and nucleus. Hsps are involved in the correct three-dimensional folding, assembly and disassembly of macromolecular protein structures, and in their translocation and degradation during ordinary cellular growth and development,[221, 223] performing *molecular chaperone* function. Also, the members of this family take part in the refolding and reactivation of unfolded and misfolded proteins, damaged by stress conditions[224, 225]

The five major families of HSPs are Hsp100 (in plants), Hsp90, Hsp70, Hsp60, and small HSP (sHSP, 15-30 kDa) which include Hsp27.

Clp/Hsp100 (casein lytic proteinases/heat shock proteins 100) are chaperones belonging to the larger AAA+ family of proteins (ATPases Associated with various cellular Activities) that act to remodel/disassemble protein complexes and/or protein aggregates using the energy of ATP. This substrate remodeling may serve many functions, including regulating the activity of protein complexes, unfolding proteins for presentation to proteases or facilitating the refolding of denatured protein aggregates. [226, 227] Hsp90 (heat shock protein 90) proteins interact with the protein substrate after binding with Hsp70. They do not act in nascent protein folding, but at a later stage of

folding.[228] Hsp70 (heat shock protein 70) is a class of chaperone system involved in different functions, such as import of proteins into cellular compartments (mitochondria, endoplasmic reticulum), folding of proteins in mitochondria and of a subset of proteins in the endoplasmic reticulum and the cytosol, disassembly of protein complexes, degradation of unstable proteins and the bacterial heat shock transcription factor, control of the activity of regulatory proteins such as heat shock transcription factors and the initiator protein of plasmid replication. Critical drivers of the activities of these proteins are Hsp40 family proteins.[229-231] Considering Hsp60 (heat shock protein 60) or chaperonins, they are key components of cellular chaperone machinery. Chaperonins form a part of the elaborate, co-operative network of chaperones that ensure correct folding of newly synthesized or stress-denatured proteins. The primary sequence of several polypeptides in the cell consists of multiple domains with α/β fold. Such proteins with complex topologies require the assistance of these specialized folding machines. Chaperonins form oligomeric, high molecular weight complexes of ~800 kD. It forms a large cage-like structure formed by two heptameric rings, each enclosing a central cavity. The heptamer is made of similar subunits, each having a molecular weight of 57 kD [228] Finally, sHSP (small heat shock proteins), also induced in stress conditions, are a very diverse group of chaperones that play an important role in maintaining the protein quality control in the cell. One of the most important protein which belongs to this family is Hsp27. The affinity of small HSPs for the target is not modulated by ATP binding, but it is determined by their oligomerization status. Only large oligomers (up to 1000 kDa) of Hsp27 have a chaperone activity and confer thermoprotection. Hsp27 oligomerization is a dynamic process that depends,

in part, on the phosphorylation status (it could be phosphorylated at three serine residues) of the protein and exposure to stress.[232]

5.2 Heat shock protein 90

Hsp90 family is one of the most investigated from both industry and academic research institute, as it is the most conserved and represents 1-2% of the total cytosolic proteins in non-stressed conditions, with an increase to 4-6% in stress-conditions, such as in tumoral states.[233-235] Two major isoforms have been found in the cytosol: the constitutive Hsp90β and the inducible Hsp90α.[236] Also, there are two non-cytosolic isoforms: the Hsp75/tumor necrosis factor receptor associated protein 1 (Trap1)[237] that is located in the mitochondrial matrix and is implicated in the oxidative cell death, and the endoplasmic reticulum resident Hsp90 isoform, 94 -kDa glucose-regulated protein (Grp94),[238] which plays a crucial role in cell adhesion, immune response, Ca^{2+} balance and folding of proteins.

Hsp90 inhibitors with cytotoxic effects induce the degradation of client proteins (to date, the maturation of more than 300 proteins is regulated by Hsp90) that are then submitted to ubiquitinylation-mediated proteasomal degradation.[239, 240] Compounds endowed with these features are excellent potential anticancer drugs,[241] while non-cytotoxic compounds able to block the functions of the chaperone are responsible of an up-regulation of HPSs levels and a subsequently solubilization of protein aggregates, suggesting application as neuroprotective agents.[242-244] Hsp90 chaperone is overexpressed in cancer cells, with an increase up to 10-fold than in normal cells, and takes part in the progression of malignancy,[245] since it prevents the aggregation and regulates the folding of client oncoproteins, such as ErbB2, Akt, p53, Bcr-Abl, Her-2,

Cdk4, Cdk6, Raf-1, v-Src, MET, telomerase and survivin.[246, 247] Furthermore, the interference with Hsp90 machinery activity affects all hallmarks of cancer, blocking the maturation of oncoproteins associated with each hallmark.[248] In light of this, the chaperone is interestingly a significant and promising target for cancer therapy. [241]

Also, Hsp90 is involved in the biogenesis, homeostasis and activation of IκB kinase (IKK) connected to the transcription factor NF-κB.[249] Experimentally, the inhibition of NF-κB pathway was observed after treatment with the N-terminal Hsp90 inhibitor geldanamycin.[250, 251] This may suggest a potential in the prevention of cancer-related inflammation. Several experimental data[252] confirmed a connection between inflammation and chaperones, as Hsp90 is involved in different kind of inflammatory responses, such as gastric inflammation,[253] colitis,[254] liver injury,[255] myopathies,[256] endotoxin-induced uveitis.[257]

5.2.1 Structure and conformational cycle of Hsp90

Structurally, it is a homodimer whose conformation plays a crucial role in the activity of the protein. The monomer is organized in three highly conserved domains: amino-terminal (NTD), middle (MTD) and carboxy-terminal (CTD), which are active components of the conformational cycle.[258] The ATP hydrolysis in the N-terminal site is the starting point for the conformational change of the protein, and provides the energy needed for the chaperoning activities;[259] the middle domain is responsible of the regulation of client proteins binding and interacts with the γ-phosphate of ATP;[260] finally, the C-terminal contains a second nucleotide binding region, but is not endowed with ATPase activity,[261, 262] and is involved in the regulation of

Hsp90 conformational rearrangement. The N-terminal and the middle domains are connected by a long and flexible linker which regulates the contacts between the two parts. Furthermore, an additional C-terminal motif could be identified which consist of the amino acid sequence Met-Glu-Glu-Val-Asp.[263] Heat shock proteins bind co-chaperones to perform most of their functions. Specifically, the C-terminal motif of Hsp90 chaperone is involved in the interaction with the tetratricopeptide repeat (TPR) domains belonging to co-chaperone molecules.[263]
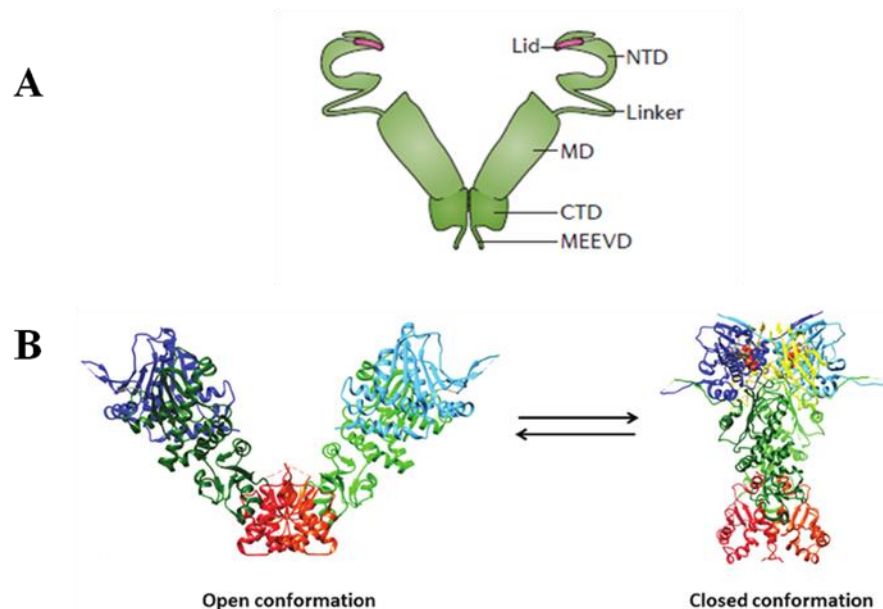
Figure 81 A) Hsp90 domains; **B)** Equilibrium between open and closed conformation of Hsp90 upon ATP binding; the C-terminal domain is colored in red, the middle in green, and the N-terminal in blue.

The ATPase activity is the key of the open-closed-open conformational changes of the chaperone and, as a consequence, of the total functions that the

protein plays in the organism. A 15 Å deep pocket region in the N-terminal domain is involved in the binding of the ATP/ADP molecule. As a member of the gyrase, Hsp90, His kinase and Mutl superfamily of "split ATPases", the association between the N-terminal and the middle domains is crucial for the ATP hydrolysis.[258] In details, the binding of two molecules of ATP, one for each monomer, induces a rearrangement in which a loop of conserved amino-acids, called lid region, closes over the bound ATP affording the intermediate state.[258, 264] The dimerization of the two NTDs leads to the closed 1 state, and the association between the NTDs and the MTDs induces the closed 2 state, which leads the repositioning of the catalytic group in the middle domain and the hydrolysis activity. After the release of ADP and inorganic phosphate, the protein returns to the open conformation. [258, 265] In general, the enzymatic activity of Hsp90 is very low, with a dissociation constant (K_D) of 400 μM. The conformational rearrangements for the formation of the split ATPase domain are the rate-limiting steps of this slow reaction. In this process, Hsp90 interacts with a number of co-chaperones which also mediate the maturation of client proteins.[266]
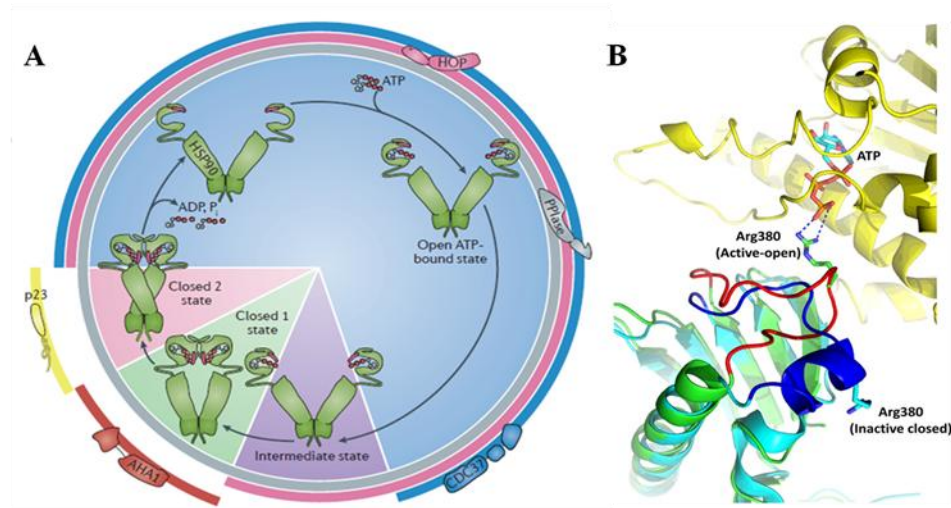
Figure 82 A) Open-closed-open conformational changes. **B)** Catalytic loop of Hsp90. The N-terminal domain is represented in yellow, while the middle domain is shown by two superimposed molecules of Hsp90 (cyan and green), one in the closed inactive state (blue) and the other one in the open active state (red). In the latter, Arg380 of the catalytic loop establishes hydrogen bonds (broken blue lines) with ATP bound in the N-terminal domain. [267]

5.2.2 Regulation of heat shock protein 90 function

Expression. The heat shock factors (HSF-1, HSF-2 and HSF-4)[268-270] are ubiquitous proteins in the human cells. They consist of a DBD (DNA-binding domain), a trimerization domain containing three leucine zipper repeats called HR-A/B, the HR-C region which leads the regulation of HR-A/B domain and a CTA (C-terminal transactivation) domain, controlled by the central RD (regulatory domain).[267] The stress-related transcription factor HSF1 (heat shock factor 1) is mainly involved in the regulation of the expression of Hsp90. When the amount of the chaperone is sufficiently available for the functions of the cell, HSF1 becomes a client of the protein and the complex Hsp90-HSF1 inhibits its activity.[271] Stress conditions induce the release of

HSF-1 from its repressed association with Hsp90, the homotrimerization of the protein and the translocation to the nucleus. After the binding of HSF-1 to the heat shock promoter element (HSE), a series of phosphorylations transforms the HSF1 trimer into an active transcription factor, which stimulates the expression of responsive genes and the increase of heat shock proteins in the cytosol.[272] Thus, Hsp90 (as well as Hsp70) is involved in the heat shock response (HSR).[268, 270]
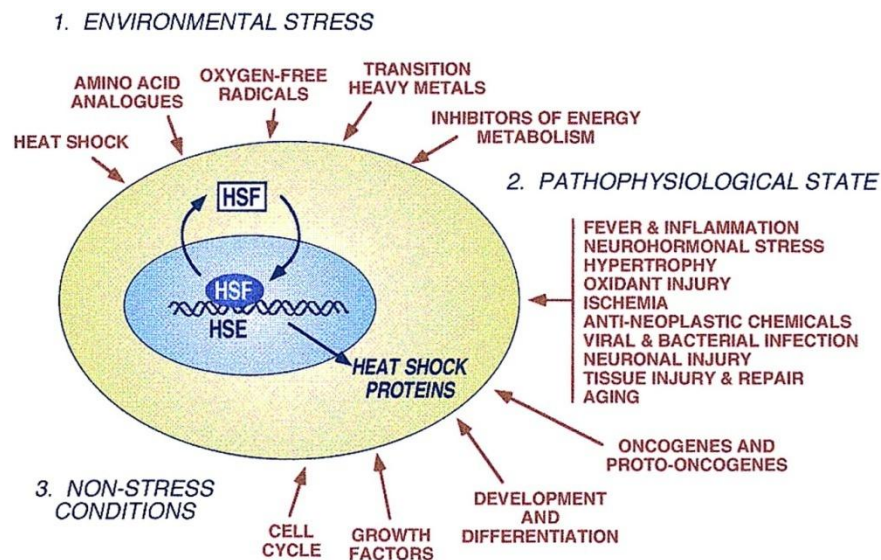
Figure 83 HSR (heat shock response).

Post-transcriptional modifications (PTMs).[273] Phosphorylation,[274] sumoylation,[275, 276] acetylation[277, 278] and S-nitrosylation[279] are the most significant post-transcriptional modifications in which Hsp90 is involved.[273] Hyperphosphorylation and hyperacetylation slow down the conformational cycle and regulate negatively the interaction with co-chaperones. S-

nitrosylation of cysteine residue in the C-terminal domain interferes with both the chaperone and the ATPase activities and, interacting with endothelial nitric oxide synthase (eNOS), inhibits its activation.[279] Summarily, the PTMs regulate the accessibility of binding sites and the interdomain communication across the Hsp90 homodimer. [273]

5.2.3 Heat shock protein 90 inhibitors

Based on the position of the binding site of the ligands in the protein, three different classes of inhibitors are known: N-terminal, middle and C-terminal.

In recent years different structurally unrelated natural or synthetic N-terminal inhibitors have been disclosed. Some of them perform an excellent antitumor activity and have entered clinical trials. One of the most famous is Geldanamycin[280, 281] (Figure 84), a 1,4-benzoquinone ansamycin antibiotic product in the organism of *Streptomyces hygroscopicus*. This natural compound is endowed with a great ability to inhibit the activity of Hsp90 and leads to the degradation of its client proteins (p53, Raf-1, Akt, ErbB2) by binding the ADP/ATP pocket of the chaperone. However, in spite of the anti-cancer activity on the animals demonstrated in the pre-clinical phase, the limitation in solubility and the hepatotoxicity prevented the selection of Geldanamycin as a drug candidate.[282] In light of this, some analogues have been developed in order to overcome the above mentioned limitations increasing the hydrophilicity.[280] The most important derivatives are 17-*N*-allylamino-17-demethoxygeldanamycin (17-AAG)[283] and 17-Dimethylaminoethylamino-17-demethoxygeldanamycin (17-DMAG),[284, 285] in which the methoxy group at position 17 is substituted respectively from an *N*-allylamino and a dimethylamino group. Both the named derivatives have

149

completed phase I of the clinical trials and are entering phase II, for the evaluation of the anti-cancer activity on solid tumors.

Radicicol (RDC) is another known binder of the N-terminal domain of the chaperone, which interferes with its functions at nanomolar concentration and induces the following degradation of the client proteins. Structurally, it represents the first and unique non-benzoquinone ansamycin capable of binding Hsp90 in the same region of Geldanamycin and inducing the same responses, such as the inhibition of the maturation of oncogenic proteins.[286] Also, the studies concerning the effects of the purine-scaffold on the protein occupied a fundamental role in the discovering of new hits. Several purine derivatives have been developed in the last years, and some of them showed nanomolar potency (IC_{50} = 50 nM) in both cellular and animal models of cancer, entering the clinical trials.[287, 288] A representative example is reported below. Other chemical items able to inhibit the activity of Hsp90 interacting with its N-terminal domain are pyrazole derivatives (Figure 84).[289]
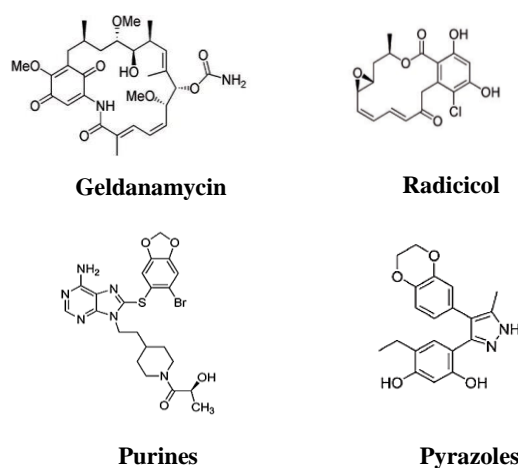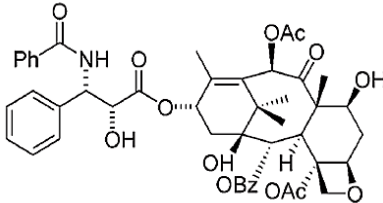
Figure 84 Hsp90 N-terminal inhibitors.
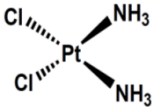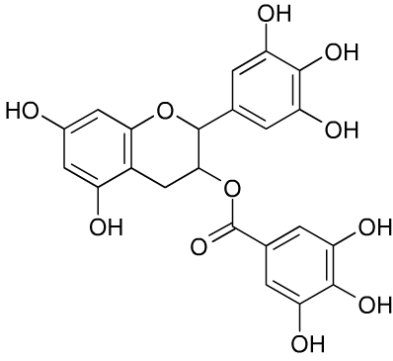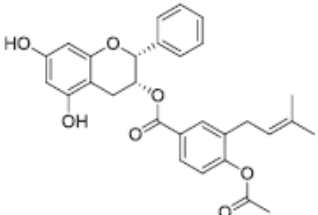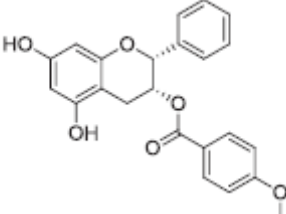
Moreover, although some N-terminal inhibitors are still in the clinical trials,[290, 291] many have failed due to toxicity issues and to the occurrence of heat shock response (HSR) associated with resistance.[292]

Concerning C-terminal inhibitors, only a few compounds have been developed in the last years, since the lack of structural information represented a limitation. The first identified C-terminus inhibitor was the natural antibiotic Novobiocin,[56] from which chlorobiocin and coumermycin A1 analogues were developed.[293] Its binding site includes amino-acids 538-728 in the C-terminal region. Experimentally, the binding of Novobiocin induces a conformational rearrangement such that the cleavage with proteolytic enzymes in correspondence of Arg400 and Lys615/Arg620 in the C-terminus is blocked, [294] and the binding of TPR of co-chaperones to the MEEVD motif is prevented.[295] Since Novobiocin presented a weak interaction with Hsp90 (IC_{50} = 700 μM in SKBr-3 breast cancer cells), several more potent analogues were synthesized (Table 9).[296-298] Furthermore, Epigallocatechin gallate (EGCG),[299] Cisplatin,[300] Taxol[301] and Sansalvamide A[302] derivatives are able to inhibit the activity of the chaperone interacting with the C-terminus domain (Table 9).

Table 9 C-terminal Hsp90 inhibitors.

Lead compound	Optimized derivatives
Taxol[56, 301]	–

Cisplatin[56]

–

Epigallocatechine-3-gallate[299, 303, 304]

IC_{50} (MCF-7): 74.40 µM

IC_{50} (SKBr3): 100.16 µM

IC_{50} (MCF-7): 13.10 µM

IC_{50} (SKBr3): 15.42 µM

IC_{50} (MCF-7): 3.99 µM

IC_{50} (SKBr3): 21.45 µM
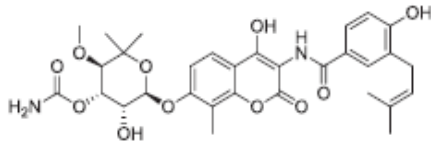
Novobiocin

IC$_{50}$ (SKBr3): 700 µM
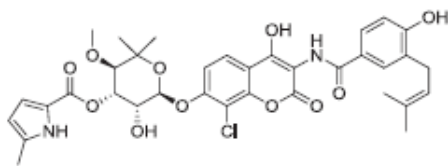
Chlorobiocin

IC$_{50}$ (SKBr3): 60 µM
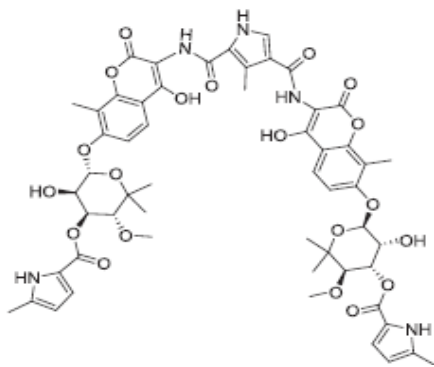
Coumermycin A1

IC$_{50}$ (SKBr3): 70 µM
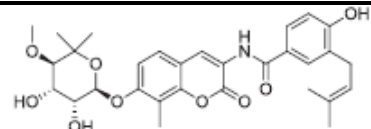
IC$_{50}$ (SKBr3) = 0.5 µM

IC$_{50}$ (SKBr3) = 0.8 µM

IC$_{50}$ (SKBr3) = 0.21 µM

IC$_{50}$ (SKBr3) = 0.11 µM

IC$_{50}$ (SKBr3) = 0.2 µM

Sansalvamide A (Hsp90 allosteric modulator)

IC$_{50}$ (mean against the NCl cell line panel) = 27.4 μM

IC$_{50}$ (HCT-116) = 7.4 μM

IC$_{50}$ (HCT-116) = 5.0 μM
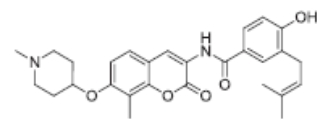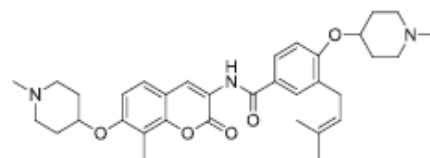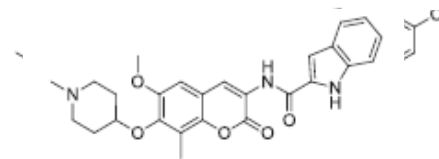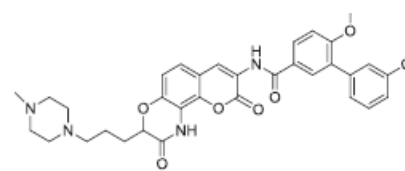
IC$_{50}$ (HCT-116) = 2.9 μM
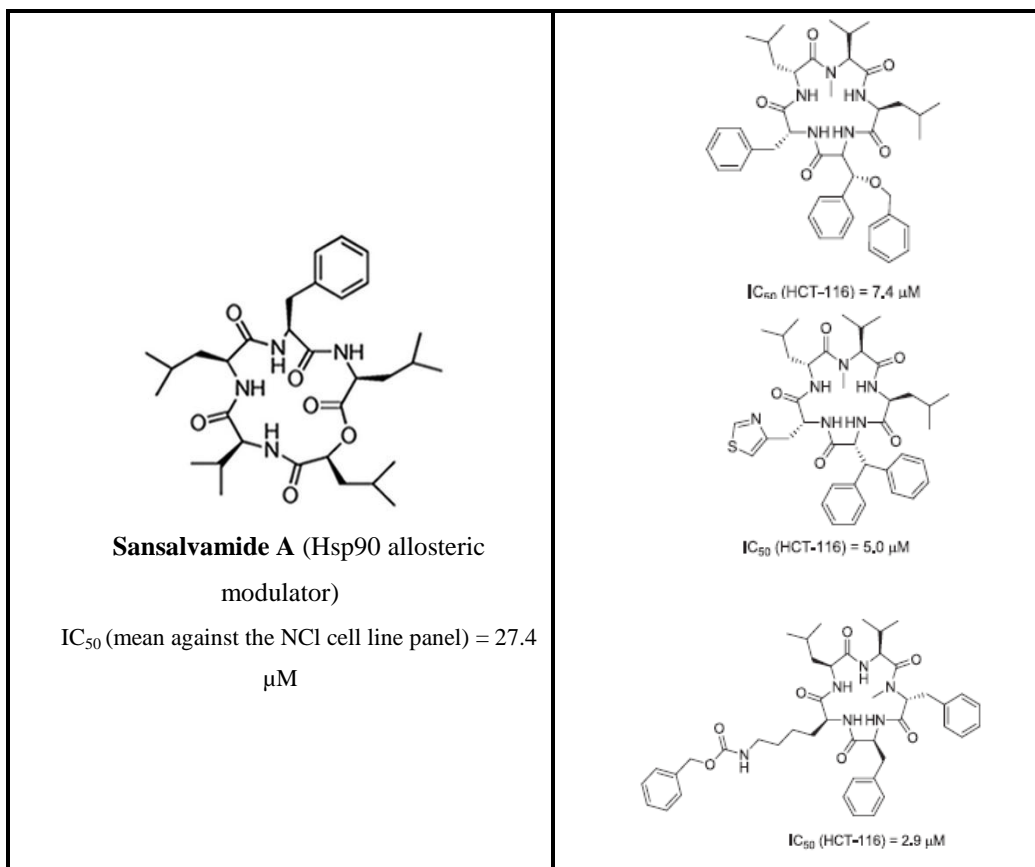
5.2.4 C-terminal inhibitors vs N-terminal inhibitors

Stressing the difference between N-terminus and C-terminus inhibitors of Hsp90 is important to understand why the latter class is more promising and preferred for cancer therapy. N-terminal modulators, in fact, presented several problems in clinical investigation (high concentration for a biological effect, poor aqueous solubility and hepatotoxicity) and induce heat shock response (HSR) related to cancer resistance.[55, 291, 292] Conversely, the C-terminal inhibitors do not induce resistance mechanism and may be an alternative therapeutic strategy for the treatment of malignant cancers.[292] The described HSR mechanism ensures the survival of cells in stressful conditions such as

exposure to heat, oxidative stress, toxins, bacterial infections and heavy metals.[270] Specifically, N-terminal Hsp90 inhibitors induce the dissociation of HSF-1 from Hsp90, and the heat shock factor triggers its response. The increase of HSPs levels helps cancer cells to avoid the cytotoxic effect.[305] In contrast, C-terminal Hsp90 inhibitors lock HSF-1 into its inactive Hsp90-bound state and promote its degradation *via* the proteasome.[306-308]

According to the importance of the discovery of novel C-terminal inhibitors, a purpose of this research work was the identification of new hits. However, the broad conformational space of this flexible chaperone is still a strong limitation.

5.3 Discovery of new molecular entities able to strongly interfere with Hsp90 C-terminal domain

In light of the above considerations, a specific protocol was applied in order to identify new inhibitors from commercially available structural unrelated small compounds. The purpose of expanding the number of molecules able to inhibit the activity of Hsp90 interacting with the C-terminal domain is the reason for which variability in the chemical structure of the selected small candidates was adopted. The exploration of the chemical space encoded by different scaffolds plays a fundamental role in the discovery of new hits. [309]
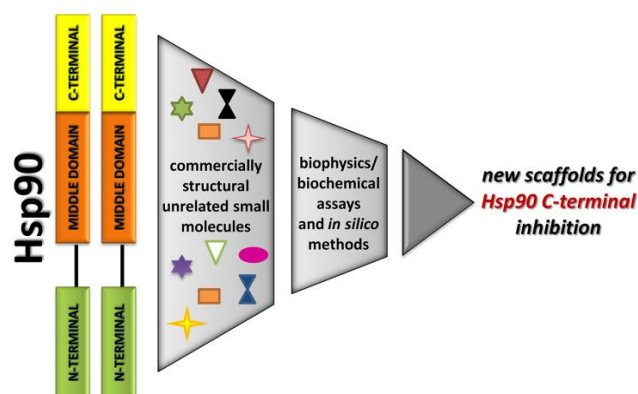
Figure 85 General workflow for the individuation of new C-terminal Hsp90.

5.3.1 Biological screening of a small library of molecules on Hsp90

Considering that only a few C-terminal domain inhibitors [56-59] have been disclosed so far, a set of 48 compounds was undergone to the mentioned workflow (Figure 85). As a starting point, the biophysical surface plasmon resonance (SPR) assay[57-59, 310] was performed on recombinant Hsp90α with the aim of screening the compounds and testing their ability to bind to the immobilized protein. Based on these analyses, 16 molecules (Figure 87) were selected for their ability to bind the molecular chaperone with high affinity and low K_D values (Table 10). In the next step, the anti-proliferative activity was evaluated, in particular against Jurkat (human T-lymphocyte) and U937 (human monocyte form histiocytic lymphoma) cell lines. The cells were exposed to increasing concentrations of the 16 selected compounds or the well known C-terminal inhibitor Novobiocin for a duration of both 24 and 48 hours, and the MTT assay was carried out to measure the cell viability. The IC_{50} values listed below confirm compounds **100** and **103** as the best

candidates for the following analysis. The evaluation of their anti-proliferative activity against non-tumor cell line PHA-stimulated human peripheral blood mononuclear cells (PBMC) demonstrated that both **100** and **103** compounds are not able to increase the non-viable cells percentage after 24 or 48 h, in comparison to the percentage observed in DMSO treated control cells. The experimental data show the following values of percentages: about $6 \pm 1.8\%$, $8 \pm 1.5\%$ and $7 \pm 1.3\%$, $9 \pm 1.8\%$ respectively for the compounds **100** and **103** at 25 μM for 24 and 48 h, and $5 \pm 0.9\%$ for the control. Then, an elucidation of their mechanism in the cell cycle was very useful to confirm the anti-proliferative activity. Jurkat (human T-lymphocyte) cell lines were used to perform the additional analysis for the characterization of the mechanism, since they were two-fold more susceptible than U936 (human monocyte form histiocytic lymphoma). The biological test provided the incubation of the cells with a concentration of compounds **100** and **103** close to their IC_{50} values or two and four times higher for 24 or 48 h. A comparison with Novobiocin was carried out, performing the test at the same conditions with concentrations close to its IC_{50} value (200 μM) or at lower doses (50 or 100 μM).

157

94

95

96

97

98

99

100

101

102

103

104

105

106

107

108

109

110

111

112

113

114

115

116

117

118

119

120
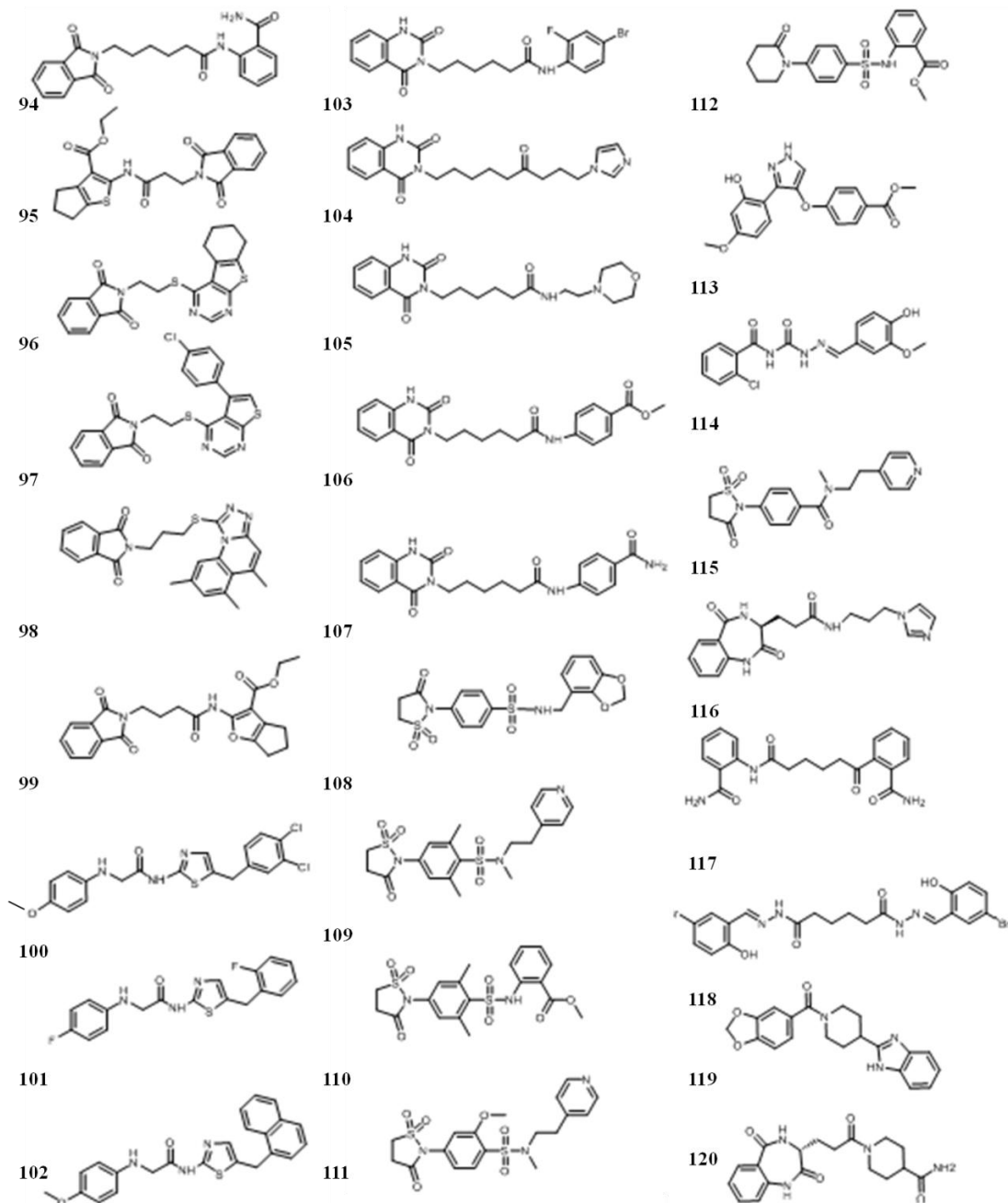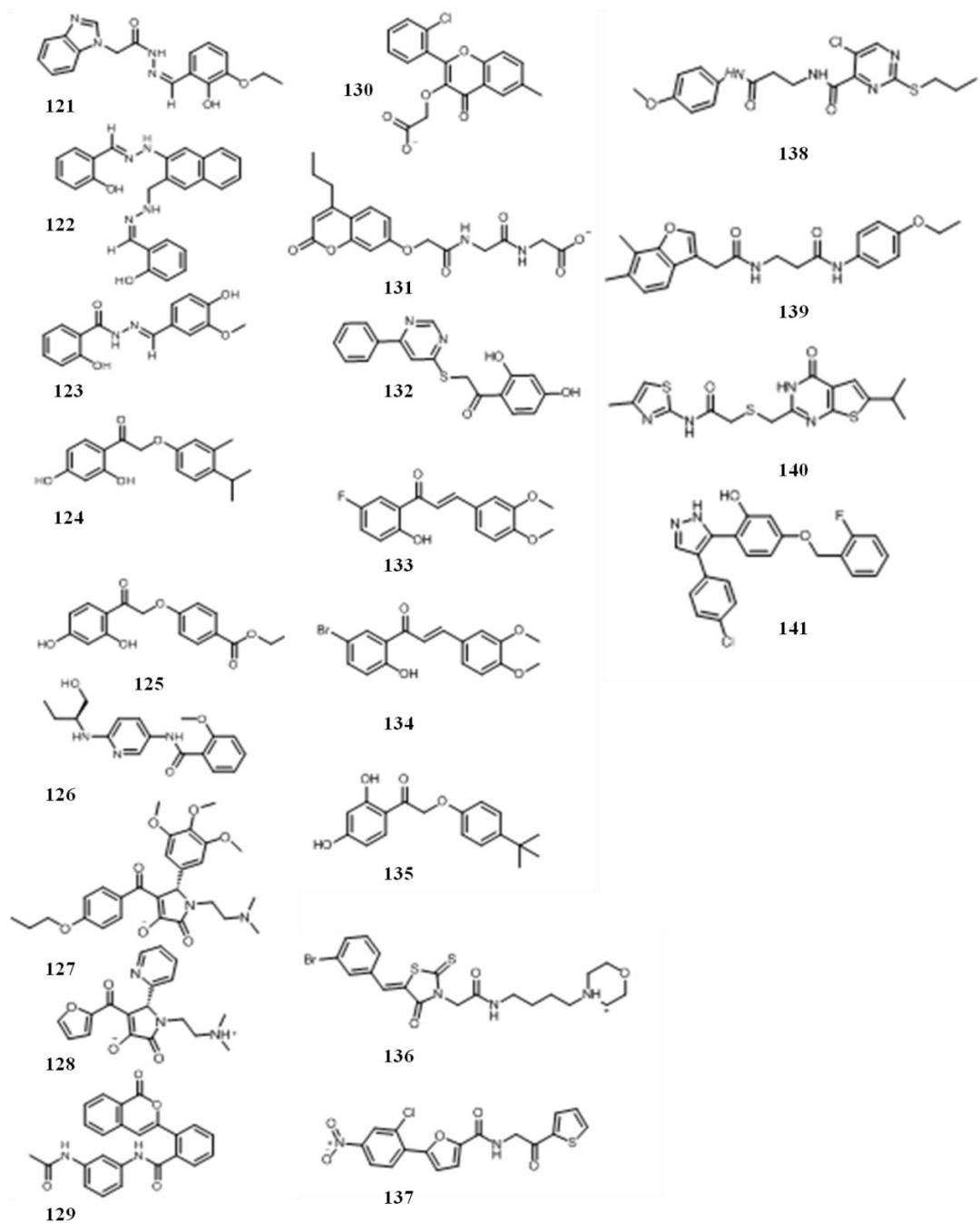
Figure 86 Library of 48 molecules screened for the individuation of Hsp90 inhibitors.

159
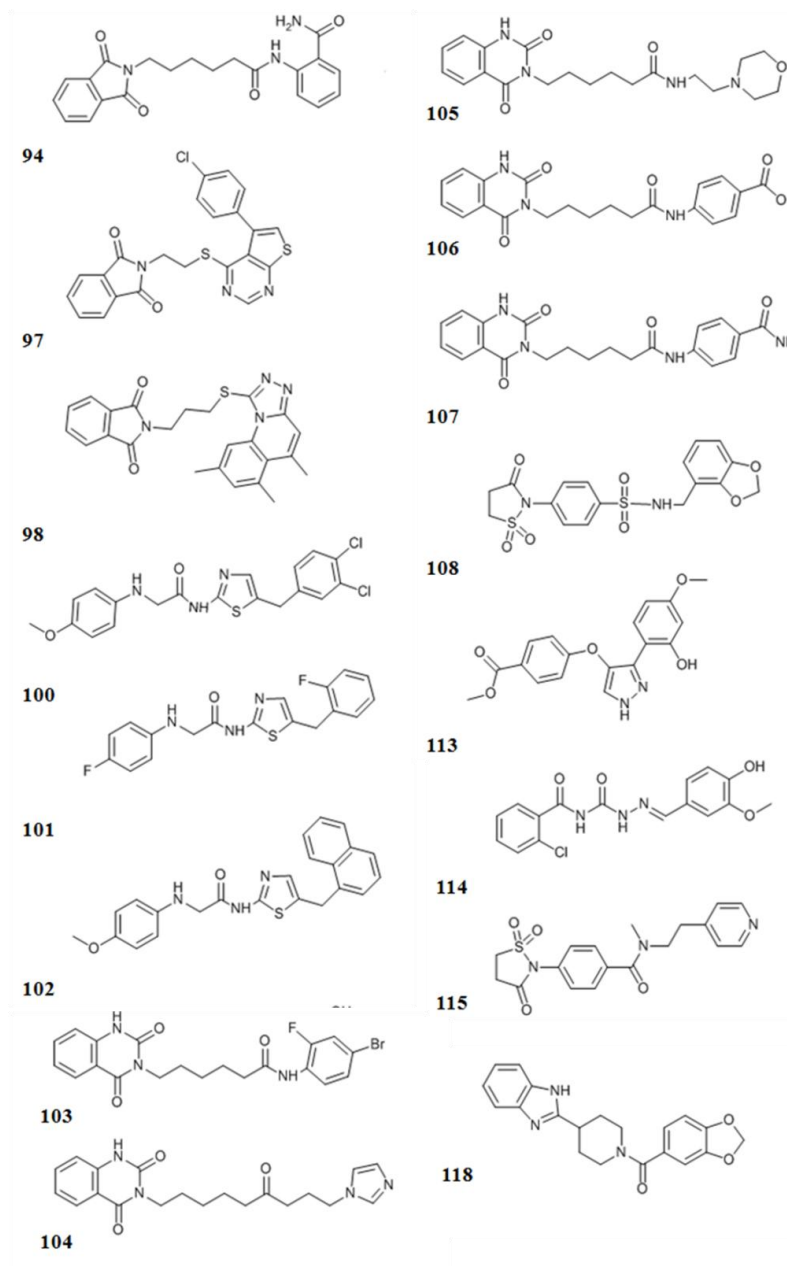
Figure 87 Chemical structures of the selected compounds with high affinity for Hsp90 from SPR screening.

Compound	K_D(nM) ± SD
94	1.5 ± 0.5
97	3.2 ± 1.1
98	14.7 ± 9.4
100	5.2 ± 3.8
101	2.4 ± 0.6
102	20.9 ± 9.5
103	20.8 ± 8.7
104	79.3 ± 7.2
105	95.1 ± 5.7
106	300 ± 19.3
107	260.2 ± 8.4
108	4.8 ± 2.9
113	14.2 ± 4.9
114	13.2 ± 2.3
115	4.1 ± 2.6
118	25.7 ± 8.4

Table 10 SPR (Surface Plasmon Resonance) assay results of the 16 compounds able to bind Hsp90.

Based on the results, compounds **100** and **103** demonstrated a cytostatic activity at concentration close to their IC_{50} values, since the cells blocked their growth in G0/G1 or S phase respectively without any significant increase of subG0/G1 cell fraction, for a duration of both 24 and 48 h. At 100 μM for 48 h, the compounds were able to exhibit a cytotoxic activity. From a comparison of these results to the anti-proliferative activity of Novobiocin, which was able

to induce cell death at high concentration (200 µM), with a loss of the activity at lower concentration (50 and 100 µM), it is possible to confirm that compounds **100** and **103** perform improved cytostatic/cytotoxic effects. A monitoring of the expression levels of cell cycle cyclin-dependent kinases is a further demonstration of the above biological results. Cyclin D and CDK4, which regulate the G0/G1 phase cycle, were slightly down-regulated in Jurkat cells with the exposure to compound **100**, in the other hand Cyclin A and CDK2, involved in normal S-phase progression, decreased with compound **103** treatment.

Western Blot was another deeper analysis to confirm that cell death was determined by Hsp90 activity inhibition. The lysates of Jurkat cells treated with compounds **100** and **103** were analyzed to determine the levels of some representative oncogenic Hsp90-client proteins, discovering a significant degradation (50–60%) of Hsp90-dependent client proteins Raf-1, p-Akt, p-Erk and p53 in a concentration-dependent way, without affecting actin levels, which is not dependent upon Hsp90, and a minimal reduction of Hsc70 (15–20%). The expression of ER chaperone grp94 was not observed. Finally, limited proteolysis experiments were performed with the purpose to individuate the region of the C-terminal domain in which the compounds are placed in the inhibitory activity of the chaperone. It is possible to identify the binding site through the differences in the proteolytic patterns observed in presence or in absence of putative protein ligands.[311, 312] The experiments were carried out on Hsp90α, Hsp90α/**100** and Hsp90α/**103** complexes, and on Hsp90α/Novobiocin, the positive control.[59]

Based on MALDI analysis of the digestion mixtures of the several complexes, exposed to trypsin and chymotrypsin, a reduction of the cleavage

of Lys484, Lys498 and Lys656 was individuated in the complexes of the chaperone with both the compounds. Thus, the middle and C-terminal domains of Hsp90α are preferentially involved in the molecular binding.

Compound	IC$_{50}$±SD (µM) (on Jurkat cell lines)	IC$_{50}$±SD (µM) (on U937 cell lines)
100	25.1 ± 0.4	51.0 ± 0.7
103	26.1 ± 0.7	50.0 ± 0.7

Table 11 IC$_{50}$ values of compounds **100** and **103**, from cells viability assay on human monocytic cell line U397, from histiocytic lymphoma, and human leukemic T lymphocyte cell line
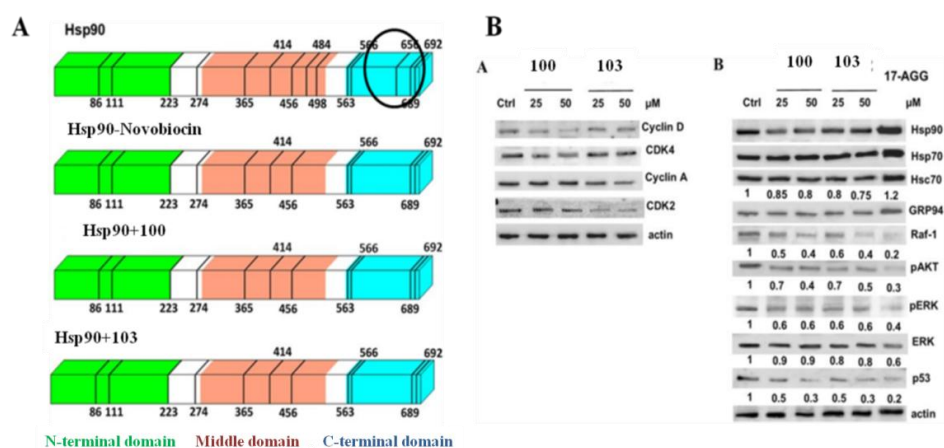
Figure 88 A) Limited proteolysis experiments on compounds **100** and **103; B)** Western blot analysis.

5.3.2 Computational rationalization

In this thesis, a detailed description of the final docking experiments for the rationalization of the activity of compounds **100** and **103** is reported. Several

computational experiments were performed to investigate the inhibitory effect at a molecular level. Molecular docking experiments were performed. Since the X-ray structure of human Hsp90 is not available in the protein data bank (PDB) database, the selection of a substitutive homologue crystal structure was essential to start the calculation. A research work published in 2011[313] reports the structure-based sequence alignment between the yeast Hsp82 (PDB code: 2CG9)[266] and the human Hsp90α. In the comparison between the middle and the C-terminal domains of the two chaperones, they showed about 60% identity in 438 residues, and the superimposition reported an rmsd of 0.91 Å for 219 Cα atoms. [313] A similar comparison was also applied with the canine GRP94 (PDB: 2O1V),[314] but lower values of identity and superimposition were identified (about 49% identity in 414 residues and a rmsd of 1.02 Å for 241 Cα atoms). [313] For this reason, the Hsp82 X-ray structure was chosen as the best candidate for the computational experiments. The selected 3D structure of the protein, complexed with the co-chaperone Sba1 in the active closed conformation, was deposited in 2006 and is characterized by a resolution of 3.1 Å. [266]

After applying the Protein Preparation Wizard Workflow, [117] in which water molecules were removed, all hydrogen atoms were added, and the bond orders were assigned, the PDB file was converted to the Maestro (MAE) format. Starting from the results of limited proteolysis experiments reported above, the region including the Arg 670 of Hsp82, which corresponds to the Lys 656 of Hsp90 involved in the binding site, was considered during the conformational searches. The 16 compounds screened by SPR experiments were docked onto the close active crystal structure of Hsp82, using the Induced Fit Docking Protocol (Schrödinger Suite),[103, 104] to account for

flexibility of ligands and receptor.[315] Considering that compounds **100** and **103** were disclosed as two novel Hsp90 C-terminal inhibitors, a comparison of the binding mode between the active compounds and the structural analogues of the tested commercially available library was crucial for a detailed investigation at a molecular level. Specifically, compound **100** was compared with its structurally related compounds **101** and **102**, and **103** with respect to **104–107**.

Considering the group of molecules **100-101**, the different biological activity has been attributed to the substituents at C-5 of thiazole ring, from the structural point of view. The main force of the interactions which the three compounds establish with the receptor counterpart is the pattern of H-bonds between their phenylamino acetamide and Leu671 and Leu674 of both the chains A and B in a specific site of the C-terminal domain. In spite of the three compounds occupy the same region of the protein, only the 3,4-dichlorobenzyl moiety of **100** is involved in a peculiar halogen bond with the side chain of Arg670 $_{\text{ChainA.}}$

On the other hand, for the second group of molecules (**103–107**), the quinazolinedione moiety is able to establish H-bond contacts with Leu674, Leu676 and Ile672, as well as the substituted *N*-hexanamide portion with Asp641$_{\text{ChainA}}$. Also, compound **103** shows an additional docking pose deriving from the inversion of the *N*-(4-bromo-2-fluorophenyl)hexamide and quinazolinedione moiety. This orientation of the molecule in the binding site leads to several hydrogen bonds between Leu674$_{\text{ChainB}}$, Leu671$_{\text{ChainA}}$, Gly675$_{\text{ChainB}}$ and amide group of *N*-hexanamide, and between the fluorine atom of bromofluorophenyl and Leu676$_{\text{ChainA}}$. Other additional bonds were observed: a halogen bond between its bromine and the CO of Thr638$_{\text{ChainB}}$

165

and a hydrogen bond between the quinazolinedione and Arg670$_{ChainA}$ and Leu674$_{ChainA}$. In light of this, the substitution on *N*-hexanamide is crucial for the biological activity of this set of molecules, due to additional interactions of this moiety with the receptor counterpart are essential for the inhibition of the conformational cycle of the protein. From the considerations above, the placement of compound **100** and **103** at the interface of the two Hsp90 A and B chains is induced by the precise pattern of hydrogen bonds with the leucine amino acids (Leu671, Leu674, Leu676), and the halogen interactions with Thr638$_{ChainB}$ for **100** and Asp641$_{ChainA}$ for **103** have been confirmed as fundamental interactions suitable for the design of novel more effective C-terminal Hsp90 inhibitors.[58, 316]
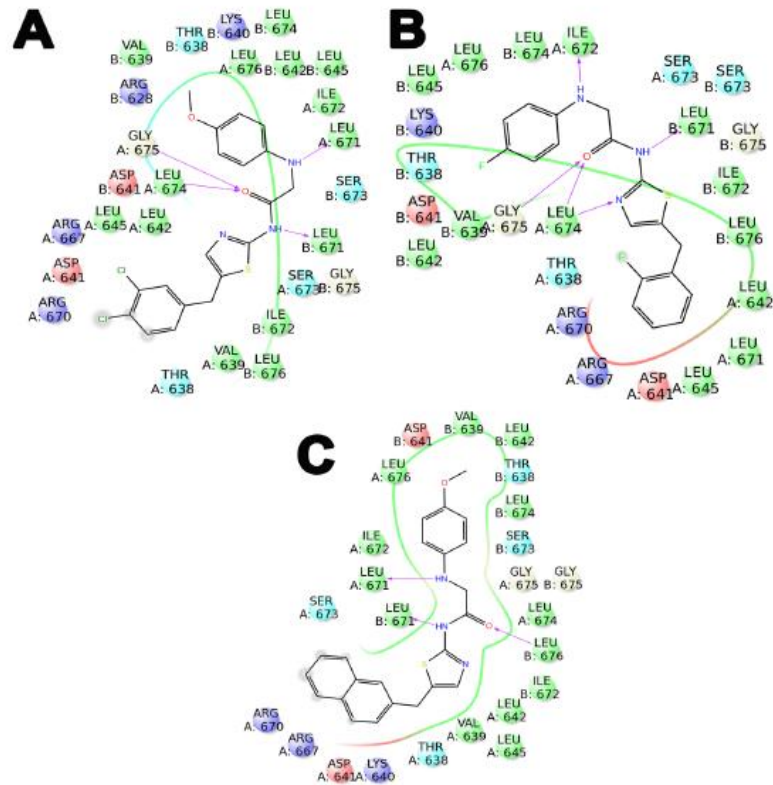
Figure 89 2D diagram interactions (panel A, B and C) of **100**, **101** and **102** with C-terminal domain of Hsp82 yeast analogue of Hsp90α (PDB: 2CG9). Positive charged residues are colored in violet, negative charged residues are colored in red, polar residues are colored in light blue, hydrophobic residues are colored in green. H-bond (side chain) are reported as dotted pink arrows.

167
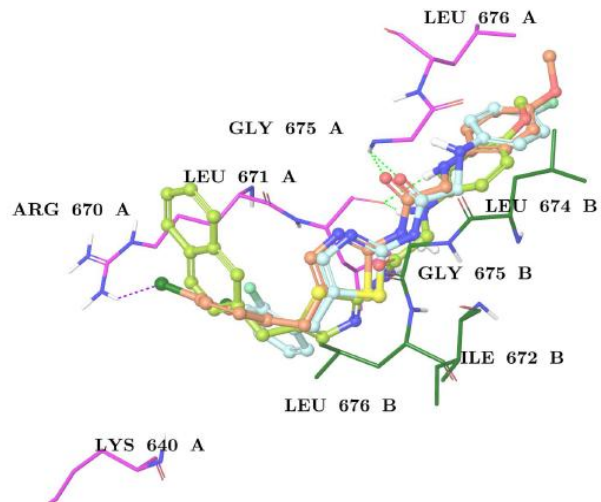
Figure 90 Superimposition of **100** (light pink sticks), **101** (sky-blue sticks) and **102** (light green sticks) with C-terminal domain of Hsp82 yeast analogue of Hsp90α (PDB: 2CG9). The protein is depicted by purple (chain A) and green (chain B) sticks.

168
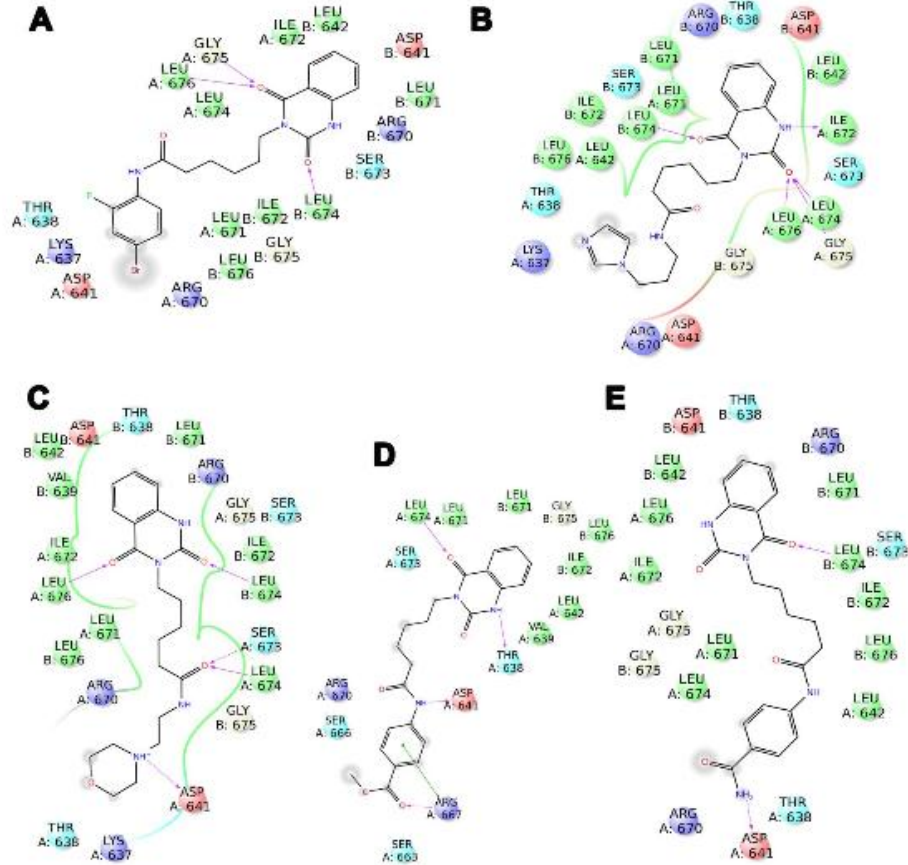
Figure 91 2D diagram interactions (panels A, B, C, D and E) of **103**, **104**, **105**, **106** and **107** with C-terminal domain of Hsp82 yeast analogue of Hsp90α (PDB: 2CG9). Positive charged residues are colored in violet, negative charged residues are colored in red, polar residues are colored in light blue, hydrophobic residues are colored in green. The π-π stacking interactions are indicated as green lines, and H-bond (side chain) are reported as dotted pink arrows.
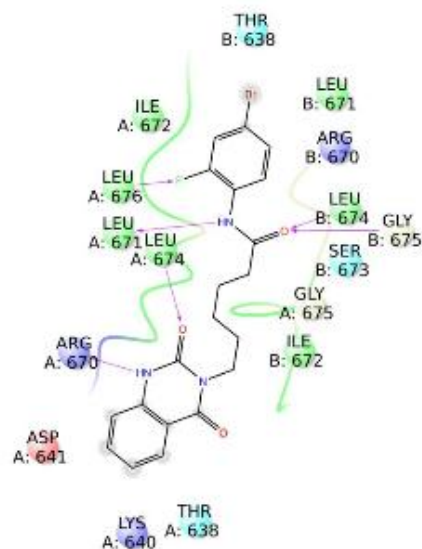
Figure 92 2D diagram interactions of second binding mode of **103** with C-terminal domain of Hsp82 yeast analogue of Hsp90α (PDB: 2CG9). The positive charged residues are colored in violet, negative charged residues are colored in red, polar residues are colored in light blue, hydrophobic residues are colored in green. H-bond (side chain) are reported as dotted pink arrows.
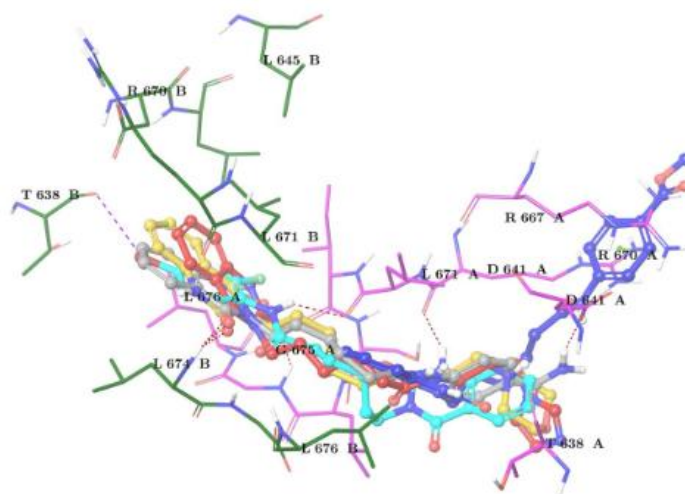
Figure 93 Superimposition of **103** (cyan sticks), **104**(red sticks), **105** (yellow sticks),**106** (blue sticks),and **107** (grey sticks) with C-terminal domain of Hsp82 yeast analogue of Hsp90α (PDB: 2CG9).The protein is depicted by purple (chain A) and green (chain B) sticks.

170
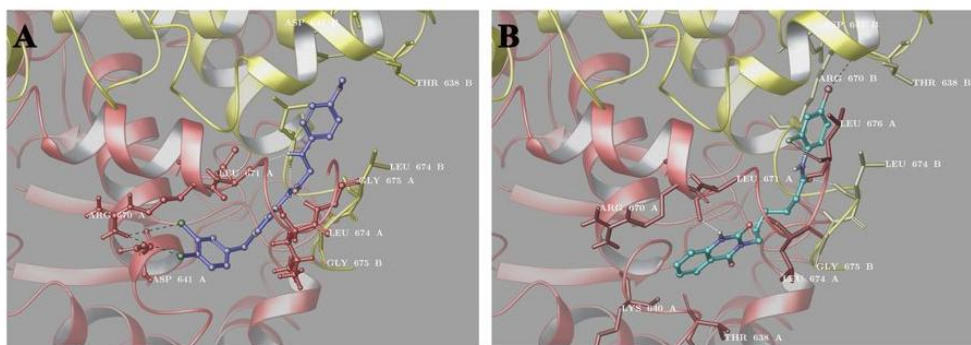
Figure 94 Three dimensional models of **100** (violet sticks, panel A) and **103** (cyan sticks, panel B) with the C-terminal domain of the Hsp82 yeast analogue of Hsp90α (chain A is depicted in red and chain B in yellow).

With the aim of performing deeper computational analysis for the investigation of ligand affinity and selectivity towards the target,[317, 318] and considering the flexibility and dynamicity of the chaperone, the best poses of the most active compounds **100** and **103** in complex with Hsp90 were used as a starting point for molecular dynamics (MD) simulations (100 ns) in explicit solvent (Desmond software).[319] In particular, for the analysis of the trajectories we have used the simulation interactions diagram (SID) (Maestro version 10.2)[94] a tool for exploring protein-ligand interactions. The simulation showed compounds **100** and **103** at the interface of the two chains of the C terminal domain, maintaining a good number of interactions with the amino acids mentioned in the previous analysis. The driving force of compound **100-Hsp90** complex consists of a pattern of hydrophobic contacts and hydrogen bonds with Leu671$_{chainB}$, maintained for more than 80% of the simulation time, in addition to further interactions with Leu676, Glu624, Asp641 of chain B (≈50%). In compound **103-Hsp90** complex, most of the contacts are retained

171

with Leu674$_{chainB}$ (>70%). Thus, the dynamic nature of protein-ligand interactions is described from a detailed pattern of hydrogen bonds and hydrophobic contacts with the C-terminal domain (Figure 95).
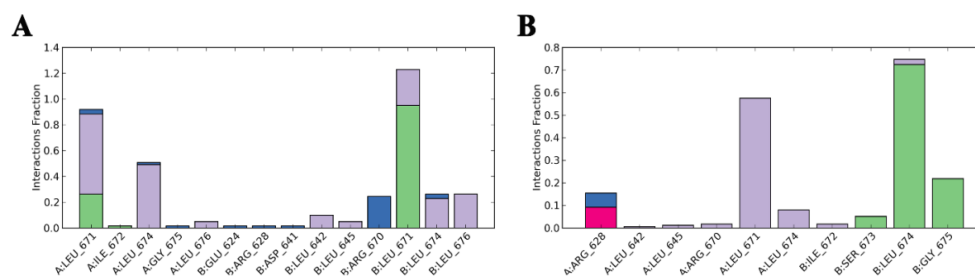
Figure 95 Bar Figure of the protein-ligand (P-L) contacts of **100** (panel A) and **103** (panel B). Hydrogen bonds are represented by green bars, hydrophobic as lilac bars, water bridges as blue bars, and ionic as fuchsia bars. The stacked bar charts are normalized over the course of the trajectory: for example, a value of 0.5 suggests that 50% of the simulation time the specific interaction is maintained.

5.4 Design of new libraries starting from the *N*-hexanamine quinazolinedione moiety of compound 103

The computational method applied for the development of novel mPGES-1 inhibitors was used in this case for the development of compound **103** derivatives. Thus, a flexible synthetic strategy was selected and novel libraries of derivatives were created.

5.4.1 Synthetic strategy for quinazolinedione derivatives

In this case, the synthetic strategy for the generation of derivatives provides the reaction between the isatoic anhydride and the amino acid with triethylamine in formic acid at reflux.[320] Then, the amide formation between the acidic group of the chain and an amine affords the final product.

172
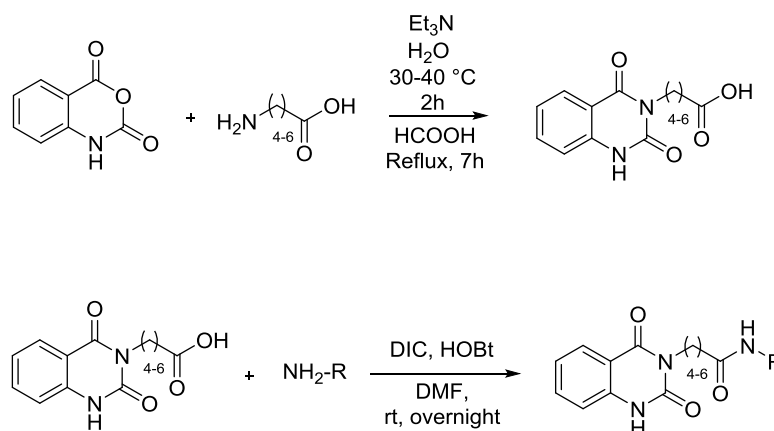
Figure 96 Synthetic strategy for quinazolinedione derivatives.

5.4.2 Generation of libraries of quinazolinedione derivatives

The design of libraries of compounds deriving from the novel disclosed hit was carried out basing on the reported chemical route. Specifically, in order to develop C-terminus Hsp90 inhibitors with an increasing activity in comparison to compound **103**, different items were considered. Length modifications of the *N*-exanamidic chain afforded two different scaffolds bearing a 5 and a 7 carbon chain respectively, in order to investigate the different binding modes onto the grid of the three-dimensional structure of the chaperone. Thus, a combinatorial approach was applied on three quinazolinedione items for the generation of three different libraries endowed with a 5, 6 or 7 carbon chain respectively. In particular, commercially available aromatic amines were combined with each selected scaffold, using Combiglide software. Then, LigPrep was applied for the generation of all possible tautomers, stereoisomers and protonation states at physiological pH, while QikProp determined pharmacokinetic parameters for each item of the libraries.

173
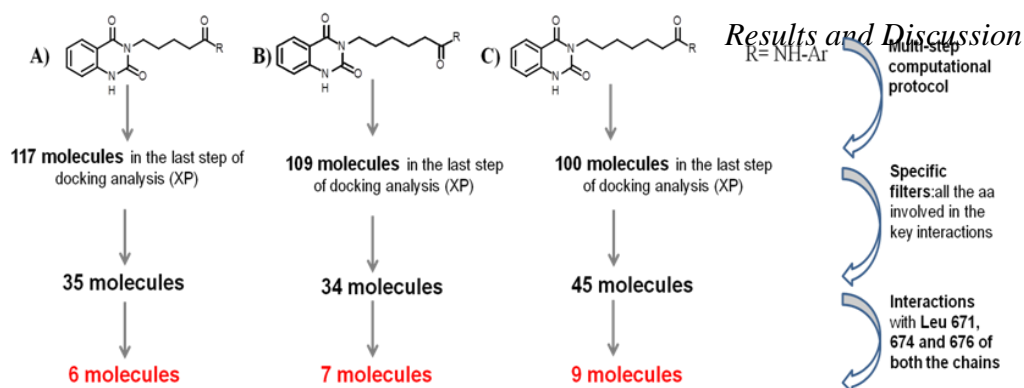
Figure 97 Design and selection of the most promising analogues of compound **103** using the multi-step computational protocol.

5.4.3 Docking studies and selection of the best candidates

Semi-flexible docking experiments were performed onto the close active crystal structure of yeast Hsp82. Starting from a detailed analysis of the interactions and the binding mode of compounds filtered via structure-based approach, 21 molecules were chosen from the three libraries for the next synthetic step. Most of the items present a halogen at position 4 of the benzene ring, according to the importance of the halogen bonds in the previously disclosed hits. Furthermore, based on the analysis of the docking score, compounds bearing a 7 carbon chain showed the best results. All the selected compounds present the typical pattern of hydrogen bonds with leucines residues previously reported. A representative example is reported below (Figure 98). Compound **157**, in fact, is able to establish hydrogen bonds with Leu676$_{chainA}$, Gly675$_{chainA}$, Leu674$_{chainB}$ and Ile672$_{chainB}$, and further hydrogen bonds with residues of chain A. Also, the iodide at position 4 interacts with Arg670$_{chainA}$ via halogen bond, a peculiarity of the hits reported above.
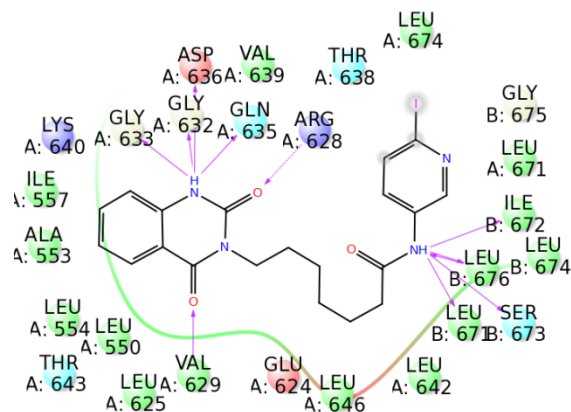
Figure 98 2D panel representation of compound **157** in the C-terminal domain of the 3D crystal structure of Hsp82 (PDB code: 2CG9).[313] Positive charged residues are colored in violet, negative charged residues are colored in red, polar residues are colored in light blue, hydrophobic residues are colored in green. The π-π stacking interactions are indicated as green lines, and H-bond are reported as dotted pink arrows.
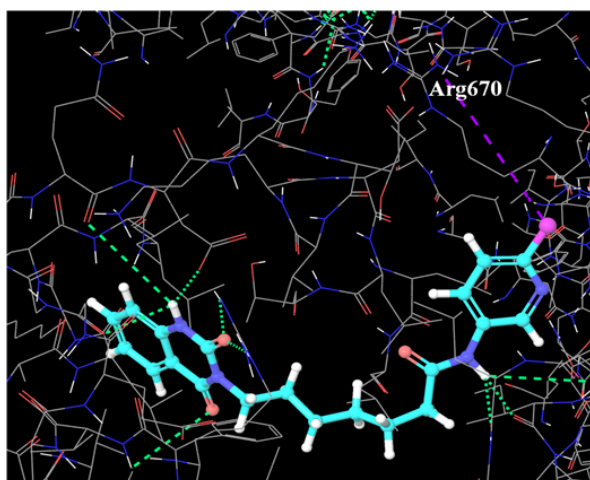
Figure 99 Three-dimensional representation of compound **157** in the C-terminal domain of the 3D crystal structure of Hsp82 (PDB code: 2CG9).[313] Purple lines represent specific halogen bonds with the receptor counterpart. A selective representation of halogen bond interactions is reported.

175
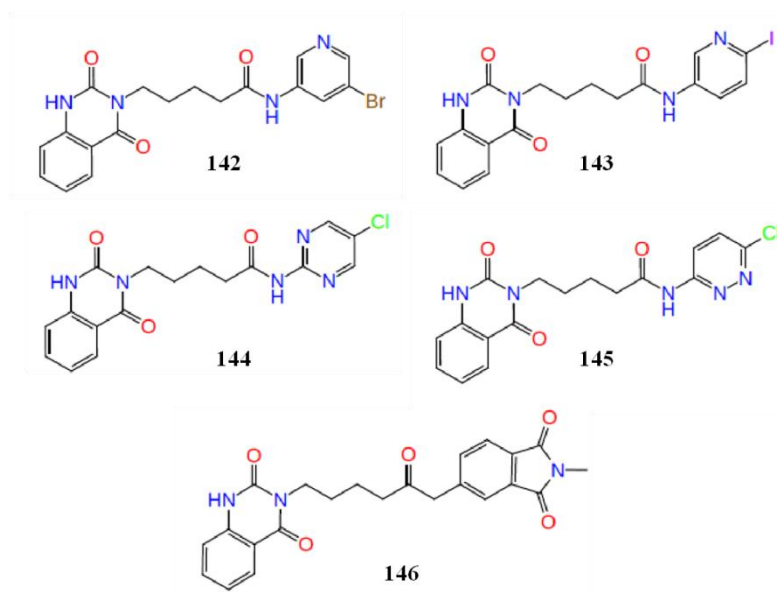
Figure 100 5 carbon chain selected compounds

.
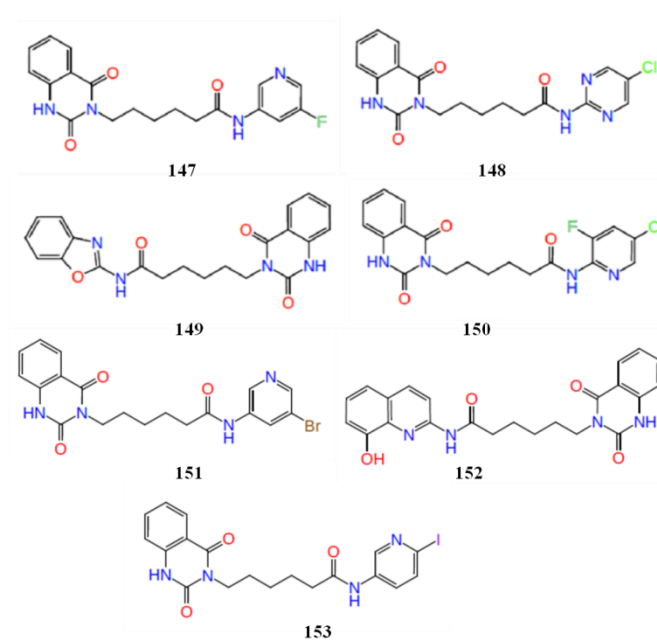
Figure 101 6 carbon chain selected compounds.

176
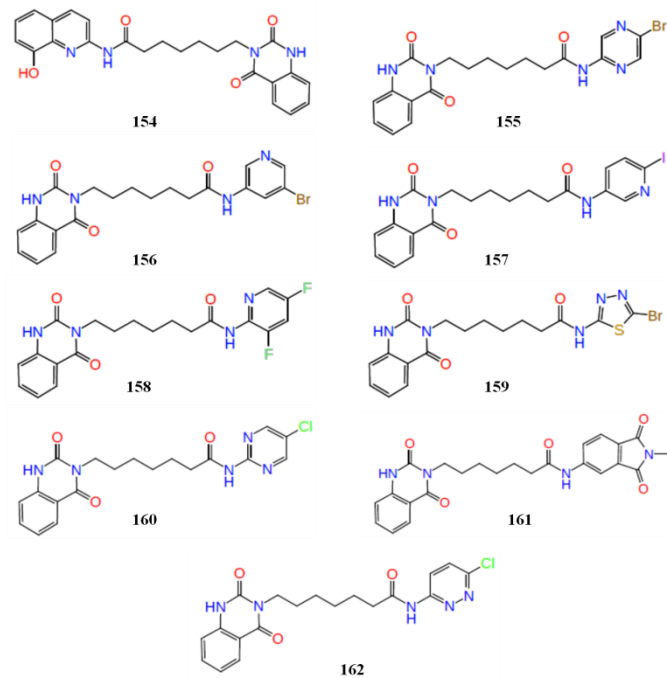
Figure 102 7 carbon chain selected compounds.

-CONCLUSIONS-

Conclusions

The research work carried out in the frame of my three years PhD has been focused on the development and the identification of new molecular platforms for the treatment of inflammation and cancer. Among the proteins of interest, the inducible microsomal Prostaglandin E$_2$ Synthase-1 (mPGES-1) was the main target, due to its biological importance in both the mentioned pathologies. Thus, the application of a protocol based on a combination of computational chemistry tools and experimental synthesis was for me very useful to identify different chemical items able to inhibit the activity of the synthase. In particular, benzothiazole **1**, **3**, **6**, **9** and **13**, thiadiazole **18-20** and **22**, pyrrole **45** and **47** based molecules presented promising results in the biological evaluation on mPGES-1 in both cell-free and cell lines tests. Furthermore, I applied my protocol to SnAP (Stannyl Amine Protocol) chemistry and I had the opportunity to move to the Department of Chemistry and Applied Biosciences at ETH for the synthetic part. Currently, biological tests are in progress for the 20 synthesized compounds.

SnAP chemistry took place in the generation of a database of about 1,300,000 synthetically accessible compounds. A new generation of SnAP reagents, called iSnAP (Iterative SnAP) reagents, provided for the possibility of further substitutions and functionalization of the saturated heterocyclic core.

Also, computational chemistry techniques based on both ligand and structure based approaches were crucial for disclosing two novel 3-hydroxy-3-pyrrolin-2-one-based hits (compounds **87** and **88**).

Another important protein target selected as a good candidate in this research project is the molecular chaperone Hsp90, whose inhibition is considered one of the most important therapeutic strategy for the treatment of

several cancers. A multidisciplinary approach was applied for the discovery of new C-terminus inhibitors, considering the numerous advantages in comparison to N-terminal inhibitors. Thus, two novel structurally unrelated hits (compounds **100** and **103**) were identified among 48 commercially available compounds, with a high binding affinity for C-terminal Hsp90. A computational rationalization was very useful to understand the molecular fingerprints of the interactions between the new hits and the receptor counterpart. These findings gave the input for an optimization campaign, which was carried out following the multi-step computational protocol applied for the discovery of novel mPGES-1 inhibitors. Thus, 21 molecules were selected from three libraries of compounds derived from the new hit **103**.

All these promising results may stimulate further research towards the individuation of novel inhibitors or the optimization of the identified hits, considering the high potential that the inhibition of the activity of the two protein targets has in the treatment of two related inflammation and cancer pathologies.

-EXPERIMENTAL SECTION-

-CHAPTER 6-

Computational details and synthesis of 2-amino-1,3-benzothiazole derivatives as mPGES-1 inhibitors

6.1 Computational details

The structures of the reagents, namely all commercially available acid-chlorides and boronates at Sigma Aldrich Company, were converted from 2D structures to 3D structures suitable for the docking stage of the process, using LigPrep software (v. 3.4; Schrödinger, LLC, 2015). Then, the compounds were prepared using Reagent Preparation: in the acyl chlorides, a cleavage between the chloride and the carbonyl group was applied in order to select the carbonyl moiety as building block, while the acidic moiety was removed in the boronic acids. The final .bld files were combined with the scaffolds obtaining the novel libraries (**A** and **B**). LigPrep performed calculation increased the number to 607,602 molecules for libraries **A** and **B**, and a final energy minimization of the two libraries with Optimized Potentials for Liquid Simulations (OPLS) 2005 force field was performed. After the application of QikProp[110] and LigFilter, [117] the final libraries **A**+**B** contained 233,273.

In the docking step, mPGES-1 three-dimensional crystal structure (PDB code: 4BPM)[209] was used for the structure-based molecular docking experiments. The three-dimensional model of the protein was prepared using the Schrödinger Protein Preparation Wizard,[117] starting from the aforementioned crystal structure co-complexed with the inhibitor LVJ (2-[[2,6-bis(chloranyl)-3-[(2,2-dimethylpropanoylamino)methyl]phenyl]amino]-1-methyl-6-(2-methyl-2-oxidanyl-propoxy)-N-[2,2,2-tris(fluoranyl)ethyl]benzimidazole-5-carboxamide) (PDB code: 4BPM).[209] The combinatorial libraries were submitted to structure-based molecular docking experiments on the mPGES-1 3D protein structure, using Glide software.[103, 104] Basically, the virtual screening workflow[117] (section 3.3.3) was used: a first round of docking experiments was performed setting the High-Throughput

Virtual Screening (HTVS) precision mode of Glide that allows a first enrichment from the starting library of compounds with a high fastness. The 30% top-ranked poses, filtered according to docking score values, were then submitted to a second round of docking experiments, using the Standard Precision (SP) which outperforms the first step in both sampling and scoring performances. Again, the 30% top-ranked poses were then submitted to the Extra-Precision (XP) Glide mode experiment, the final and most accurate docking step. During the molecular docking calculation, the adopted receptor grid was focused onto the co-crystallized ligand binding site (LVJ) with inner- and outer-box dimensions of 18×18×18 and 34.7×34.7×34.7, respectively.

6.2 General synthetic methods

The compounds 2-amino-6-bromo-1,3-benzothiazole and 2-amino-5-bromo-1,3-benzothiazole were purchased from Sigma Aldrich and used as received. All solvents used for the synthesis were of HPLC grade, and were purchased from Sigma-Aldrich and Carlo Erba Reagenti. NMR spectra were recorded on 300 or 400 MHz Bruker Avance instrument. All compounds were dissolved in 0.5 mL of the following solvents: chloroform-d (Sigma-Aldrich, 99.8 Atom % D); methanol-d_4 (Sigma-Aldrich, 99.8 Atom % D); dimethylsulfoxyde-d_6 (Sigma-Aldrich, 99.8 Atom % D). Coupling constants (*J*) are reported in Herz, and chemical shifts are expressed in parts per million (ppm) on the delta (δ) scale relative to $CHCl_3$ (7.19 ppm for ^1H and 77.0 ppm for ^{13}C) or CH_3OH (3.31 ppm for ^1H and 49.15 ppm for ^{13}C) or DMSO (2.50 ppm for ^1H and 39.51 ppm for ^{13}C) as internal reference. Multiplicities are reported as follows: s, singlet; d, doublet; t, triplet; m, multiplet; dd, doublet of doublets. ^{13}C NMR spectra were obtained at 100 MHz and referenced to the internal solvent signal. High Resolution Mass Spectrometry spectra (HRMS)

184

were performed on a LCQ DECA TermoQuest (San Josè, California, USA) mass spectrometer. Reactions were monitored on silica gel 60 F254 plates (Merck), and the spots were visualized under UV light. Analytical and semi-preparative reversed-phase HPLC was performed on Agilent Technologies 1200 Series high performance liquid chromatography using a Synergi Fusion C18 reversed-phase column (250 x 4.60mm, 4μ, 80 Å, flow rate = 1 mL/min; 250 x 10.00mm, 10μ, 80 Å, flow rate = 4 mL/min respectively, Phenomenex®). The binary solvent system (A/B) was as follows: 0.1% TFA in water (A) and 0.1% TFA in CH_3CN (B); gradient condition: from 5% B to 100 % B in 50 min. The absorbance was detected at 240 nm. All tested compounds were obtained with high purity (> 98% detected by HPLC analysis) and were fully characterized by HRMS, and NMR spectra.

6.3 General prodecure for the synthesis of compounds 1-3, 7-10 and 11-13
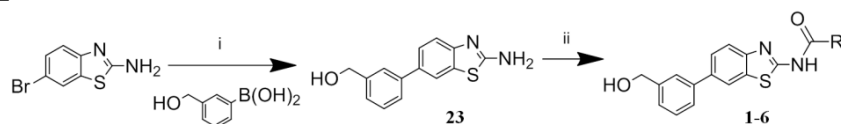
Reagents and conditions: **i**: $Pd(PPh_3)_4$, K_2CO_3, 1,4-dioxane-H_2O, 80°C; **ii:** a) TMSCl, py, dry CH_3CN, r.t.; b) RCOCl, r.t.
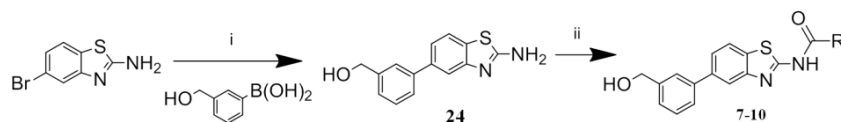
Reagents and conditions: **i**: $Pd(PPh_3)_4$, K_2CO_3, 1,4-dioxane-H_2O, 80°C; **ii:** a) TMSCl, py, dry CH_3CN, r.t.; b) RCOCl, r.t.
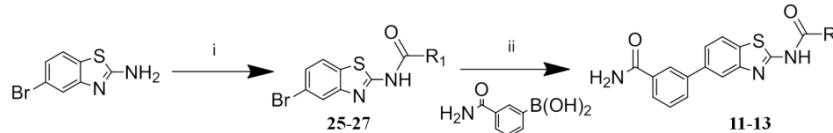
Reagents and conditions: **i**) RCOCl, py, CH_3CN dry, r.t. **ii**) $Pd(PPh_3)_4$, K_2CO_3, 1,4-dioxane-H_2O, 80°C.
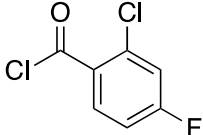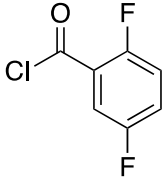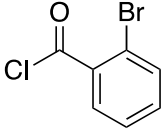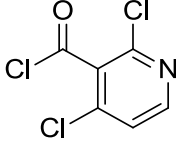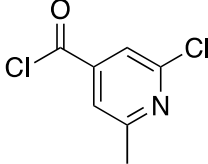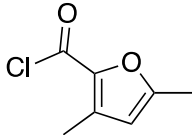
Scheme 1 Synthetic method for the synthesis of benzothiazole-based derivatives (**1-13**).

The synthesis of benzothiazole derivatives was carried out according to the selected synthetic route depicted in scheme 1. Pd-catalyzed Suzuki-Miyaura cross-coupling was performed between 3-(hydroxymethyl)phenylboronic acid and 2-amino-6-bromobenzothiazole or 2-amino-5-bromobenzothiazole respectively. The Suzuki-Miyaura reaction was chosen for our purpose because it is an efficient and versatile method for highly functionalized biaryls synthesis, in good yields under mild conditions. For the preparation of our compounds, the cross-coupling was performed under standard conditions using Pd(PPh$_3$)$_4$ as catalyst and aqueous carbonate base in a mixture of dioxane (80%) and H$_2$O (20%) at 80 °C. Reactions proceeded with good yields (75% and 88%). Since the (hydroxymethyl)phenyl portion presented a primary alcohol it was necessary the protection of hydroxyl group before acylation reaction. We opted for a transient protection by trimethylsilyl ether which was formed *in situ* in dry acetonitrile at room temperature with pyridine and removed with acidic work-up. Acylation of the protected aminobenzothiazole nucleus was then accomplished adding to the reaction mixture the proper acyl chloride (**a-h**, Table 12). Compound **1-6** and **7-10** were obtained with moderate to high yields (32–85%). For compounds **11-13** we opted for a different synthetic approach because acylation of 2-amino-5-bromobenzothiazole gave less polar compounds with consequently easier purifications. Acylation reactions were conducted in dry acetonitrile with pyridine at room temperature, between 2-amino-5-bromobenzothiazole and the proper acyl chloride (**f-h**, Table 12). Compounds **25-27** were then subjected to Suzuki-Miyaura coupling with 3-aminocarbonylphenylboronic acid to give **11**, **12** and **13** (32%, 42% and 45% yields respectively). All compounds were

purified by reverse phase HPLC or flash column chromatography using different EtOAc:hexane mixtures, and were obtained with >98% purity.

Compound	Acyl chloride
a	
b	
c	
d	
e	
f	

187

g	
h	

Table 12 List of acyl chlorides used for the synthesis of benzothiazole derivatives.

6.3.1 Synthesis of 3[3-(2-Amino-benzothiazol-6-yl)-phenyl]-methanol (compound 23)
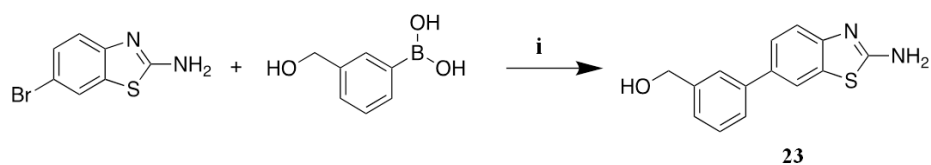
2-Amino-6-bromobenzothiazole (460 mg, 1.0 equiv.), 3-(hydroxymethyl)phenylboronic acid (365 mg, 1.2 equiv.), and tetrakis(triphenylphosphine)palladium(0) (115 mg, 5 mol%), were sequentially added to a degassed mixture of 1,4-dioxane (80%) and water (20%) (10 mL) and the mixture was stirred at r.t. for 30 min. Degassed aqueous Na_2CO_3 solution (1 M, 2 equiv.) was added and the reaction mixture was heated under argon at 80 °C for 16 h. The mixture was transferred to a separating funnel, ethyl acetate was added and the organic layer was washed with brine, separated, and dried over $MgSO_4$. The solvent was removed under reduced pressure, and the residue was purified by chromatography on silica gel eluting

with a mixture of ethyl acetate (70%) and hexane (30%) to give 0.365 g (75%) of compound **23** as a pale oil.

^{1}H NMR (CD$_3$OD, 300 MHz): δ 7.74 (d, *J* = 1.8 Hz, 1H), 7.50 (s, 1H), 7.42 (dd, *J* = 8.4, 1.9 Hz, 1H), 7.39 (m, 1H), 7.33 (d, *J* = 8.4 Hz, 1H), 7.28 (t, *J* = 7.6 Hz, 1H), 7.16 (dd, *J* = 7.6 Hz, 1H), 4.56 (s, 2H).

6.3.2 Synthesis of [3-(2-Amino-benzothiazol-5-yl)-phenyl]-methanol (compound 24)
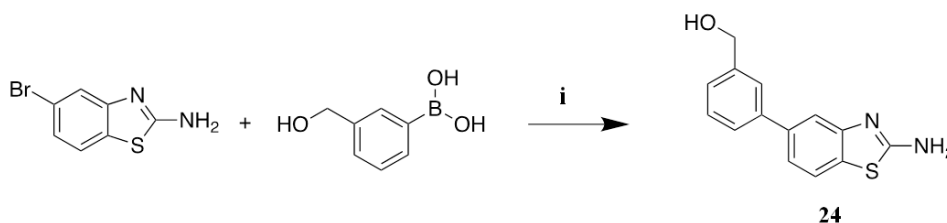
2-Amino-5-bromobenzothiazole (300 mg, 1.0 equiv.), 3-(hydroxymethyl)phenylboronic acid (237 mg, 1.2 equiv.), and tetrakis(triphenylphosphine)palladium(0) (75 mg, 5 mol%), were sequentially added to a degassed mixture of 1,4-dioxane (80%) and water (20%) (50 mL) and the mixture was stirred at r.t. for 30 min. Degassed aqueous Na$_2$CO$_3$ solution (1 M, 2 equiv.) was added and the reaction mixture was heated under argon at 80 °C for 16 h. The mixture was transferred to a separating funnel, ethyl acetate was added and the organic layer was washed with brine, separated, and dried over MgSO$_4$. The solvent was removed under reduced pressure, and the residue was purified by flash chromatography on silica gel eluting with a mixture of ethyl acetate (70%) and hexane (30%) to give 0.278 g (88%) of compound **24** as a pale oil.

^{1}H NMR (CD$_3$OD, 400 MHz): δ 7.49 (d, *J* = 1.7 Hz, 1H), 7.46 (s, 1H), 7.35 (d, *J* = 8.1 Hz, 1H), 7.30 (dd, *J* = 7.6, 1.7 Hz, 1H), 7.19 (t, *J* = 7.5 Hz, 1H), 7.14 (dd, *J* = 7.6, 1.6 Hz, 1H), 7.10 (dd, *J* = 8.2, 1.8 Hz, 1H), 4.51 (s, 2H).

6.3.3 General procedure for acylation reactions (compounds 1-10)
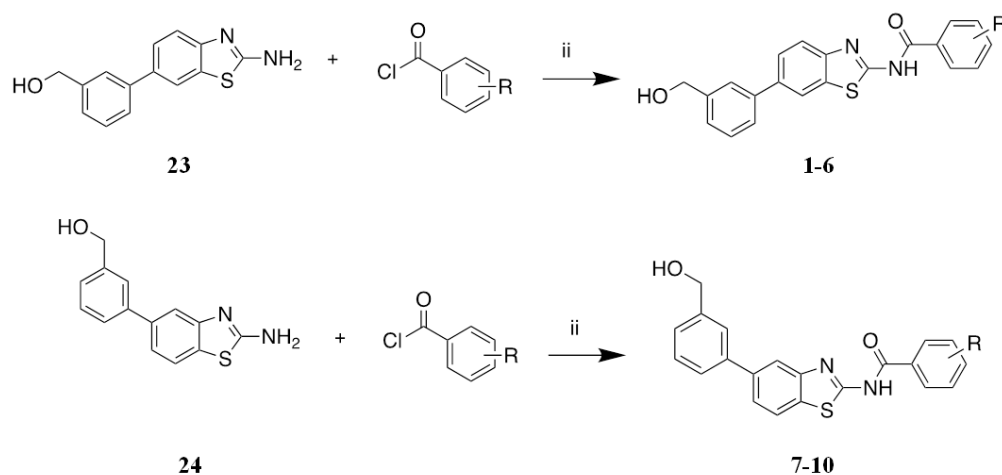
To a solution of compounds **23** or **24** (50 mg, 1 equiv.) in dry acetonitrile (10 mL) and pyridine (0.49 mL, 30 equiv.) was added chlorotrimethylsilane (0.26 mL, 10 equiv.) at 0 °C. The resulting mixture was stirred at r.t. for 3 h, then the proper acyl chloride (Table 12) was added (1.5 equiv) and the reaction mixture was stirred overnight. The mixture was diluted with ethyl acetate, washed with 0.5 N HCl (10 mL x 3) and brine (10 mL) and dried (MgSO$_4$). The solvent was removed under reduced pressure, and the residue was purified by flash column chromatography using different EtOAc:hexane mixtures or by semi-preparative reversed-phase HPLC, using a Sinergy Fusion, C18 reversed-phase column and the following conditions: a

mutigradient from 5% to 100% CH_3CN over 50 min, flow rate = 4 mL/min, UV detector at 240 nm. Yields for each compound are reported below.

2-chloro-4-fluoro-*N*-(6-(3-(hydroxymethyl)phenyl)benzo[*d*]thiazol-2-yl)benzamide (compound 1)
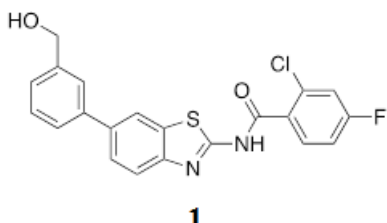
was obtained by following the general procedure, using 2-chloro-4-fluorobenzoyl chloride (**a**) (65% yield).

^{1}H NMR (CD$_3$OD, 400 MHz): δ 8.08 (d, *J* = 1.8 Hz, 1H), 7.73 (d, *J* = 8.4 Hz, 1H), 7.64 (dd, *J* = 8.3, 2.1 Hz, 2H), 7.59 (s, 1H), 7.50 (m, 1H), 7.34 (t, *J* = 7.5 Hz, 1H), 7.32 (dd, *J* = 8.4, 2.5 Hz, 1H), 7.26 (m, 1H), 7.16 (td, *J* = 8.4, 2.5 Hz, 1H), 4.60 (s, 2H); ^{13}C NMR (CD$_3$OD, 100 MHz): δ 167.0; 165.3 (d, *J* = 252 Hz), 160.0, 149.5, 145.3, 143.6, 142.3, 139.0, 134.3 (d, *J* = 13.8 Hz), 132.6 (d, *J* = 9.6 Hz), 132.3 (d, *J* = 3.0 Hz), 130.1, 127.3, 127.1, 126.9, 126.9, 122.3, 120.8, 118.9 (d, *J* = 25.0 Hz), 115.8 (d, *J* = 22.0 Hz), 65.31; ESI-HRMS calcd for $C_{21}H_{15}ClFN_2O_2S$ [M+ H]$^+$ 413.0527, found 413.05237.

2,5-difluoro-*N*-(6-(3-(hydroxymethyl)phenyl)benzo[*d*]thiazol-2-yl)benzamide (compound 2)

2
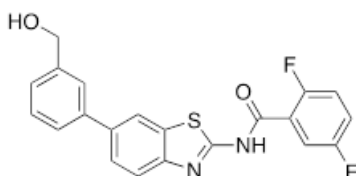
was obtained by following the general procedure, using 2,5-difluorobenzoyl chloride (**b**). Purification was performed by semi-preparative reversed-phase HPLC, t_R = 36 min. The pure product was obtained as a white solid. (72% yield).

^{1}H NMR (CD$_3$OD, 400 MHz): δ 8.20 (d, *J* = 1.8 Hz, 1H), 7.87 (d, *J* = 8.4 Hz, 1H), 7.77 (dd, *J* = 8.4, 1.8 Hz, 1H), 7.71 (s, 1H), 7.65 (m, 2H), 7.47 (t, *J* = 7.6 Hz, 1H), 7.40 (m, 3H), 4.72 (s, 2H); ^{13}C NMR (CD$_3$OD, 100 MHz): δ 160.1 (d, *J* = 32.0 Hz), 157.6, 156.9 (d, *J* = 214.0 Hz), 156.5 (d, *J* = 228.0 Hz), 147.4, 141.5, 140.9, 137.7, 129.8, 129.1, 126.6, 126.2, 126.2, 125.9, 122.1 (dd, J = 24.5, 9.8 Hz), 121.2, 120.1 (m), 119.8, 118.4 (d, *J* = 26.0 Hz), 118.1 (dd, *J* = 17.0, 8.0 Hz), 65.3; ESI-HRMS calcd for C$_{21}$H$_{15}$F$_2$N$_2$O$_2$S 397.0822 [M+ H]$^+$, found 397.08175.

2-bromo-*N*-(6-(3-(hydroxymethyl)phenyl)benzo[*d*]thiazol-2-yl)benzamide (compound 3)

3
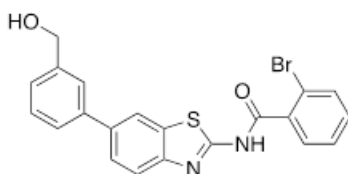
was isolated by following the general procedure, using 2-bromobenzoyl chloride (**c**). Purification was performed by semi-preparative reversed-phase HPLC, t_R = 41 min. The pure product was obtained as a colorless oil (78% yield).

^{1}H NMR (CD$_3$OD, 400 MHz): δ 8.19 (d, J = 1.8 Hz, 1H), 7.85 (d, J = 8.4 Hz, 1H), 7.76 (d, J = 8.2 Hz, 2H), 7.71 (s, 1H), 7.62 (m, 2H), 7.54 (td, J = 7.5, 1.2 Hz, 1H), 7.47 (m, 2H), 7.37 (d, J = 7.5 Hz, 1H), 4.72 (s, 2H); ^{13}C NMR (CD$_3$OD, 100 MHz): δ 168.7, 160.0, 149.5, 143.6, 142.2, 139.0, 138.0, 134.6, 134.4, 133.7, 133.3, 130.4, 130.1, 128.9, 127.2, 127.1, 126.9, 126.9, 122.3, 120.8, 65.3; ESI-HRMS calcd for C$_{21}$H$_{14}$BrN$_2$O$_2$S [M- H]$^-$ 436.0038, found 436.99646.

_N_-(5-(3-(hydroxymethyl)phenyl)benzo[_d_]thiazol-2-yl)-2,4-dimethylnicotinamide (compound 4)
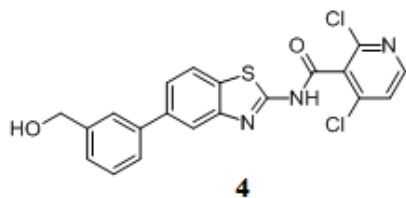
was isolated as a white solid using 2,4-dichloropyridine-3-carbonyl chloride (**d**) (51% yield).

^{1}H NMR (CD$_3$OD, 400 MHz): δ 8.48 (d, J = 5.5 Hz, 1H), 8.22 (d, J = 1.8 Hz, 1H), 7.87 (d, J = 8.5 Hz, 1H), 7.77 (dd, J = 8.5, 1.8 Hz, 1H), 7.71 (s, 1H), 7.66 (d, J = 5.4 Hz, 1H), 7.62 (d, J = 8.0 Hz, 1H), 7.45 (t, J = 7.6 Hz, 1H), 7.37 (d, J = 7.7 Hz, 1H), 4.71 (s, 2H).

2-chloro-*N*-(5-(3-(hydroxymethyl)phenyl)benzo[*d*]thiazol-2-yl)-6-methylisonicotinamide (compound 5)

5
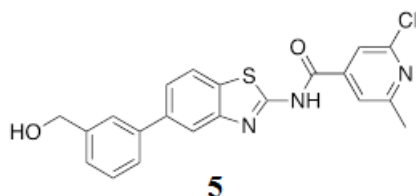
was isolated as a white solid using 2-chloro-6-methylpyridine-4-carbonyl chloride (**e**) (53% yield).

^{1}H NMR (CDCl$_3$, 400 MHz): δ 8.03 (d, J = 1.6 Hz, 1H), 7.87 (m, 3H), 7.80 (dd, *J* = 8.5, 1.7 Hz, 1H), 7.59 (s, 1H), 7.51 (d, *J* = 7.5 Hz, 1H), 7.44 (t, *J* = 7.6 Hz, 1H), 7.35 (d, *J* = 7.5 Hz, 1H), 4.77 (s, 2H), 2.63 (s, 3H).

N-(6-(3-(hydroxymethyl)phenyl)benzo[*d*]thiazol-2-yl)-3,5-dimethylfuran-2-carboxamide (compound 6)

6
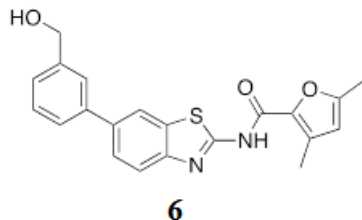
was obtained by following the general procedure, using 2,5-dimethylfuran-3-carbonyl chloride (**f**). Purification was performed by semi-preparative reversed-phase HPLC, t$_R$ = 36 min. The pure product was obtained as a colorless oil (80% yield).

^{1}H NMR (CDCl$_3$, 400 MHz): δ 7.96 (d, *J* = 1.6 Hz, 1H), 7.83 (d, *J* = 8.5 Hz, 1H), 7.75 (d, *J* = 8.5 Hz, 1H), 7.58 (s, 1H), 7.49 (d, *J* = 7.8 Hz, 1H), 7.42 (t, *J* = 7.6 Hz, 1H), 7.34 (d, *J* = 7.5 Hz, 1H), 6.77 (s, 1H), 4.75 (s, 2H), 2.61 (s, 3H), 2.27 (s, 3H); ^{13}C NMR (CDCl$_3$, 100 MHz): δ 162.0, 161.7, 160.4, 151.2,

141.7, 140.3, 138.6, 129.9, 129.2, 127.1, 126.6, 126.3, 125.8, 120.0, 118.3, 114.5, 113.9, 103.7, 65.1, 14.1, 13.3; ESI-HRMS calcd for $C_{21}H_{19}N_2O_3S$ [M+ H]$^+$ 379.1116, found 379.11122.

2-bromo-*N*-(5-(3-(hydroxymethyl)phenyl)benzo[*d*]thiazol-2-yl)benzamide (compound 7)
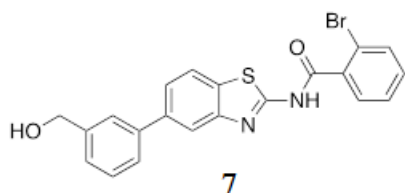
7

was obtained by following the general procedure, using 2-bromobenzoyl chloride (**c**). Purification was performed by semi-preparative reversed-phase HPLC, t_R = 36 min. The pure product was obtained as a colorless oil (78% yield).

^{1}H NMR (CDCl$_3$, 400 MHz): δ 7.89 (m, 2H), 7.77 (dd, *J* = 7.6, 1.8 Hz, 1H), 7.61 (m, 3H), 7.53 (m, 1H), 7.44 (t, *J* = 7.6 Hz, 1H), 7.39 (m, 2H), 7.31 (td, *J* = 7.7, 1.8 Hz, 1H), 4.77 (s, 2H); ^{13}C NMR (CDCl$_3$, 100 MHz): δ 165.7, 161.0, 144.9, 141.5, 140.6, 140.4, 134.1, 133.9, 132.9, 130.1, 129.1, 129.0, 127.7, 126.7, 126.3, 125.9, 124.3, 121.8, 120.2, 117.5, 65.2; ESI-HRMS calcd for $C_{21}H_{16}BrN_2O_2S$ [M+ H]$^+$ 439.0116, found 439.01075.

2-chloro-4-fluoro-*N*-(5-(3-(hydroxymethyl)phenyl)benzo[*d*]thiazol-2-yl)benzamide (compound 8)

8
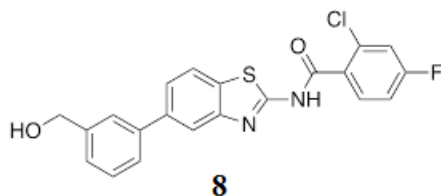
was obtained as a white solid using 2-chloro-4-fluorobenzoyl chloride (**a**) (82% yield).

^{1}H NMR (CDCl$_3$, 400 MHz): δ 7.85 (d, J = 8.3 Hz, 1H), 7.77 (dd, J = 8.7, 5.9 Hz, 1H); 7.58 (m, 2H), 7.44 (m, 3H), 7.38 (m, 1H), 6.90 (dd, J = 8.3, 2.4 Hz, 1H), 6.84 (td, J = 8.1, 2.4 Hz, 1H), 4.77 (s, 2H); ^{13}C NMR (CDCl$_3$, 100 MHz): δ 164.5 (d, J = 255 Hz), 163.5, 161.4, 158.2, 141.8, 141.3, 140.0, 134.4, 132.8 (d, J = 9.8 Hz), 129.6, 129.3, 127.2, 126.6, 126.6, 126.0, 125.0, 122.2, 118.9 (d, J = 25.0 Hz), 117.0, 115.2 (d, J = 21.8 Hz), 65.18; ESI-HRMS calcd for C$_{21}$H$_{15}$ClFN$_2$O$_2$S [M+ H]$^+$ 413.0527, found 413.05191.

N-(5-(3-(hydroxymethyl)phenyl)benzo[*d*]thiazol-2-yl)-3,5-dimethylfuran-2-carboxamide (compound 9)
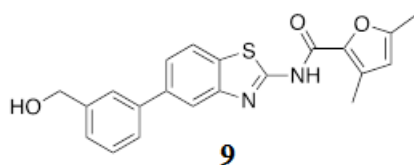
was isolated as a colorless oil using 2,5-dimethylfuran-3-carbonyl chloride (**f**) (65% yield).

^{1}H NMR (CDCl$_3$, 400 MHz): δ 7.83 (d, J = 8.2 Hz, 1H), 7.77 (d, J = 1.5 Hz, 1H), 7.56 (s, 1H), 7.51 (dd, J = 8.2, 1.5 Hz, 1H), 7.48 (m, 1H), 7.42 (t, J = 7.5 Hz, 1H), 7.35 (m, 1H), 6.28 (s, 1H), 4.76 (s, 2H), 2.63 (s, 3H), 2.17 (s, 3H); ^{13}C NMR (CDCl$_3$, 100 MHz): δ 162.7, 161.4, 160.7, 151.5, 141.8, 141.7, 139.8, 129.3, 129.1, 126.7, 126.5, 125.8, 125.0, 122.3, 115.7, 113.7, 113.7, 103.9, 65.1, 14.0, 13.2; ESI-HRMS calcd for C$_{21}$H$_{19}$N$_2$O$_3$S [M+ H]$^+$ 379.1116, found 379.11113.

2,6-dichloro-*N*-(5-(3-(hydroxymethyl)phenyl)benzo[*d*]thiazol-2-yl)benzamide (compound 10)
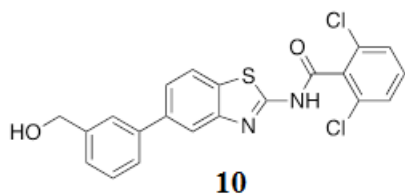
was obtained by following the general procedure, using 2,6-dichlorobenzoyl chloride (**g**). The pure product was obtained as a white solid (85% yield).

^{1}H NMR (CDCl$_3$, 400 MHz): δ 7.83 (d, *J* = 8.3 Hz, 1H), 7.59 (s, 1H), 7.53 (dd, *J* = 8.4, 1.4 Hz, 1H), 7.49 (m, 2H), 7.39 (m, 1H), 7.36 (s, 1H), 6.84 (m, 2H), 6.77 (dd, *J* = 9.3, 6.6 Hz, 1H), 4.81 (s, 2H); ^{13}C NMR (DMSO-d$_6$ 100 MHz): δ 163.2, 157.9, 149.3, 143.3, 139.7, 139.0, 134.2, 132.3 (2C), 131.1, 130.6, 128.8, 128.3, 125.6 (2C), 125.3, 125.0, 123.0, 122.3, 118.0, 62.9; ESI-HRMS calcd for C$_{21}$H$_{15}$Cl$_2$N$_2$O$_2$S [M+ H]$^{+}$ 429.0231, found 429.02242.

6.3.4 General procedure for the preparation of compounds 25-27

25-27
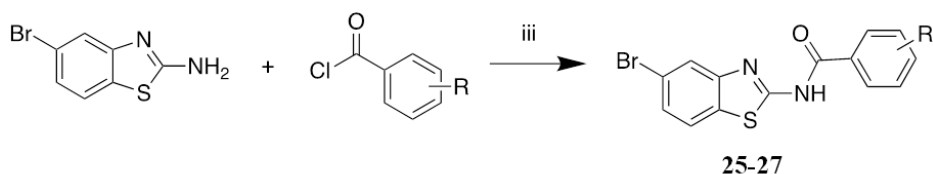
To a solution of 2-amino-5-bromobenzothiazole (200 mg, 1 equiv.) in dry acetonitrile (20 mL) and pyridine (0.11 mL, 1.5 equiv.) the proper acyl chloride was added (1.2 equiv) and the reaction mixture was stirred overnight. The mixture was diluted with ethyl acetate, washed with water (10 mL x 2) and brine (10 mL) and dried over anhydrous MgSO$_4$. The solvent was removed under reduced pressure, and the residue was purified by flash chromatography on silica gel, eluting with a ethyl acetate (70%) and hexane (30%) mixture.

N-(5-bromobenzo[*d*]thiazol-2-yl)-3,5-dimethylfuran-2-carboxamide (compound 25)

25
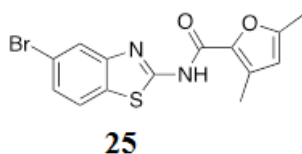
was isolated as a colorless oil using 2,5-dimethylfuran-3-carbonyl chloride (**f**) (83 % yield).

^{1}H NMR (CDCl$_3$/CD$_3$OD 1:1, 300 MHz): δ 7.86 (d, *J* = 1.9 Hz, 1H), 7.69 (d, *J* = 8.4 Hz, 1H), 7.37 (dd, *J* = 8.5, 1.9 Hz, 1H), 6.49 (s, 1H), 2.58 (s, 3H), 2.27 (s, 3H).

N-(5-bromobenzo[*d*]thiazol-2-yl)-2,6-dichlorobenzamide   (compound 26)

26
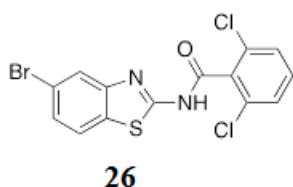
was isolated as a colorless oil using 2,6-dichlorobenzoyl chloride (**g**) (75% yield).

^{1}H NMR (CDCl$_3$, 400 MHz): δ 8.69 (d, *J* = 1.7 Hz, 1H), 7.53 (dd, *J* = 8.3, 1.8 Hz, 1H), 7.46 (d, *J* = 8.3 Hz, 1H), 6.83 (m, 2H), 6.83 (dd, *J* = 8.8, 7.3 Hz, 1H).

N-(5-bromobenzo[*d*]thiazol-2-yl)-4-fluoro-2-(trifluoromethyl)benzamide (compound 27)

27
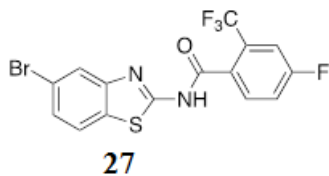
was isolated as a colorless oil using 4-fluoro-2-(trifluoromethyl)benzoyl chloride (**h**) (93% yield).

¹H NMR (DMSO-d₆, 400 MHz): δ 8.28 (d, *J* = 1.8 Hz, 1H), 8.08 (dd, *J* = 8.7, 5.2 Hz, 1H), 7.99 (d, *J* = 8.2 Hz, 1H), 7.88 (dd, *J* = 9.2, 2.5 Hz, 1H), 7.74 (dd, *J* = 8.2, 1.8 Hz, 1H), 7.68 (m, 1H).

6.3.5 General procedure for the preparation of compounds 11-13

Compounds **25-27** (1.0 equiv.), 3-aminocarbonylphenylboronic acid (1.2 equiv.), and tetrakis(triphenylphosphine)palladium(0) (5 mol%), were sequentially added to a degassed mixture of 1,4-dioxane (80%) and water (20%) (50 mL) and the mixture was stirred at r.t. for 30 min. Degassed aqueous Na₂CO₃ solution (1 M, 2 equiv.) was added and the reaction mixture was heated under argon at 80 °C for 16 h. The mixture was transferred to a separating funnel, ethyl acetate was added and the organic layer was washed

with brine, separated, and dried over MgSO$_4$. The solvent was removed under reduced pressure, and the residue was purified by semi-preparative reversed-phase HPLC.

N-(5-(3-carbamoylphenyl)benzo[*d*]thiazol-2-yl)-3,5-dimethylfuran-2-carboxamide (compound 11)
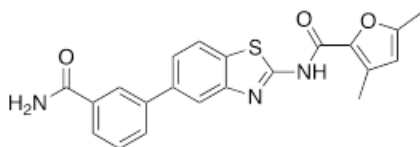
11

was obtained by following the general procedure. Purification was performed by semi-preparative reversed-phase HPLC, t_R = 38 min. The product was isolated as a white solid (32% yield).

^{1}H NMR (CDCl$_3$, 400 MHz): δ 8.08 (s, 1H), 8.00 (s, 1H), 7.91 (d, *J* = 8.3 Hz, 1H), 7.84 (d, *J* = 7.7 Hz, 2H), 7.70 (d, *J* = 8.5 Hz, 1H), 7.59 (t, *J* = 7.9 Hz, 1H), 6.81 (s, 1H), 2.65 (s, 3H), 2.31 (s, 3H); ^{13}C NMR (DMSO-d$_6$, 100MHz): δ 167.9, 162.1, 159.1, 158.0, 157.7, 149.8, 149.4, 140.2, 138.1, 135.0, 129.8, 129.0, 126.6, 125.9, 122.7, 122.2, 118.4, 115.8, 104.8, 13.7, 13.1; ESI-HRMS calcd for C$_{21}$H$_{18}$N$_3$O$_3$S [M+ H]$^+$ 392.1069, found 392.10680.

N-(5-(3-carbamoylphenyl)benzo[*d*]thiazol-2-yl)-2,6-dichlorobenzamide (compound 12)

12
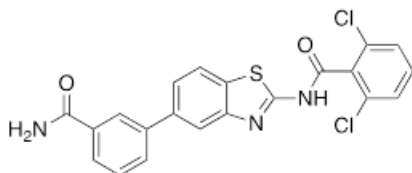
was obtained by following the general procedure and isolated as a white solid (42% yield).

^{1}H NMR (CDCl$_3$, 400 MHz): δ 8.52 (d, J = 8.4 Hz, 1H), 7.65 (d, J = 7.6 Hz, 1H), 7.53 (dd, J = 8.5, 7.5 Hz, 1H), 7.44 (m, 1H), 7.14 (m, 3H), 6.98 (d, J = 8.4 Hz, 2H), 6.87 (dd, J = 8.8, 7.3 Hz, 1H); ^{13}C NMR (CDCl$_3$, 100MHz): δ 174.0, 167.7, 164.4, 138.0, 137.2, 136.3, 133.5, 131.4 (2C), 131.0, 129.8, 129.4, 128.6, 128.2 (2C), 127.3, 127.1, 126.5, 125.5, 122.6, 117.5; ESI-HRMS calcd for C$_{21}$H$_{14}$Cl$_2$N$_3$O$_2$S [M+ H]$^+$ 442.0184, found 441.29757.

N-(5-(3-carbamoylphenyl)benzo[*d*]thiazol-2-yl)-4-fluoro-2-(trifluoromethyl)benzamide (compound 13)
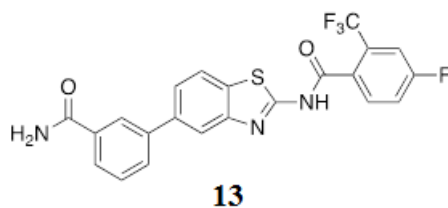
13

was obtained by following the general procedure. Purification was performed by semi-preparative reversed-phase HPLC, t$_R$ = 41 min. The product was isolated as a white solid (45% yield).

^{1}H NMR (DMSO-d$_6$ 400 MHz): δ 8.27 (s, 1H), 8.14 (m, 3H), 7.95 (dd, J = 8.6, 5.4 Hz, 1H), 7.86 (m, 2H), 7.72 (m, 3H); ^{13}C NMR (DMSO-d$_6$ 100 MHz): δ 165.7, 162.5 (d, J = 250.0 Hz), 158.7, 157.8 (d, J = 30.7 Hz), 149.2, 141.1, 136.5, 132.0 (d, J = 8.8 Hz), 131.8, 131.7, 131.1, 130.5, 130.2, 129.9, 128.7 (dd, J = 32.6, 8.5 Hz); 122.9, 122.6 (q, J = 270.0 Hz), 122.5, 119.6 (d, J = 21.4 Hz), 118.9, 118.8, 114.5 (dd, J = 26.0, 4.7 Hz); ESI-HRMS calcd for C$_{22}$H$_{14}$F$_4$N$_3$O$_2$S [M+ H]$^+$ 460.0743, found 459.89917.

-CHAPTER 7-

Computational details and synthesis of 2-amino-1,3,4-thiadiazole derivatives as mPGES-1 inhibitors

7.1 Computational details

The structures of the reagents, namely all commercially available acyl chlorides and boronates at Sigma Aldrich Company, were converted from 2D structures to 3D structures suitable for the docking stage of the process, using LigPrep software (v. 3.4; Schrödinger, LLC, 2015). Then, the compounds were prepared using Reagent Preparation: in the acyl chlorides, a cleavage between the chloride and the carbonyl group was applied in order to select the carbonyl moiety as building block, while the acidic moiety was removed in the boronic acids. The final .bld files were combined with the scaffolds obtaining the novel library (**C**). LigPrep performed calculation increased the number to 424,202 molecules for library **C**, and a final energy minimization of the library with Optimized Potentials for Liquid Simulations (OPLS) 2005 force field was performed. After the application of QikProp[110] and LigFilter, [117] the final library **C** contained 15,412 compounds

In the docking step, mPGES-1 three-dimensional crystal structure (PDB code: 4BPM)[209] was used for the structure-based molecular docking experiments. The three-dimensional model of the protein was prepared using the Schrödinger Protein Preparation Wizard,[117] starting from the aforementioned crystal structure co-complexed with the inhibitor LVJ (2-[[2,6-bis(chloranyl)-3-[(2,2-dimethylpropanoylamino)methyl]phenyl]amino]-1-methyl-6-(2-methyl-2-oxidanyl-propoxy)-N-[2,2,2-tris(fluoranyl)ethyl]benzimidazole-5-carboxamide) (PDB code: 4BPM).[209] The combinatorial library was submitted to structure-based molecular docking experiments on the mPGES-1 3D protein structure, using Glide software.[103, 104] Basically, the virtual screening workflow[117] (section 3.3.3) was used: a first round of docking experiments was performed setting the High-Throughput

Virtual Screening (HTVS) precision mode of Glide that allows a first enrichment from the starting library of compounds with a high fastness. The 30% top-ranked poses, filtered according to docking score values, were then submitted to a second round of docking experiments, using the Standard Precision (SP) which outperforms the first step in both sampling and scoring performances. Again, the 30% top-ranked poses were then submitted to the Extra-Precision (XP) Glide mode experiment, the final and most accurate docking step. During the molecular docking calculation, the adopted receptor grid was focused onto the co-crystallized ligand binding site (LVJ) with inner- and outer-box dimensions of 18×18×18 and 34.7×34.7×34.7, respectively.

7.2 General synthetic methods

The compound 2-amino-5-(4-bromophenyl)thiadiazole was purchased from Sigma-Aldrich and was used without any purification. All solvents used for the synthesis were of HPLC grade; they were purchased from Sigma-Aldrich and Carlo Erba Reagenti. NMR spectra were recorded on 300 or 400 MHz Bruker Avance instrument. All compounds were dissolved in 0.5 mL of the following solvents: chloroform-d (Sigma-Aldrich, 99.8 Atom % D); methanol-d_4 (Sigma-Aldrich, 99.8 Atom % D); dimethylsulfoxyde-d_6 (Sigma-Aldrich, 99.8 Atom % D). Coupling constants (J) are reported in Herz, and chemical shifts are expressed in parts per million (ppm) on the delta (δ) scale relative to CHCl$_3$ (7.19 ppm for ^{1}H and 77.0 ppm for ^{13}C) or CH$_3$OH (3.31 ppm for ^{1}H and 49.15 ppm for ^{13}C) or DMSO (2.50 ppm for ^{1}H and 39.51 ppm for ^{13}C) as internal reference. Multiplicities are reported as follows: s, singlet; d, doublet; t, triplet; m, multiplet; dd, doublet of doublets. ^{13}C NMR spectra were obtained at 100 MHz and referenced to the internal solvent signal. High Resolution Mass Spectrometry spectra (HRMS) were performed on a LCQ

DECA TermoQuest (San Josè, California, USA) mass spectrometer. Reactions were monitored on silica gel 60 F254 plates (Merck), and the spots were visualized under UV light. Analytical and semi-preparative reversed-phase HPLC was performed on Agilent Technologies 1200 Series high performance liquid chromatography. using a Nucleodur C8 reversed-phase column (250 x 10.00 mm, 5 µM, 110 Å, flow rate = 4 mL/min, UV detector at 240 nm). The binary solvent system (A/B) was as follows: 0.1% TFA in water (A) and 0.1% TFA in CH₃CN (B). Specific solvent gradient was applied for each compound. All tested compounds were obtained with high purity (> 98% detected by HPLC analysis) and were fully characterized by HRMS, and NMR spectra.

7.3 General procedure for the synthesis of compounds 14-22

i) pyridine, dry CH₃CN ii) K₂CO₃, Pd(dppf)Cl₂ · CH₂Cl₂, 7:3 Dioxane-H₂O, 80 °C
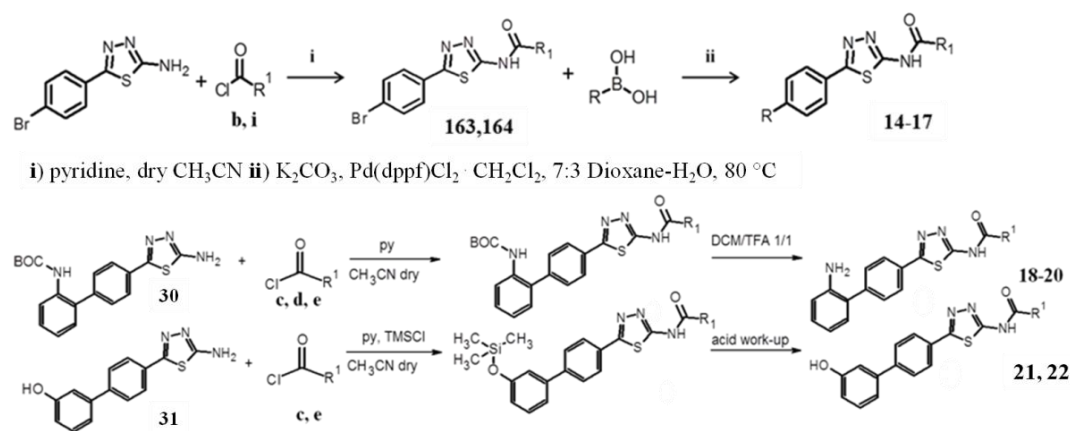
Scheme 2 Synthetic strategy for the synthesis of compounds **14-22**

The synthesis of thiadiazole derivatives was carried out according to the selected synthetic route depicted in scheme 2. Acylation reactions were performed between 2-amino-5-(4-bromophenyl)thiadiazole and acyl chlorides

206

b and **i** respectively (Table 13) to obtain the proper acylated intermediated **163** and **164**. The acylation was performed in dry acetonitrile at room temperature with pyridine. Reactions proceeded with good yields (74% and 92%).

Then, Pd-catalyzed Suzuki-Miyaura cross-coupling was performed between compound **163** and 2-aminophenylboronic acid or 3-hydroxyphenylboronic acid respectively, to obtain the final products **14** and **15**, while the coupling between compound **164** and the boronic acids above, provided products **16** and **17**. The cross-coupling was performed under standard conditions using [1,1'-bis(diphenylphosphine)ferrocene]dichloropalladium (II) (Pd(dppf)·CH$_2$Cl$_2$) as catalyst and aqueous carbonate base in a mixture 7:3 dioxane:H$_2$O at 80 °C.

For compounds **18-22** we opted for a different synthetic approach, because halogens on the acylated intermediates could be involved in the coupling. Since the aminophenyl and the hydroxyphenyl portion presented an amine and a hydroxyl group respectively, it was necessary the use of protective groups. In the synthesis of compounds **18-20**, the 2-(*N*-Boc-amino)phenylboronic acid was used, and the final deprotection step gave the desired products, while for compounds **21** and **22** chlorotrimethylsilane (TMSCl) was used for the protection of the hydroxyl group in situ during the acylation reaction, and the consequent removal with acidic work-up afforded the products. Suzuki reactions were carried out between 2-amino-5-(4-bromophenyl)thiadiazole and 2-(*N*-Boc-amino)phenylboronic acid to give compound **30,** and between 2-amino-5-(4-bromophenyl)thiadiazole and 3-hydroxyphenylboronic acid to give compound **31**. Acylation reactions were performed on compound **30** with the acyl chlorides **c**, **d** and **e** (Table 13) to obtain compounds **32**, **33**, and **34**. The deprotection step, using a mixture of DCM (50%) and TFA (50%),

afforded the final products **18-20**. Finally, compound **31** was protected by trimethylsilyl ether, formed *in situ* in dry acetonitrile at room temperature with pyridine. Acylation of the protected aminothiadiazole nucleus was then accomplished adding to the reaction mixture the proper acyl chloride (**c**, **d**).

All compounds were purified by high performance liquid chromatography (HPLC) or by flash column chromatography using different petroleum ether:ethyl acetate mixtures.
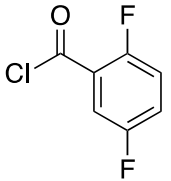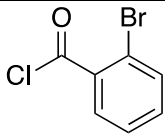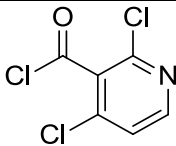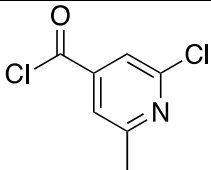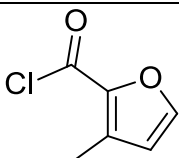
Compound	Acyl chloride
b	
c	
d	
e	
i	

Table 13 List of acyl chlorides used for the synthesis of thiadiazole derivatives.

208

7.3.1 General procedure for the synthesis of compounds 14 and 15

The common intermediate **163** was synthesized as reported below:
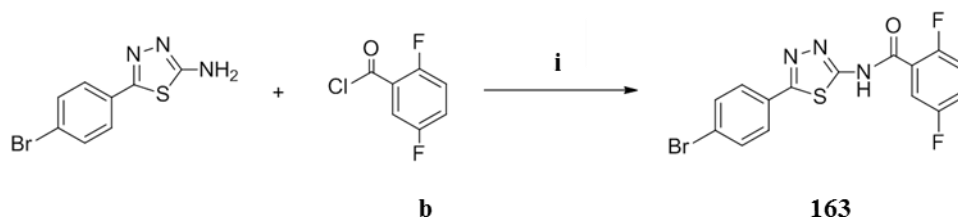
To a solution of 2-amino-5-(4-bromophenyl)thiadiazole (100 mg, 0.39 mmol) in dry CH_3CN (5 ml) were added pyridine (1.5 eq., 47 µL, 0.586 mmol) and 2,5-difluorobenzoyl chloride (1.5 eq., 72 µL, 0.586 mmol) under dry conditions. The mixture was stirred for two hours at room temperature. Then, ethyl acetate was added and the resulting mixture was washed with aqueous HCl 0.5 N (x2) and brine (x2). The organic phase was dried over anhydrous Na_2SO_4 and evaporated, affording 179 mg of white solid. Purification by flash chromatography, using a mixture 7:3 PET:EtOAc provided the pure product (114.2 mg, yield 74%).

^{1}H NMR (400 MHz, CD_3OD): δ 7.92 (d, *J* = 8.3 Hz, 2H), 7.56 (d, *J* = 8.3 Hz, 2H), 7.37 (m, 2H), 7.25 (m, 1H).

***N*-(5-(2'-amino-[1,1'-biphenyl]-4-yl)-1,3,4-thiadiazol-2-yl)-2,5-difluorobenzamide (compound 14)**
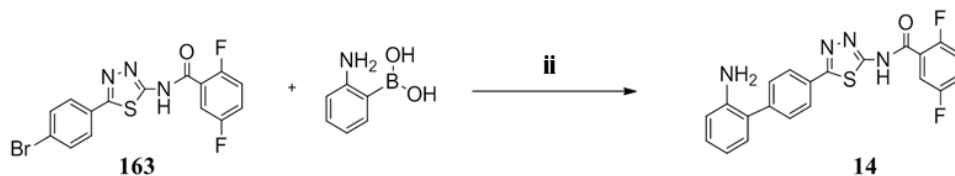
In a 25 mL flask were added compound **163** (40 mg; 0.10 mmol), K$_2$CO$_3$ (3 eq.; 41.5 mg; 0.300 mmol), 2-aminophenylboronic acid (1.5 eq.; 26 mg; 0.150 mmol) and Pd(dppf)Cl$_2$ ·CH$_2$Cl$_2$ (0.2 eq.; 16.3 mg; 0.02 mmol) and Schlenk techniques were applied. A degassed mixture (5 ml) of 1,4-dioxane (70%) and water (30%) was added and the mixture was stirred overnight at 80 °C. Ethyl acetate was added and the organic layer was washed with distilled water (x2) and brine (x2), separated, and dried over anhydrous Na$_2$SO$_4$. After concentration under reduced pressure, a brown solid was obtained (65.8 mg). A purification was performed by semi-preparative reversed-phase HPLC using the following conditions: gradient from 5% ending to 100% CH$_3$CN over 50 min, t$_R$ = 29.5 min. The pure product was obtained (21.7 mg, yield 53%) and characterized by ESI-MS and NMR spectra (purity grade >98%).

^{1}H NMR (400 MHz, CD$_3$OD) δ 8.14 (d, *J* = 8.2 Hz, 2H), 7.69–7.60 (m, 3H), 7.47–7.35 (m, 4H), 7.33 – 7.24 (m, 2H); ESI-HRMS calcd for C$_{21}$H$_{14}$F$_2$N$_4$OS [M + H]$^+$ 409.0856, found 409.0947.

2,5-difluoro-*N*-(5-(3'-hydroxy-[1,1'-biphenyl]-4-yl)-1,3,4-thiadiazol-2-yl)benzamide (compound 15)
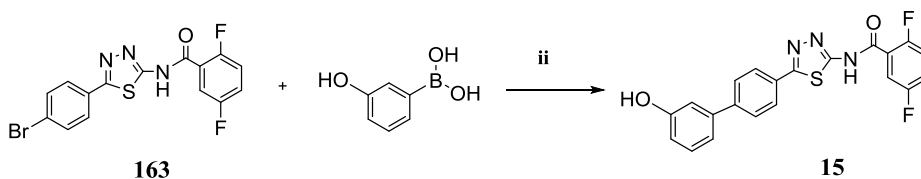
In a 25 mL flask were added: compound **163** (57 mg; 0.144 mmol), K$_2$CO$_3$ (3 eq.; 59.7 mg; 0.432 mmol), 3-hydroxyphenylboronic acid **24** (1.5 eq.; 29.8

mg; 0.216 mmol) and Pd(dppf)Cl$_2$ · CH$_2$Cl$_2$ (0.2 eq.; 23.5 mg; 0.029 mmol), applying Schlenk techniques. A degassed mixture (5 ml) of 1,4-dioxane (70%) and water (30%) was added and the mixture was stirred overnight at 80 °C under nitrogen. After the addition of ethyl acetate, the mixture was washed with distilled water (x2) and brine (x2). The organic phase was dried over anhydrous Na$_2$SO$_4$ and evaporated. A brown solid was obtained (59.5 mg). Purification by semi-preparative reversed-phase HPLC was carried out, using a multigradient H$_2$O:CH$_3$CN (0.1% TFA solutions): from 20% to 65% CH$_3$CN over 5 min, from 65% to 80% CH$_3$CN over 35 min and from 80% to 100% CH$_3$CN over 10 min, total time = 50 min; t$_R$ = 14.1 min. The pure product was obtained as a white solid (21.2 mg, yield 36%) and characterized by ESI-MS and NMR spectra (purity grade >98%).

^{1}H NMR (400MHz, DMSO-d$_6$): δ 7.92 (d, J = 8.3 Hz, 2H), 7.69 (m, 2H), 7.61 (m, 1H), 7.27 (t, J = 7.9 Hz, 1H), 7.21 (m, 2H), 7.13 (d, J = 7.6 Hz, 1H), 7.08 (s, 1H), 6.78 (dd, J = 8.2, 2.4 Hz, 1H); ^{13}C NMR (100MHz, DMSO-d$_6$): δ 162.0, 160.1 (d, J=210 Hz), 158.9, 158.5, 155.8 (d, J=246 Hz), 150.9, 141.1, 140.7, 130.4, 129.6, 127.7 (4 C), 124.7, 121.5, 120.1, 119.4 (dd, J=25.0, 8.4 Hz), 118.8 (m), 118.4 (dd, J=24.3, 8.4 Hz), 118.3 (d, J = 25.9 Hz); ESI-HRMS calcd for C$_{21}$H$_{13}$F$_2$N$_3$O$_2$S [M + H]$^+$ 410.0775, found 410.0209.

7.3.2 General procedure for the synthesis of compounds 16 and 17

The common intermediate **164** was synthesized as reported below:

211
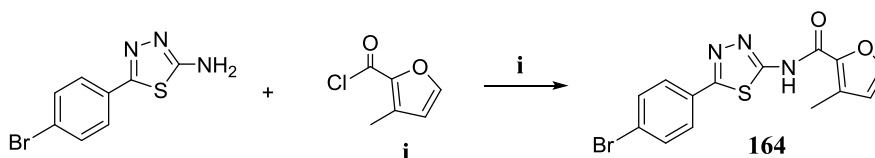
To a solution of 2-amino-5-(4-bromophenyl)thiadiazole (50 mg, 0.195 mmol) in dry CH_3CN (5 ml) were added pyridine (1.5 eq., 23.6 μL, 0.292 mmol) and 3-methyl-2-furoyl chloride (1.5 eq., 34 μL, 0.292 mmol) respectively, and the mixture was stirred for two hours at room temperature under anhydrous conditions. After dilution with ethyl acetate, the organic phase was washed with aqueous HCl 0.5 N (x2) and brine (x2), separated, dried over anhydrous Na_2SO_4 and concentrated under vacuum. A white solid was obtained (128 mg). Purification by flash column chromatography (PET:EtOAc 7:3) afforded 65.4 mg of pure product (92% yield), characterized by ^{1}H NMR.

^{1}H NMR (400 MHz, CD_3OD): δ 7.75 (d, J = 8.5 Hz, 2H); 7.59 (d, J = 8.4 Hz, 2H); 7.53 (s, 1H); 6.44 (d, J = 1.6 Hz, 1H); 2.43 (s, 3H).

N-(5-(2'-amino-[1,1'-biphenyl]-4-yl)-1,3,4-thiadiazol-2-yl)-3-methylfuran-2-carboxamide (compound 16)
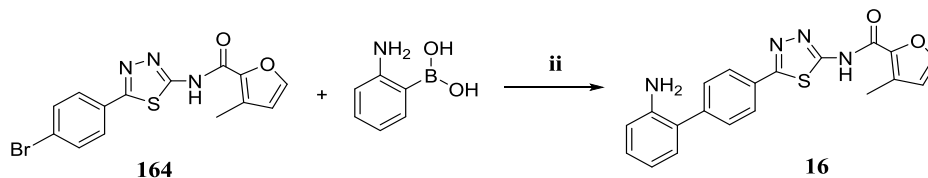
In a 25 mL flask were added: compound **164** (40 mg, 0.11 mmol), K_2CO_3 (3 eq., 45.6 mg, 0.33 mmol), 2-aminophenylboronic acid (1.5 eq., 28.6 mg, 0.165 mmol) and Pd(dppf)Cl_2·CH_2Cl_2 (0.2 eq., 18 mg, 0.022 mmol) and Schlenk techniques were performed. The mixture was dissolved in a degassed solution (5 ml) of 1,4-dioxane (70%) and H_2O (30%), and stirred at 80 °C over night. Ethyl acetate was added and the organic layer was washed with distilled

water (x2) and brine (x2), separated, dried over anhydrous Na_2SO_4 and evaporated under vacuum, affording a brown solid crude (77 mg). A purification was performed by semi-preparative reversed-phase HPLC, using the following conditions: gradient from 5% ending to 100% CH_3CN over 50 min, $t_R = 27.0$ min. The pure product was obtained as a white solid (10.8 mg, 26% yield) and characterized by ESI-MS and NMR spectra (purity grade >98%).

^{1}H NMR (400MHz, DMSO-d_6): δ 8.04 (d, *J* = 8.0 Hz, 2H), 7.90 (s, 1H), 7.62 (d, *J* = 8.0 Hz, 2H), 7.15 (m, 2H), 6.91 (d, *J* = 8.0 Hz, 1H), 6.81 (t, *J* = 7.5 Hz, 1H), 6.68 (s, 1H), 2.40 (s, 3H); ^{13}C NMR (100MHz, DMSO-d_6): δ 161.1, 158.3, 156.8, 145.6, 142.7, 141.5, 140.2, 131.3, 130.1. 129.6 (2C), 128.8, 128.6, 127.3 (2C), 126.2, 118.6, 116.8, 116.0, 11.1; ESI-HRMS calcd for $C_{20}H_{16}N_4O_2S$ [M + H]$^+$ 377.1072, found 377.0495.

N-(5-(3'-hydroxy-[1,1'-biphenyl]-4-yl)-1,3,4-thiadiazol-2-yl)-3-methylfuran-2-carboxamide (compound 17)
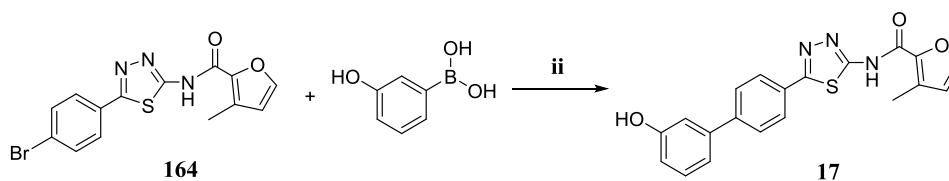
In a 25 mL bottom flask were added: compound **164** (25 mg, 0.068 mmol), K_2CO_3 (3 eq., 28 mg, 0.204 mmol), 3-hydroxyphenylboronic acid (1.5 eq., 14 mg, 0.102 mmol) and Pd(dppf)Cl$_2$·CH$_2$Cl$_2$ (0.2 eq., 11.1 mg, 0.0136 mmol) and Schlenk techniques were performed. The mixture was dissolved in a

degassed mixture (5 ml) of 1,4-dioxane (70%) and H_2O (30%), and stirred at 80 °C over night. Ethyl acetate was added and the organic layer was washed with distilled water (x2) and brine (x2), separated, dried over anhydrous Na_2SO_4 and evaporated under vacuum, affording a brown solid crude (33 mg). A purification was performed by semi-preparative reversed-phase HPLC, using a multigradient H_2O-CH_3CN (0.1% TFA solutions): from 5% to 50% over 5 min, from 50% to 70% over 30 min, from 70% ending to 100% over 10 min, total time = 45 min; t_R = 19,6 min. The pure product was obtained as a white solid (12.1 mg, 47% yield) and characterized by ESI-MS and NMR spectra (purity grade >98%).

^{1}H NMR (400MHz, DMSO-d$_6$): δ 8.03 (d, J = 8.1 Hz, 2H), 7.89 (d, J = 1.7 Hz, 1H), 7.78 (d, J = 8.1 Hz, 2H), 7.30 (t, J = 7.9 Hz, 1H), 7.16 (d, J = 7.7 Hz, 1H), 7.10 (s, 1H), 6.81 (dd, J = 8.1, 2.2 Hz, 1H), 6.67 (d, J = 1.7 Hz, 1H), 2.39 (s, 3H); ^{13}C NMR (100MHz, DMSO-d$_6$): δ 158.3, 158.0, 157.9, 157.7, 157.4, 145.6, 142.2, 140.4, 131.3, 130.1, 129.1, 127.4 (4C), 117.5, 116.0, 115.1, 113.4, 11.1; ESI-HRMS calcd for $C_{20}H_{15}N_3O_3S$ [M + H]$^+$ 378.0912, found 378.0746.

7.3.3 Synthesis of compounds 18-20

The common intermediate **30** was synthesized as reported below:

In a 25 mL flask were added: 2-amino-5-(4-bromophenyl)thiadiazole (300 mg, 1.17 mmol), K_2CO_3 (3 eq., 485 mg, 3.51 mmol), 2-(*N*-Boc-

amino)phenylboronic acid (1.5 eq., 560 mg, 1.75 mmol) and Pd(dppf)Cl$_2$·CH$_2$Cl$_2$ (0.2 eq., 191 mg, 0.234 mmol). Schlenk techniques were applied. The mixture was dissolved in a degassed mixture (10 ml) of 1,4-dioxane (70%) and H$_2$O (30%), and stirred at 80 °C over night. Ethyl acetate was added and the organic layer was washed with distilled water (x 2) and brine (x 2), separated, dried over anhydrous Na$_2$SO$_4$ and evaporated under vacuum, affording a brown solid crude (734 mg). Purification by flash column chromatography (PET:EtOAc 1:1) afforded 258.4 mg of pure product (60% yield).

^{1}H NMR (CD$_3$OD 400MHz): δ 7.82 (d, J = 7.9 Hz, 2H), 7.52 (m, 3H), 7.34 (m, 2H), 7.26 (m, 1H), 1.35 (s, 9H).

7.3.3.1 Synthesis of compound 18
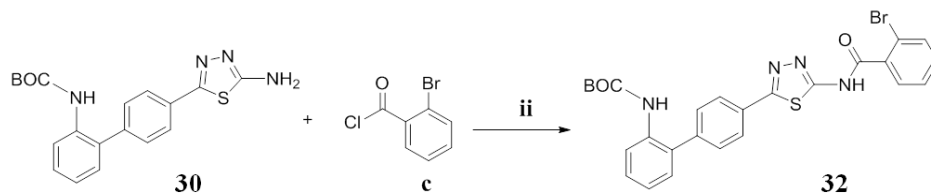
To a solution of compound **30** (40 mg, 0.109 mmol) in dry CH$_3$CN (5 ml) were added pyridine (1.5 eq., 11 μL, 0.133 mmol) and 2-bromobenzoyl chloride (1.5 eq., 17.4 μL, 0.133 mmol) under anhydrous conditions. The mixture was stirred for two hours at room temperature and diluted with ethyl acetate. The organic phase was washed with aqueous HCl 0.5 N (x2) and brine (x2), separated, dried over anhydrous Na$_2$SO$_4$ and evaporated to obtain 65 mg of solid crude. A purification was performed by semi-preparative reversed-phase HPLC, using the following conditions: gradient from 5% ending to

100% CH_3CN over 45 min, t_R = 43.7 min. ^1H NMR analysis confirmed that compound **32** was obtained (21 mg, 35% yield) as an orange solid.

^1H NMR (400MHz, CD_3OD): δ 8.08 (d, *J* = 7.9 Hz, 2H), 7.75 (d, *J* = 7.9 Hz, 1H), 7.62 (d, *J* = 7.7 Hz, 2H), 7.50 (m, 3H), 7.23 (m, 2H), 6.98 (m, 2H), 1.28 (s, 9H).

N-(5-(2'-amino-[1,1'-biphenyl]-4-yl)-1,3,4-thiadiazol-2-yl)-2-bromobenzamide (compound 18)
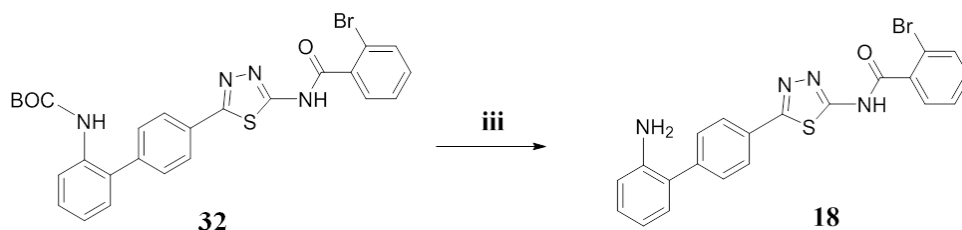
The deprotection of compound **32** (21 mg, 0.0381 mmol) was carried out. After dissolution in a mixture of DCM (50%) and TFA (50%) (2 ml), the solution was stirred over night. After concentration under vacuum, the crude was purified by semi-preparative reversed-phase HPLC using the following conditions: gradient from 5% ending to 100% CH_3CN over 45 min, flow rate = 4 mL/min, UV detector at 240 nm; t_R = 26.4 min. The pure product was obtained as a yellow solid (16.5 mg, 96% yield). The compound was characterized by ESI-MS and NMR spectra (purity grade >98%).

^1H NMR (400 MHz, CD_3OD): 8.13 (d, *J* = 8.4 Hz, 2H), 7.75 (d, *J* = 7.9 Hz, 1H), 7.62 (d, *J* = 8.0 Hz, 3H), 7.50 (m, 5H), 7.42 (d, *J* = 7.6 Hz, 1H); ^{13}C NMR (100MHz, CD_3OD): δ 168.1, 164.8, 160.5, 141.1, 137.5, 135.6, 134.7,

133.6, 132.7, 131.7, 131.3, 130.8, 130.5, 129.1 (2C), 129.0(2C), 128.6, 123.6 (2C), 120.8; ESI-HRMS calcd for $C_{21}H_{14}BrN_4O_2S$ $[M + H]^+$ 451.0228, found 450.9545.

7.3.3.2 Synthesis of compound 19
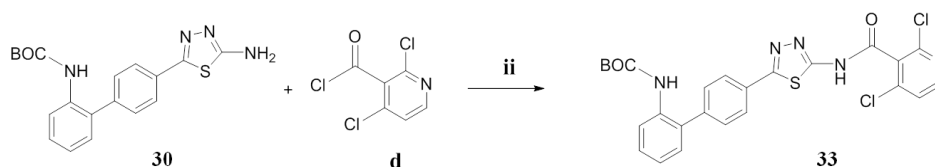
To a solution of compound **30** (20 mg, 0.0540 mmol) in dry CH$_3$CN (5 ml) were added pyridine (1,5 eq., 66 μL, 0.0815 mmol) and 2,4-dichloropyridine-3-carbonyl chloride (1.5 eq., 11.2 μL, 0.0815 mmol) under anhydrous conditions. The mixture was stirred for two hours at room temperature and diluted with ethyl acetate. The organic phase was washed with aqueous HCl 0.5 N (x 2) and brine (x2), separated, dried over anhydrous Na$_2$SO$_4$ and evaporated to obtain 76 mg of crude. A purification was performed by semi-preparative reversed-phase HPLC using the following conditions: gradient from 5% ending to 100% CH$_3$CN over 45 min, flow rate = 4 mL/min, UV detector at 240 nm; t_R = 39.8 min. ^{1}H NMR analysis confirmed that compound **33** was obtained (12.2 mg, 42% yield) as an orange solid.

^{1}H NMR (400MHz, CD$_3$OD): δ 8.48 (d, J = 5.5 Hz, 1H), 8.05 (d, J = 8.3 Hz, 2H), 7.66 (d, J = 5.4 Hz, 1H), 7.58 (d, J = 8.3 Hz, 2H), 7.38 (m, 2H), 7.29 (m, 2H), 1.36 (s, 9H).

217

N-(5-(2'-amino-[1,1'-biphenyl]-4-yl)-1,3,4-thiadiazol-2-yl)-2,4-dichloronicotinamide (compound 19)
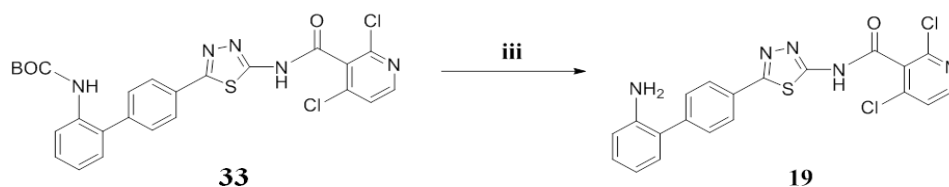
The de-protection of compound **33** (12.2 mg, 0.0223 mmol) was carried out. After dissolution in a mixture of DCM (50%) and TFA (50%) (2 ml), the solution was stirred over night. After concentration under vacuum, the crude was purified by semi-preparative reversed-phase HPLC using the following conditions: gradient from 5% ending to 100% CH_3CN over 45 min, flow rate = 4 mL/min, UV detector at 240 nm; t_R = 32 min. The pure product was obtained as a yellow solid (9.2 mg, 93% yield). The compound was characterized by ESI-MS and NMR spectra (purity grade >98%).

^{1}H NMR (400 MHz, CD_3OD) δ 8.49 (d, J = 5.5 Hz, 1H), 8.13 (d, J = 7.8 Hz, 2H), 7.66 (d, J = 5.5 Hz, 1H), 7.62 (d, J = 7.8 Hz, 2H), 7.45 (m, 2 H), 7.36 (m, 2H); ^{13}C NMR (100MHz, CD_3OD): δ 165.6, 163.5, 160.3, 153.0, 150.1 (2C), 145.1, 142.1, 134.9, 134.8, 132.9, 131.2 (2C), 131.7 (2C), 131.1, 129.5, 127.7, 125.8, 123.1; ESI-HRMS calcd for $C_{20}H_{13}Cl_2N_5OS$ [M + H]$^+$ 442.0296, found 441.9587.

7.3.3.3 Synthesis of compound 20
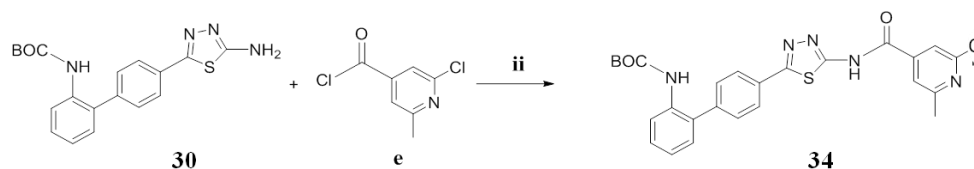
To a solution of compound **30** (15 mg, 0.0410 mmol) in dry CH_3CN (5 ml) were added pyridine (1.5 eq., 5 µL, 0.0615 mmol) and 4-carbonyl-2-chloro-6-methylpyridine chloride (1.5 eq., 6 µL, 0.0410 mmol) under anhydrous conditions. The mixture was stirred for two hours at room temperature and diluted with ethyl acetate. The organic phase was washed with aqueous HCl 0.5 N (x 2) and brine (x2), separated, dried over anhydrous Na_2SO_4 and evaporated to obtain 76 mg of solid. A purification was performed by semi-preparative reversed-phase HPLC using the following conditions: gradient from 5% ending to 100% CH_3CN over 45 min, flow rate = 4 mL/min, UV detector at 240 nm; t_R = 40.2 min. ^{1}H NMR analysis confirmed that compound **34** was obtained (4.9 mg, 23% yield) as a orange solid.

^{1}H NMR (400MHz, CD_3OD): δ 8.03 (d, *J* = 7.9 Hz, 2H); 7.84 (d, *J* = 11.0 Hz, 2H); 7.57 (d, *J* = 8.0 Hz, 2H); 7.50 (d, *J* = 8.0 Hz, 1H); 7.37 (m, 2H); 7.29 (m, 1H); 2.62 (s, 3H); 1.35 (s, 9H).

N-(5-(2'-amino-[1,1'-biphenyl]-4-yl)-1,3,4-thiadiazol-2-yl)-2-chloro-6-methylisonicotinamide (compound 20)
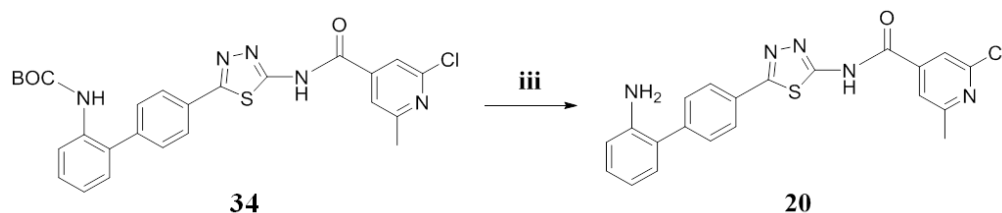
The de-protection of compound **34** (4.9 mg, 0.0116 mmol) was carried out. After dissolution in a mixture of DCM (50%) and TFA (50%) 1/1 (2 ml), the solution was stirred over night. After concentration under vacuum, the crude was purified by semi-preparative reversed-phase HPLC using the following conditions: gradient from 5% ending to 100% CH_3CN over 45 min, flow rate = 4 mL/min, UV detector at 240 nm; t_R = 29.1 min. The pure product was obtained as a yellow solid (4.7 mg, 96% yield). The compound was characterized by ESI-MS and NMR spectra (purity grade >98%).

^{1}H NMR (400 MHz, DMSO-d_6) δ 8.06 (d, J = 7.9 Hz, 2H), 7.96 (s, 1H), 7.91 (s, 1H), 7.62 (d, J = 8.0 Hz, 2H), 7.12 − 7.03 (m, 2H), 6.80 (d, J = 8.0 Hz, 1H), 6.68 (t, J = 7.4 Hz, 1H), 2.59 (s, 3H); ^{13}C NMR (100MHz, DMSO-d_6): δ 162.1, 160.4, 158.1, 157.7, 150.0, 144.4, 142.9, 142.2, 130.0, 129.6 (2 C), 128.8, 128.3, 127.4 (2 C), 125.1, 121.0, 119.8, 117.4, 116.0, 23.7; ESI-HRMS calcd for $C_{21}H_{16}ClN_5OS$ [M + H]$^+$ 422.0842, found 422.6523.

7.3.4 Synthesis of compound 31
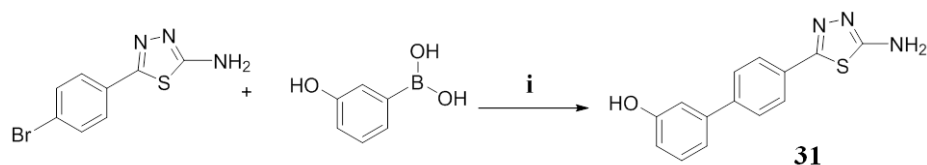
In a 25 mL flask were added: 2-amino-5-(4-bromophenyl)thiadiazole (300 mg, 1.17 mmol), K_2CO_3 (3 eq., 485 mg, 3.51 mmol), 3-hydroxyphenylboronic acid (1.5 eq., 243 mg, 1.75 mmol) and Pd(dppf)Cl$_2$·CH$_2$Cl$_2$ (0.2 eq., 191 m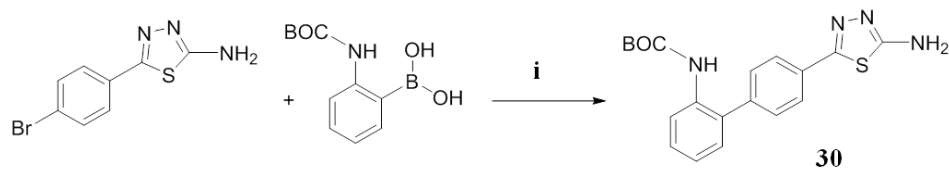g, 0.234 mmol). Schlenk techniques were applied. The mixture was dissolved in a degassed mixture (10 ml) of 1,4-dioxane (70%) and water (30%) and stirred at 80 °C overnight. Ethyl acetate was added and the organic layer was washed with distilled water (x2) and brine (x2), separated, dried over anhydrous Na_2SO_4 and evaporated under vacuum, affording a brown solid crude (440 mg). Purification by flash column chromatography (PET:EtOAc 8:2) afforded 150 mg of pure product (48% yield).

^{1}H NMR (400 MHz, CDCl$_3$): δ 9.34 (s, 1H, OH); 7.56 (d, J = 8.4 Hz, 2H); 7.43 (d, J = 8.4 Hz, 2H); 7.02 (t, J = 7.9 Hz, 1H); 6.85 (d, J = 7.7 Hz, 1H); 6.80 (m, 1H); 6.53 (dd, J = 8.0, 1.6 Hz, 1H).

7.3.5 General procedure for the synthesis of compounds 21 and 22

To a solution of compound **31** (40 mg, 0.148 mmol) in dry CH$_3$CN (5 ml) was added pyridine (30 eq., 359 µL, 4.44 mmol). The mixture was cooled to 0°C, and chlorotrimethylsilane (10 eq., 856 µL 1.48 mmol) was added. The reaction proceeded for two hours stirred at room temperature. Then, the proper

acyl chloride (1.5 eq) was added and the resulting mixture was stirred for two hours. After dilution with ethyl acetate, the organic phase was washed with aqueous HCl 0.5 N (x2) and brine (x2), separated, dried over anhydrous Na$_2$SO$_4$ and evaporated. Purification by semi-preparative reversed-phase HPLC and flash chromatography afforded the products.

2-bromo-*N*-(5-(3'-hydroxy-[1,1'-biphenyl]-4-yl)-1,3,4-thiadiazol-2-yl)benzamide (compound 21)

21
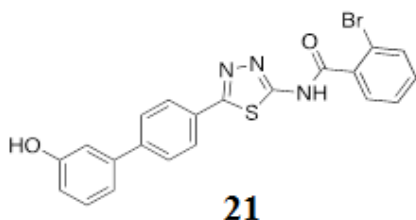
was obtained as a brown solid by following the general procedure, using acyl chloride **c**. A purification was performed by semi-preparative reversed-phase HPLC using the following conditions: a mutigradient from 5% to 40% CH$_3$CN over 5 min, from 40% to 60% CH$_3$CN over 30 min, from 60% ending to 100% CH$_3$CN over 5 min (total time = 40 min), flow rate = 4 mL/min, UV detector at 240 nm; t$_R$ = 9.3 min. The pure product was obtained (38.9 mg, 58% yield) as a white solid. The compound was characterized by ESI-MS and NMR spectra (purity grade >98%).

^{1}H NMR (400 MHz, DMSO-d_6) δ 9.66 (s, OH, 1H), 8.04 (d, *J* = 8.0 Hz, 2H), 7.76 (m, 3H), 7.67 (d, *J* = 7.4 Hz, 1H), 7.49 (m, 2H), 7.30 (t, *J* = 7.9 Hz, 1H), 7.16 (d, *J* = 7.7 Hz, 1H), 7.10 (s, 1H), 6.81 (d, *J* = 8.0 Hz, 1H); ^{13}C NMR (100MHz, DMSO-d$_6$): δ 166.1, 161.9, 157.9, 157.7, 142.3, 140.4, 138.3,

132.9, 132.2, 130.1, 129.9, 129.1, 127.7, 127.6 (2 C), 127.46 (2 C), 119.2, 117.5, 115.1, 113.4; ESI-HRMS calcd for $C_{21}H_{14}BrN_3O_2S$ [M + H]$^+$ 454.0068, found 453.9680.

2-chloro-*N*-(5-(3'-hydroxy-[1,1'-biphenyl]-4-yl)-1,3,4-thiadiazol-2-yl)-6-methylisonicotinamide (compound 22)

22
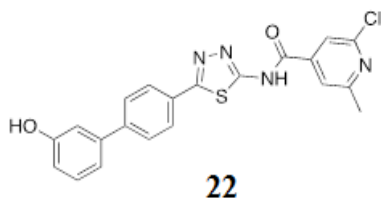
was obtained by following the general procedure, using acyl chloride **e**. Purification by flash column chromatography using a mixture of PET (60%) and EtOAc (40%) afforded the pure product (49.4 mg, 79% yield) as a white solid. The compound was characterized by ESI-MS and NMR spectra (purity grade >98%).

^{1}H NMR (400 MHz, DMSO-d_6) δ 9.66 (s, 1H, OH), 8.07 (d, *J* = 8.3 Hz, 2H), 7.96 (s, 1H), 7.91 (s, 1H), 7.80 (d, *J* = 8.4 Hz, 2H), 7.31 (t, *J* = 7.9 Hz, 1H), 7.17 (d, *J* = 7.9 Hz, 1H), 7.12 (s, 1H), 6.84 (d, *J* = 6.5 Hz, 1H), 2.59 (s, 3H); ^{13}C NMR (100MHz, DMSO-d_6): δ 161.4, 160.2, 157.9, 157.7, 149.9, 143.9, 143.8, 142.2, 140.4, 130.1, 129.2, 127.4 (4 C), 121.0, 119.7, 117.5, 115.1, 113.4, 25.7; ESI-HRMS calcd for $C_{21}H_{15}ClN_4O_2S$ [M + H]$^+$ 423.0682, found 423.0240.

-CHAPTER 8-

Computational details and synthesis of substituted saturated N-heterocycles as mPGES-1 inhibitors

8.1 Computational details

For the docking analysis a different X-ray structure of the protein was used, since the co-crystallized ligand 6PW,[321] a 3,3-dimethyl substituted *N*-aryl piperidine, presents a saturated heterocycle moiety in its structure.

Protein 3D input file of mPGES-1 was obtained from the Protein Data Bank database (PDB codes: 5K0I).[321] The Schrodinger Protein Preparation Wizard Workflow (Schrödinger, LLC, NY, USA, 2013) was performed for the preparation of the protein, which provides the removal of water molecules, the addition of cap termini and all hydrogen atoms, the assignment of bond orders.

The resulting PDB file was converted to the Maestro (MAE) format. The grid for the structure-based docking experiments was prepared in the ligand binding site of 6PW, and the virtual screening workflow[117] (Glide software[103, 104]) was applied (section 3.3.3). The three rounds of experiments (HTVS, SP and XP) were performed with a gradually increasing precision, keeping the 30% top-ranked poses for each step. During the molecular docking calculation, the adopted receptor grid was focused onto the co-crystallized ligand binding site with inner- and outer-box dimensions of 10×10×10 and 27.4×27.4×27.4, respectively.

8.2 General synthetic methods

Chemicals were purchased from ABCR, Acros, Alfa Aesar, Apollo Scientific, Fluorochem, Maybridge, Merck, Sigma-Aldrich, Strem, or TCI, and were used without further purification. Common organic solvents were used as supplied (ACS or HPLC grade). SnAP reagents starting materials were synthesized in the laboratory of Prof. Jeffrey Bode at the Department of Chemistry and Applied Biosciences of ETH. 1,1,1,3,3,3-Hexafluoro-2-

propanol is abbreviated to HFIP. Thin layer chromatography (TLC) was performed for reaction monitoring and visualized by UV quenching and by staining with basic $KMnO_4$, ninhydrin solution, or phosphomolybdic acid.

Flash column chromatography[322] was performed on silica gel (Silicycle SiliaFlash F60, 230–400 mesh) using a forced flow of eluent at 0.4–0.5 bar.

NMR spectra were recorded on Bruker Avance 400 MHz, and Varian Mercury 300 MHz spectrometers. All compounds were dissolved in 0.5 mL of the following solvents: chloroform-d (Sigma-Aldrich, 99.8 Atom % D); methanol-d_4 (Sigma-Aldrich, 99.8 Atom % D); dimethylsulfoxyde-d_6 (Sigma-Aldrich, 99.8 Atom % D), D_2O (Sigma-Aldrich, 99.8 Atom % D). Coupling constants (*J*) are reported in Herz, and chemical shifts are expressed in parts per million (ppm) on the delta (δ) scale relative to $CHCl_3$ (7.19 ppm for ^1H and 77.0 ppm for ^{13}C) or CH_3OH (3.31 ppm for ^1H and 49.15 ppm for ^{13}C) or DMSO (2.50 ppm for ^1H and 39.51 ppm for ^{13}C) or H_2O (4.8 ppm for ^1H) as internal reference. Multiplicities are reported as follows: s, singlet; d, doublet; t, triplet; m, multiplet; dd, doublet of doublets. ^{13}C NMR spectra were obtained at 101 MHz and referenced to the internal solvent signal. High resolution mass spectra were measured by the Mass Spectrometry Service Facility of Laboratorium of Organic Chemistry at ETH Zürich on a Bruker Daltonics maXis for ESI-Qq-TOF spectrometer (ESI-MS) or Micromass (Waters) AutoSpec Ultima for EI spectrometer (EI-MS). All compounds were obtained with high purity (> 98% detected by HPLC analysis) and were fully characterized by HRMS and NMR spectra.

8.3 Methods and materials

SnAP-M (Morpholine), SnAP-TM (Thiomorpholine), SnAP-PIP (Piperazine) were available in the laboratory where the synthesis of compounds **62-78** was carried out. SnAP-TM was purified by flash chromatography before use. SnAP-Cys (Cysteine) was synthesized as follow.

8.3.1 Synthesis of ethyl 2-amino-3-((((tributylstannyl)methyl)thio)propanoate (compound 85, SnAP-Cys).
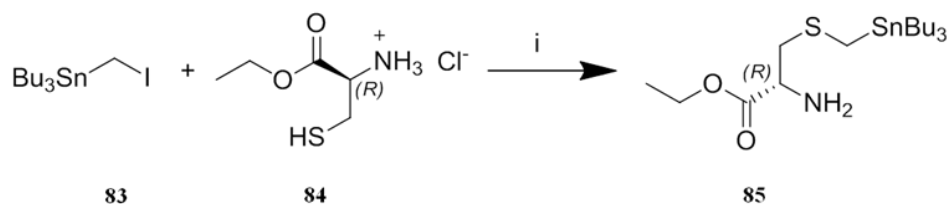
To a solution of Tributyl(iodomethyl)stannane (**83**) (2.324 g, 5.38 mmol, 1.00 equiv) in EtOH (40 mL) was added L-ethyl cysteine hydrochloride (**84**) (1 g, 5.38 mmol, 1.00 equiv), followed by a solution of K_2CO_3 (0.892 g, 6.456 mmol, 1.20 equiv) in H_2O (11 mL) at rt. The reaction mixture was refluxed at 70 °C. After 4 h, the mixture was concentrated under reduced pressure to remove the solvent; the resulting residue was dissolved in H_2O and extracted with EtOAc (x3). The combined organic solutions were dried over anhydrous Na_2SO_4, filtered and concentrated under reduced pressure. Purification by flash column chromatography (2:1 hexane:EtOAc) afforded **85** (2.102 g, 86% yield) as a clear, colorless liquid.

[^1]H NMR (400 MHz, CDCl3) δ 4.19 (q, *J* = 7.1 Hz, 2H), 3.67 (dd, *J* = 8.0, 4.5 Hz, 1H), 2.89 (dd, *J* = 13.4, 4.5 Hz, 1H), 2.70 (dd, *J* = 13.4, 8.0 Hz, 1H), 1.92 (dd, *J* = 35.0, 9.3 Hz, 2H), 1.69 (s, 4H), 1.58 − 1.44 (m, 5H), 1.38 − 1.23 (m, 10H), 0.99 − 0.84 (m, 15H); [^13]C NMR (101 MHz, CDCl3) δ 174.6, 61.2, 53.2, 43.9, 29.1, 27.4, 14.4, 13.8, 9.7, 9.2; ESI-HRMS calcd for $C_{18}H_{40}NO_2SSn$ [M + H]$^+$ 454.1798, found 454.1794.

8.3.2 General method for the preparation of the substituted saturated heterocycles

The assigned name for each compound derives from the starting SnAP reagent (**TM**, **M**, **PIP** or **Cys**) and the aldehydes (**a-g**).
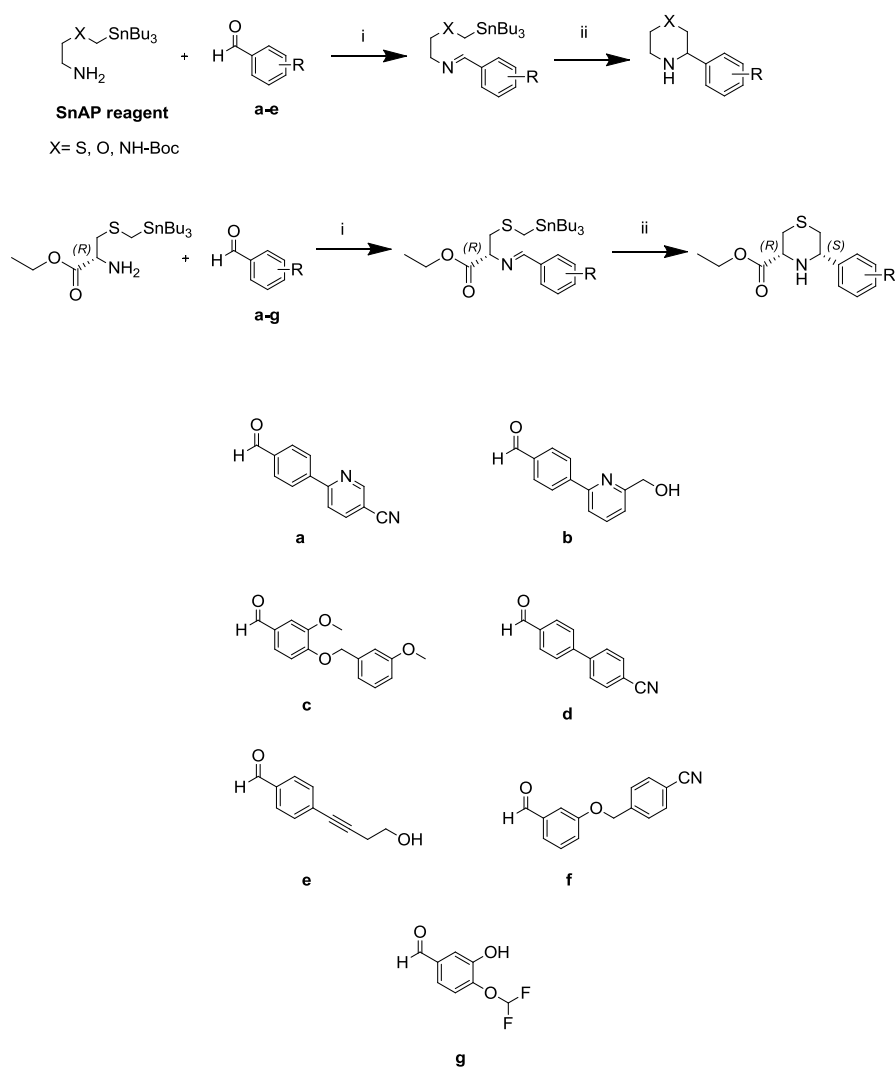
Scheme 3. Synthetic method for the synthesis of **62-78; i)** MS 4 Å, dry DCM, rt **ii)** Cu(Otf)$_2$, 2,6-lutidine, DCM:HFIP 4:1, rt, overnight.

The general procedure for the synthesis of compounds **62-78** is depicted in scheme 3 (SnAP chemistry). To a solution of the amino tributylstannane-SnAP reagent (0.1-0.3 mmol, 1.00 equiv) in CH_2Cl_2 at rt was added the proper aldehyde (**a-g**, 1.0 equiv) and MS 4 Å (150 mg/mmol). The reaction mixture was stirred at rt overnight, filtered through a short layer of Celite and concentrated under reduced pressure. The imine formation was checked by ^{1}H NMR.

A suspension of anhydrous $Cu(OTf)_2$ (1.00 equiv) in HFIP (hexafluoroisopropanol) was prepared, and 2,6-lutidine (1.00 equiv) was added in one portion. The mixture was stirred for 1 h at rt, during which time a homogeneous green suspension was formed. The previous imine was dissolved in dry DCM and added to the solution in one portion, and the resulting mixture was stirred overnight at rt. Schlenk techniques were applied to all reactions.

The reaction was quenched with 10% aq NH_4OH, and stirred for 15 min. Then, the layers were separated and the aqueous layer was extracted with CH_2Cl_2 (3 x 3 ml). The combined organic layers were washed with H_2O (3 x 5 ml) and brine (5 ml), dried over Na_2SO_4, filtered, concentrated, and purified by flash chromatography using mixtures of hexane and ethyl-acetate in different proportions, to provide the desired substituted saturated heterocycles.

Boc moiety of SnAP-PIP is useful to avoid the imine formation at the amine group close to tributyltin group. For the synthesis of compounds **69-71**, a final deprotection step afforded the desired products.

All the compounds were obtained as racemic mixtures.

Concerning SnAP-Cys derivatives (**72-78**), experimental data demonstrated a diastereoselectivity of the reaction for the *cis* product (20:1).

Notes about the purification:

- Purification was performed by flash column chromatography using mixtures of hexane and ethyl acetate in different proportions.

- 0.1% of Et$_3$N was added to the solvent mixture prepared for the flash chromatography for the most polar compounds.

- Tin traces were removed applying this method: the product was dissolved in acetonitrile and washed a few times with hexane, and the combined hexane layers were extracted with a small amount of acetonitrile. The combined acetonitrile layers were concentrated under reduced pressure to provide the pure product.

- Traces of aldehyde in the product after flash chromatography were removed using a small column of propyl sulfonic acid supported on silica (loading/capacity mmol/g 0.62) (SCX$_2$) for not basic aldehydes.

6-(4-(thiomorpholin-3-yl)phenyl)nicotinonitrile (compound 62, TMa)
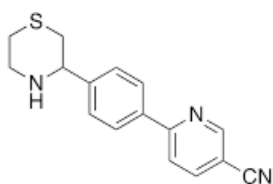
62

Was obtained by following the general procedure (scheme 3, 0.1 mmol). Purification by flash column chromatography (hexane-EtOAc 2:1 to 0:3) afforded the pure product as an orange solid (21 mg, 71% yield).

¹H NMR (400 MHz, CDCl$_3$) δ 8.95 (dd, *J*= 2.2, 0.9 Hz, 1H), 8.06-8.01 (m, 3H), 7.85 (dd, *J*= 8.3, 0.9 Hz, 1H), 7.55 (d, *J* = 8.3 Hz, 2H), 4.08 (dd, *J* = 10.7, 2.3 Hz, 1H), 3.53-3.49 (m, 1H), 3.23 (td, *J*= 12.0, 2.4 Hz, 1H), 3.03-2.91 (m, 2H), 2.58-2.46 (m, 2H); ¹³C NMR (101 MHz, CDCl$_3$) δ 160.0, 152.5, 145.9, 139.9, 137.0, 127.7 (2C), 127.4 (2C), 119.9, 117.0, 107.9, 62.5, 48.8, 34.4, 27.0; ESI-HRMS calcd for C$_{16}$H$_{16}$N$_3$S [M + H]$^+$ 282.1059, found 282.1060.

6-(4-(thiomorpholin-3-yl)phenyl)pyridin-2-yl)methanol (compound 63, TMb)

63

Was obtained by following the general procedure (scheme 3, 0.3 mmol). Purification by flash column chromatography (EtOAc-hexane 1:1 to 2:0) afforded the pure product as an orange oil (38 mg, 44% of yield).

Note: not stable at rt. Stored at 2ºC - 8ºC.

¹H NMR (400 MHz, CDCl$_3$) δ 7.98 (d, *J* = 8.3 Hz, 2H), 7.74 (t, *J* = 7.7 Hz, 1H), 7.62 (dd, *J* = 7.8, 0.8 Hz, 1H), 7.48 (d, *J* = 8.2 Hz, 2H), 7.18 (dd, *J* = 7.6, 0.8 Hz, 1H), 4.81 (s, 2H), 4.02 (dd, *J* = 10.7, 2.3 Hz, 1H), 3.49 (dt, *J* = 12.0, 3.1 Hz, 3H), 3.20 (td, *J* = 11.9, 2.3 Hz, 1H), 3.01 − 2.86 (m, 2H), 2.50 (ddt, *J* = 26.4, 13.3, 2.3 Hz, 2H); ¹³C NMR (101 MHz, CDCl$_3$) δ 158.7, 155.6, 144.7, 138.4, 137.5, 127.2 (2C), 127.05 (2C), 119.0, 118.9, 64.0, 62.6, 49.0, 34.6, 27.2; ESI-HRMS calcd for C$_{16}$H$_{19}$N$_2$OS [M + H]$^+$ 287.1213, found 287.1210.

3-(3-methoxy-4-((3-methoxybenzyl)oxy)phenyl)thiomorpholine (compound 64, TMc)
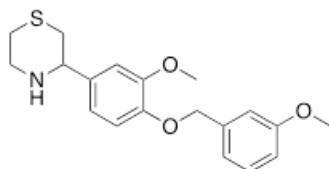
64

Was obtained by following the general procedure (scheme 3, 0.1 mmol). Purification by flash column chromatography (EtOAc-hexane 2:1 to 3:0) afforded the product as a yellow solid.

<u>Notes</u>: Traces of Tin in the sample were removed following the described method (10 mg, 23% of yield).

^{1}H NMR (400 MHz, CDCl$_3$) δ 7.32-7.27 (m, 1H), 7.04-7.01 (m, 2H), 6.98 (s, 1H), 6.87-6.84 (m, 3H), 5.14 (s, 2H), 3.93-3.89 (m, 4H), 3.83 (s, 3H), 3.45 (d, *J*= 12 Hz, 1H), 3.18 (t, *J*= 11.8 Hz, 1H), 2.99-2.84 (m, 2H), 2.47 (dd, *J*= 20.8, 13.2, 2H); ^{13}C NMR (101 MHz, CDCl$_3$) δ 159.8, 149.7, 147.7, 138.8, 129.6 (2C), 119.4, 118.8, 113.9, 113.4, 112.7, 110.2, 71.0, 62.8, 56.1, 55.3, 49.1, 34.7, 27.2; ESI-HRMS calcd for C$_{19}$H$_{24}$NO$_3$S [M + H]$^+$ 346.1471, found 346.1469.

4'-(thiomorpholin-3-yl)-[1,1'-biphenyl]-4-carbonitrile (compound 65, TMd)

65

Was obtained by following the general procedure (scheme 3, 0.1 mmol). Purification by flash column chromatography (EtOAc-hexane 1:1 to 2:0) afforded the pure product as an orange oil (6 mg, 22% yield).

Note: performed NMR analysis demonstrated it is not stable at rt. Stored at 2ºC - 8ºC.

^{1}H NMR (400 MHz, CDCl$_3$) δ 7.75 (d, *J*= 8.6 Hz, 2H), 7.69 (d, J= 8.7 Hz, 2H), 7.59 (d, J = 8.3 Hz, 2H), 7.51 (d, J= 8.3 Hz, 2H), 4.04 (dd, *J* = 10.6, 2.3 Hz, 1H), 3.51 (d, *J* = 11.8 Hz, 1H), 3.23 (td, *J* = 11.9, 2.3 Hz, 1H), 3.00 − 2.86 (m, 2H), 2.52 (dd, *J* = 24.9, 13.2 Hz, 2H); ^{13}C NMR (126 MHz, CDCl$_3$) δ 145.2, 144.6, 138.6 (2C), 132.6 (2C), 127.6 (2C), 127.5 (2C), 127.4, 118.9, 111.0, 62.5, 49.0, 34.8, 27.4; ESI-HRMS calcd for C$_{17}$H$_{17}$N$_2$S [M + H]$^+$ 281.1107, found 281.1106.

6-(4-(morpholin-3-yl)phenyl)nicotinonitrile (compound 66, Ma)

66

was obtained by following the general procedure (scheme 3, 0.1 mmol). Purification by flash column chromatography (EtOAc-hexane 2:1 to 3:0) provided the product as a white solid (11 mg, 41% of yield). Tin traces were removed as described previously.

^{1}H NMR (400 MHz, CDCl$_3$) δ 8.96 (dd, J= 2.2, 0.9 Hz, 1H), 8.04 (ddd, J = 8.4, 6.8, 2.0 Hz, 3H), 7.87 (dd, J = 8.4, 0.9 Hz, 1H), 7.58 (d, J= 8.1 Hz, 2H), 4.04 (dd, J= 10.3, 3.2 Hz, 1H), 3.91 (ddd, J= 18.0, 11.3, 3.0 Hz, 2H), 3.70 (td, J = 11.3, 2.7 Hz, 1H), 3.44 (dd, J = 11.0, 10.0 Hz, 1H), 3.19 (td, J = 11.6, 3.3 Hz, 1H), 3.06 (d, J = 11.7 Hz, 1H); ^{13}C NMR (100 MHz, CDCl$_3$) δ 160.0, 152.5, 143.3 139.9, 136.8, 127.9 (2C), 127.5 (2C), 119.9, 117.0, 107.9, 73.5, 67.2, 60.2, 46.4; ESI-HRMS calcd for C$_{16}$H$_{16}$N$_3$O [M + H]$^+$ 266.1288, found 266.1291.

(6-(4-(morpholin-3-yl)phenyl)pyridin-2-yl)methanol (compound 67, Mb)

67

Was obtained by following the general procedure (scheme 3, 0.3 mmol). Purification by flash column chromatography (EtOAc-hexane 2:1 to 3:0) provided the pure product as an orange oil (55 mg, 68% of yield).

^{1}H NMR (400 MHz, CDCl$_3$) δ 7.98 (d, J = 7.9 Hz, 2H), 7.74 (t, J = 7.7 Hz, 1H), 7.61 (d, J = 7.8 Hz, 1H), 7.52 (d, J = 7.9 Hz, 2H), 7.19 (d, J = 7.6 Hz, 1H), 4.81 (s, 2H), 4.02 (dd, J = 10.2, 3.1 Hz, 1H), 3.89 (td, J = 11.2, 2.9 Hz, 2H), 3.77 − 3.68 (m, 1H), 3.54 − 3.44 (m, 1H), 3.15 (t, J = 11.9 Hz, 1H), 3.04

(d, J = 11.8 Hz, 1H); ^{13}C NMR (101 MHz, CDCl3) δ 158.9, 155.7, 140.7, 138.6, 137.5, 127.7 (2C), 127.1 (2C), 118.9, 118.8, 73.0, 66.8, 64.0, 60.1, 46.2; ESI-HRMS calcd for C16H19N2O2 [M + H]$^{+}$ 271.1441, found 271.1445.

Ethyl (3*R*,5*S*)-5-(4-(4-hydroxybut-1-yn-1-yl)phenyl)thiomorpholine-3-carboxylate (compound 72, CYSe)

was obtained by following the general procedure (scheme 3, 0.3 mmol). Purification by flash column chromatography (hexane-EtOAc 3:2 to 0:3) provided the pure product as a yellow oil (54 mg, 56% of yield).

^{1}H NMR (400 MHz, CDCl$_3$) δ 7.42 (d, *J*= 8.5 Hz, 2H), 7.36 (d, *J*= 8.3 Hz, 2H), 4.30-4.18 (m, 2H), 4.01 (dd, J= 10.7, 2.3 Hz, 1H), 3.86-3.78 (m, 3H), 2.93-2.69 (m, 5H), 2.47 (dt, *J*= 13.2, 2.0 Hz, 2H), 1.31 (t, *J*= 7.1 Hz, 3H); ^{13}C NMR (101 MHz, CDCl$_3$) δ 171.0, 143.0, 132.0 (2C), 126.6 (2C), 123.0, 86.8, 82.0, 63.1, 61.5, 61.1, 60.7, 34.2, 28.8, 23.8, 14.1; ESI-HRMS calcd for C$_{17}$H$_{22}$NO$_3$S [M + H]$^{+}$ 320.1315, found 320.1319.

Ethyl (3R,5S)-5-(3-((4-cyanobenzyl)oxy)phenyl)thiomorpholine-3-carboxylate (compound 73, CYSf)
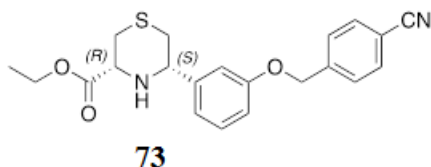
was obtained by following the general procedure (scheme 3, 0.2 mmol) as a yellow oil (24 mg, 63% of yield)

^{1}H NMR (400 MHz, CDCl$_3$) δ 7.71 (d, J= 8.3 Hz, 2H), 7.58 (d, J= 8.5 Hz, 2H), 7.31-7.27 (m, 1H), 7.09-6.99 (m, 2H), 6.90 (ddd, *J*= 8.3, 2.7, 1.0 Hz, 1H), 5.15 (s, 2H), 4.30-4.19 (m, 2H), 4.01 (dd, *J*=10.6, 2.3 Hz, 1H), 3.81 (dd, *J*= 10.6, 2.7 Hz, 1H), 2.94-2.73 (m, 3H), 2.49 (dt, *J*= 13.1, 2.1 Hz, 1H), 1.31 (t, J = 7.1 Hz, 3H); ^{13}C NMR (101 MHz, CDCl$_3$) δ 171.0, 158.5, 145.2, 142.4, 132.5 (2C), 130.0, 127.6 (2C), 125.5, 120.0, 118.7, 114.2, 111.7, 68.9, 63.4, 61.5, 60.8, 34.4, 28.8, 14.2; ESI-HRMS calcd for C$_{21}$H$_{23}$N$_2$O$_3$S [M + H]$^+$ 383.1424, found 383.1425.

Ethyl (3*R*,5*S*)-5-(3-methoxy-4-((3-methoxybenzyl)oxy)phenyl)thiomorpholine-3-carboxylate (compound 74, CYSc)
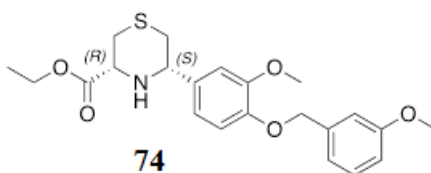
was obtained by following the general procedure (scheme 3, 0.2 mmol). The imine formation required an increase of the temperature at 40 C. Purification by flash column chromatography (hexane-EtOAc 2:1) afforded the pure product as a yellow oil (29 mg, 35% of yield)

^{1}H NMR (400 MHz, CDCl$_3$) δ 7.32-7.27 (m, 1H), 7.05-6.96 (m, 3H), 6.89-6.83 (m, 3H), 5.15 (s, 2H), 4.30-4.17 (m, 3H), 3.96-3.92 (m, 4H), 3.84-3.77 (m, 4H), 2.92-2.73 (m, 3H), 2.46 (dt, *J*= 13.1, 2.0 Hz, 1H), 1.30 (t, *J*= 7.1 Hz, 3H); ^{13}C NMR (101 MHz, CDCl$_3$) δ 171.0, 159.8, 149.7, 147.8, 138.8, 136.7, 129.6, 119.4, 118.9, 113.9, 113.4, 112.6, 110.4, 70.9, 63.4, 61.4, 61.0, 56.1, 55.2, 34.4, 28.8, 14.2; ESI-HRMS calcd for C$_{22}$H$_{28}$NO$_5$S [M + H]$^+$ 418.1683, found 418.1676.

Ethyl (3*R*,5*S*)-5-(4-(6-(hydroxymethyl)pyridin-2-yl)phenyl)thiomorpholine-3-carboxylate (compound 75, CYSb)
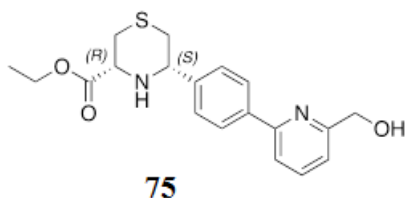
75

was obtained by following the general procedure (scheme 3, 0.3 mmol). Purification by flash column chromatography (hexane-EtOAc 1:1) afforded the pure product as a yellow oil (52 mg, 48% of yield)

^{1}H NMR (400 MHz, CDCl$_3$) δ 8.01 (d, *J* = 8.4 Hz, 2H), 7.77 (t, *J* = 7.7 Hz, 1H), 7.65 (dd, *J*= 7.8, 0.9 Hz, 1H), 7.53 (d, *J* = 8.2 Hz, , 2H), 7.19 (dd, *J* = 7.6, 0.9 Hz, 1H), 4.83 (s, 2H), 4.31-4.18 (m, 2H), 4.09 (dd, *J* = 10.6, 2.3 Hz, 1H), 3.84 (dd, *J* = 10.5, 2.9 Hz, 1H), 2.96-2.76 (m, 3H), 2.52 (dt, *J*= 13.1, 2.1 Hz, 1H), 1.31 (t, *J* = 7.1 Hz, 3H); ^{13}C NMR (101 MHz, CDCl$_3$) δ 171.0, 158.6,

155.7, 144.3, 138.6, 137.5, 127.2 (2C), 127.1 (2C), 119.0, 118.8, 63.9, 63.2, 61.5, 60.8, 34.3, 28.8, 14.2; ESI-HRMS calcd for $C_{19}H_{23}N_2O_3S$ [M + H]$^+$ 359.1424, found 359.1419.

Ethyl (3R,5S)-5-(4'-cyano-[1,1'-biphenyl]-4-yl)thiomorpholine-3-carboxylate (compound 76, CYSd)
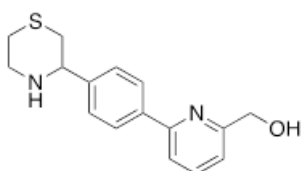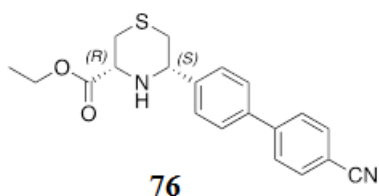

Was obtained by following the general procedure (scheme 3, 0.2 mmol). Purification by flash column chromatography (hexane-EtOAc 1:1) provided the pure product as a yellow solid (21 mg, 30% of yield).

^{1}H NMR (400 MHz, CDCl$_3$) δ 7.75 (d, *J* = 8.7 Hz, 2H), 7.70 (d, *J* = 8.7 Hz, 2H), 7.60 (d, *J* = 8.5 Hz, 2H), 7.54 (d, *J* = 8.2 Hz, 2H), 4.30-4.21 (m, 2H), 4.09 (dd, *J* = 10.6, 2.3 Hz, 1H), 3.84 (dd, *J* = 10.6, 2.7 Hz, 1H), 2.96 − 2.77 (m, 3H), 2.53 (dt, *J* = 13.1, 2.1 Hz, 1H), 1.32 (t, *J* = 7.1 Hz, 3H); ^{13}C NMR (101 MHz, CDCl$_3$) δ 171.0, 145.1, 143.9, 138.8, 132.6 (2C), 127.7 (2C), 127.5 (4C), 118.9, 111.0, 63.1, 61.5, 60.7, 34.4, 28.9, 14.2; ESI-HRMS calcd for $C_{20}H_{21}N_2O_2S$ [M + H] 353.1318, found 353.1315.

Ethyl (3R,5S)-5-(4-(5-cyanopyridin-2-yl)phenyl)thiomorpholine-3-carboxylate (compound 77, CYSa)
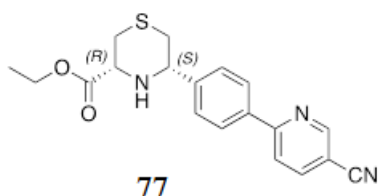
Was obtained by following the general procedure (scheme 3, 0.1 mmol). The imine formation required an increase of both temperature and of reaction time to induce 97% of conversion. After the cyclization reaction, a purification by flash column chromatography (hexane-EtAOc 1:1) afforded the product. A crystallization by hexane-EtOAc 8:2 was useful to remove traces of aldehyde in the sample. The pure product was obtained as a yellow oil (27 mg, 76% yield).

^{1}H NMR (400 MHz, CDCl$_3$) δ 8.96 (dd, J = 2.2, 0.9 Hz, 1H), 8.08 – 8.01 (m, 3H), 7.87 (dd, J = 8.3, 0.9 Hz, 1H), 7.58 (d, J = 8.3 Hz, 2H), 4.25 (qd, J = 7.1, 3.8 Hz, 2H), 4.11 (dd, J = 10.6, 2.4 Hz, 1H), 3.84 (dd, J = 10.6, 2.7 Hz, 1H), 2.97 – 2.75 (m, 3H), 2.53 (dt, J = 13.2, 2.1 Hz, 1H), 1.32 (t, J = 7.1 Hz, 3H); ^{13}C NMR (101 MHz, CDCl$_3$) δ 170.9, 160.0, 152.5, 145.9, 139.9, 137.0, 127.8 (2C), 127.4 (2C), 119.9, 117.0, 107.9, 63.1, 61.5, 60.7, 34.3, 28.8, 14.2; ESI-HMRS calcd for C$_{19}$H$_{20}$N$_3$O$_2$S [M + H]$^+$ 354.1271, found 354.1264.

Ethyl **(3*R*,5*S*)-5-(3-(difluoromethoxy)-4-hydroxyphenyl)thiomorpholine-3-carboxylate (compound 78, CYSg)**

78
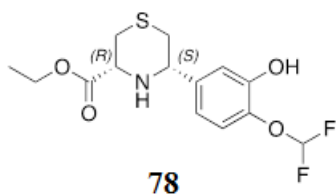
Was obtained by following the general prodecure (scheme 3, 0.5 mmol). After the cyclization reaction, a purification by flash column chromatography (EtAOc-hexane 1:1) provided the pure product as a brown oil (99 mg, 60% yield).

^{1}H NMR (400 MHz, CDCl$_3$) δ 6.99 (s, 2H), 6.83 (d, J = 8.1 Hz, 1H), 6.44 (t, J_{H-F} = 73.9 Hz, 1H), 4.17 (m, 2H), 3.86 (d, J = 10.4 Hz, 1H), 3.71 (d, J = 10.4 Hz, 1H), 2.84 - 2.51 (m, 3H), 2.36 (d, J = 13.0 Hz, 1H), 1.21 (t, J = 7.1 Hz, 3H); ESI-HRMS calcd for C$_{14}$H$_{18}$F$_2$NO$_4$S [M + H]$^+$ 334.0919, found 334.0924.

8.3.2.1 Synthesis of compounds 69-71

***tert*-butyl** **3-(4-(6-(hydroxymethyl)pyridin-2-yl)phenyl)piperazine-1-carboxylate (compound 168)**
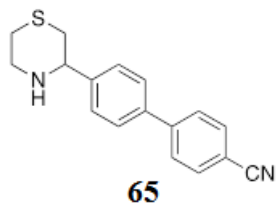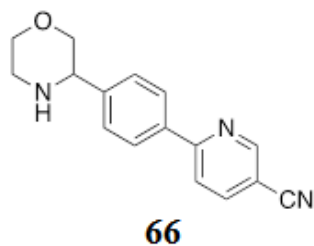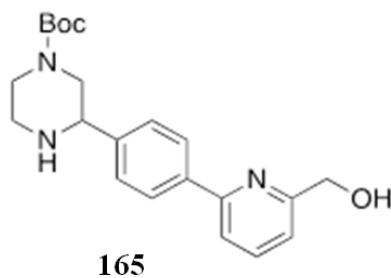

165

241

Was obtained by following the general procedure (scheme 3. 0.3 mmol). Purification by flash column chromatography (EtOAc-hexane 2:1 to 3:0) afforded the pure product as a yellow solid (76 mg, 68% of yield).

^{1}H NMR (400 MHz, CDCl$_3$) δ 7.98 (d, J = 7.9 Hz, 2H), 7.73 (t, J = 7.7 Hz, 1H), 7.62 (d, J = 7.8 Hz, 1H), 7.51 (d, J = 8.0 Hz, 2H), 7.19 (d, J = 7.6 Hz, 1H), 4.80 (s, 2H), 4.06 (s, 2H), 3.78 (d, J = 10.4 Hz, 1H), 3.27 (s, 2H), 3.10 (d, J = 9.9 Hz, 1H), 2.99-2.70 (m, 3H), 1.49 (s, 9H).

(6-(4-(piperazin-2-yl)phenyl)pyridin-2-yl)methanol (compound 69, PIPa)

69
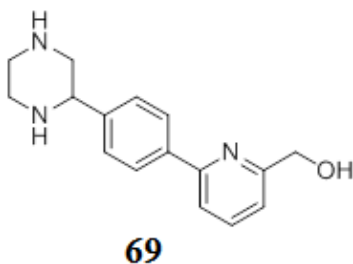
To a solution of compound **165** (76.0 mg, 0.205 mmol) in DCM (3 ml) was added trifluoroacetic acid (3 ml). The mixture was stirred at room temperature for two hours and concentrated. NaOH aqueous solution (1 N) was added dropwise, and the mixture was extracted with EtAOc. The layers were separated and the organic layer was washed with aqueous NaHCO$_3$ and with brine, dried over anhydrous Na$_2$SO$_4$, filtered, and concentrated under reduced pressure to give compound **69** (97% yield).

^{1}H NMR (400 MHz, D$_2$O) δ 8.49 (t, J = 8.0 Hz, 1H), 8.04 (dd, J = 8.1, 1.2 Hz, 1H), 7.92 (dd, J = 8.1, 1.0 Hz, 1H), 7.87 (d, J = 8.5 Hz, 2H), 7.69 (d, J =

8.4 Hz, 2H), 4.96 (s, 2H), 4.84 (dd, J = 12.5, 3.4 Hz, 1H), 3.91 − 3.44 (m, 6H); ^{13}C NMR (101 MHz, D$_2$O) δ 156.0, 151.4, 147.1, 134.3, 133.1, 129.7 (2C), 128.6 (2C), 125.3, 123.4, 59.7, 55.6, 44.4, 41.2, 39.7; ESI-HRMS calcd for C$_{16}$H$_{20}$N$_3$O [M + H]$^+$ 270.1601, found 270.1602.

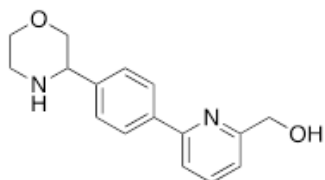***tert*-butyl 3-(4-(4-hydroxybut-1-yn-1-yl)phenyl)piperazine-1-carboxylate (compound 169)**
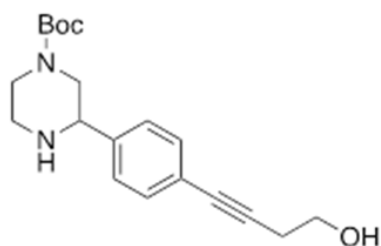
166

Was obtained by following the general procedure (scheme 3, 0.3 mmol). Purification by flash column chromatography (EtOAc-hexane 2:1 to 3:0) provided the pure product as a yellow solid (70 mg, 71% of yield).

^{1}H NMR (400 MHz, CDCl$_3$) δ 7.39 (d, J = 8.3 Hz, 2H), 7.35 (d, J = 8.4 Hz, 2H), 4.05 (br s, 2H), 3.81 (t, J = 6.3 Hz, 2H), 3.73 (dd, J = 10.8, 3.1 Hz, 1H), 3.11–2.93 (m, 4H), 2.93-2.78 (m, 2H), 2.69 (t, J = 6.3 Hz, 2H), 1.48 (s, 9H).

4-(4-(piperazin-2-yl)phenyl)but-3-yn-1-ol (compound 70, PIPe)
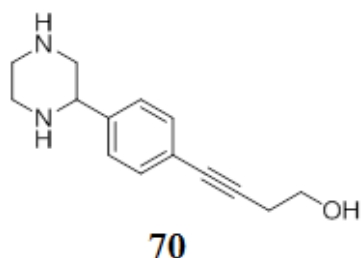
To a solution of compound **166** (70 mg, 0.212 mmol) in DCM (2.5 ml) was added trifluoroacetic acid (2.5 ml). The mixture was stirred at room temperature for two hours and concentrated. NaOH aqueous solution (1 N) was added dropwise, and the mixture was extracted with EtAOc. The layers were separated and the organic layer was washed with aqueous $NaHCO_3$ and with brine, dried over anhydrous Na_2SO_4, filtered, and concentrated under reduced pressure to give compound **70** (92% yield).

^{1}H NMR (400 MHz, D_2O) δ 7.52 (d, *J* = 8.4 Hz, 2H), 7.42 (d, *J* = 8.4 Hz, 2H), 3.86 – 3.44 (m, 9H), 2.60 (t, *J* = 6.3 Hz, 2H); ^{13}C NMR (101 MHz, D_2O) δ 132.7, 130.3 (2C), 127.6 (2C), 125.5, 90.0, 80.6, 59.86, 55.8, 44.4, 41.1, 39.7, 22.4; ESI-HMRS calcd for $C_{14}H_{19}N_2O$ [M + H]$^+$ 231.1492, found 231.149.

tert-butyl   3-(3-methoxy-4-((3-methoxybenzyl)oxy)phenyl)piperazine-1-carboxylate (compound 170)
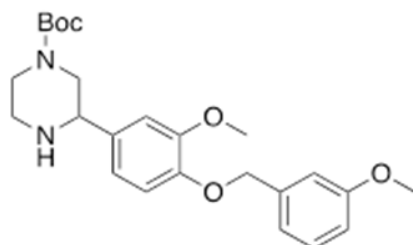
167
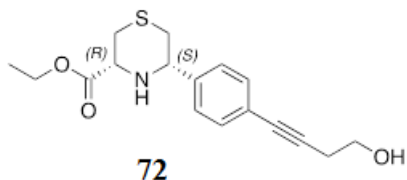
Was obtained following the general procedure (scheme 3, 0.1 mmol). Purification by flash column chromatography (EtOAc-hexane 1:1) provided the product as an orange solid (15 mg, 35% of yield).

Note: Traces of aldehyde were removed using a small column of propyl sulfonic acid supported on silica.

^{1}H NMR (400 MHz, CDCl$_3$) δ 7.32 − 7.27 (m, 3H), 7.06 − 6.98 (m, 3H), 6.89 − 6.83 (m, 3H), 5.13 (s, 2H), 3.96 − 3.87 (m, 3H), 3.85 − 3.77 (m, 5H), 3.17 − 2.90 (m, 5H), 2.78 (t, J = 11.3 Hz, 1H), 1.48 (s, 9H).

2-(3-methoxy-4-((3-methoxybenzyl)oxy)phenyl)piperazine
(compound 71, PIPc)
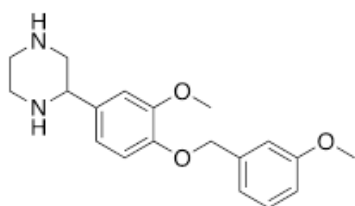
71

To a solution of compound **167** (15 mg, 0.035 mmol) in DCM (2.5 ml) was added trifluoroacetic acid (2.5 ml). The mixture was stirred at room temperature for two hours and concentrated. NaOH aqueous solution (1 N)

was added dropwise, and the mixture was extracted with EtAOc. The layers were separated and the organic layer was washed with aqueous $NaHCO_3$ and with brine, dried over anhydrous Na_2SO_4, filtered, and concentrated under reduced pressure to give compound **71** (94% yield).

^{1}H NMR (400 MHz, $CDCl_3$) δ 7.33 − 7.27 (m, 3H), 7.06 − 6.98 (m, 3H), 6.89 − 6.83 (m, 3H), 5.13 (s, 2H), 3.96 − 3.87 (m, 4H), 3.85 − 3.77 (m, 5H), 3.17 − 2.90 (m, 5H), 2.78 (t, *J* = 11.3 Hz, 1H); ESI-HMRS calcd for $C_{19}H_{25}N_2O_3$ $[M + H]^+$ 329.1860, found 329.1856.

8.3.3 General procedure for the synthesis of compounds 79-82

A solution of 10 mg of compounds **72-75** in methanol (1 ml) was treated with 10% NaOH solution (1 ml). The resulting mixture was stirred for 3 hours at rt and concentrated under reduced pressure at 40 °C. The remaining aqueous solution was acidified with HCl 2N (pH=6) and extracted with EtOAc (10 x 3). The organic layer was dried over Na_2SO_4 and concentrated to obtain the final products **79-82**.

(3*R*,5*S*)-5-(4-(4-hydroxybut-1-yn-1-yl)phenyl)thiomorpholine-3-carboxylic acid (compound 79)
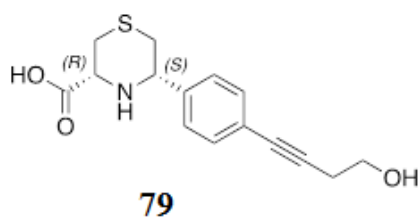
Was obtained by following the general prodecure as a transparent oil (91% yield).

^{1}H NMR (400 MHz, MeOD) δ 7.54 (d, J = 7.3 Hz, 2H), 7.48 (d, J = 7.5 Hz, 2H), 4.63 (d, J = 11.7 Hz, 1H), 4.43 (d, J = 11.6 Hz, 1H), 3.75 (t, J = 6.0 Hz, 2H), 3.30 – 3.12 (m, 3H), 2.92 (d, J = 14.9 Hz, 1H), 2.65 (t, J = 6.0 Hz, 2H); ^{13}C NMR (101 MHz, MeOD) δ 167.8, 134.9, 132.3 (2C), 127.2 (2C), 125.3, 88.9, 79.8, 62.3, 60.0, 59.8, 29.6, 25.9, 22.8; ESI-HRMS calcd for $C_{15}H_{18}NO_3S$ [M + H]$^+$ 292.1002, found 292.0999.

(3R,5S)-5-(3-((4-cyanobenzyl)oxy)phenyl)thiomorpholine-3-carboxylic acid (compound 80)
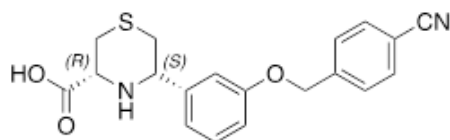
80

Was obtained by following the general prodecure as a white solid (95% yield).

^{1}H NMR (400 MHz, MeOD) δ 7.92 (d, J = 7.6, 2H), 7.57 (d, J = 7.6, 2H), 7.45 (t, J = 7.9, 1H), 7.22 (s, 1H), 7.14 (t, J = 7.3, 2H), 5.24 (s, 2H), 4.60 (d, J = 11.6, 1H), 4.40 (d, J = 11.5, 1H), 3.33 – 3.13 (m, 4H), 2.92 (d, J = 14.6, 1H); ^{13}C NMR (101 MHz, MeOD) δ 170.4, 168.7, 159.4, 141.1, 137.3, 133.1, 130.7, 127.6 (2C), 126.8 (2C), 118.9, 115.5, 113.8, 69.1, 62.7, 59.6, 29.9, 26.1.

(3*R*,5*S*)-5-(3-methoxy-4-((3-methoxybenzyl)oxy)phenyl)thiomorpholine-3-carboxylic acid (compound 81)

81
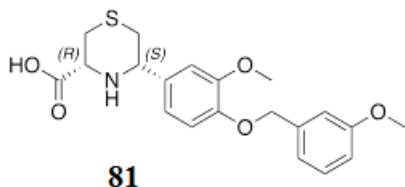
Was obtained by following the general prodecure as an orange solid (71.4% yield).

^{1}H NMR (400 MHz, MeOD) δ 7.20-7.12 (m, 2H), 7.06 (s, 1H), 7.00-6.90 (m, 3H), 6.76 (d, *J* = 7.5 Hz, 1H), 5.04 (s, 2H), 4.42 (d, J = 11.5 Hz, 1H), 4.24 (d, *J* = 11.7 Hz, 1H), 3.79 (s, 3H), 3.68 (s, 3H), 3.25-3.01 (m, 3H), 2.78 (d, *J* = 14.6, 1H); ^{13}C NMR (101 MHz, MeOD) δ 168.0, 150.1, 149.2 (2C), 138.5, 129.2, 128.9, 119.6, 119.2, 114.4, 112.9, 112.7, 110.9, 70.5, 62.7, 59.8, 55.4, 54.2, 29.8, 25.8. ESI-HRMS calcd for $C_{20}H_{22}NO_5S$ [M - H]$^-$ 388.1297, found 388.1212.

(3*R*,5*S*)-5-(4-(6-(hydroxymethyl)pyridin-2-yl)phenyl)thiomorpholine-3-carboxylic acid (compound 82)

82
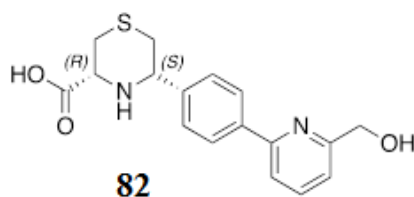
Was obtained by following the general prodecure as an orange solid (93% yield).

^{1}H NMR (400 MHz, D$_2$O) δ 8.55 (t, *J* = 8.1 Hz, 1H), 8.10 (dd, *J* = 8.1, 1.1 Hz, 1H), 7.97 (dd, *J* = 8.0, 1.1 Hz, 1H), 7.89 (d, *J* = 8.5 Hz, 1H), 7.72 (d, *J* =

8.5 Hz, 2H), 4.75 (dd, *J* = 11.9, 2.7 Hz, 1H), 4.36 (dd, *J* = 11.1, 3.9 Hz, 1H), 3.40 – 3.10 (m, 3H), 2.94 (ddd, *J* = 14.8, 2.7, 1.6 Hz, 1H); ^{13}C NMR (101 MHz, MeOD) δ 167.6, 158.2, 151.9, 145.8, 139.4, 133.2, 129.3 (2C), 128.1 (2C), 124.3, 122.7, 62.3, 60.2, 59.6, 29.6, 25.6; ESI-HRMS calcd for $C_{17}H_{19}N_2O_3S$ 331.1111, found 331.1115.

-CHAPTER 9-

Computational details

9.1 2-Carboxamide pyrrole derivatives targeting mPGES-1

9.1.1 Generation of libraries

Commercially available methyl ketones and aromatic amines were converted from 2D structures to 3D structures using LigPrep software (v. 3.4; Schrödinger, LLC, 2015). The methyl moiety in the ketones and the amine group in the amines were removed to provide the building blocks for the next step in the Reagent Preparation phase, and Combiglide was used for the generation of the final libraries **D** and **E**. LigPrep performed calculation increased the number to 57,541 for each library, and a final energy minimization of the three libraries with *Optimized Potentials for Liquid Simulations* (OPLS) *2005 force field* was performed. After the application of QikProp[110] and LigFilter, [117] the number was reduced to 4,300 and 458 molecules for the libraries **D** and **E** respectively.

9.1.2 Docking analysis

In the structure-based molecular docking experiments, the same mPGES-1 three-dimensional crystal structure (PDB code: 4BPM)[209] used for the calculation concerning 2-amino benzothiazole and thiadiazole derivatives was adopted (see section 3.4.3). Also in this specific case, Glide software[103, 104] was used for docking analysis and the virtual screening workflow[117] was applied (see sections 3.3.3 and 3.4.3), in the same size receptor grid focused onto the co-crystallized ligand binding site (LVJ).

For the calculation regarding reported pyrrole alkanoic acid derivatives (Table 6), chemical structures of pyrroles were built with Maestro's Build

Panel (v. 9.6; Schrödinger, LLC, 2015) and processed with LigPrep, (v. 3.4; Schrödinger, LLC, 2013) in order to generate all the possible stereoisomers, tautomers and protonation states at a pH of 7.4 ± 1.0, and a final energy minimization with the OPLS 2005 force field. Then, the Ligand Docking was performed using the same crystal structure and the same grid adopted for the virtual screening workflow for libraries **D** and **E**. Glide software package (Standard Precision [SP] mode, version 6.1, Schrödinger package) was used in order to analyze the binding mode of the compounds into the crystal structure of the protein (PDB code: 4BPM). [209] For this step, an expansion of the sampling mode (2×) was set, keeping 10,000 poses in the starting phase of docking and selecting 800 poses for energy minimization. Specifically, one output structure was saved for each binder, with a scaling factor of 0.8 related to van der Waals radii with a partial charge cutoff of 0.15. Basing on a 0.5 kcal/mol rejection cutoff for the obtained minimized poses, a maximum of one pose was chosen in the post-docking optimization phase. The selected outputs were then submitted to another docking round, the Extra Precision Glide mode (Extra Precision [XP] mode, version 6.1, Schrödinger package) setting the same parameters applied in the previous SP-docking experiments. In the output file, 20 poses for each compound were saved, and in the post-docking optimization of the docking poses, a maximum of 20 poses was selected.

9.2 Discovery of novel 3-hydroxy-3-pyrrolin-2-one derivatives as mPGES-1 inhibitors

9.2.1 Input files preparation for molecular docking

The starting library of compounds was purchased from the Otava Chemicals database (~ 3.1×10^5 compounds). LigPrep software (Schrodinger Suite) was used for the preparation of the library and all the possible stereoisomers, tautomers, and protonation states at physiological pH were added to each compound, and a minimization was performed using OPLS 2005 force field. Protein 3D model was prepared using the Schrödinger Protein Preparation Wizard, [117] starting from the mPGES-1 X-ray structure in the active form co-complexed with the inhibitor LVJ (2-[[2,6-bis(chloranyl)-3-[(2,2-dimethylpropanoylamino)methyl]phenyl]amino]-1-methyl-6-(2-methyl-2-oxidanyl-propoxy)-N-[2,2,2-tris(fluoranyl)ethyl]benzimidazole-5-carboxamide) (PDB code: 4BPM). [209] The visual inspection of the protein crystal structure showed that the binding of LVJ inhibitor in the ligand binding site was not assisted by structural water molecules, the reason why they were removed. All hydrogen atoms were added, and bond orders were assigned. Docking calculations were performed on the protein structure in the presence of the cofactor GSH, whereas LVJ was removed.

9.2.2 Molecular Docking and structure-based shape screening

The molecular docking virtual screening campaign was performed using the Virtual Screening Workflow (Glide software), following the scheme:

- High-Throughput Virtual Screening scoring/sampling (HTVS): an input file containing 7,220 compounds, saved 10 maximum number of poses for each compound, saved first 10,000 ranked poses (selection filter: docking score) as output, corresponding to 4546 compounds

- Standard Precision scoring/sampling phase (SP), and structure-based shape screening: 4,546 unique compounds from HTVS phase as input, saved 10 maximum number of poses for each compound. Each produced pose was submitted to an "in place" shape screening (See Results and Discussion) against LVJ. Choosing a threshold = 0.400, 4120 unique compounds were selected for the subsequent step

- Extra Precision scoring/ sampling phase (XP), and structure-based shape screening: 4,120 unique compounds from SP/shape screening step as input, saved 100 maximum number of poses for each compound. The produced poses were submitted to an "in place" shape screening (See Results and Discussion) against LVJ. Choosing a threshold = 0.500, 914 unique compounds were selected. The selected compounds were then further filtered considering their binding mode with the receptor counterpart.

9.3 Discovery of new molecular entities able to strongly interfere with Hsp90 C-terminal domain: rationalization

9.3.1 Molecular docking studies.

Schrödinger Protein Preparation Wizard workflow[117] was used to prepare the ATP-bound active state of Hsp82, a yeast Hsp90α homologue (PDB code: 2CG9)[313] removing the water molecules that were found 5 Å or more and cap termini were included. Additionally, all hydrogen atoms were added and bond orders were assigned. Chemical structures of investigated compounds were built with Maestro's Build Panel (version 10.2) [117] and subsequently processed with LigPrep (version 3.4)[123] in order to generate all the possible tautomers and protonation states at a pH of 7.4 ± 1.0; the resulting ligands were finally minimized employing the OPLS 2005 force field.

9.3.2 Induced fit docking.

Binding site for the first Glide docking phase (Glide Standard Precision Mode) of the Induced Fit Workflow (Induced Fit Docking, protocol 2015–2, Glide version 6.4, Prime version 3.7, Schrödinger)[103, 104] is calculated on the 2CG9 structure[313], mapping onto a grid with dimensions of 36 Å (outer box) and 20 Å (inner box), centered on residues 628–630, 640–641, 670–675 (Hsp90 residues numbering as in the PDB entry 2CG9). Maestro's default protocol was used for the first (Initial Glide docking) and the second step (Prime Induced Fit) considering 20 poses per ligand; these poses were retained from the initial docking and then were passed to Prime (Prime version 3.7, Schrödinger 2015), for the Prime refinement step. Finally, the ligands were re-

docked (third step) into their corresponding low energy protein structures (Glide Extra Precision Mode) with resulting complexes ranked according to GlideScore.

9.3.3 Molecular Dynamics Simulations

The starting structures for the Molecular Dynamics (MD) simulations were prepared with the System Builder in Desmond.[319] Na+ ions were added to the system to ensure electroneutrality, and the SPC[323] (simple point charge) water model was used for solvation in a rectangular box with a 10 Å buffer distance, resulting in a system with approximately 17,8000 atoms. OPLS-2005 force field parameters available in the Schrödinger Suite was used for the entire system (protein and substrates). The MD simulation workflow was run with the default parameters in the Maestro interface to Desmond[319] accounting for a total simulation time of 100 ns, using a recording interval of 1.2 ps, and an ensemble class NPT (300 K and 1.01 bar). Before the simulation, a relaxation of the system was performed using the default equilibration protocol in Desmond[319] with multisim procedure, which is a vital step to prepare a molecular system for production-quality MD simulation. In particular, Maestro's default relaxation protocol was used, which have included two stages of minimization (restrained and unrestrained) followed by four stages of MD runs with gradually diminishing restraints.

9.3.4 Generation of three libraries of compounds deriving from the new disclosed inhibitor 103 and docking studies

The structures of the amines, commercially available at Sigma Aldrich Company, were converted from 2D structures to 3D structures suitable for the docking stage of the process, using LigPrep software (v. 3.4; Schrödinger,

LLC, 2015). Reagent Preparation was used for the generation of the building blocks, with a cleavage of a hydrogen atom of the amine group. By means of Combiglide, the final .bld file was combined with the scaffolds obtaining the novel libraries, each containing 1,629 compounds, which were processed with LigPrep and minimized with *Optimized Potentials for Liquid Simulations* (OPLS) *2005 force field*. The final libraries contained 2887 compounds.

The same prepared three-dimensional protein used for docking experiments performed on compounds **100** and **103** was used for the calculation (PDB code: 2CG9).[313] The final libraries were submitted to the virtual screening workflow onto the crystal structure of the chaperone, performing the three rounds of docking experiments: the High-Throughput Virtual Screening (HTVS), the Standard Precision (SP) and the Extra-Precision (XP) Glide mode experiment, with a gradually increasing precision in sampling and scoring. The final small libraries of compounds filtered in the last step (XP) were undergone to a set of filters and selected setting the key interactions with Leu671, Leu674 and Leu676 of both the chains as qualitative filter.

References

1.   Balkwill, F.; Mantovani, A., Inflammation and cancer: back to Virchow? *Lancet* **2001,** *357* (9255), 539-45.

2.   Dvorak, H. F., Tumors: wounds that do not heal. Similarities between tumor stroma generation and wound healing. *N Engl J Med* **1986,** *315* (26), 1650-9.

3.   Pardoll, D. M., Spinning molecular immunology into successful immunotherapy. *Nat Rev Immunol* **2002,** *2* (4), 227-38.

4.   Philip, M.; Rowley, D. A.; Schreiber, H., Inflammation as a tumor promoter in cancer induction. *Semin Cancer Biol* **2004,** *14* (6), 433-9.

5.   Laveti, D.; Kumar, M.; Hemalatha, R.; Sistla, R.; Naidu, V. G.; Talla, V.; Verma, V.; Kaur, N.; Nagpal, R., Anti-inflammatory treatments for chronic diseases: a review. *Inflamm Allergy Drug Targets* **2013,** *12* (5), 349-61.

6.   Chen, K.; Huang, J.; Gong, W.; Iribarren, P.; Dunlop, N. M.; Wang, J. M., Toll-like receptors in inflammation, infection and cancer. *Int Immunopharmacol* **2007,** *7* (10), 1271-85.

7.   Munn, L. L., Cancer and inflammation. *Wiley Interdiscip Rev Syst Biol Med* **2017,** *9* (2).

8.   Kidane, D.; Chae, W. J.; Czochor, J.; Eckert, K. A.; Glazer, P. M.; Bothwell, A. L.; Sweasy, J. B., Interplay between DNA repair and inflammation, and the link to cancer. *Crit Rev Biochem Mol Biol* **2014,** *49* (2), 116-39.

9.   Chong, D. L.; Sriskandan, S., Pro-inflammatory mechanisms in sepsis. *Contrib Microbiol* **2011,** *17*, 86-107.

10.   De Caterina, R.; Libby, P.; Peng, H. B.; Thannickal, V. J.; Rajavashisth, T. B.; Gimbrone, M. A., Jr.; Shin, W. S.; Liao, J. K., Nitric oxide decreases cytokine-induced endothelial activation. Nitric oxide selectively reduces endothelial expression of adhesion molecules and proinflammatory cytokines. *J Clin Invest* **1995,** *96* (1), 60-8.

11.   Savill, J. S.; Wyllie, A. H.; Henson, J. E.; Walport, M. J.; Henson, P. M.; Haslett, C., Macrophage phagocytosis of aging neutrophils in inflammation. Programmed cell death in the neutrophil leads to its recognition by macrophages. *J Clin Invest* **1989,** *83* (3), 865-75.

12.   Hoffmann, B. R.; Wagner, J. R.; Prisco, A. R.; Janiak, A.; Greene, A. S., Vascular endothelial growth factor-A signaling in bone marrow-derived endothelial progenitor cells exposed to hypoxic stress. *Physiol Genomics* **2013,** *45* (21), 1021-34.

13.   Nakanishi, M.; Rosenberg, D. W., Multifaceted roles of PGE2 in inflammation and cancer. *Semin Immunopathol* **2013,** *35* (2), 123-37.

14.   Dey, I.; Lejeune, M.; Chadee, K., Prostaglandin E2 receptor distribution and function in the gastrointestinal tract. *Br J Pharmacol* **2006,** *149* (6), 611-23.

15.   Omori, K.; Kida, T.; Hori, M.; Ozaki, H.; Murata, T., Multiple roles of the PGE2 - EP receptor signal in vascular permeability. *Br J Pharmacol* **2014,** *171* (21), 4879-89.

16.   Duffy, D. M., Novel contraceptive targets to inhibit ovulation: the prostaglandin E2 pathway. *Hum Reprod Update* **2015,** *21* (5), 652-70.

17.   Tan, S.; Chen, X.; Xu, M.; Huang, X.; Liu, H.; Jiang, J.; Lu, Y.; Peng, X.; Wu, B., PGE2 /EP4 receptor attenuated mucosal injury via beta-arrestin1/Src/EGFR-mediated proliferation in portal hypertensive gastropathy. *Br J Pharmacol* **2017,** *174* (9), 848-866.

18.   Gonzalez, A. A.; Salinas-Parra, N.; Leach, D.; Navar, L. G.; Prieto, M. C., PGE2 upregulates renin through E-prostanoid receptor 1 via PKC/cAMP/CREB pathway in M-1 cells. *Am J Physiol Renal Physiol* **2017,** *313* (4), F1038-F1049.

19.   Pratt, C. L.; Brown, C. R., The role of eicosanoids in experimental Lyme arthritis. *Front Cell Infect Microbiol* **2014,** *4*, 69.

20.   Wang, D.; Fu, L.; Sun, H.; Guo, L.; DuBois, R. N., Prostaglandin E2 Promotes Colorectal Cancer Stem Cell Expansion and Metastasis in Mice. *Gastroenterology* **2015,** *149* (7), 1884-1895 e4.

21.   Nandi, P.; Girish, G. V.; Majumder, M.; Xin, X.; Tutunea-Fatan, E.; Lala, P. K., PGE2 promotes breast cancer-associated lymphangiogenesis by activation of EP4 receptor on lymphatic endothelial cells. *BMC Cancer* **2017,** *17* (1), 11.

22.   Noverr, M. C.; Erb-Downward, J. R.; Huffnagle, G. B., Production of Eicosanoids and Other Oxylipins by Pathogenic Eukaryotic Microbes. *Clin Microbiol Rev* **2003,** *16* (3), 517-533.

23.   Folco, G.; Murphy, R. C., Eicosanoid Transcellular Biosynthesis: From Cell-Cell Interactions to in Vivo Tissue Responses. *Pharmacol Rev* **2006,** *58* (3), 375-388.

24.   Rovati, G. E.; Baroffio, M.; Citro, S.; Brichetto, L.; Ravasi, S.; Milanese, M.; Crimi, E.; Brusasco, V., Cysteinyl-leukotrienes in the regulation of beta2-adrenoceptor function: an in vitro model of asthma. *Respir Res* **2006,** *7*, 103.

25.   Aggarwal, B. B., Signalling pathways of the TNF superfamily: a double-edged sword. *Nat Rev Immunol* **2003,** *3* (9), 745-56.

26.   Balkwill, F., Tumor necrosis factor or tumor promoting factor? *Cytokine Growth Factor Rev* **2002,** *13* (2), 135-41.

27.   Courtois, G.; Gilmore, T. D., Mutations in the NF-kappaB signaling pathway: implications for human disease. *Oncogene* **2006,** *25* (51), 6831-43.

28.   Rodriguez, M.; Domingo, E.; Municio, C.; Alvarez, Y.; Hugo, E.; Fernandez, N.; Sanchez Crespo, M., Polarization of the innate immune response by prostaglandin E2: a puzzle of receptors and signals. *Mol Pharmacol* **2014,** *85* (1), 187-97.

29.   Hawkey, C. J., COX-1 and COX-2 inhibitors. *Best Pract Res Clin Gastroenterol* **2001,** *15* (5), 801-20.

30.   Hu, C.; Ma, S., Recent development of lipoxygenase inhibitors as anti-inflammatory agents. *Medchemcomm* **2018,** *9* (2), 212-225.

31.   Garavito, R. M.; DeWitt, D. L., The cyclooxygenase isoforms: structural insights into the conversion of arachidonic acid to prostaglandins. *Biochim Biophys Acta* **1999,** *1441* (2-3), 278-87.

32.   Alabaster, V. A., Metabolism of arachidonic acid and its endoperoxide (PGH2) to myotropic products in guinea-pig and rabbit isolated lungs. *Br J Pharmacol* **1980,** *69* (3), 479-89.

33.   Smith, W. L.; Urade, Y.; Jakobsson, P. J., Enzymes of the cyclooxygenase pathways of prostanoid biosynthesis. *Chem Rev* **2011,** *111* (10), 5821-65.

34.   Tsuboi, K.; Sugimoto, Y.; Ichikawa, A., Prostanoid receptor subtypes. *Prostaglandins Other Lipid Mediat* **2002,** *68-69*, 535-56.

35.   Maiuri, M. C.; Tajana, G.; Iuvone, T.; De Stefano, D.; Mele, G.; Ribecco, M. T.; Cinelli, M. P.; Romano, M. F.; Turco, M. C.; Carnuccio, R., Nuclear factor-kappaB regulates inflammatory cell apoptosis and phagocytosis in rat carrageenin-sponge implant model. *Am J Pathol* **2004,** *165* (1), 115-26.

36.   Levy, B. D.; Clish, C. B.; Schmidt, B.; Gronert, K.; Serhan, C. N., Lipid mediator class switching during acute inflammation: signals in resolution. *Nat Immunol* **2001,** *2* (7), 612-9.

37.   Hodge-Dufour, J.; Marino, M. W.; Horton, M. R.; Jungbluth, A.; Burdick, M. D.; Strieter, R. M.; Noble, P. W.; Hunter, C. A.; Pure, E., Inhibition of interferon gamma induced interleukin 12 production: a potential mechanism for the anti-inflammatory activities of tumor necrosis factor. *Proc Natl Acad Sci U S A* **1998,** *95* (23), 13806-11.

38.   Nathan, C., Points of control in inflammation. *Nature* **2002,** *420* (6917), 846-52.

39.   Savill, J.; Fadok, V., Corpse clearance defines the meaning of cell death. *Nature* **2000,** *407* (6805), 784-8.

40.   Birbrair, A.; Zhang, T.; Wang, Z. M.; Messi, M. L.; Olson, J. D.; Mintz, A.; Delbono, O., Type-2 pericytes participate in normal and tumoral angiogenesis. *Am J Physiol Cell Physiol* **2014,** *307* (1), C25-38.

41.   Clark, W. H., Tumour progression and the nature of cancer. *Br J Cancer* **1991,** *64* (4), 631-44.

42.   Hanahan, D.; Weinberg, R. A., The hallmarks of cancer. *Cell* **2000,** *100* (1), 57-70.

43.   Sarkar, S.; Horn, G.; Moulton, K.; Oza, A.; Byler, S.; Kokolus, S.; Longacre, M., Cancer development, progression, and therapy: an epigenetic overview. *Int J Mol Sci* **2013,** *14* (10), 21087-113.

44.   Maeda, H.; Akaike, T., Nitric oxide and oxygen radicals in infection, inflammation, and cancer. *Biochemistry (Mosc)* **1998,** *63* (7), 854-65.

45.   Pollard, J. W., Tumour-educated macrophages promote tumour progression and metastasis. *Nat Rev Cancer* **2004,** *4* (1), 71-8.

46.   Rainsford, K. D., Profile and mechanisms of gastrointestinal and other side effects of nonsteroidal anti-inflammatory drugs (NSAIDs). *Am J Med* **1999,** *107* (6A), 27S-35S; discussion 35S-36S.

47.   McGettigan, P.; Henry, D., Cardiovascular risk and inhibition of cyclooxygenase: a systematic review of the observational studies of selective and nonselective inhibitors of cyclooxygenase 2. *JAMA* **2006,** *296* (13), 1633-44.

48.   Chang, H. H.; Meuillet, E. J., Identification and development of mPGES-1 inhibitors: where we are at? *Future Med Chem* **2011,** *3* (15), 1909-34.

49.   Claveau, D.; Sirinyan, M.; Guay, J.; Gordon, R.; Chan, C. C.; Bureau, Y.; Riendeau, D.; Mancini, J. A., Microsomal prostaglandin E synthase-1 is a major terminal synthase that is selectively up-regulated during cyclooxygenase-2-dependent prostaglandin E2 production in the rat adjuvant-induced arthritis model. *J Immunol* **2003,** *170* (9), 4738-44.

50.   Schopf, F. H.; Biebl, M. M.; Buchner, J., The HSP90 chaperone machinery. *Nat Rev Mol Cell Biol* **2017,** *18* (6), 345-360.

51.   Mahalingam, D.; Swords, R.; Carew, J. S.; Nawrocki, S. T.; Bhalla, K.; Giles, F. J., Targeting HSP90 for cancer therapy. *British Journal Of Cancer* **2009,** *100*, 1523.

52.   Wayne, N.; Mishra, P.; Bolon, D. N., Hsp90 and client protein maturation. *Methods Mol Biol* **2011,** *787*, 33-44.

53.   Wu, Y.; Huang, B.; Liu, Q.; Liu, Y., Heat shock protein 90-beta over-expression is associated with poor survival in stage I lung adenocarcinoma patients. *Int J Clin Exp Pathol* **2015,** *8* (7), 8252-9.

54.   Jarzab, M.; Kowal, M.; Bal, W.; Oczko-Wojciechowska, M.; Rembak-Szynkiewicz, J.; Kowalska, M.; Stobiecka, E.; Chmielik, E.; Tyszkiewicz, T.; Kaszuba, M.; Nowicka, E.; Lange, B.; Czarniecka, A.; Krajewska, J.; Dyla, A.; Dobrut, M.; Lange, D.; Jarzab, B.; Bobek-Billewicz, B.; Tarnawski, R., Ratio of proliferation markers and HSP90 gene expression as a predictor of pathological complete response in breast cancer neoadjuvant chemotherapy. *Folia Histochem Cytobiol* **2016,** *54* (4), 202-209.

55.   Heath, E. I.; Hillman, D. W.; Vaishampayan, U.; Sheng, S.; Sarkar, F.; Harper, F.; Gaskins, M.; Pitot, H. C.; Tan, W.; Ivy, S. P.; Pili, R.; Carducci, M. A.; Erlichman, C.; Liu, G., A phase II trial of 17-allylamino-17-demethoxygeldanamycin in patients with hormone-refractory metastatic prostate cancer. *Clin Cancer Res* **2008,** *14* (23), 7940-6.

56.   Donnelly, A.; Blagg, B. S., Novobiocin and additional inhibitors of the Hsp90 C-terminal nucleotide-binding pocket. *Curr Med Chem* **2008,** *15* (26), 2702-17.

57.   Strocchia, M.; Terracciano, S.; Chini, M. G.; Vassallo, A.; Vaccaro, M. C.; Dal Piaz, F.; Leone, A.; Riccio, R.; Bruno, I.; Bifulco, G., Targeting the Hsp90 C-terminal domain by the chemically accessible dihydropyrimidinone scaffold. *ChemComm* **2015,** *51* (18), 3850-3853.

58.   Terracciano, S.; Foglia, A.; Chini, M. G.; Vaccaro, M. C.; Russo, A.; Piaz, F. D.; Saturnino, C.; Riccio, R.; Bifulco, G.; Bruno, I., New dihydropyrimidin-2(1H)-one based Hsp90 C-terminal inhibitors. *RSC Advances* **2016,** *6* (85), 82330-82340.

59.   Terracciano, S.; Chini, M. G.; Vaccaro, M. C.; Strocchia, M.; Foglia, A.; Vassallo, A.; Saturnino, C.; Riccio, R.; Bifulco, G.; Bruno, I., Correction: Identification of the key structural elements of a dihydropyrimidinone core driving toward more potent Hsp90 C-terminal inhibitors. *Chem Commun (Camb)* **2016,** *52* (92), 13515.

60.   Samarasinghe, B.; Wales, C. T.; Taylor, F. R.; Jacobs, A. T., Heat shock factor 1 confers resistance to Hsp90 inhibitors through p62/SQSTM1 expression and promotion of autophagic flux. *Biochem Pharmacol* **2014,** *87* (3), 445-55.

61.   Sliwoski, G.; Kothiwale, S.; Meiler, J.; Lowe, E. W., Jr., Computational methods in drug discovery. *Pharmacol Rev* **2014,** *66* (1), 334-95.

62.   Poulsen, A.; Liljefors, T.; Gundertofte, K.; Bjornholm, B., A pharmacophore model for NK2 antagonist comprising compounds from several structurally diverse classes. *J Comput Aided Mol Des* **2002,** *16* (4), 273-86.

63.   Abi Hussein, H.; Geneix, C.; Petitjean, M.; Borrel, A.; Flatters, D.; Camproux, A. C., Global vision of druggability issues: applications and perspectives. *Drug Discov Today* **2017,** *22* (2), 404-415.

64.   Hopkins, A. L.; Groom, C. R., Target analysis: a priori assessment of druggability. *Ernst Schering Res Found Workshop* **2003,** (42), 11-7.

65.   Hopkins, A. L.; Groom, C. R., The druggable genome. *Nat Rev Drug Discov* **2002,** *1* (9), 727-30.

66.   Lipinski, C. A.; Lombardo, F.; Dominy, B. W.; Feeney, P. J., Experimental and computational approaches to estimate solubility and permeability in drug discovery and development settings. *Adv Drug Deliv Rev* **2001,** *46* (1-3), 3-26.

67.   Macalino, S. J.; Gosu, V.; Hong, S.; Choi, S., Role of computer-aided drug design in modern drug discovery. *Arch Pharm Res* **2015,** *38* (9), 1686-701.

68.   Flory, P. J.; Volkenstein, M., Statistical mechanics of chain molecules. *Biopolymers* **1969,** *8* (5), 699-700.

69.   Sledz, P.; Caflisch, A., Protein structure-based drug design: from docking to molecular dynamics. *Curr Opin Struct Biol* **2018,** *48*, 93-102.

70.   Hatherley, R.; Brown, D. K.; Glenister, M.; Tastan Bishop, O., PRIMO: An Interactive Homology Modeling Pipeline. *PLoS One* **2016,** *11* (11), e0166698.

71.   Kumar Deokar, H.; Barch, H. P.; Buolamwini, J. K., Homology Modeling of Human Concentrative Nucleoside Transporters (hCNTs) and Validation by Virtual Screening and Experimental Testing to Identify Novel hCNT1 Inhibitors. *Drug Des* **2017,** *6* (1).

72.   Schrödinger Release 2017-1 *SiteMap*, LLC, Schrödinger New York, NY, 2017.

73.   Schrödinger Release 2017-1 *QSite*, LLC, Schrödinger New York, NY, 2017.

74.   Binkowski, T. A.; Naghibzadeh, S.; Liang, J., CASTp: Computed Atlas of Surface Topography of proteins. *Nucleic Acids Res* **2003,** *31* (13), 3352-5.

75.   von Behren, M. M.; Rarey, M., Ligand-based virtual screening under partial shape constraints. *J Comput Aided Mol Des* **2017,** *31* (4), 335-347.

76.   Vuorinen, A.; Odermatt, A.; Schuster, D., Reprint of "In silico methods in the discovery of endocrine disrupting chemicals". *J Steroid Biochem Mol Biol* **2015,** *153*, 93-101.

77.   Kuntz, I. D.; Blaney, J. M.; Oatley, S. J.; Langridge, R.; Ferrin, T. E., A geometric approach to macromolecule-ligand interactions. *J Mol Biol* **1982,** *161* (2), 269-88.

78.   Rarey, M.; Kramer, B.; Lengauer, T.; Klebe, G., A fast flexible docking method using an incremental construction algorithm. *J Mol Biol* **1996,** *261* (3), 470-89.

79.   Jones, G.; Willett, P.; Glen, R. C.; Leach, A. R.; Taylor, R., Development and validation of a genetic algorithm for flexible docking. *J Mol Biol* **1997,** *267* (3), 727-48.

80.   Huey, R.; Morris, G. M.; Olson, A. J.; Goodsell, D. S., A semiempirical free energy force field with charge-based desolvation. *J Comput Chem* **2007,** *28* (6), 1145-52.

81.   Morris, G. M.; Huey, R.; Lindstrom, W.; Sanner, M. F.; Belew, R. K.; Goodsell, D. S.; Olson, A. J., AutoDock4 and AutoDockTools4: Automated docking with selective receptor flexibility. *J Comput Chem* **2009,** *30* (16), 2785-91.

82.   Trott, O.; Olson, A. J., AutoDock Vina: improving the speed and accuracy of docking with a new scoring function, efficient optimization, and multithreading. *J Comput Chem* **2010,** *31* (2), 455-61.

83.   Friesner, R. A.; Banks, J. L.; Murphy, R. B.; Halgren, T. A.; Klicic, J. J.; Mainz, D. T.; Repasky, M. P.; Knoll, E. H.; Shelley, M.; Perry, J. K.; Shaw, D. E.; Francis, P.; Shenkin, P. S., Glide: a new approach for rapid, accurate docking and scoring. 1. Method and assessment of docking accuracy. *J Med Chem* **2004,** *47* (7), 1739-49.

84.   Halgren, T. A.; Murphy, R. B.; Friesner, R. A.; Beard, H. S.; Frye, L. L.; Pollard, W. T.; Banks, J. L., Glide: A New Approach for Rapid, Accurate Docking and Scoring. 2. Enrichment Factors in Database Screening. *J Med Chem* **2004,** *47* (7), 1750-1759.

85.   Friesner, R. A.; Murphy, R. B.; Repasky, M. P.; Frye, L. L.; Greenwood, J. R.; Halgren, T. A.; Sanschagrin, P. C.; Mainz, D. T., Extra Precision Glide: Docking and Scoring Incorporating a Model of Hydrophobic Enclosure for Protein−Ligand Complexes. *J Med Chem* **2006,** *49* (21), 6177-6196.

86.   Schrödinger Release 2015-2 *Glide*, LLC, Schrödinger New York, NY, 2015.

87.   Schrödinger Release 2017-1 *Glide*, LLC, Schrödinger New York, NY, 2017.

88.   Halperin, I.; Ma, B.; Wolfson, H.; Nussinov, R., Principles of docking: An overview of search algorithms and a guide to scoring functions. *Proteins* **2002,** *47* (4), 409-43.

89.   Kitchen, D. B.; Decornez, H.; Furr, J. R.; Bajorath, J., Docking and scoring in virtual screening for drug discovery: methods and applications. *Nat Rev Drug Discov* **2004,** *3* (11), 935-49.

90.   Verkhivker, G. M.; Bouzida, D.; Gehlhaar, D. K.; Rejto, P. A.; Arthurs, S.; Colson, A. B.; Freer, S. T.; Larson, V.; Luty, B. A.; Marrone, T.; Rose, P. W., Deciphering common failures in molecular docking of ligand-protein complexes. *J Comput Aided Mol Des* **2000,** *14* (8), 731-51.

91.   Park, H.; Lee, J.; Lee, S., Critical assessment of the automated AutoDock as a new docking tool for virtual screening. *Proteins* **2006,** *65* (3), 549-54.

92.   Chen, J.; Houk, K. N., Molecular Modeling: Principles and Applications By Andrew R. Leach. Addison Wesley Longman Limited: Essex, England, 1996. 595 pp. ISBN 0-582-23933-8. $35. J *Chem Inf Comput Sci* **1998,** *38* (5), 939-939.

93.   Brooijmans, N.; Kuntz, I. D., Molecular recognition and docking algorithms. *Annu Rev Biophys Biomol Struct* **2003,** *32*, 335-73.

94.   Di Nola, A.; Roccatano, D.; Berendsen, H. J., Molecular dynamics simulation of the docking of substrates to proteins. *Proteins* **1994,** *19* (3), 174-82.

95.   Durrant, J. D.; McCammon, J. A., Molecular dynamics simulations and drug discovery. *BMC Biol* **2011,** *9*, 71.

96.   McCammon, J. A.; Gelin, B. R.; Karplus, M., Dynamics of folded proteins. *Nature* **1977,** *267* (5612), 585-90.

97.   Huang, N.; Kalyanaraman, C.; Irwin, J. J.; Jacobson, M. P., Physics-based scoring of protein-ligand complexes: enrichment of known inhibitors in large-scale virtual screening. *J Chem Inf Model* **2006,** *46* (1), 243-53.

98.   Bohm, H. J., The development of a simple empirical scoring function to estimate the binding constant for a protein-ligand complex of known three-dimensional structure. *J Comput Aided Mol Des* **1994,** *8* (3), 243-56.

99.   Krammer, A.; Kirchhoff, P. D.; Jiang, X.; Venkatachalam, C. M.; Waldman, M., LigScore: a novel scoring function for predicting binding affinities. *J Mol Graph Model* **2005,** *23* (5), 395-407.

100.   Eldridge, M. D.; Murray, C. W.; Auton, T. R.; Paolini, G. V.; Mee, R. P., Empirical scoring functions: I. The development of a fast empirical scoring function to estimate the binding affinity of ligands in receptor complexes. *J Comput Aided Mol Des* **1997,** *11* (5), 425-45.

101.   Greenwood, J. R.; Calkins, D.; Sullivan, A. P.; Shelley, J. C., Towards the comprehensive, rapid, and accurate prediction of the favorable tautomeric states of drug-like molecules in aqueous solution. *J Comput Aided Mol Des* **2010,** *24* (6-7), 591-604.

102.   Shelley, J. C.; Cholleti, A.; Frye, L. L.; Greenwood, J. R.; Timlin, M. R.; Uchimaya, M., Epik: a software program for pK(a) prediction and protonation state generation for drug-like molecules. *J Comput Aided Mol Des* **2007,** *21* (12), 681-91.

103.   Sherman, W.; Day, T.; Jacobson, M. P.; Friesner, R. A.; Farid, R., Novel procedure for modeling ligand/receptor induced fit effects. *J Med Chem* **2006,** *49* (2), 534-53.

104.   Sherman, W.; Beard, H. S.; Farid, R., Use of an induced fit receptor structure in virtual screening. *Chem Biol Drug Des* **2006,** *67* (1), 83-4.

105.   Induced Fit Docking, protocol 2015-2 *Glide version 6.4, Prime version 3.7*, LLC, Schrödinger New York, NY, 2015.

106.   Schrödinger Release 2015-2 *Prime*, LLC, Schrödinger New York, NY, 2015.

107.   Lauro, G.; Cantone, V.; Potenza, M.; Fischer, K.; Koeberle, A.; Werz, O.; Riccio, R.; Bifulco, G., Discovery of 3-hydroxy-3-pyrrolin-2-one-based mPGES-1 inhibitors using a multi-step virtual screening protocol. *MedChemComm* **2018,** *9* (12), 2028-2036.

108.   Dixon, S. L.; Smondyrev, A. M.; Knoll, E. H.; Rao, S. N.; Shaw, D. E.; Friesner, R. A. J. o. C.-A. M. D., PHASE: a new engine for pharmacophore perception, 3D QSAR model development, and 3D database screening: 1. Methodology and preliminary results. *J Comput Aided Mol Des* **2006,** *20* (10), 647-671.

109.   Schrödinger Release 2017-1 *Phase*, LLC, Schrödinger New York, NY, 2017.

110.   Schrödinger Release 2015-2 *QikProp*, LLC, Schrödinger New York, NY, 2015.

111.   Schrödinger Release 2017-1 *QikProp*, LLC, Schrödinger New York, NY, 2017.

112.   Schrödinger Release 2015-2 *CombiGlide*, LLC, Schrödinger New York, NY, 2015.

113.   Schrödinger Release 2017-1 *CombiGlide*, LLC, Schrödinger New York, NY, 2017.

114.   Benet, L. Z.; Hosey, C. M.; Ursu, O.; Oprea, T. I., BDDCS, the Rule of 5 and drugability. *Adv Drug Deliv Rev* **2016,** *101*, 89-98.

115.   Wenlock, M. C.; Austin, R. P.; Barton, P.; Davis, A. M.; Leeson, P. D., A comparison of physiochemical property profiles of development and marketed oral drugs. *J Med Chem* **2003,** *46* (7), 1250-6.

116.   Congreve, M.; Carr, R.; Murray, C.; Jhoti, H., A 'rule of three' for fragment-based lead discovery? *Drug Discov Today* **2003,** *8* (19), 876-7.

117.   Schrödinger Release 2015-2 *Maestro*, LLC, Schrödinger New York, NY, 2015.

118.   Schrödinger Release 2017-1 *Maestro*, LLC, Schrödinger New York, NY, 2017.

119.   Liu, R.; Li, X.; Lam, K. S., Combinatorial chemistry in drug discovery. *Curr Opin Chem Biol* **2017,** *38*, 117-126.

120.   Hajduk, P. J., Fragment-Based Drug Design: How Big Is Too Big? *J Med Chem* **2006,** *49* (24), 6972-6976.

121.   Song, X.; Liu, C.; Chen, P.; Zhang, H.; Sun, R., Natural Product-Based Pesticide Discovery: Design, Synthesis and Bioactivity Studies of N-Amino-Maleimide Derivatives. *Molecules* **2018,** *23* (7).

122.   Fang, G.; Xue, M.; Su, M.; Hu, D.; Li, Y.; Xiong, B.; Ma, L.; Meng, T.; Chen, Y.; Li, J.; Li, J.; Shen, J., CCLab--a multi-objective genetic algorithm based combinatorial library design software and an application for histone deacetylase inhibitor design. *Bioorg Med Chem Lett* **2012,** *22* (14), 4540-5.

123.   Schrödinger Release 2015-2 *LigPrep*, LLC, Schrödinger New York, NY, 2015.

124.   Schrödinger Release 2017-1 *LigPrep*, LLC, Schrödinger New York, NY, 2017.

125.   Jorgensen, W. L.; Maxwell, D. S.; Tirado-Rives, J., Development and Testing of the OPLS All-Atom Force Field on Conformational Energetics and Properties of Organic Liquids. *J. Am. Chem. Soc.* **1996,** *118* (45), 11225-11236.

126.   Stichtenoth, D. O.; Thoren, S.; Bian, H.; Peters-Golden, M.; Jakobsson, P. J.; Crofford, L. J., Microsomal prostaglandin E synthase is regulated by proinflammatory cytokines and glucocorticoids in primary rheumatoid synovial cells. *J Immunol* **2001,** *167* (1), 469-74.

127.   Jakobsson, P. J.; Thoren, S.; Morgenstern, R.; Samuelsson, B., Identification of human prostaglandin E synthase: a microsomal, glutathione-dependent, inducible enzyme, constituting a potential novel drug target. *Proc Natl Acad Sci U S A* **1999,** *96* (13), 7220-5.

128.   Jakobsson, P. J.; Morgenstern, R.; Mancini, J.; Ford-Hutchinson, A.; Persson, B., Common structural features of MAPEG -- a widespread superfamily of membrane associated proteins with highly divergent functions in eicosanoid and glutathione metabolism. *Protein Sci* **1999,** *8* (3), 689-92.

129.   Jakobsson, P. J.; Mancini, J. A.; Ford-Hutchinson, A. W., Identification and characterization of a novel human microsomal glutathione S-transferase with leukotriene C4 synthase activity and significant sequence identity to 5-lipoxygenase-activating protein and leukotriene C4 synthase. *J Biol Chem* **1996,** *271* (36), 22203-10.

130.   Jegerschold, C.; Pawelzik, S. C.; Purhonen, P.; Bhakat, P.; Gheorghe, K. R.; Gyobu, N.; Mitsuoka, K.; Morgenstern, R.; Jakobsson, P. J.; Hebert, H., Structural basis for induced formation of the inflammatory mediator prostaglandin E2. *Proc Natl Acad Sci U S A* **2008,** *105* (32), 11110-5.

131.   Sjogren, T.; Nord, J.; Ek, M.; Johansson, P.; Liu, G.; Geschwindner, S., Crystal structure of microsomal prostaglandin E2 synthase provides insight into diversity in the MAPEG superfamily. *Proc Natl Acad Sci U S A* **2013,** *110* (10), 3806-11.

132.   Brock, J. S.; Hamberg, M.; Balagunaseelan, N.; Goodman, M.; Morgenstern, R.; Strandback, E.; Samuelsson, B.; Rinaldo-Matthis, A.; Haeggstrom, J. Z., A dynamic Asp-Arg interaction is essential for catalysis in microsomal prostaglandin E2 synthase. *Proc Natl Acad Sci U S A* **2016,** *113* (4), 972-7.

133.   Luz, J. G.; Antonysamy, S.; Kuklish, S. L.; Condon, B.; Lee, M. R.; Allison, D.; Yu, X.-P.; Chandrasekhar, S.; Backer, R.; Zhang, A.; Russell, M.; Chang, S. S.; Harvey, A.; Sloan, A. V.; Fisher, M. J., Crystal Structures of mPGES-1 Inhibitor Complexes Form a Basis for the Rational Design of Potent Analgesic and Anti-Inflammatory Therapeutics. *J Med Chem* **2015,** *58* (11), 4727-4737.

134.   Quraishi, O.; Mancini, J. A.; Riendeau, D., Inhibition of inducible prostaglandin E(2) synthase by 15-deoxy-Delta(12,14)-prostaglandin J(2) and polyunsaturated fatty acids. *Biochem Pharmacol* **2002,** *63* (6), 1183-9.

135.   Gillard, J.; Ford-Hutchinson, A. W.; Chan, C.; Charleson, S.; Denis, D.; Foster, A.; Fortin, R.; Leger, S.; McFarlane, C. S.; Morton, H.; et al., L-663,536 (MK-886) (3-[1-(4-chlorobenzyl)-3-t-butyl-thio-5-isopropylindol-2-yl]-2,2 - dimethylpropanoic acid), a novel, orally active leukotriene biosynthesis inhibitor. *Can J Physiol Pharmacol* **1989,** *67* (5), 456-64.

136.   Riendeau, D.; Aspiotis, R.; Ethier, D.; Gareau, Y.; Grimm, E. L.; Guay, J.; Guiral, S.; Juteau, H.; Mancini, J. A.; Methot, N.; Rubin, J.; Friesen, R. W., Inhibitors of the inducible microsomal prostaglandin E2 synthase (mPGES-1) derived from MK-886. *Bioorg Med Chem Lett* **2005,** *15* (14), 3352-5.

137.   Xu, D.; Rowland, S. E.; Clark, P.; Giroux, A.; Cote, B.; Guiral, S.; Salem, M.; Ducharme, Y.; Friesen, R. W.; Methot, N.; Mancini, J.; Audoly, L.; Riendeau, D., MF63 [2-(6-chloro-1H-phenanthro[9,10-d]imidazol-2-yl)-isophthalonitrile], a selective microsomal prostaglandin E synthase-1 inhibitor, relieves pyresis and pain in preclinical models of inflammation. *J Pharmacol Exp Ther* **2008,** *326* (3), 754-63.

138.   Finetti, F.; Terzuoli, E.; Bocci, E.; Coletta, I.; Polenzani, L.; Mangano, G.; Alisi, M. A.; Cazzolla, N.; Giachetti, A.; Ziche, M.; Donnini, S., Pharmacological inhibition of microsomal prostaglandin E synthase-1 suppresses epidermal growth factor receptor-mediated tumor growth and angiogenesis. *PLoS One* **2012,** *7* (7), e40576.

139.   Arhancet, G. B.; Walker, D. P.; Metz, S.; Fobian, Y. M.; Heasley, S. E.; Carter, J. S.; Springer, J. R.; Jones, D. E.; Hayes, M. J.; Shaffer, A. F.; Jerome, G. M.; Baratta, M. T.; Zweifel, B.; Moore, W. M.; Masferrer, J. L.; Vazquez, M. L., Discovery and SAR of PF-4693627, a potent, selective and orally bioavailable mPGES-1 inhibitor for the potential treatment of inflammation. *Bioorg Med Chem Lett* **2013,** *23* (4), 1114-9.

140.   Kuklish, S. L.; Antonysamy, S.; Bhattachar, S. N.; Chandrasekhar, S.; Fisher, M. J.; Fretland, A. J.; Gooding, K.; Harvey, A.; Hughes, N. E.; Luz, J. G.; Manninen, P. R.; McGee, J. E.; Navarro, A.; Norman, B. H.; Partridge, K. M.; Quimby, S. J.; Schiffler, M. A.; Sloan, A. V.; Warshawsky, A. M.; York, J. S.; Yu, X. P., Characterization of 3,3-dimethyl substituted N-aryl piperidines as potent microsomal prostaglandin E synthase-1 inhibitors. *Bioorg Med Chem Lett* **2016,** *26* (19), 4824-4828.

141.   Nikolaou, A.; Kokotou, M. G.; Limnios, D.; Kokotos, G., Microsomal prostaglandin E2 synthase-1 inhibitors: a patent review AU - Psarra, Anastasia. *Expert Opin Ther Pat.* **2017,** *27* (9), 1047-1059.

142.   Guerrero, M. D.; Aquino, M.; Bruno, I.; Terencio, M. C.; Paya, M.; Riccio, R.; Gomez-Paloma, L., Synthesis and pharmacological evaluation of a selected library of new potential anti-inflammatory agents bearing the gamma-hydroxybutenolide scaffold: a new class of inhibitors of prostanoid production through the selective modulation of microsomal prostaglandin E synthase-1 expression. *J Med Chem* **2007,** *50* (9), 2176-84.

143.   Banerjee, A.; Pawar, M. Y.; Patil, S.; Yadav, P. S.; Kadam, P. A.; Kattige, V. G.; Deshpande, D. S.; Pednekar, P. V.; Pisat, M. K.; Gharat, L. A., Development of 2-aryl substituted quinazolin-4(3H)-one, pyrido[4,3-d]pyrimidin-4(3H)-one and pyrido[2,3-d]pyrimidin-4(3H)-one derivatives as microsomal prostaglandin E(2) synthase-1 inhibitors. *Bioorg Med Chem Lett* **2014,** *24* (20), 4838-44.

144.   Jin, Y.; Smith, C. L.; Hu, L.; Campanale, K. M.; Stoltz, R.; Huffman, L. G., Jr.; McNearney, T. A.; Yang, X. Y.; Ackermann, B. L.; Dean, R.; Regev, A.; Landschulz, W., Pharmacodynamic comparison of LY3023703, a novel microsomal prostaglandin e synthase 1 inhibitor, with celecoxib. *Clin Pharmacol Ther* **2016,** *99* (3), 274-84.

145.   Moon, Y.; Glasgow, W. C.; Eling, T. E., Curcumin suppresses interleukin 1beta-mediated microsomal prostaglandin E synthase 1 by altering early growth response gene 1 and other signaling pathways. *J Pharmacol Exp Ther* **2005,** *315* (2), 788-95.

146.   Bauer, J.; Kuehnl, S.; Rollinger, J. M.; Scherer, O.; Northoff, H.; Stuppner, H.; Werz, O.; Koeberle, A., Carnosol and Carnosic Acids from Salvia officinalis Inhibit Microsomal Prostaglandin E$_2$ Synthase-1. *J Pharmacol Exp Ther* **2012,** *342* (1), 169-176.

147.   Koeberle, A.; Bauer, J.; Verhoff, M.; Hoffmann, M.; Northoff, H.; Werz, O., Green tea epigallocatechin-3-gallate inhibits microsomal prostaglandin E(2) synthase-1. *Biochem Biophys Res Commun* **2009,** *388* (2), 350-4.

148.   Koeberle, A.; Northoff, H.; Werz, O., Identification of 5-lipoxygenase and microsomal prostaglandin E2 synthase-1 as functional targets of the anti-inflammatory and anti-carcinogenic garcinol. *Biochem Pharmacol* **2009,** *77* (9), 1513-21.

149.   Trebino, C. E.; Stock, J. L.; Gibbons, C. P.; Naiman, B. M.; Wachtmann, T. S.; Umland, J. P.; Pandher, K.; Lapointe, J. M.; Saha, S.; Roach, M. L.; Carter, D.; Thomas, N. A.; Durtschi, B. A.; McNeish, J. D.; Hambor, J. E.; Jakobsson, P. J.; Carty, T. J.; Perez, J. R.; Audoly, L. P., Impaired inflammatory and pain responses in mice lacking an inducible prostaglandin E synthase. *Proc Natl Acad Sci U S A* **2003,** *100* (15), 9044-9.

150.   Kamei, D.; Yamakawa, K.; Takegoshi, Y.; Mikami-Nakanishi, M.; Nakatani, Y.; Oh-Ishi, S.; Yasui, H.; Azuma, Y.; Hirasawa, N.; Ohuchi, K.; Kawaguchi, H.; Ishikawa, Y.; Ishii, T.; Uematsu, S.; Akira, S.; Murakami, M.; Kudo, I., Reduced pain hypersensitivity and inflammation in mice lacking microsomal prostaglandin e synthase-1. *J Biol Chem* **2004,** *279* (32), 33684-95.

151.   Korotkova, M.; Jakobsson, P. J., Microsomal prostaglandin e synthase-1 in rheumatic diseases. *Front Pharmacol* **2010,** *1*, 146.

152.   Wang, M.; Song, W. L.; Cheng, Y.; Fitzgerald, G. A., Microsomal prostaglandin E synthase-1 inhibition in cardiovascular inflammatory disease. *J Intern Med* **2008,** *263* (5), 500-5.

153.   Saha, S.; Engstrom, L.; Mackerlova, L.; Jakobsson, P. J.; Blomqvist, A., Impaired febrile responses to immune challenge in mice deficient in microsomal prostaglandin E synthase-1. *Am J Physiol Regul Integr Comp Physiol* **2005,** *288* (5), R1100-7.

154.   Murakami, M.; Kudo, I., Prostaglandin E synthase: a novel drug target for inflammation and cancer. *Curr Pharm Des* **2006,** *12* (8), 943-54.

155.   Mattila, S.;   Tuominen, H.;   Koivukangas, J.;   Stenback, F., The terminal prostaglandin synthases mPGES-1, mPGES-2, and cPGES are all overexpressed in human gliomas. *Neuropathology* **2009,** *29* (2), 156-65.

156.   Gudis, K.; Tatsuguchi, A.; Wada, K.; Hiratsuka, T.; Futagami, S.; Fukuda, Y.; Kiyama, T.; Tajiri, T.; Miyake, K.; Sakamoto, C., Clinical significance of prostaglandin E synthase expression in gastric cancer tissue. *Hum Pathol* **2007,** *38* (12), 1826-35.

157.   Mehrotra, S.; Morimiya, A.; Agarwal, B.; Konger, R.; Badve, S., Microsomal prostaglandin E2 synthase-1 in breast cancer: a potential target for therapy. *J Pathol* **2006,** *208* (3), 356-63.

158.   Omi, Y.;   Shibata, N.;   Okamoto, T.;   Obara, T.;   Kobayashi, M., Immunohistochemical demonstration of membrane-bound prostaglandin E2 synthase-1 in papillary thyroid carcinoma. *Acta Histochem Cytochem* **2009,** *42* (4), 105-9.

159.   Yoshimatsu, K.;   Altorki, N. K.;   Golijanin, D.;   Zhang, F.;   Jakobsson, P. J.; Dannenberg, A. J.; Subbaramaiah, K., Inducible prostaglandin E synthase is overexpressed in non-small cell lung cancer. *Clin Cancer Res* **2001,** *7* (9), 2669-74.

160.   Herfs, M.; Herman, L.; Hubert, P.; Minner, F.; Arafa, M.; Roncarati, P.; Henrotin, Y.;   Boniver, J.; Delvenne, P., High expression of PGE2 enzymatic pathways in cervical (pre)neoplastic lesions and functional consequences for antigen-presenting cells. *Cancer Immunol Immunother* **2009,** *58* (4), 603-14.

161.   Rask, K.; Zhu, Y.; Wang, W.; Hedin, L.; Sundfeldt, K., Ovarian epithelial cancer: a role for PGE2-synthesis and signalling in malignant transformation and progression. *Mol Cancer* **2006,** *5*, 62.

162.   Stamatakis, K.;   Jimenez-Martinez, M.;   Jimenez-Segovia, A.;   Chico-Calero, I.; Conde, E.; Galan-Martinez, J.; Ruiz, J.; Pascual, A.; Barrocal, B.; Lopez-Perez, R.; Garcia-Bermejo, M. L.; Fresno, M., Prostaglandins induce early growth response 1 transcription factor mediated microsomal prostaglandin E2 synthase up-regulation for colorectal cancer progression. *Oncotarget* **2015,** *6* (37), 39941-59.

163.   Svouraki, A.; Garscha, U.; Kouloura, E.; Pace, S.; Pergola, C.; Krauth, V.; Rossi, A.;   Sautebin, L.;   Halabalaki, M.;   Werz, O.;   Gaboriaud-Kolar, N.; Skaltsounis, A. L., Evaluation of Dual 5-Lipoxygenase/Microsomal Prostaglandin E2 Synthase-1 Inhibitory Effect of Natural and Synthetic Acronychia-Type Isoprenylated Acetophenones. *J Nat Prod* **2017,** *80* (3), 699-706.

164.   Chini, M. G.; De Simone, R.; Bruno, I.; Riccio, R.; Dehm, F.; Weinigel, C.; Barz, D.;   Werz, O.; Bifulco, G., Design and synthesis of a second series of triazole-based compounds as potent dual mPGES-1 and 5-lipoxygenase inhibitors. *Eur J Med Chem* **2012,** *54*, 311-23.

165.   Chini, M. G.; Ferroni, C.; Cantone, V.; Dambruoso, P.; Varchi, G.; Pepe, A.; Fischer, K.; Pergola, C.; Werz, O.; Bruno, I.; Riccio, R.; Bifulco, G., Elucidating new structural features of the triazole scaffold for the development of mPGES-1 inhibitors. *MedChemComm* **2015,** *6* (1), 75-79.

166.   Terracciano, S.; Lauro, G.; Strocchia, M.; Fischer, K.; Werz, O.; Riccio, R.; Bruno, I.; Bifulco, G., Structural Insights for the Optimization of Dihydropyrimidin-2(1H)-one Based mPGES-1 Inhibitors. *ACS Med Chem Lett* **2015,** *6* (2), 187-91.

167.   Melo-Filho, C. C.;   Braga, R. C.; Andrade, C. H., 3D-QSAR approaches in drug design: perspectives to generate reliable CoMFA models. *Curr Comput Aided Drug Des* **2014,** *10* (2), 148-59.

168.   Lauro, G.; Romano, A.; Riccio, R.; Bifulco, G., Inverse Virtual Screening of Antitumor Targets: Pilot Study on a Small Database of Natural Bioactive Compounds. *J Nat Prod* **2011,** *74* (6), 1401-1407.

169.   Dadmal, T. L.; Katre, S. D.; Mandewale, M. C.; Kumbhare, R. M., Contemporary progress in the synthesis and reactions of 2-aminobenzothiazole: a review. *New J Chem* **2018,** *42* (2), 776-797.

170.   Koeberle, A.; Siemoneit, U.; Buehring, U.; Northoff, H.; Laufer, S.; Albrecht, W.; Werz, O., Licofelone suppresses prostaglandin E(2) formation by interference with the inducible microsomal prostaglandin E(2) synthase-1. *J. Pharmacol. Exp. Ther.* **2008,** *326* (3), 975-982.

171.   Kim, S. H.; Hashimoto, Y.; Cho, S. N.; Roszik, J.; Milton, D. R.; Dal, F.; Kim, S. F.; Menter, D. G.; Yang, P.; Ekmekcioglu, S.; Grimm, E. A., Microsomal PGE2 synthase-1 regulates melanoma cell survival and associates with melanoma disease progression. *Pigment Cell Melanoma Res* **2016,** *29* (3), 297-308.

172.   Sharma, P. C.; Sinhmar, A.; Sharma, A.; Rajak, H.; Pathak, D. P., Medicinal significance of benzothiazole scaffold: an insight view. *J Enzyme Inhib Med Chem* **2013,** *28* (2), 240-66.

173.   Keri, R. S.; Patil, M. R.; Patil, S. A.; Budagumpi, S., A comprehensive review in current developments of benzothiazole-based molecules in medicinal chemistry. *Eur J Med Chem* **2015,** *89*, 207-51.

174.   Kamal, A.; Syed, M. A.; Mohammed, S. M., Therapeutic potential of benzothiazoles: a patent review (2010 - 2014). *Expert Opin Ther Pat* **2015,** *25* (3), 335-49.

175.   Luz, J. G.; Antonysamy, S.; Kuklish, S. L.; Condon, B.; Lee, M. R.; Allison, D.; Yu, X. P.; Chandrasekhar, S.; Backer, R.; Zhang, A.; Russell, M.; Chang, S. S.; Harvey, A.; Sloan, A. V.; Fisher, M. J., Crystal Structures of mPGES-1 Inhibitor Complexes Form a Basis for the Rational Design of Potent Analgesic and Anti-Inflammatory Therapeutics. *J Med Chem* **2015,** *58* (11), 4727-37.

176.   Muthukaman, N.; Deshmukh, S.; Sarode, N.; Tondlekar, S.; Tambe, M.; Pisal, D.; Shaikh, M.; Kattige, V. G.; Honnegowda, S.; Karande, V.; Kulkarni, A.; Jadhav, S. B.; Mahat, M. Y. A.; Gudi, G. S.; Khairatkar-Joshi, N.; Gharat, L. A., Discovery of 2-((2-chloro-6-fluorophenyl)amino)-N-(3-fluoro-5-(trifluoromethyl)phenyl)-1-methy   l-7,8-dihydro-1H-[1,4]dioxino[2',3':3,4]benzo[1,2-d]imidazole-5-carboxamide   as   potent,   selective   and efficacious microsomal prostaglandin E2 synthase-1 (mPGES-1) inhibitor. *Bioorg Med Chem Lett* **2016,** *26* (24), 5977-5984.

177.   Serban, G.; Stanasel, O.; Serban, E.; Bota, S., 2-Amino-1,3,4-thiadiazole as a potential scaffold for promising antimicrobial agents. *Drug Des Devel Ther* **2018,** *12*, 1545-1566.

178.   Holla, B. S.; Poojary, K. N.; Rao, B. S.; Shivananda, M. K., New bis-aminomercaptotriazoles and bis-triazolothiadiazoles as possible anticancer agents. *Eur J Med Chem* **2002,** *37* (6), 511-7.

179.   Miyaura, N.; Yamada, K.; Suzuki, A., A new stereospecific cross-coupling by the palladium-catalyzed reaction of 1-alkenylboranes with 1-alkenyl or 1-alkynyl halides. *Tetrahedron Lett* **1979,** *20* (36), 3437-3440.

180.   Miyaura, N.; Suzuki, A., Stereoselective synthesis of arylated (E)-alkenes by the reaction of alk-1-enylboranes with aryl halides in the presence of palladium catalyst. *J Chem Soc, ChemComm* **1979,** (19), 866-867.

181.   Miyaura, N.; Suzuki, A., Palladium-Catalyzed Cross-Coupling Reactions of Organoboron Compounds. *Chemical Reviews* **1995,** *95* (7), 2457-2483.

182.   Lauro, G.; Manfra, M.; Pedatella, S.; Fischer, K.; Cantone, V.; Terracciano, S.; Bertamino, A.; Ostacolo, C.; Gomez-Monterrey, I.; De Nisco, M.; Riccio, R.; Novellino, E.; Werz, O.; Campiglia, P.; Bifulco, G., Identification of novel microsomal prostaglandin E2 synthase-1 (mPGES-1) lead inhibitors from Fragment Virtual Screening. *Eur J Med Chem* **2017,** *125*, 278-287.

183.   Di Micco, S.; Terracciano, S.; Cantone, V.; Fischer, K.; Koeberle, A.; Foglia, A.; Riccio, R.; Werz, O.; Bruno, I.; Bifulco, G., Discovery of new potent molecular entities able to inhibit mPGES-1. *Eur J Med Chem* **2018,** *143*, 1419-1427.

184.   Daina, A.; Michielin, O.; Zoete, V., SwissADME: a free web tool to evaluate pharmacokinetics, drug-likeness and medicinal chemistry friendliness of small molecules. *Sci Rep* **2017,** *7*, 42717.

185.   Baell, J. B.; Holloway, G. A., New substructure filters for removal of pan assay interference compounds (PAINS) from screening libraries and for their exclusion in bioassays. *J Med Chem* **2010,** *53* (7), 2719-40.

186.   Klayman, D. L.; Maul, J.; Milne, G. W., 2-Amino-2-thiazoline. 3. The differing behavior of phenylisothiocyanate and phenylisocyanate toward 2-amino-2-thiazoline. *Tetrahedron Lett* **1967,** *3*, 281-4.

187.   Bosc, J. J.; Jarry, C., 2-Amino-2-oxazolines, Part 9: Synthesis and pharmacological evaluation of N-phenyl-N'-[1-[3-(1-aryl-4-piperazinyl)propan-2-ol]]ureas. *Arch Pharm (Weinheim)* **1998,** *331* (9), 291-3.

188.   Bhosale, J. D.; Dabur, R.; Jadhav, G. P.; Bendre, R. S., Facile Syntheses and Molecular-Docking of Novel Substituted 3,4-Dimethyl-1H-pyrrole-2-carboxamide/carbohydrazide Analogues with Antimicrobial and Antifungal Properties. *Molecules* **2018,** *23* (4).

189.   Ragno, R.; Marshall, G. R.; Di Santo, R.; Costi, R.; Massa, S.; Rompei, R.; Artico, M., Antimycobacterial pyrroles: synthesis, anti-Mycobacterium tuberculosis activity and QSAR studies. *Bioorg Med Chem* **2000,** *8* (6), 1423-32.

190.   Battilocchio, C.; Poce, G.; Alfonso, S.; Porretta, G. C.; Consalvi, S.; Sautebin, L.; Pace, S.; Rossi, A.; Ghelardini, C.; Di Cesare Mannelli, L.; Schenone, S.; Giordani, A.; Di Francesco, L.; Patrignani, P.; Biava, M., A class of pyrrole derivatives endowed with analgesic/anti-inflammatory activity. *Bioorg Med Chem* **2013,** *21* (13), 3695-701.

191.   Persico, M.; Ramunno, A.; Maglio, V.; Franceschelli, S.; Esposito, C.; Carotenuto, A.; Brancaccio, D.; De Pasquale, V.; Pavone, L. M.; Varra, M.; Orteca, N.; Novellino, E.; Fattorusso, C., New anticancer agents mimicking protein recognition motifs. *J Med Chem* **2013,** *56* (17), 6666-80.

192.   Wiegard, A.; Hanekamp, W.; Griessbach, K.; Fabian, J.; Lehr, M., Pyrrole alkanoic acid derivatives as nuisance inhibitors of microsomal prostaglandin E2 synthase-1. *Eur J Med Chem* **2012,** *48*, 153-63.

193.   Wattanasuepsin, W.; Intra, B.; Euanorasetr, J.; Watanabe, Y.; Mingma, R.; Fukasawa, W.; Mori, M.; Matsumoto, A.; Shiomi, K.; Panbangred, W., 1-Methoxypyrrole-2-carboxamide-A new pyrrole compound isolated from Streptomyces griseocarneus SWW368. *J Gen Appl Microbiol* **2017,** *63* (4), 207-211.

194.   Janupally, R.; Medepi, B.; Brindha Devi, P.; Suryadevara, P.; Jeankumar, V. U.; Kulkarni, P.; Yogeeswari, P.; Sriram, D., Design and Biological Evaluation of

Furan/Pyrrole/Thiophene-2-carboxamide Derivatives as Efficient DNA GyraseB Inhibitors of Staphylococcus aureus. *Chem Biol Drug Des* **2015,** *86* (4), 918-25.

195.   Stubbing, L. A.; Li, F. F.; Furkert, D. P.; Caprio, V. E.; Brimble, M. A., Access to 2-alkyl chromanones via a conjugate addition approach. *Tetrahedron* **2012,** *68* (34), 6948-6956.

196.   Luescher, M. U.; Bode, J. W., Catalytic Synthesis of N-Unprotected Piperazines, Morpholines, and Thiomorpholines from Aldehydes and SnAP Reagents. *Angew Chem Int Ed Engl* **2015,** *54* (37), 10884-8.

197.   Vo, C. V.; Mikutis, G.; Bode, J. W., SnAP reagents for the transformation of aldehydes into substituted thiomorpholines--an alternative to cross-coupling with saturated heterocycles. *Angew Chem Int Ed Engl* **2013,** *52* (6), 1705-8.

198.   Vo, C.-V. T.; Bode, J. W., Synthesis of Saturated N-Heterocycles. *J Org Chem* **2014,** *79* (7), 2809-2815.

199.   Yoshikai, N.; Mieczkowski, A.; Matsumoto, A.; Ilies, L.; Nakamura, E., Iron-catalyzed C-C bond formation at alpha-position of aliphatic amines via C-H bond activation through 1,5-hydrogen transfer. *J Am Chem Soc* **2010,** *132* (16), 5568-9.

200.   Pastine, S. J.; Gribkov, D. V.; Sames, D., sp3 C-H bond arylation directed by amidine protecting group: alpha-arylation of pyrrolidines and piperidines. *J Am Chem Soc* **2006,** *128* (44), 14220-1.

201.   McNally, A.; Prier, C. K.; MacMillan, D. W., Discovery of an alpha-amino C-H arylation reaction using the strategy of accelerated serendipity. *Science* **2011,** *334* (6059), 1114-7.

202.   Jurberg, I. D.; Peng, B.; Wostefeld, E.; Wasserloos, M.; Maulide, N., Intramolecular redox-triggered C-H functionalization. *Angew Chem Int Ed Engl* **2012,** *51* (8), 1950-3.

203.   Hirotaka, K.; Kohei, S., Copper(II) Triflate-mediated Addition Reaction of α-Oxygenated Alkylstannanes to Imines for the Synthesis of vicinal-Amino Alcohol Derivatives. *Synth Commun* **2003,** *32* (6), 514-515.

204.   Luescher, M. U.; Vo, C. V.; Bode, J. W., SnAP reagents for the synthesis of piperazines and morpholines. *Org Lett* **2014,** *16* (4), 1236-9.

205.   Geoghegan, K.; Bode, J. W., Bespoke SnAP Reagents for the Synthesis of C-Substituted Spirocyclic and Bicyclic Saturated N-Heterocycles. *Org Lett* **2015,** *17* (8), 1934-1937.

206.   Vo, C.-V. T.; Luescher, M. U.; Bode, J. W., SnAP reagents for the one-step synthesis of medium-ring saturated N-heterocycles from aldehydes. *Nat Chem* **2014,** *6*, 310.

207.   Duan, J.; Dixon, S. L.; Lowrie, J. F.; Sherman, W., Analysis and comparison of 2D fingerprints: Insights into database screening performance using eight fingerprint methods. *J Mol Graph Model* **2010,** *29* (2), 157-170.

208.   Sastry, M.; Lowrie, J. F.; Dixon, S. L.; Sherman, W., Large-scale systematic analysis of 2D fingerprint methods and parameters to improve virtual screening enrichments. *J Chem Inf Model* **2010,** *50* (5), 771-84.

209.   Li, D.; Howe, N.; Dukkipati, A.; Shah, S. T. A.; Bax, B. D.; Edge, C.; Bridges, A.; Hardwicke, P.; Singh, O. M. P.; Giblin, G.; Pautsch, A.; Pfau, R.; Schnapp, G.; Wang, M.; Olieric, V.; Caffrey, M., Crystallizing Membrane Proteins in the Lipidic Mesophase. Experience with Human Prostaglandin E2 Synthase 1 and an Evolving Strategy. *Cryst Growth Des* **2014,** *14* (4), 2034-2047.

210.   Phase; Schrödinger; LLC, *New York, NY* **2017**.

211.   Sastry, G. M.; Inakollu, V. S.; Sherman, W., Boosting virtual screening enrichments with data fusion: coalescing hits from two-dimensional fingerprints, shape, and docking. *J Chem Inf Model* **2013,** *53* (7), 1531-42.

212.   Pala, D.; Beuming, T.; Sherman, W.; Lodola, A.; Rivara, S.; Mor, M., Structure-based virtual screening of MT2 melatonin receptor: influence of template choice and structural refinement. *J Chem Inf Model* **2013,** *53* (4), 821-35.

213.   LigPrep.; Schrödinger; LLC, *New York, NY* **2017**.

214.   Glide; Schrödinger; LLC, *New York, NY* **2017**.

215.   Shymanska, N. V.; Pierce, J. G., Stereoselective Synthesis of Quaternary Pyrrolidine-2,3-diones and beta-Amino Acids. *Org. Lett.* **2017,** *19* (11), 2961-2964.

216.   Mori, M.; Tintori, C.; Christopher, R. S.; Radi, M.; Schenone, S.; Musumeci, F.; Brullo, C.; Sanita, P.; Delle Monache, S.; Angelucci, A.; Kissova, M.; Crespan, E.; Maga, G.; Botta, M., A combination strategy to inhibit Pim-1: synergism between noncompetitive and ATP-competitive inhibitors. *ChemMedChem* **2013,** *8* (3), 484-96.

217.   Pace, P.; Spieser, S. A.; Summa, V., 4-Hydroxy-5-pyrrolinone-3-carboxamide HIV-1 integrase inhibitors. *Bioorg. Med. Chem. Lett.* **2008,** *18* (14), 3865-9.

218.   Radmark, O.; Samuelsson, B., Microsomal prostaglandin E synthase-1 and 5-lipoxygenase: potential drug targets in cancer. *J. Intern. Med.* **2010,** *268* (1), 5-14.

219.   Park, H. G.; Han, S. I.; Oh, S. Y.; Kang, H. S., Cellular responses to mild heat stress. *Cell Mol Life Sci* **2005,** *62* (1), 10-23.

220.   Boston, R. S.; Viitanen, P. V.; Vierling, E., Molecular chaperones and protein folding in plants. *Plant Mol Biol* **1996,** *32* (1-2), 191-222.

221.   Lindquist, S.; Craig, E. A., The heat-shock proteins. *Annu Rev Genet* **1988,** *22*, 631-77.

222.   Derocher, A. E.; Helm, K. W.; Lauzon, L. M.; Vierling, E., Expression of a Conserved Family of Cytoplasmic Low Molecular Weight Heat Shock Proteins during Heat Stress and Recovery. *Plant Physiol* **1991,** *96* (4), 1038-47.

223.   Wang, Z.; Li, L., Adenovirus-mediated RNA interference against collagen-specific molecular chaperone 47-KDa heat shock protein suppresses scar formation on mouse wounds. *Cell Biol Int* **2008,** *32* (5), 484-93.

224.   Sitia, R.; Braakman, I., Quality control in the endoplasmic reticulum protein factory. *Nature* **2003,** *426* (6968), 891-4.

225.   Whitley, D.; Goldberg, S. P.; Jordan, W. D., Heat shock proteins: a review of the molecular chaperones. *J Vasc Surg* **1999,** *29* (4), 748-51.

226.   Lee, U.; Rioflorido, I.; Hong, S. W.; Larkindale, J.; Waters, E. R.; Vierling, E., The Arabidopsis ClpB/Hsp100 family of proteins: chaperones for stress and chloroplast development. *Plant J* **2007,** *49* (1), 115-27.

227.   R, R. K.; N, S. N.; S, P. A.; Sinha, D.; Veedin Rajan, V. B.; Esthaki, V. K.; D'Silva, P., HSPIR: a manually annotated heat shock protein information resource. *Bioinformatics* **2012,** *28* (21), 2853-5.

228.   Lund, P. A., Microbial molecular chaperones. *Adv Microb Physiol* **2001,** *44*, 93-140.

229.   Mayer, M. P.; Brehmer, D.; Gassler, C. S.; Bukau, B., Hsp70 chaperone machines. *Adv Protein Chem* **2001,** *59*, 1-44.

230.   Mayer, M. P.; Bukau, B., Hsp70 chaperones: cellular functions and molecular mechanism. *Cell Mol Life Sci* **2005,** *62* (6), 670-84.

231. Garrido, C.; Brunet, M.; Didelot, C.; Zermati, Y.; Schmitt, E.; Kroemer, G., Heat shock proteins 27 and 70: anti-apoptotic proteins with tumorigenic properties. *Cell Cycle* **2006,** *5* (22), 2592-601.

232. Park, C. J.; Seo, Y. S., Heat Shock Proteins: A Review of the Molecular Chaperones for Plant Immunity. *Plant Pathol J* **2015,** *31* (4), 323-33.

233. Pratt, W. B.; Toft, D. O., Regulation of signaling protein function and trafficking by the hsp90/hsp70-based chaperone machinery. *Exp Biol Med (Maywood)* **2003,** *228* (2), 111-33.

234. Whitesell, L.; Lindquist, S. L., HSP90 and the chaperoning of cancer. *Nat Rev Cancer* **2005,** *5* (10), 761-72.

235. Zhang, H.; Burrows, F., Targeting multiple signal transduction pathways through inhibition of Hsp90. *J Mol Med (Berl)* **2004,** *82* (8), 488-99.

236. Sreedhar, A. S.; Kalmar, E.; Csermely, P.; Shen, Y. F., Hsp90 isoforms: functions, expression and clinical importance. *FEBS Lett* **2004,** *562* (1-3), 11-5.

237. Altieri, D. C.; Stein, G. S.; Lian, J. B.; Languino, L. R., TRAP-1, the mitochondrial Hsp90. *Biochim Biophys Acta* **2012,** *1823* (3), 767-73.

238. Marzec, M.; Eletto, D.; Argon, Y., GRP94: An HSP90-like protein specialized for protein folding and quality control in the endoplasmic reticulum. *Biochim Biophys Acta* **2012,** *1823* (3), 774-87.

239. Theodoraki, M. A.; Caplan, A. J., Quality control and fate determination of Hsp90 client proteins. *Biochim Biophys Acta* **2012,** *1823* (3), 683-8.

240. McDonough, H.; Patterson, C., CHIP: a link between the chaperone and proteasome systems. *Cell Stress Chaperones* **2003,** *8* (4), 303-8.

241. Workman, P., Combinatorial attack on multistep oncogenesis by inhibiting the Hsp90 molecular chaperone. *Cancer Lett* **2004,** *206* (2), 149-57.

242. Muchowski, P. J.; Wacker, J. L., Modulation of neurodegeneration by molecular chaperones. *Nat Rev Neurosci* **2005,** *6* (1), 11-22.

243. Luo, G. R.; Le, W. D., Collective roles of molecular chaperones in protein degradation pathways associated with neurodegenerative diseases. *Curr Pharm Biotechnol* **2010,** *11* (2), 180-7.

244. Batulan, Z.; Taylor, D. M.; Aarons, R. J.; Minotti, S.; Doroudchi, M. M.; Nalbantoglu, J.; Durham, H. D., Induction of multiple heat shock proteins and neuroprotection in a primary culture model of familial amyotrophic lateral sclerosis. *Neurobiol Dis* **2006,** *24* (2), 213-25.

245. Li, Y.; Zhang, T.; Schwartz, S. J.; Sun, D., New developments in Hsp90 inhibitors as anti-cancer therapeutics: mechanisms, clinical perspective and more potential. *Drug Resist Updat* **2009,** *12* (1-2), 17-27.

246. Zuehlke, A.; Johnson, J. L., Hsp90 and co-chaperones twist the functions of diverse client proteins. *Biopolymers* **2010,** *93* (3), 211-7.

247. Blagosklonny, M. V., Hsp-90-associated oncoproteins: multiple targets of geldanamycin and its analogs. *Leukemia* **2002,** *16* (4), 455-62.

248. Miyata, Y.; Nakamoto, H.; Neckers, L., The therapeutic target Hsp90 and cancer hallmarks. *Curr Pharm Des* **2013,** *19* (3), 347-65.

249. Broemer, M.; Krappmann, D.; Scheidereit, C., Requirement of Hsp90 activity for IkappaB kinase (IKK) biosynthesis and for constitutive and inducible IKK and NF-kappaB activation. *Oncogene* **2004,** *23* (31), 5378-86.

250.   Bucci, M.; Roviezzo, F.; Cicala, C.; Sessa, W. C.; Cirino, G., Geldanamycin, an inhibitor of heat shock protein 90 (Hsp90) mediated signal transduction has anti-inflammatory effects and interacts with glucocorticoid receptor in vivo. *Br J Pharmacol* **2000,** *131* (1), 13-6.

251.   Pittet, J. F.; Lee, H.; Pespeni, M.; O'Mahony, A.; Roux, J.; Welch, W. J., Stress-induced inhibition of the NF-kappaB signaling pathway results from the insolubilization of the IkappaB kinase complex following its dissociation from heat shock protein 90. *J Immunol* **2005,** *174* (1), 384-94.

252.   Zhao, Y.; Huang, Z. J.; Rahman, M.; Luo, Q.; Thorlacius, H., Radicicol, an Hsp90 inhibitor, inhibits intestinal inflammation and leakage in abdominal sepsis. *J Surg Res* **2013,** *182* (2), 312-8.

253.   Choi, S. R.; Lee, S. A.; Kim, Y. J.; Ok, C. Y.; Lee, H. J.; Hahm, K. B., Role of heat shock proteins in gastric inflammation and ulcer healing. *J Physiol Pharmacol* **2009,** *60 Suppl 7*, 5-17.

254.   Tomasello, G.; Sciume, C.; Rappa, F.; Rodolico, V.; Zerilli, M.; Martorana, A.; Cicero, G.; De Luca, R.; Damiani, P.; Accardo, F. M.; Romeo, M.; Farina, F.; Bonaventura, G.; Modica, G.; Zummo, G.; Conway de Macario, E.; Macario, A. J.; Cappello, F., Hsp10, Hsp70, and Hsp90 immunohistochemical levels change in ulcerative colitis after therapy. *Eur J Histochem* **2011,** *55* (4), e38.

255.   Ambade, A.; Catalano, D.; Lim, A.; Mandrekar, P., Inhibition of heat shock protein (molecular weight 90 kDa) attenuates proinflammatory cytokines and prevents lipopolysaccharide-induced liver injury in mice. *Hepatology* **2012,** *55* (5), 1585-95.

256.   De Paepe, B.; Creus, K. K.; Martin, J. J.; Weis, J.; De Bleecker, J. L., A dual role for HSP90 and HSP70 in the inflammatory myopathies: from muscle fiber protection to active invasion by macrophages. *Ann N Y Acad Sci* **2009,** *1173*, 463-9.

257.   Poulaki, V.; Iliaki, E.; Mitsiades, N.; Mitsiades, C. S.; Paulus, Y. N.; Bula, D. V.; Gragoudas, E. S.; Miller, J. W., Inhibition of Hsp90 attenuates inflammation in endotoxin-induced uveitis. *FASEB J* **2007,** *21* (9), 2113-2123.

258.   Wandinger, S. K.; Richter, K.; Buchner, J., The Hsp90 chaperone machinery. *J Biol Chem* **2008,** *283* (27), 18473-7.

259.   Prodromou, C.; Roe, S. M.; O'Brien, R.; Ladbury, J. E.; Piper, P. W.; Pearl, L. H., Identification and structural characterization of the ATP/ADP-binding site in the Hsp90 molecular chaperone. *Cell* **1997,** *90* (1), 65-75.

260.   Hawle, P.; Siepmann, M.; Harst, A.; Siderius, M.; Reusch, H. P.; Obermann, W. M., The middle domain of Hsp90 acts as a discriminator between different types of client proteins. *Mol Cell Biol* **2006,** *26* (22), 8385-95.

261.   Soti, C.; Racz, A.; Csermely, P., A Nucleotide-dependent molecular switch controls ATP binding at the C-terminal domain of Hsp90. N-terminal nucleotide binding unmasks a C-terminal binding pocket. *J Biol Chem* **2002,** *277* (9), 7066-75.

262.   Soti, C.; Vermes, A.; Haystead, T. A.; Csermely, P., Comparative analysis of the ATP-binding sites of Hsp90 by nucleotide affinity cleavage: a distinct nucleotide specificity of the C-terminal ATP-binding site. *Eur J Biochem* **2003,** *270* (11), 2421-8.

263.   Chadli, A.; Bruinsma, E. S.; Stensgard, B.; Toft, D., Analysis of Hsp90 cochaperone interactions reveals a novel mechanism for TPR protein recognition. *Biochemistry* **2008,** *47* (9), 2850-7.

264.   Shiau, A. K.; Harris, S. F.; Southworth, D. R.; Agard, D. A., Structural Analysis of E. coli hsp90 reveals dramatic nucleotide-dependent conformational rearrangements. *Cell* **2006,** *127* (2), 329-40.

265.   Huai, Q.; Wang, H.; Liu, Y.; Kim, H. Y.; Toft, D.; Ke, H., Structures of the N-terminal and middle domains of E. coli Hsp90 and conformation changes upon ADP binding. *Structure* **2005,** *13* (4), 579-90.

266.   Ali, M. M.; Roe, S. M.; Vaughan, C. K.; Meyer, P.; Panaretou, B.; Piper, P. W.; Prodromou, C.; Pearl, L. H., Crystal structure of an Hsp90-nucleotide-p23/Sba1 closed chaperone complex. *Nature* **2006,** *440* (7087), 1013-7.

267.   Prodromou, C., Mechanisms of Hsp90 regulation. *Biochem J* **2016,** *473* (16), 2439-52.

268.   Pirkkala, L.; Nykanen, P.; Sistonen, L., Roles of the heat shock transcription factors in regulation of the heat shock response and beyond. *FASEB J* **2001,** *15* (7), 1118-31.

269.   Sorger, P. K.; Pelham, H. R., Yeast heat shock factor is an essential DNA-binding protein that exhibits temperature-dependent phosphorylation. *Cell* **1988,** *54* (6), 855-64.

270.   Sorger, P. K., Heat shock factor and the heat shock response. *Cell* **1991,** *65* (3), 363-6.

271.   Zou, J.; Guo, Y.; Guettouche, T.; Smith, D. F.; Voellmy, R., Repression of heat shock transcription factor HSF1 activation by HSP90 (HSP90 complex) that forms a stress-sensitive complex with HSF1. *Cell* **1998,** *94* (4), 471-80.

272.   Sakurai, H.; Takemori, Y., Interaction between heat shock transcription factors (HSFs) and divergent binding sequences: binding specificities of yeast HSFs and human HSF1. *J Biol Chem* **2007,** *282* (18), 13334-41.

273.   Mollapour, M.; Neckers, L., Post-translational modifications of Hsp90 and their contributions to chaperone regulation. *Biochim Biophys Acta* **2012,** *1823* (3), 648-55.

274.   Bachman, A. B.; Keramisanou, D.; Xu, W.; Beebe, K.; Moses, M. A.; Vasantha Kumar, M. V.; Gray, G.; Noor, R. E.; van der Vaart, A.; Neckers, L.; Gelis, I., Phosphorylation induced cochaperone unfolding promotes kinase recruitment and client class-specific Hsp90 phosphorylation. *Nat Commun* **2018,** *9* (1), 265.

275.   Preuss, K. D.; Pfreundschuh, M.; Weigert, M.; Fadle, N.; Regitz, E.; Kubuschok, B., Sumoylated HSP90 is a dominantly inherited plasma cell dyscrasias risk factor. *J Clin Invest* **2015,** *125* (1), 316-23.

276.   Mollapour, M.; Bourboulia, D.; Beebe, K.; Woodford, M. R.; Polier, S.; Hoang, A.; Chelluri, R.; Li, Y.; Guo, A.; Lee, M. J.; Fotooh-Abadi, E.; Khan, S.; Prince, T.; Miyajima, N.; Yoshida, S.; Tsutsumi, S.; Xu, W.; Panaretou, B.; Stetler-Stevenson, W. G.; Bratslavsky, G.; Trepel, J. B.; Prodromou, C.; Neckers, L., Asymmetric Hsp90 N domain SUMOylation recruits Aha1 and ATP-competitive inhibitors. *Mol Cell* **2014,** *53* (2), 317-29.

277.   Oh, J. H.; Hyun, J. Y.; Varshavsky, A., Control of Hsp90 chaperone and its clients by N-terminal acetylation and the N-end rule pathway. *Proc Natl Acad Sci U S A* **2017,** *114* (22), E4370-E4379.

278.   Scroggins, B. T.; Robzyk, K.; Wang, D.; Marcu, M. G.; Tsutsumi, S.; Beebe, K.; Cotter, R. J.; Felts, S.; Toft, D.; Karnitz, L.; Rosen, N.; Neckers, L., An acetylation site in the middle domain of Hsp90 regulates chaperone function. *Mol Cell* **2007,** *25* (1), 151-9.

279.   Martinez-Ruiz, A.; Villanueva, L.; Gonzalez de Orduna, C.; Lopez-Ferrer, D.; Higueras, M. A.; Tarin, C.; Rodriguez-Crespo, I.; Vazquez, J.; Lamas, S., S-nitrosylation of Hsp90 promotes the inhibition of its ATPase and endothelial nitric oxide synthase regulatory activities. *Proc Natl Acad Sci U S A* **2005,** *102* (24), 8525-30.

280.   Jurczyszyn, A.; Zebzda, A.; Czepiel, J.; Perucki, W.; Bazan-Socha, S.; Cibor, D.; Owczarek, D.; Majka, M., Geldanamycin and Its Derivatives Inhibit the Growth of Myeloma Cells and Reduce the Expression of the MET Receptor. *J Cancer* **2014,** *5* (6), 480-90.

281.   Gorska, M.; Popowska, U.; Sielicka-Dudzin, A.; Kuban-Jankowska, A.; Sawczuk, W.; Knap, N.; Cicero, G.; Wozniak, F., Geldanamycin and its derivatives as Hsp90 inhibitors. *Front Biosci (Landmark Ed)* **2012,** *17*, 2269-77.

282.   Samuni, Y.; Ishii, H.; Hyodo, F.; Samuni, U.; Krishna, M. C.; Goldstein, S.; Mitchell, J. B., Reactive oxygen species mediate hepatotoxicity induced by the Hsp90 inhibitor geldanamycin and its analogs. *Free Radic Biol Med* **2010,** *48* (11), 1559-63.

283.   Li, Y.; Chen, Y.; Qiu, C.; Ma, X.; Lei, K.; Cai, G.; Liang, X.; Liu, J., 17-allylamino-17-demethoxygeldanamycin impeded chemotherapy through antioxidant activation via reducing reactive oxygen species-induced cell death. *J Cell Biochem* **2018.**

284.   Kummar, S.; Gutierrez, M. E.; Gardner, E. R.; Chen, X.; Figg, W. D.; Zajac-Kaye, M.; Chen, M.; Steinberg, S. M.; Muir, C. A.; Yancey, M. A.; Horneffer, Y. R.; Juwara, L.; Melillo, G.; Ivy, S. P.; Merino, M.; Neckers, L.; Steeg, P. S.; Conley, B. A.; Giaccone, G.; Doroshow, J. H.; Murgo, A. J., Phase I trial of 17-dimethylaminoethylamino-17-demethoxygeldanamycin (17-DMAG), a heat shock protein inhibitor, administered twice weekly in patients with advanced malignancies. *Eur J Cancer* **2010,** *46* (2), 340-7.

285.   Aregbe, A. O.; Sherer, E. A.; Egorin, M. J.; Scher, H. I.; Solit, D. B.; Ramanathan, R. K.; Ramalingam, S.; Belani, C. P.; Ivy, P. S.; Bies, R. R., Population pharmacokinetic analysis of 17-dimethylaminoethylamino-17-demethoxygeldanamycin (17-DMAG) in adult patients with solid tumors. *Cancer Chemother Pharmacol* **2012,** *70* (1), 201-5.

286.   Schulte, T. W.; Akinaga, S.; Soga, S.; Sullivan, W.; Stensgard, B.; Toft, D.; Neckers, L. M., Antibiotic radicicol binds to the N-terminal domain of Hsp90 and shares important biologic activities with geldanamycin. *Cell Stress Chaperones* **1998,** *3* (2), 100-8.

287.   Taldone, T.; Chiosis, G., Purine-scaffold Hsp90 inhibitors. *Curr Top Med Chem* **2009,** *9* (15), 1436-46.

288.   He, H.; Zatorska, D.; Kim, J.; Aguirre, J.; Llauger, L.; She, Y.; Wu, N.; Immormino, R. M.; Gewirth, D. T.; Chiosis, G., Identification of potent water soluble purine-scaffold inhibitors of the heat shock protein 90. *J Med Chem* **2006,** *49* (1), 381-90.

289.   McDonald, E.; Jones, K.; Brough, P. A.; Drysdale, M. J.; Workman, P., Discovery and development of pyrazole-scaffold Hsp90 inhibitors. *Curr Top Med Chem* **2006,** *6* (11), 1193-203.

290.   Goldman, J. W.; Raju, R. N.; Gordon, G. A.; El-Hariry, I.; Teofilivici, F.; Vukovic, V. M.; Bradley, R.; Karol, M. D.; Chen, Y.; Guo, W.; Inoue, T.; Rosen, L. S., A first in human, safety, pharmacokinetics, and clinical activity phase I study of once weekly administration of the Hsp90 inhibitor ganetespib (STA-9090) in patients with solid malignancies. *BMC Cancer* **2013,** *13*, 152.

291.   Oki, Y.; Copeland, A.; Romaguera, J.; Fayad, L.; Fanale, M.; Faria Sde, C.; Medeiros, L. J.; Ivy, P.; Younes, A., Clinical experience with the heat shock protein-90 inhibitor, tanespimycin, in patients with relapsed lymphoma. *Leuk Lymphoma* **2012,** *53* (5), 990-2.

292.   Bagatell, R.; Paine-Murrieta, G. D.; Taylor, C. W.; Pulcini, E. J.; Akinaga, S.; Benjamin, I. J.; Whitesell, L., Induction of a heat shock factor 1-dependent stress response alters the cytotoxic activity of hsp90-binding agents. *Clin Cancer Res* **2000,** *6* (8), 3312-8.

293.   Marcu, M. G.; Schulte, T. W.; Neckers, L., Novobiocin and related coumarins and depletion of heat shock protein 90-dependent signaling proteins. *J Natl Cancer Inst* **2000,** *92* (3), 242-8.

294.   Yun, B. G.; Huang, W.; Leach, N.; Hartson, S. D.; Matts, R. L., Novobiocin induces a distinct conformation of Hsp90 and alters Hsp90-cochaperone-client interactions. *Biochemistry* **2004,** *43* (25), 8217-29.
295.   Ardi, V. C.; Alexander, L. D.; Johnson, V. A.; McAlpine, S. R., Macrocycles that inhibit the binding between heat shock protein 90 and TPR-containing proteins. *ACS Chem Biol* **2011,** *6* (12), 1357-66.
296.   Zhao, H.; Donnelly, A. C.; Kusuma, B. R.; Brandt, G. E.; Brown, D.; Rajewski, R. A.; Vielhauer, G.; Holzbeierlein, J.; Cohen, M. S.; Blagg, B. S., Engineering an antibiotic to fight cancer: optimization of the novobiocin scaffold to produce anti-proliferative agents. *J Med Chem* **2011,** *54* (11), 3839-53.
297.   Zhao, H.; Garg, G.; Zhao, J.; Moroni, E.; Girgis, A.; Franco, L. S.; Singh, S.; Colombo, G.; Blagg, B. S., Design, synthesis and biological evaluation of biphenylamide derivatives as Hsp90 C-terminal inhibitors. *Eur J Med Chem* **2015,** *89*, 442-66.
298.   Zhao, H.; Moroni, E.; Yan, B.; Colombo, G.; Blagg, B. S., 3D-QSAR Assisted Design, Synthesis and Evaluation of Novobiocin Analogues. *ACS Med Chem Lett* **2012,** *4* (1), 57-62.
299.   Palermo, C. M.; Westlake, C. A.; Gasiewicz, T. A., Epigallocatechin gallate inhibits aryl hydrocarbon receptor gene transcription through an indirect mechanism involving binding to a 90 kDa heat shock protein. *Biochemistry* **2005,** *44* (13), 5041-52.
300.   Itoh, H.; Ogura, M.; Komatsuda, A.; Wakui, H.; Miura, A. B.; Tashima, Y., A novel chaperone-activity-reducing mechanism of the 90-kDa molecular chaperone HSP90. *Biochem J* **1999,** *343 Pt 3*, 697-703.
301.   Byrd, C. A.; Bornmann, W.; Erdjument-Bromage, H.; Tempst, P.; Pavletich, N.; Rosen, N.; Nathan, C. F.; Ding, A., Heat shock protein 90 mediates macrophage activation by Taxol and bacterial lipopolysaccharide. *Proc Natl Acad Sci U S A* **1999,** *96* (10), 5645-50.
302.   Vasko, R. C.; Rodriguez, R. A.; Cunningham, C. N.; Ardi, V. C.; Agard, D. A.; McAlpine, S. R., Mechanistic studies of Sansalvamide A-amide: an allosteric modulator of Hsp90. *ACS Med Chem Lett* **2010,** *1* (1), 4-8.
303.   Yin, Z.; Henry, E. C.; Gasiewicz, T. A., (-)-Epigallocatechin-3-gallate is a novel Hsp90 inhibitor. *Biochemistry* **2009,** *48* (2), 336-45.
304.   Khandelwal, A.; Hall, J. A.; Blagg, B. S., Synthesis and structure-activity relationships of EGCG analogues, a recently identified Hsp90 inhibitor. *J Org Chem* **2013,** *78* (16), 7859-84.
305.   Wang, Y.; McAlpine, S. R., N-terminal and C-terminal modulation of Hsp90 produce dissimilar phenotypes. *Chem Commun (Camb)* **2015,** *51* (8), 1410-3.
306.   Conde, R.; Belak, Z. R.; Nair, M.; O'Carroll, R. F.; Ovsenek, N., Modulation of Hsf1 activity by novobiocin and geldanamycin. *Biochem Cell Biol* **2009,** *87* (6), 845-51.
307.   Shelton, S. N.; Shawgo, M. E.; Matthews, S. B.; Lu, Y.; Donnelly, A. C.; Szabla, K.; Tanol, M.; Vielhauer, G. A.; Rajewski, R. A.; Matts, R. L.; Blagg, B. S.; Robertson, J. D., KU135, a novel novobiocin-derived C-terminal inhibitor of the 90-kDa heat shock protein, exerts potent antiproliferative effects in human leukemic cells. *Mol Pharmacol* **2009,** *76* (6), 1314-22.
308.   Li, Y.; Zhang, T.; Jiang, Y.; Lee, H. F.; Schwartz, S. J.; Sun, D., (-)-Epigallocatechin-3-gallate inhibits Hsp90 function by impairing Hsp90 association with cochaperones in pancreatic cancer cell line Mia Paca-2. *Mol Pharm* **2009,** *6* (4), 1152-9.

309.   Terracciano, S.; Russo, A.; Chini, M. G.; Vaccaro, M. C.; Potenza, M.; Vassallo, A.; Riccio, R.; Bifulco, G.; Bruno, I., Discovery of new molecular entities able to strongly interfere with Hsp90 C-terminal domain. *Sci Rep* **2018,** *8* (1), 1709.

310.   Christopeit, T.; Carlsen, T. J.; Helland, R.; Leiros, H. K., Discovery of Novel Inhibitor Scaffolds against the Metallo-beta-lactamase VIM-2 by Surface Plasmon Resonance (SPR) Based Fragment Screening. *J Med Chem* **2015,** *58* (21), 8671-82.

311.   Vassallo, A.; Vaccaro, M. C.; De Tommasi, N.; Dal Piaz, F.; Leone, A., Identification of the plant compound geraniin as a novel Hsp90 inhibitor. *PLoS One* **2013,** *8* (9), e74266.

312.   Piaz, F. D.; Vassallo, A.; Temraz, A.; Cotugno, R.; Belisario, M. A.; Bifulco, G.; Chini, M. G.; Pisano, C.; De Tommasi, N.; Braca, A., A Chemical–Biological Study Reveals C9-type Iridoids as Novel Heat Shock Protein 90 (Hsp90) Inhibitors. *J Med Chem* **2013,** *56* (4), 1583-1595.

313.   Lee, C. C.; Lin, T. W.; Ko, T. P.; Wang, A. H., The hexameric structures of human heat shock protein 90. *PLoS One* **2011,** *6* (5), e19961.

314.   Dollins, D. E.; Warren, J. J.; Immormino, R. M.; Gewirth, D. T., Structures of GRP94-nucleotide complexes reveal mechanistic differences between the hsp90 chaperones. *Mol Cell* **2007,** *28* (1), 41-56.

315.   Chini, M. G.; Malafronte, N.; Vaccaro, M. C.; Gualtieri, M. J.; Vassallo, A.; Vasaturo, M.; Castellano, S.; Milite, C.; Leone, A.; Bifulco, G.; De Tommasi, N.; Dal Piaz, F., Identification of Limonol Derivatives as Heat Shock Protein 90 (Hsp90) Inhibitors through a Multidisciplinary Approach. *Chemistry* **2016,** *22* (37), 13236-13250.

316.   Terracciano, S.; Chini, M. G.; Vaccaro, M. C.; Strocchia, M.; Foglia, A.; Vassallo, A.; Saturnino, C.; Riccio, R.; Bifulco, G.; Bruno, I., Identification of the key structural elements of a dihydropyrimidinone core driving toward more potent Hsp90 C-terminal inhibitors. *ChemComm* **2016,** *52* (87), 12857-12860.

317.   Moroni, E.; Zhao, H.; Blagg, B. S.; Colombo, G., Exploiting conformational dynamics in drug discovery: design of C-terminal inhibitors of Hsp90 with improved activities. *J Chem Inf Model* **2014,** *54* (1), 195-208.

318.   Vettoretti, G.; Moroni, E.; Sattin, S.; Tao, J.; Agard, D. A.; Bernardi, A.; Colombo, G., Molecular Dynamics Simulations Reveal the Mechanisms of Allosteric Activation of Hsp90 by Designed Ligands. *Sci Rep* **2016,** *6*, 23830.

319.   Schrödinger Suite 2015-2 *Maestro-Desmond Interoperability Tools, version 4.2*, LLC, Schrödinger New York, NY, 2015.

320.   Vaisburg, A.; Bernstein, N.; Frechette, S.; Allan, M.; Abou-Khalil, E.; Leit, S.; Moradei, O.; Bouchain, G.; Wang, J.; Woo, S. H.; Fournel, M.; Yan, P. T.; Trachy-Bourget, M. C.; Kalita, A.; Beaulieu, C.; Li, Z.; MacLeod, A. R.; Besterman, J. M.; Delorme, D., (2-amino-phenyl)-amides of omega-substituted alkanoic acids as new histone deacetylase inhibitors. *Bioorg Med Chem Lett* **2004,** *14* (1), 283-7.

321.   Kuklish, S. L.; Antonysamy, S.; Bhattachar, S. N.; Chandrasekhar, S.; Fisher, M. J.; Fretland, A. J.; Gooding, K.; Harvey, A.; Hughes, N. E.; Luz, J. G.; Manninen, P. R.; McGee, J. E.; Navarro, A.; Norman, B. H.; Partridge, K. M.; Quimby, S. J.; Schiffler, M. A.; Sloan, A. V.; Warshawsky, A. M.; York, J. S.; Yu, X.-P., Characterization of 3,3-dimethyl substituted N-aryl piperidines as potent microsomal prostaglandin E synthase-1 inhibitors. *Bioorg Med Chem Lett* **2016,** *26* (19), 4824-4828.

322.   Still, W. C.; Kahn, M.; Mitra, A., Rapid chromatographic technique for preparative separations with moderate resolution. *J Org Chem* **1978,** *43* (14), 2923-2925.

323.   Berendsen, H. J. C.; Grigera, J. R.; Straatsma, T. P., The missing term in effective pair potentials. *J Phys Chem* **1987,** *91* (24), 6269-6271.

List of Abbreviations

17-AAG	17-N-allylamino-17-demethoxygeldanamycin
17-DMAG	17-Dimethylaminoethylamino-17 demethoxygeldanamycin
AA	Arachidonic Acid
ADME	Absorption, Distribution, Metabolism, Elimination
ADP	Adenosine Diphosphate
ATP	Adenosine Triphosphate
CADD	Computer-aided drug discovery
CDK	Cyclin-Dependent Kinase
CH_3CN	Acetonitrile
cPGES	cytosolic Prostaglandin E_2 Synthase
COX	Cyclooxygenase
COXib	COX-2 selective inhibitor
Cys	Cysteine
DIPEA	N,N-Diisopropylethylamine
DMSO	Dimethyl Sulfoxide
EGCG	(-)-Epigallocatechin-3-gallate
EtOAc	Ethyl acetate
ESI-MS	Electrospray mass spectrometry

FISA	Hydrophilic component of the SASA
FLAP	5-Lipoxygenase Activating Protein
GA	Genetic Alghoritm
GPCR	G-Protein Coupled Receptors
Grp94	94 kDa gluclose-regulated protein
GSH	Glutathione
HFIP	Hexafluoroisopropanol
Hsc70	Heat Shock Cognate 70
HSF1	Heat Shock Factor 1
Hsp	Heat Shock Protein
HSR	Heat Shock Response
HTVS	High-throughput virtual screening
IC_{50}	Half Maximal Inhibitory Concentration
IFD	Induced Fit Docking
IKK	IκB Kinase
IL	Interleukin
iSnAP	Iterative Stannyl Amine Protocol
K_D	Dissociation Constant
LBDD	Ligand-based Drug Design
LBS	Ligand Binding Site
LO	Lipoxygenase

LT	Leukotriene
LTC4S	Leukotriene C4 Synthase
LVJ	2-[[2,6-bis(chloranyl)-3-[(2,2dimethylpropanoylamino)-methyl]phenyl]amino]-1-methyl-6-(2-methyl-2-oxidanyl-propoxy)-N-[2,2,2-tris-(fluoranyl)ethyl]-benzimidazole-5-carboxamide
M	Morpholine
MAPEG	Membrane-Associated Proteins in Eicosanoid and Glutathione metabolism
MD	Molecular Dinamics
MGST	Microsomal Glutathione S-Transferase
MOM	Methoxymethyl
mPGES-1	microsomal Prostaglandin E_2 Synthase-1
mPGES-2	microsomal Prostaglandin E_2 Synthase-2
MS	Mass Spectrometry
NET	Neutrophil extracellular traps
NF-κB	Nuclear factor kappa-light-chain-enhancer of activated B cells

NMR	Nuclear Magnetic Resonance
NO	Nitric oxide
NSAID	Non-Steroideal Antiinflammatory Drug
PAINS	Pan assay interference compounds
PG	Prostaglandin
PIP	Piperazine
PLA2	Phospholipase A2
PRR	Pattern Recognition Receptors
PET	Petroleum ether
RDC	Radicicol
ROS	Reactive oxygen species
RP-HPLC	Reverse Phase- High Performance Liquid Chromatogrphy
QPlogBB	Predicted brain/blood partition coefficient
QPlogPo/w	Predicted octanol/water partition coefficien
QPlogS	Predicted aqueous solubility
QPPCaco	Predicted apparent Caco-2 cell permeability in nm/sec
QPPMDCK	Predicted apparent MDCK cell permeability in nm/sec.

QPlogHERG	Predicted IC50 value for blockage of HERG K+ channels
RtvFG	Number of reactive functional groups
SASA	Total solvent accessible surface area (SASA) in square angstroms using a probe with a 1.4 Å radius
SBDD	Structure-based Drug Design
SCX_2	Propyl Sulfonic acid supported on silica
SnAP	Stannyl Amine Protocol
SP	Standard Precision
SPR	Surface Plasmon Resonance
STAT3	Signal Transducer and Activator of Transcription 3
TLRs	Toll-Like Receptors
TM	Thiomorpholine
TMSCl	Chlorotrimethylsilane
TNFα	Tumor Necrosis Factor alpha
Trap1	Hsp75/tumor necrosis factor receptor associated protein 1
TXA_2	Tromboxane
VEGF	Vascular Endothelial cell Growth Factor
VSW	Virtual screening workflow

283

XP   Extra Precision